University of Alberta

Investigating the role of the D0 domain of KIR3DL1 in ligand interaction
and exploring the effect of LILRB1 on KIR3DL1 signaling

by

Li Fu

A thesis submitted to the Faculty of Graduate Studies and Research
in partial fulfillment of the requirements for the degree of

Doctor of Philosophy

in

Immunology

Department of Medical Microbiology and Immunology

©Li Fu
Fall 2013
Edmonton, Alberta

ABSTRACT

Natural killer (NK) cells are crucial in early defense against viral infections by rapidly terminating infected cells and by secreting cytokines to shape adaptive immune responses. The activity of NK cells is regulated by balance of activating and inhibitory signals during interaction with target cells. Inhibitory receptors are important as they trigger inhibitory signals to prevent damage of normal health tissue through interaction with self MHC-I molecules. KIR3DL1 is one of inhibitory receptors implicated in resistance to viral diseases such as HIV/AIDS. Structurally, KIR3DL1 contains three Ig domains and has specificity for MHC-I molecules belonging to the HLA-Bw4 serogroup. The receptor's second (D1) and third (D2) Ig domains confer the Bw4 specificity, but the role of the first Ig domain (D0) in ligand recognition remained enigmatic until recently.

In this thesis, I found that KIR3DL1 expressed in YTS cells and as a soluble receptor can weakly recognize additional MHC-I molecules including HLA-B*0702 and HLA-G. This interaction is highly sensitive to blocking with antibodies to the MHC-I α3-domain and the anti-KIR3DL1-D0 antibody, Z27, but not the canonical blocking antibody DX9. Using chimeric receptors between KIR3DL1 and KIR2DL1 expressed on YTS cells and as soluble Fc-fusion proteins, I showed that the presence of a second and independent site of interaction between the KIR3DL1-D0 domain and MHC-I proteins. This data is consistent with the finding of the D0 domain interaction with the MHC-I α1 region in the co-crystal structure reported by Vivian JP et al in 2012. However, after reconciling antibody blocking results with the published co-crystal structure, I proposed a new model in which a third site of interaction occurs. Moreover, using same strategies, I showed KIR3DL1 binding to xenogenic MHC-I, such as mouse MHC-I.

Similarly as shown in HLA, either anti-α3 antibodies or Z27 dramatically inhibited the binding. In addition, mutagenesis studies showed that position 194 at the α3 domain somehow interferes KIR3DL1 binding with unknown mechanism.

Collectively, the results may shed light on how KIRs evolved from LILRs, and be used to interpret genetic association of KIR with diseases such as HIV/AIDS.

ACKNOWLEDGEMENTS

First, I would like to thank my supervisor, Dr. Deborah Burshtyn, for letting me to have opportunity to do graduate studies in her laboratory. She has been a strong and supportive advisor to me throughout my whole graduate study, but she has always given me enough freedom to pursue independent work. In addition, thanks for her kind supports to my general life.

Special thanks to the members of my supervisory committee, Drs Kevin Kane and Bart Hazes, for their support, guidance and helpful suggestion.

As well, thank you to the past and present Burshtyn lab members to technical assistance and friendship.

Also, special thanks to administrative staffs, Anne Giles, Debbie Doudiet and Tabitha Vasquez in the department to help me all the issues throughout my school years. As well, thank you to Dorothy for help cell sorting, Donger for help producing fusion proteins.

Also, thank you to the many friends I have made over the past few years. The encouragement and support from Deanna, Selena, Nick, Chelsea, Kinola, Wayne, Carlo and Elsa.

I would like to thank my dear husband, Zhanpeng Zhang and two lovely kids, Ricky and Jesse Zhang. Finally, I would like to dedicate this work to my in-laws for their unconditional support. Especially, to my father-in-law, who left us too soon. I hope that this work makes you proud.

TABLE OF CONTENTS

CHAPTER 4. THE FIRST IG DOMAIN OF KIR3DL1 CONTACTS MHC CLASS I AT A SECONDARY SITE

CHAPTER 5. XENORECOGNITION OF MOUSE MHC-I BY KIR3DL1

CHAPTER 6. THE INFLUENCE OF POSITION 194 OF MHC-I ON KIR3DL1-D0 BINDING

CHAPTER 7. FINAL DISCUSSION

LIST OF TABLES:

LIST OF FIGURES:

List of Abbreviations

ADCC   antibody dependent cell-mediated cytotoxicity
AIDS   acquired immunodeficiency syndrome
BiP   binding immunoglobulin protein
CTL   cytotoxic T cells
EBV   Epstein-Barr Virus
EGFP   enhanced green fluorescent protein
ER   endoplasmic reticulum
FBS   fetal bovine serum
HBS   HEPES buffered saline
HCMV   human cytomegalovirus
HCV   hepatitis C virus
HIV   human immunodeficiency virus
HFE   Hemochromatosis
HLA   human leukocyte antigen
LILR   leukocyte Ig like receptor
Ig   immunoglobulin
IgSF   immunoglobulin superfamily
ILT2   immuno transcript 2
IS   immunological synapse
ITAM   immunoreceptor tyrosine-based activation motifs
ITIM   immunoreceptor tyrosine-based inhibitory motifs
KIR   killer Ig like receptor
kDa   kilodalton
LFA-1   lymphocyte function-associate antigen-1
LRC   leukocyte receptor complex
MCMV   mouse cytomegalovirus
2-ME   2-mercaptoethanol
MFI   Mean fluorescent intensity
MHC   major histocompability complex
NCR   natural cytotoxic receptor
NEAA   Non-essential amino acid
NK   natural killer
NKC   natural killer complex
PCR   polymerase chain reaction
SFK   src-family tyrosine kinases
SH2   Src homology 2
SPR   surface plasmon resonance

Chapter 1

GENERAL INTRODUCTION

1.1. Natural killer cells

Natural killer (NK) cells are bone marrow derived lymphocytes containing large granules in the cytoplasm. They were discovered in the early 1970's as cells able to spontaneously lyse tumors in the absence of prior antigen stimulation in a mouse model (1, 2). Subsequent studies uncovered the important role of NK cells in responding to infections and tumorgenesis. NK cells comprise 10-15% of circulating peripheral blood lymphocytes, and they are distributed in diverse tissues such as the liver, spleen, peritoneal cavity and in the uterus during pregnancy. Mature human NK cells are defined by the surface expression of Neural Cell Adhesion Molecule 1 (NCAM1), also known as CD56, but lack of the expression of T lymphocyte marker, CD3 (3).

To lay the foundation for understanding my research, in this Chapter, I will cover aspects of NK function and their molecular basis, particularly the complicated receptor systems that are involved.

1.1.1 NK functions

NK cells are differentiated from a common lymphoid progenitor cell, which is the same origin as T and B cells. However, in comparison to the adaptive immune cells, NK cells are effectors of the innate immune system as they rapidly respond to invading pathogens without prior antigen exposure (4, 5). In particular, NK cells are pivotal in defending against viral infection as most viruses have developed mechanisms to evade the adaptive immune response (6).

In general, NK cells act in two ways: cytotoxicity and cytokine secretion. NK cells serve as "natural killers" using a similar mechanism as cytotoxic T cells (CTL). Equipped with a unique receptor system, NK cells have the ability of direct lysis of abnormal or virally infected cells by releasing stored cytotoxic molecules such as perforin and granzymes, upon contacting target cells. In addition, NK cells can use their Fc receptors expressed on the surface to lyse the

antibody coated cells via antibody dependent cell-mediated cytotoxicity (ADCC). On the other hand, NK cells secrete cytokines, such as interferon- γ (IFN-γ) and tumor necrosis factor α (TNF-α), which have direct antiviral effects and modulate subsequent adaptive immune responses (3, 7).

1.1.2 Controlling NK function

NK cells have the ability to kill cells. Therefore, this function must be carefully controlled to prevent damage to healthy tissues. To distinguish pathogen infected and transformed cells from healthy self cells, T cells are equipped with a T cell receptor (TCR) to recognize foreign peptides in the context of the Major Histocompability Complex class I proteins (MHC-I), whereas NK cells use a number of receptors to sense the reduction of MHC-I on target cells. This detection of MHC-I reduction therefore regulates NK functional responses, either positively towards activation or negatively towards inhibition (8, 9).

In association with certain alleles of MHC-I molecules, particular alleles of several NK receptors are strongly linked to resistance of important pathogens such as Hepatitis C Virus (HCV) and Human Immunodeficiency Virus (HIV) (10-13). In addition to the response to infection, NK cells have been implicated in susceptibility to autoimmune diseases, prevention of tumor growth, bone marrow transplant rejection, and protection of embryonic development during pregnancy (14-17). Thus, NK cells are crucial in human health. Better understanding of NK function may aid in disease prevention and treatment.

1.2. Target cell recognition

1.2.1. Distinguishing between "self" and "non-self"

To defend against pathogen invasion, the immune system developed a precise strategy to discriminate healthy self-cells from abnormal self-cells and foreign agents (non-self). This discrimination is monitored through MHC-I (the

details of MHC will be described in section 1.3). The MHC locus was originally defined as an important factor in tissue transplantation (18,19), and the proteins present self and non-self peptides to the TCR (19). The recognition of non-self antigens in the context of MHC-I by the TCR leads to T cell activation and results in tissue rejection. A typical example is skin graft rejection, mediated by T cells. An F1 hybrid offspring generated by mating two strains of mice expresses MHC alleles from both parents. A skin graft from either parent is accepted by the F1 recipient, however, a skin graft from the F1 hybrid is rejected by either parent due to the mismatched inherited non-self MHC from the other parent. Studies of bone marrow transplantation revealed another mechanism. F1 hybrid recipients vigorously reject bone marrow grafts from either parent, despite the fact that donor bone marrow grafts have only self-MHC-I (20-23). This observation, also known as hybrid resistance, was later determined to be mediated by NK cells, and led to the "missing self hypothesis" to explain how NK cells sense the absence of self-MHC-I (24, 25).

1.2.2. Missing self hypothesis

Early experiments in mice revealed that NK cells have the ability to lyse tumor cells that lack MHC-I expression, but spare autologous cells (24, 25). Subsequent *in vitro* studies with human cell lines revealed a similar phenomenon. An Epstein-Barr Virus (EBV) transformed B cell line, 721, was resistant to NK cells whereas its MHC-I deficient variant was lysed by the same NK cells (26). These observations led to the formation of the missing self hypothesis, initially proposed by K. Karre. He predicted that the absence or altered expression of MHC-I would render target cells susceptible to NK cell attack (27). The hypothesis was then validated by numerous subsequent studies and the molecular basis is now better understood. The current explanation of the missing self hypothesis is that self MHC-I engages inhibitory receptors on the surface of NK

cells to transmit inhibitory signals to prevent NK activation, and that NK activity is related to "missing self" when a loss/reduction of self MHC-I occurs.

1.2.3. Induced self hypothesis

In addition to a decrease in inhibitory signals, increases in activating signals also play an important role in controlling NK cells. This idea, known as "induced self activation", was formed by understanding what the activating receptor NKG2D recognized and when its ligand was upregulated (28). NKG2D is a homodimeric molecule expressed by the majority of NK cells, which mediates NK cytotoxicity and cytokine secretion when binding to stress induced molecules on target cells. Besides NKG2D, other activating receptors, such as natural cytotoxic receptors (NCRs), including NKp30, NKp44 and NKp46, have also been reported to control NK response to tumor cells. For example, NKp46 deficient mice are prone to tumorgenesis (29), and molecules on tumor cells are found to be NKp46 ligands (30).

1.2.4. Non-self recognition

A third way for NK-target cell recognition was revealed by the finding that a mouse activating receptor, Ly49H, could be engaged by an MHC-I like molecule derived from Mouse Cytomegalovirus (MCMV) (31, 32). In human, a protein encoded by influenza virus, hemagglutinin, was reported to be a potential ligand for the activating receptors, NKp44 and NKp46 (33). These observations suggest another mechanism of activating receptor involvment in NK responses, through direct interaction with non-self molecules.

1.2.5. The modified missing self hypothesis

With more molecular information being uncovered, there is now agreement that NK activity is actually based on the integration of activating and inhibitory signals (Fig 1-1). Under normal conditions, the presence of self-peptides in the context of MHC-I prevents NK action due to the predominant inhibitory signals.

However, when MHC-I is down-regulated during viral infection, as a common viral strategy to escape T cell responses, it causes a reduction in inhibitory signaling, permitting NK activation. Alternatively, activating pathways are turned on by the appearance or up-regulation of ligands for activating receptors, such as stress molecules, viral proteins and tumor antigens. Ultimately, overriding the inhibitory signaling by enhancing activating signals, allows for NK activation.

Given that the MHC family is important in distinguishing self from non-self by NK cells, I will describe both classical and non-classical MHC-I as they pertain to the studies presented in this thesis.
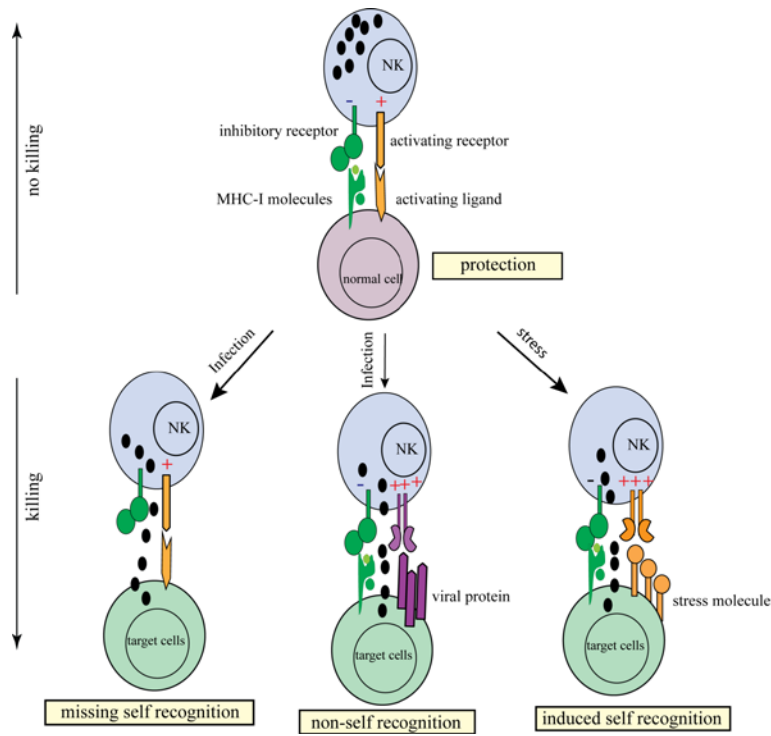
Fig 1-1. Illustration of the missing self hypothesis

The activity of NK cells is based on the integration of inhibitory and activating signals. The balance of activating and inhibitory signals protects normal cells from damage. Abnormal conditions, such as viral infections and tumor transformation, offset the balance and consequently induce NK activation.

Table 1-1. MHC evolution and diverse gene organization between species.

Time of Emergence	Class	Representative Species	Key Features
500 million years ago (MYA)	Teleost	Cartilaginous Fish	I, II and III region
		Zebra Fish	Unlinked I, II and III region
350 MYA	Amphibia	Frog	I, II and III region in the order of II, I, III
	Reptile	Crocodile	I, II region, MHC organization remains unclear.
300 MYA	Avian	Chicken	Minimal and essential, only 19 genes are distributed in I, II, III regions.
100 MYA	Mammal	Mouse	H-2, has I, II and III region with unique genes compared to human. Class I region is separated by II and III regions. The order is I, II, III, I
		Chimpanzee	The most homologous MHC to human
		Human	Over 260 genes in I, II and III region and extended regions. The order is II, III, I region

1.3. Major histocompatibility antigen (MHC)

The Major Histocompatibility Antigens (MHC) are encoded by a group of genes clustered in a confined genomic region. The MHC cluster contains a large number of genes, controlling both immune and non-immune functions. The MHC was originally discovered in mice (34) and later in humans (35) through studying tissue rejection. Subsequently, MHC has been identified in all jawed vertebrates examined to date, and has rapidly evolved from an ancient ancestor 500 million years ago (Table 1-1) (36). In mammals, MHC genes are scattered into three condensed but distinct regions known as class I, II and III, but the number and type of genes are different between species due to gene duplications and mutations. Despite the great genetic differences, the overall function and structure of the MHC proteins is conserved between species.

Aside from being a barrier to transplantation as described in *section 1.2*, the MHC gene complex has been reported to be linked to autoimmune disease (37-39), resistance to infection (40, 41) and fertility (42, 43). Additionally, MHC is involved in non-immune related functions such as central nervous system development (44). Here, I will provide some basic information about human MHC and focus on particular members of the MHC class I locus that are most relevant to this thesis.

1.3.1. Human leukocyte antigen

MHC in humans is called Human Leukocyte Antigen (HLA). The extremely gene-dense region is located on the short arm of human chromosome 6. Thus far, a total of 253 different genes have been identified within the MHC cluster (44). The gene complex contains five regions, including the extended Class I, Class I, III, II and the extended Class II from the telomeric to the centromeric end (Fig 1-2a). The distinct regions encode more than 150 glycoproteins that are categorized into three groups: class I, II and III molecules. Furthermore, Class I molecules are

divided into classical and non-classical groups. Classical MHC-I are encoded by the genes in region A, B and C shown as grey blocks in Fig 1-2a, while non-classical MHC-I are encoded by genes located in region E, F and G shown as black blocks in Fig 1-2a. Classical MHC-I genes are highly polymorphic. Thus far, 2,132 alleles of HLA-A, 2,798 alleles of HLA-B and 1,672 alleles of HLA-C have been identified in human populations (45). However, non-classical genes have limited polymorphism, such that the reported alleles of HLA-E, F and G are 11, 22 and 50, respectively (45).

1.3.1.1. Nomenclature of HLA

A naming system was developed to distinguish individual HLA genes and alleles. The nomenclature of HLA is based on guidelines provided by the World Health Organization (WHO) Nomenclature committee, established in 1968. Figure 1-3 exemplifies the recent strategy for assigning a new HLA gene name (46). In brief, a letter and four sets of digits are used to describe identified alleles. The letter denotes the location of the locus. Four sets of digits are separated by colons, each set representing aspects of the changes in sequence. The optional suffixes (N,L,S,C,Q and A) that indicate the alterations in expression, are also used at the end if applicable. Every allele has at least the first two sets of digits. The last two pairs of digits are added only if necessary. Alleles that differ in the first two sets of digits have at least one different amino acid in the sequence.

a).

Centromeric   Telomeric

Extended Class II   Class II   Class III   Extended Class I

                                                          Class I

b).
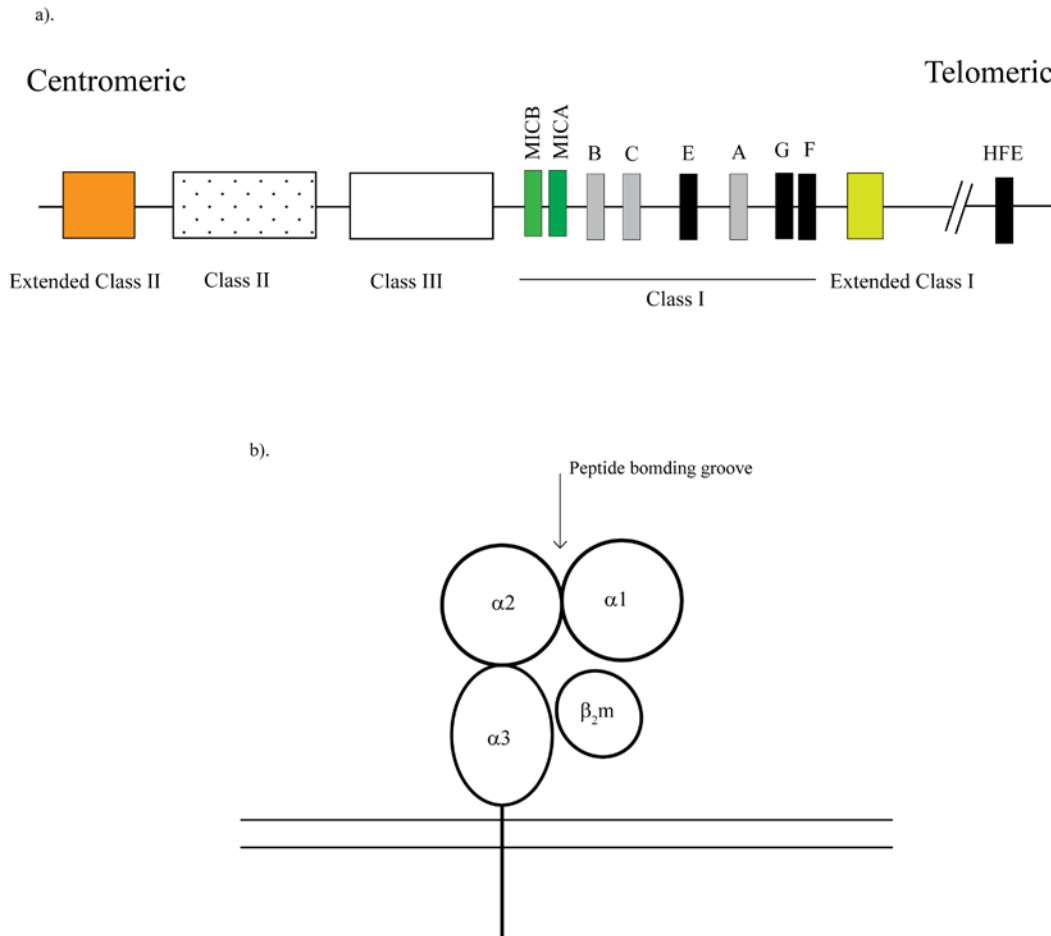
Fig 1-2. The organization of selected genes in human MHC cluster and basic structure of an MHC-I molecule.

a) Distribution of HLA genes on human chromosome 6 from the centromeric to the telomeric end. The organization of the indicated genes in the Class I region is shown. *b)* Schematic of the basic structure of MHC-I.

11

A* 02 : 02 : 02 : 02 N

locus serological antigen or allele family specific HLA protein synonymous changes within the coding region changes in a non-coding region

N denotes null allele does not show on cell surface.
L indicates an allele is expressed with low level compared to normal level.
S denotes an allele expressed in soluble form .
C means allele product stays in cytoplasm.
Q denotes questionable expression
A refers to aberrant expression that is debated

Fig 1-3. Example of the recent nomenclature for a given HLA allele

1.3.1.2. The basic structure of MHC class I molecules

In spite of the vast genetic variation, the encoded MHC-I molecules share a basic structure. The structure consists of two polypeptide chains: a 45 kilodalton (kDa) alpha (α) chain and a 12-kDa beta 2-microglobulin (β_2m) (47) shown in Fig 1-2b. β_2m is encoded by a conserved gene located on chromosome 15. The α chain is a transmembrane glycoprotein composed of three extracellular domains (α1, α2 and α3), a transmembrane region and a short cytoplasmic tail. Each individual extracellular domain contains approximately 90 amino acids. The extremely polymorphic α1 and α2 domains create a groove that fits an approximately 8-11 amino acid long peptide derived from self or non-self proteins. The α3 domain is conserved and it is linked with a short stem that anchors the MHC-I molecule to the cell membrane.

The α chain, β_2m domain of MHC-I and corresponding peptides are assembled in the endoplasmic reticulum (ER) with the assistance of chaperones such as calnexin, calreticulin, ERp57 and binding immunoglobulin protein (BiP). The formed trimeric complex egresses through the Golgi compartment to the cell membrane (48). The structure of the α/β_2m heterodimer is stabilized with a disulfide bond between the α2 and α3 domains and with a non-covalent association of the α3 chain with β_2m (49, 50). In addition, the bound peptide is required for the stability of the complex, and assists in stabilizing the structure of the MHC-I complex on the cell surface (27). Apart from the basic structure, small conformational changes occur due to sequence variations (51). For some alleles, a free α chain without β_2m is observed (52).

Table 1-2. The comparison of the Bw4 and Bw6 determinants

	77	78	79	80	81	82	83	Representative subtypes
Bw4	N	L	R	I/T	A/L	L/A	R	B*27, B*51, B*58,
Bw6	S	L	R	N	L	R	G	B*07, B*35,

The residue that is important for determination of the Bw4/Bw6 specificity is indicated red.

Table 1-3. The comparison of HLA-C1 and C2 serological groups

	77	78	79	80	81	82	83	Representative subtypes
C1	S	L	R	N	L	R	G	Cw01, 03,07,
C2	N	L	R	K	L	R	G	Cw02,06,15

The residue that is important for determination of the C1/C2 specificity is indicated red.

1.3.1.3. Classical HLA

As described in section 1.3.1.1, classical HLA molecules are extremely polymorphic and are expressed on almost all nucleated cells. The polymorphisms are mainly located near the peptide binding cleft and this restricts the types of peptide that can be bound to each subtype. Different subtypes confer distinct specificities for T and NK cell recognition. In the subsequent text, subtypes that are most relevant to this thesis will be described, which include HLA-B and C.

1.3.1.3.1. HLA-B

Of all the classical molecules, the HLA-B locus has the highest diversity, having over 2000 variants. Human Bw4/Bw6 antisera were originally used to define two HLA-B antigens (53), but later, these two antigens were found to represent shared determinants of a larger family of HLA-B alleles (54), also known as public epitopes (55). Presently, the variants of HLA-B are categorized into the Bw4 group or Bw6 group, based upon detectability by either Bw4 or Bw6 specific antisera. Among all the identified HLA-B molecules, the Bw4 motif is present in one third of HLA-B molecules, while the Bw6 epitope is expressed in the remaining two thirds of HLA-B molecules (56).

Sequence comparisons of variants reacting with Bw4 or Bw6 antibodies revealed that these two serological groups bear distinct amino acid sequences at positions 77-83 located in the α-helix of the α_1 domain (specifically residues 77, 80, 81, 82, and 83) (57, 58). The sequence variations are described in Table 1-2. Of these residues, the amino acid at position 80 is the dominant determinant for serological specificity (56). Bw4 variants are defined by polymorphisms at positions 80, 81 and 82. Functionally, polymorphisms in this region are known to affect peptide binding (59) and modify T cell and NK cell responses (56, 60).

HLA-B alleles were initially classified by serological evidence and then by molecular methods. In most scenarios, the serological classification agrees with

the amino acid sequences observed at the public epitopes. However, there are a few exceptions as several alleles bearing the Bw4 sequence also react with anti-Bw6 antibodies (61). Moreover, the Bw4 and Bw6 epitopes are not restricted to HLA-B molecules. For example, the Bw4 motif is found in several HLA-A molecules (62, 63).

As previously mentioned, the HLA-B locus is highly polymorphic as compared to the other two classical MHC-I groups. To further distinguish individual members in the Bw4 or Bw6 groups, other antibodies are utilized to divide HLA-B groups into a number of subtypes, such as B27 and B7, shown in Table 1-2. Of those, the B27 subtype is unique because of the presence of an extra cysteine (C) at position 67 (52). This cysteine contributes to the formation of a homodimer comprising only heavy chains (52, 64). The complexity of this subtype and its impact on NK response will be described in Chapter 6.

1.3.1.3.2. HLA-C

Studies of HLA-C were neglected until the findings of NK cells in the 1990s. The observations that HLA-C impacts the response of alloreactive human NK cells (65, 66) led to subsequent studies. Now, HLA-C mismatch is known to be responsible for the graft versus leukemia response during bone marrow transplantation (17).

The surface level of HLA-C is much lower than that of HLA-A and B (67) despite a similar level of transcript (68). In terms of function, HLA-C molecules are less efficient at triggering T cell responses in comparison to HLA-A and B molecules (69). However, they are important to NK cell activity. Based on their specificities to NK cells, HLA-C molecules are classified into two groups: C1 and C2 (70). Residues involved in the specificity are mapped to positions 77 and 80 of the α1 domain (71) (Table 1-3). The influence of polymorphism of these residues on NK recognition will be described in section 1.5.1.

1.3.1.4. Non-classical HLA

Unlike classical HLA, non-classical HLA molecules have limited diversity. Expression of HLA-E on the cell surface was thought to be restricted to peptides derived from signal sequences of other MHC-I molecules (72), and HLA-E is recognized by NK cells (73-75). However, recently, the presentation of peptides from pathogens or stress molecules by HLA-E has been reported (76-79). The association of other peptides impacts the recognition by NK cells (80). In addition, the non-self peptides derived from viral products that associate with HLA-E also permit recognition by a subset of CD8+ T cells (81, 82).

Of the three non-classical MHC-I, HLA-F is the least characterized. HLA-F molecules are mostly expressed intracellularly in various healthy tissues and immune cells (83). Surface expression of HLA-F is detected on activated lymphocytes (84) and on invading fetal cells (trophoblasts) during pregnancy (85). In comparison to canonical MHC-I, HLA-F has non-synonymous changes at residues required for antigen presentation, yielding a different structure (86). The cytoplasmic tail directs the protein to the surface bypassing the classical antigen presentation pathway (87). In addition, surface expression of HLA-F is independent of peptides (88). In terms of receptor interaction, tetramers of HLA-F were found to stain cells expressing leukocyte Ig-like receptors, and the direct binding was confirmed with BIAcore analysis (89). However, the function of HLA-F remains enigmatic.

HLA-G has a similar structure to other MHC-I molecules, but contains a short cytoplasmic tail that lacks an endocytosis motif, resulting in a longer half-life in comparison to other class I molecules (90). HLA-G dimers are formed due to extra cysteines in the α1 and α2 domains (91). To date, 7 isoforms of HLA-G have been reported, of these, several variants have truncated extracellular domains (42). In addition, free heavy chains have been observed, and they bind different NK receptors (92). HLA-G has a restricted tissue distribution. Under normal

conditions, it is only found in medullary thymic epithelial cells and in the cornea (93, 94). During pregnancy, several HLA-G variants are expressed on extravillous trophoblasts, the fetal cells invading the maternal decidua (95). The presence of HLA-G is believed to inhibit maternal NK cytotoxicity and thereby permit the development of the embryo. However, abnormal expression of HLA-G is an indicator for disease. For example, reduction of HLA-G level on the trophoblast is linked with pregnancy disorders such as miscarriage and pre-eclampsia (42). Upregulation of membrane bound and soluble HLA-G are frequently detected in cancer patients and people diagnosed with autoimmune diseases or infection (42).

In comparison to conventional MHC-I molecules, human hemochromatosis protein (HFE) has a similar structure but a distinctly different function. HFE was initially discovered in 1996 and was named as HLA-H (96). Later, it was renamed as heredity hemochromatosis (HH) and was finally defined as HFE, to distinguish it from the HLA pseudogene HLA-H. This gene is one megabase (Mb) away from the telomeric end of the classical HLA-A gene region (Fig 1-2a). An aberrant HFE gene, due to a mutation at position 282, results in an iron metabolic disorder, known as hemochromatosis (96). The primary amino acid sequence of HFE compared to HLA is quite distinct, but it shows a similar MHC-I structure that has a heavy α chain non-covalently associated with β_2m (97). However, the α1 and α2 domains are not polymorphic and the resulting peptide binding groove is narrow, which does not accommodate for any peptide (97). Rather than antigen presentation, HFE interacts with an iron transporter to maintain iron metabolism (98).

1.4. NK receptor systems

To identify and respond to various stimuli, NK cells express several unique and diverse germline encoded receptor systems. The majority of these receptors are structurally classified into two superfamilies: the C-type lectin like family and the Immunoglobulin (Ig) Superfamily (IgSF). These receptors have their specific

ligands. In some cases, one ligand is recognized by several NK receptors. Each NK cell can express a distinct subset of receptors and each individual has their own repertoire of NK receptors.

1.4.1. Human NK receptors

Genes encoding IgSF is known as Leukocyte Receptor Complex (LRC), while the gene cluster encoding C-type lectin like are located on a different chromosome, called the Natural Killer Complex (NKC) (Fig 1-4a).

Members of the IgSF are type I transmembrane proteins. They are commonly referred to as "paired receptors" since these receptors have highly homologous extracellular domains but contain distinct transmembrane segments and cytoplasmic tails, transmitting either activating or inhibitory signals. The IgSF receptors expressed in humans are the Leukocyte Ig-like Receptors (LILRs) and the Killer cell Ig-like Receptors (KIRs). The LILR family is comprised of a group of immunoreceptors expressed on the surface of lymphoid and myeloid cells (99, 100). KIRs are polygenic and polymorphic and are predominately expressed on NK cells and a subset of T cells. These diverse proteins have been classified according to the number of extracellular Ig domains, cytoplasmic tail length and sequence similarity (101). More details of LILR and KIR will be described in *section 1.5*.

The receptors of the C-type lectin like families exhibit distinct structures as shown in Fig 1-4b. However, similar to IgSF receptors, C-type lectin like receptors either trigger activating or inhibitory signals upon engagement with self ligands. For example, CD94/NKG2A is a hetrodimer of CD94 with NKG2A with limited polymorphism. It inhibits NK activation through interaction with a non-classical MHC-I molecule, HLA-E.
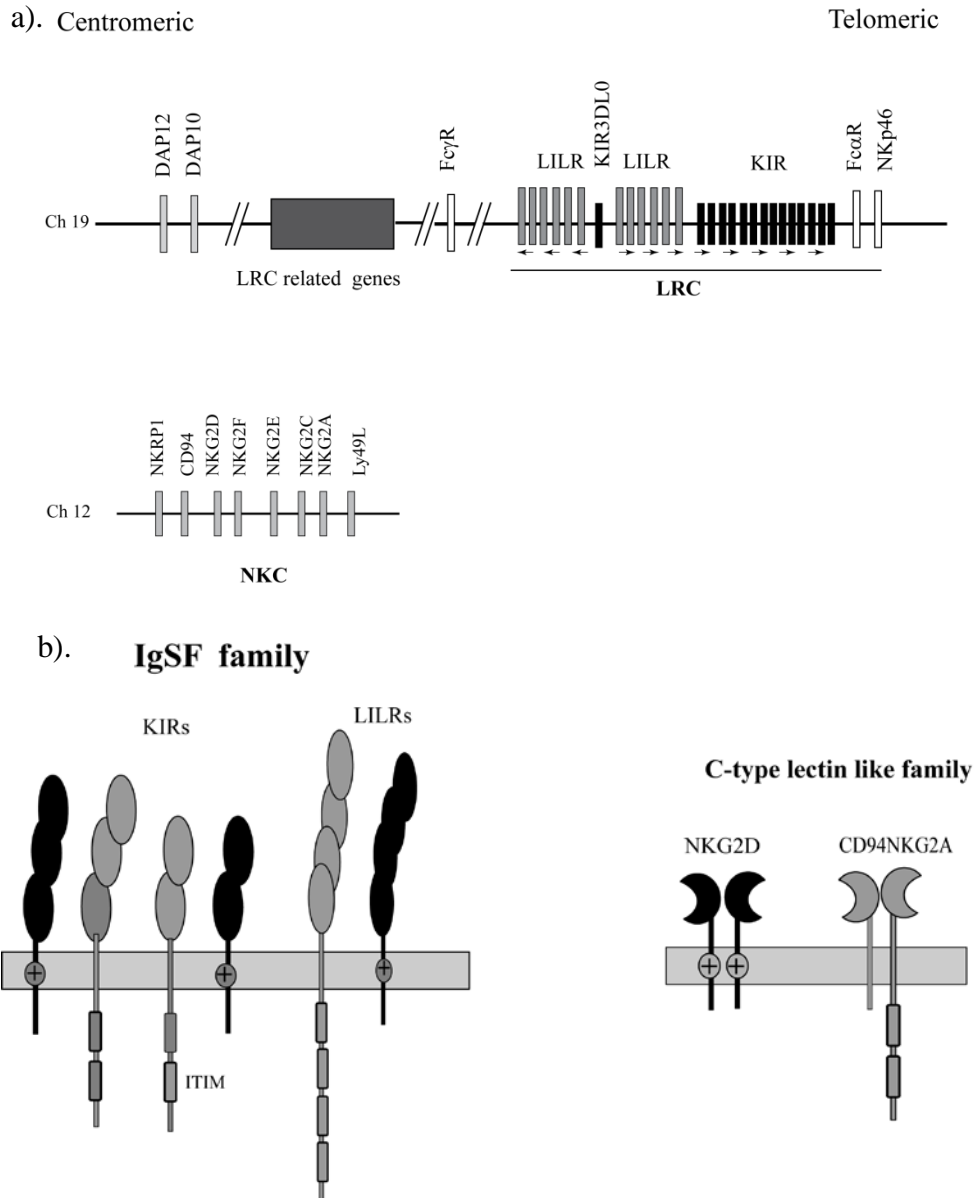
Fig 1-4. Genomic organization of genes encoding NK receptors and illustration of diverse receptors.

a) The gene distribution of the LRC and NKC on human chromosomes 19 and 12. The maps are not to scale. *Adapted from Trowsdale, J: Genetic and Functional Relationships between MHC and NK Receptor Genes. Immunity, 2001, 15: 363-374.* *b)* Illustration of selected members of the IgSF and C-type lectin like superfamilies. Activating receptors are in black and inhibitory receptors are in grey.

20

1.4.2. Receptors that regulate NK function

NK receptors are functionally grouped into either activating or inhibitory categories. Each family has activating and inhibitory receptors depending on their transmembrane regions and cytoplasmic tails as shown in Fig 1-4b. As described in section 1.2.4, activating receptors interact with induced self or non-self antigens to transmit activating signals, while inhibitory receptors bind self MHC-I molecules to deliver inhibitory signals. The interplay of these two signals regulates NK activities.

1.4.2.1. NK activating receptors and their signaling pathway

Although the main focus of this thesis is an inhibitory receptor, it is important to put the inhibitory signaling in the context of how NK cells are activated. A few important activating receptors were described briefly in sections 1.1 and 1.2, including CD16 (Fc receptor for ADCC mentioned in *section 1.1.1*), NKG2D and the NCRs (*section 1.2.3*). Although they have different structures as shown in Fig 1-4, these receptors have a common feature in that they contain short cytoplasmic tails. These tails do not contain any sequence motifs typically required for the activation of signaling cascades. Instead, they have a positively charged amino acid in the transmembrane region which associates with negatively charged residues of adaptor molecules such as DAP10, DAP12, CD3 and Fc receptor γ chain (FcεRIγ) that transmit activating signals (8) (Fig 1-5). These adaptor moleculess bear immunoreceptor tyrosine-based activation motifs (ITAMs). The consensus sequence of an ITAM is $(D/E)xxYxx(L/I)_{X6-8}Yxx(L/I)$ with the exception of DAP10, which is YxxM. In the sequence, x denotes any amino acid, and two YxxL/I sequences are separated by any 6-8 amino acids.

Interaction of activating receptors with their ligands permits membrane proximal src-family tyrosine kinases (SFKs) such as Lck to phosphorylate tyrosine residues in ITAMs. Subsequentially, the phosphorylated ITAMs recruit tyrosine kinases, Syk and ZAP70. The recruitments then initiate a cascade of

downstream signaling pathways including a number of key signaling molecules as illustrated in Fig 1-6. Ultimately, this leads to NK effector functions including cytotoxicity and/or cytokine secretion.

Fig 1-6 shows multiple activating cascades by one activating receptor. The actual activating system is much more complex than the figure depicts in that different activating receptors deliver distinct and sometimes similar signaling pathways. Aside from classical activating receptors, adhesion molecules also contribute to initiation of activation signaling. For example, lymphocyte function-associate antigen-1 (LFA-1) dependent cytotoxicity was shown when its ligand, intercellular adhesion molecule (ICAM), was present, and LFA-1 was found to control lytic granule polarization (102).

1.4.2.2. The mechanism of inhibition

The hallmark of inhibitory receptors is an immunoreceptor tyrosine-based inhibitory motif (ITIM) sequence in their long cytoplasmic tails (Fig 1-7). The ITIM consensus sequence is (I/L/V)xYxx (L/V) (103). Engagement of self-MHC-I by inhibitory receptors permits phosphorylation of the tyrosine residues in the ITIM by kinases, such as SFK (104, 105), as described in section 1.4.2.1.

The inhibitory function is primarily dependent on tyrosine phosphatases, SHP-1 and SHP-2, which contain two Src homology 2 (SH2) domains at the N-terminus and a tyrosine phosphatase domain at the C-terminal end. Under normal circumstances, the catalytic domain is blocked and the phosphatase is inactive. Engagement of phosphorylated tyrosines by the SH2 domains leads to exposure of the enzymatic site, allowing for the subsequent events (Fig 1-7). The observation that overexpressing a catalyticaly inactive SHP-1 mutant caused elimination of inhibition (103) suggests a vital role for the enzymatic domain in negative signaling. In the case of NK cells, both SHP-1 and SHP-2 (106) molecules have been reported to dephosphorylate phosphoproteins in the close proximity of SHP-

1 or SHP-2, such as Vav1 (107), and also to prevent downstream signaling events that occur in the activating pathway in direct and indirect manners (108, 109).
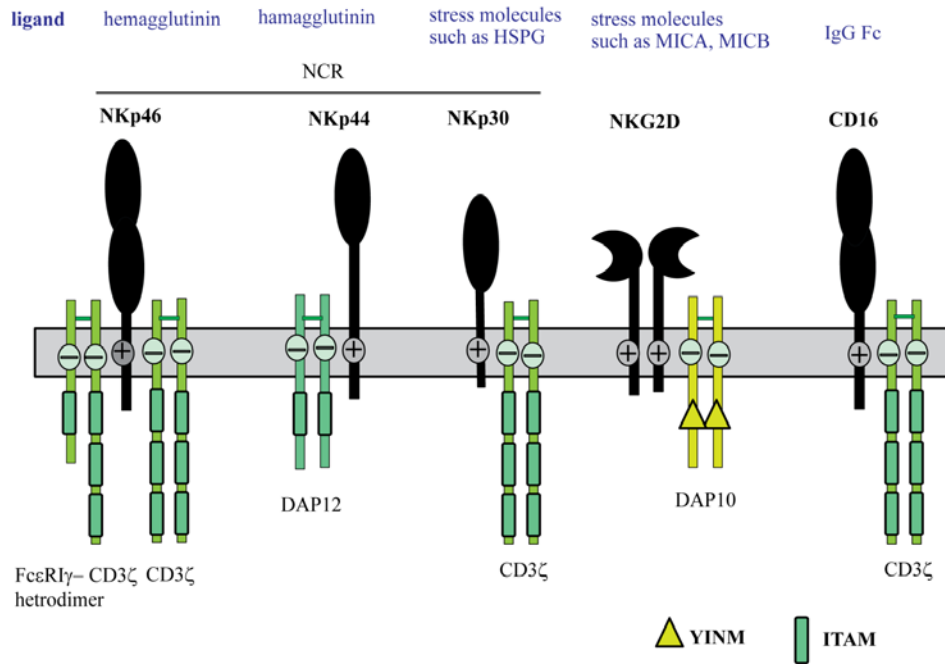
Fig 1-5. Illustration of selected activating receptors on human NK cells.

The five activating receptors described in chapter 1 and their associations with corresponding adaptor molecules are shown. The ligands are indicated in blue.
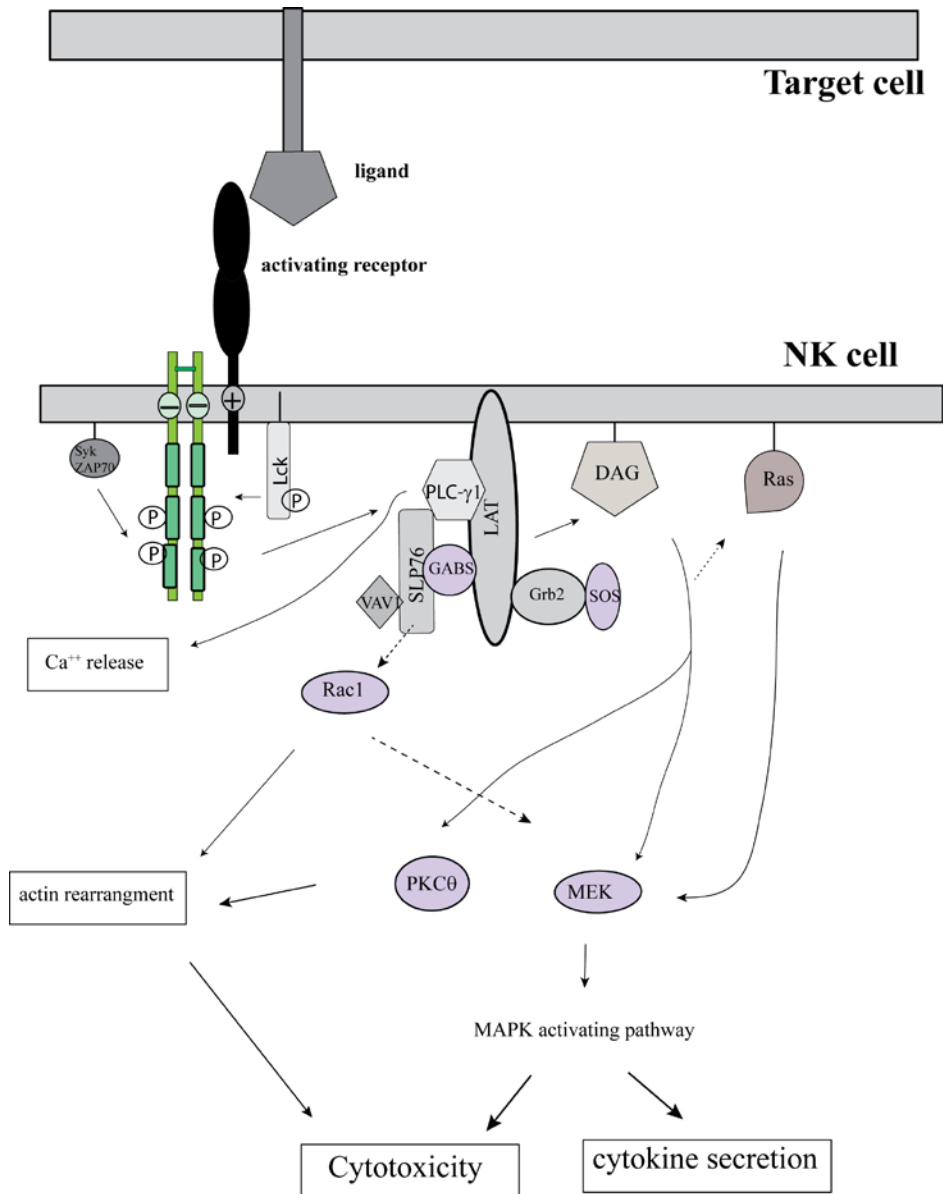
Fig 1-6. Illustration of NK activating pathways

Engagement of an activating receptor with a ligand triggers the phosphorylation of tyrosines in ITAM motifs of the associated adaptor molecules by membrane proximal kinases, such as Lck. The phosphorylated ITAMs then allow for the recruitment of Syk and ZAP70, initiating a cascade of downstream signaling. Some of the key molecules and downstream events are shown.
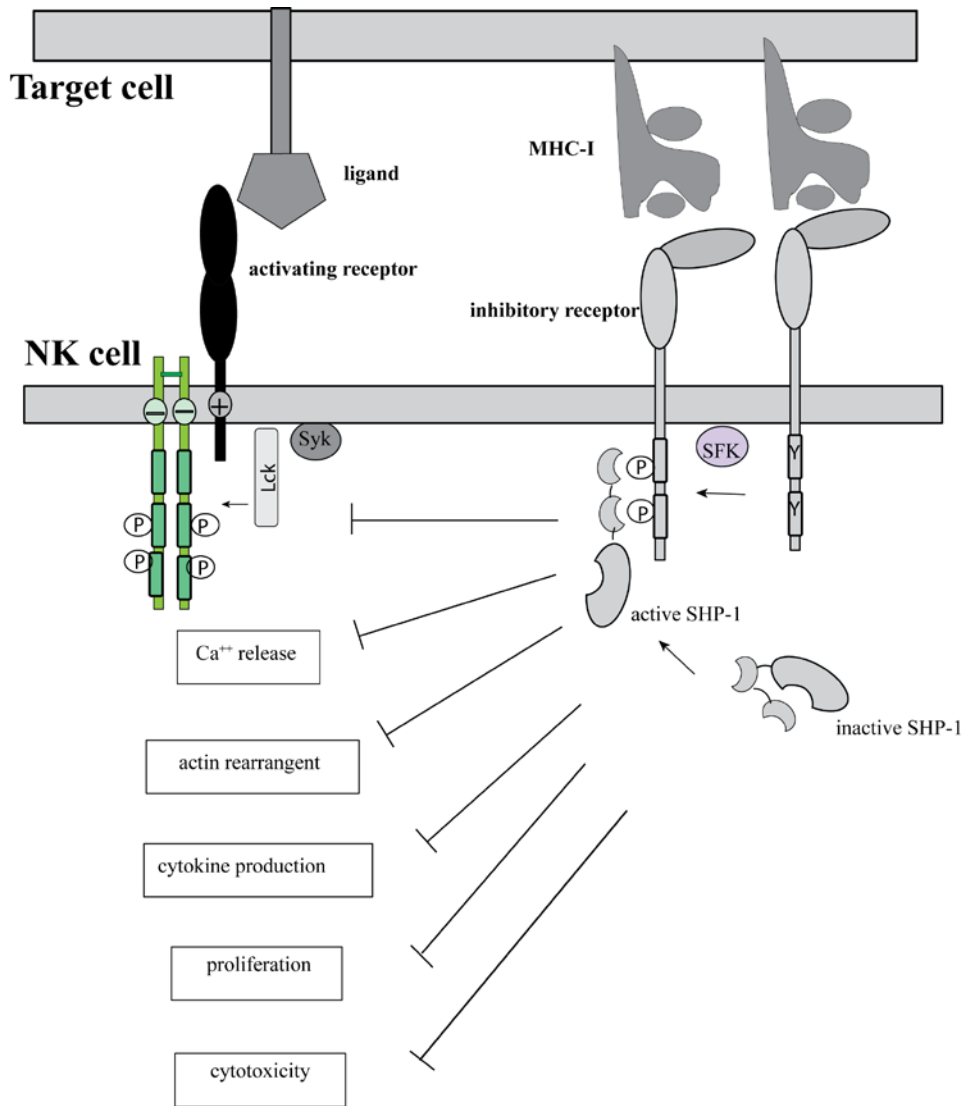
Fig 1-7. Schematic of the mechanism of KIR mediated inhibition.

Engagement of KIR by MHC-I leads to the phosphorylation of the ITIMs by membrane proximal kinase, SFK. Subsequently, the binding of phosphorylated tyrosines in ITIMs by SHP-1 yields the conformational change of SHP-1 from an inactive form to an active form. Active SHP-1 then results in the dephosphorylation of kinases in the vicinity and prevents downstream activating signaling cascades.

1.5. KIR and LILR

1.5.1. KIR

In humans, KIRs are expressed on the surface of NK cells and a subset of T cells. To date, there are 17 distinct KIR genes and each gene is highly polymorphic. Their encoded KIR receptors bind specific subsets of MHC class I such as HLA-A, B or C. In addition to humans, KIRs are also present in other mammalian species, such as primates, but with less diversity. In mice, KIR genes are located on chromosome X, but are not expressed by mouse NK cells. These cells have the Ly49 family of C-type lectin receptors as a functional equivalent to the KIRs.

As KIR is the focus of my research, I will provide details of this receptor family including KIR nomenclature, diversity, evolution, ligand specificity and the specific receptor studied in this thesis.

1.5.1.1. KIR nomenclature

KIR genes and alleles are named by the KIR Nomenclature Committee (110). Based on the number of Ig domains encoded, the KIR genes are named as 2D or 3D. Fig 1-8 demonstrates an example of how to describe a KIR allele. In brief, "D" refers to the extracellular Ig domains, and the first digit before D indicates the number of Ig domains. "L" or "S" refers to the length of the cytoplasmic tail as "long" or "short", generally indicating inhibiting or activating. "P" denotes pseudogenes. KIR alleles are named similarly to HLA alleles. In brief, the first three digits refer to the non-synonymous changes. The next two digits represent synonymous differences within exons, and the last two digits suggest variations in introns, promoters or other non-coding regions. Table 1-4 shows the KIR family members identified to date in humans. Fig 1-9 illustrates the classification and structures of the typical members. In general, the long tailed KIRs are inhibitory KIRs, whereas short tail KIRs exert activating functions. The

exception is KIR2DL4. KIR2DL4 has an ITIM motif and a charged residue at the transmembrane region that associates with an ITAM contained adaptor molecule, FcεRI γ chain (111) (Fig 1-9). Therefore, KIR2DL4 has the potential for both inhibitory or activating functions (112, 113).

first 3DL protein
described

3DL1 * 005 02 02

numbers of
Ig domain

domain

short or long tail

non-synony-
mous changes

synonymous
changes in
exons

changes in
non-coding regions
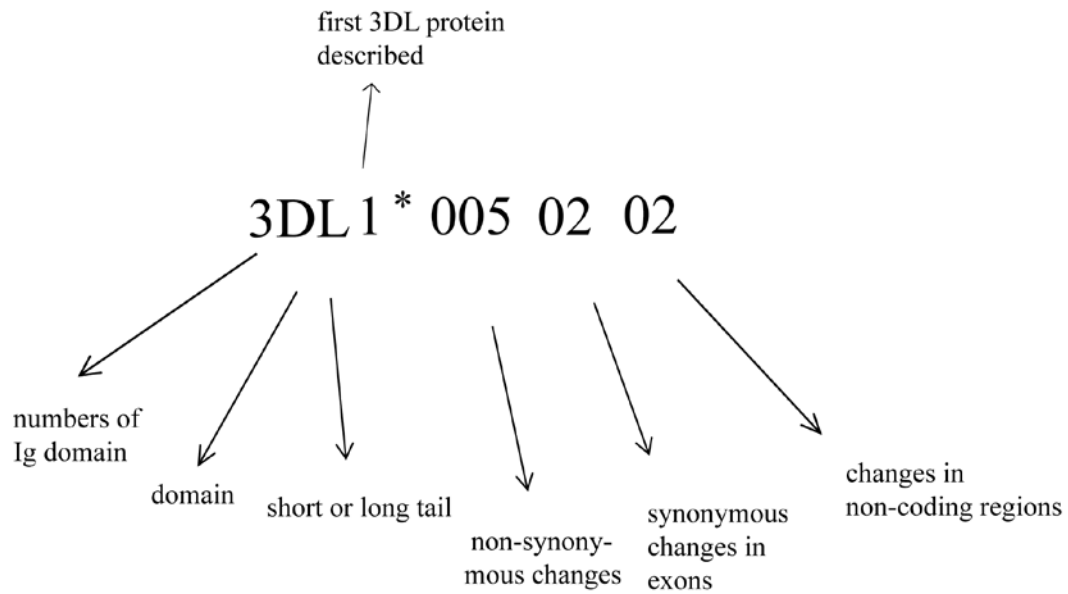
Fig 1-8. KIR nomenclature.

The illustration explains the various elements for an example of naming a KIR allele.

Table 1-4. Members of the KIR Family

KIR Genes/Alleles	Ligand	Function
2DL1	HLA-C2	Inhibition
2DL2	HLA-C1	Inhibition
2DL3	HLA-C1	Inhibition
2DL4	HLA-G	Activation
2DL5A	HLA-A11, and some C	Inhibition
2DL5B	N/A	Inhibition
2DS1	HLA-C2	Activation
2DS2	HLA-C1	Activation
2DS3	HLA-C2	Activation
2DS4	HLA-C, A11	Activation
2DS5	N/A	Activation
3DL1	Subset of HLA-A and B carrying Bw4 epitiope	Inhibition
3DL2	HLA-A	Inhibition
3DL3	N/A	Inhibition
3DS1	N/A	Activation
2DP1	N/A	N/A
3DP1	N/A	N/A
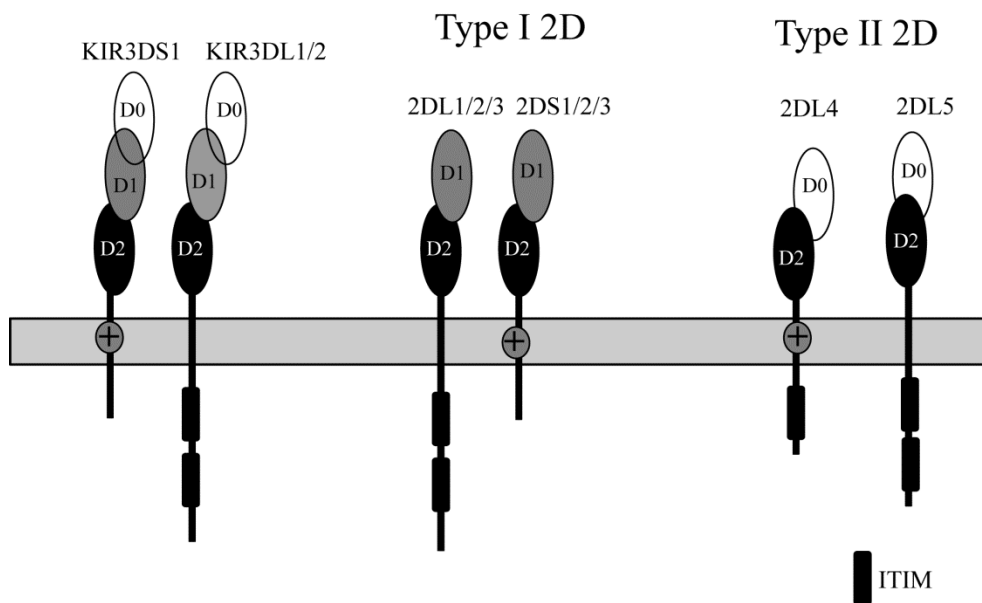
Fig 1-9. Illustration of human KIR proteins.

Paired KIRs are shown with either long or short tails. KIR2D are type I or type II based on the relationship of the extracellular Ig domains.
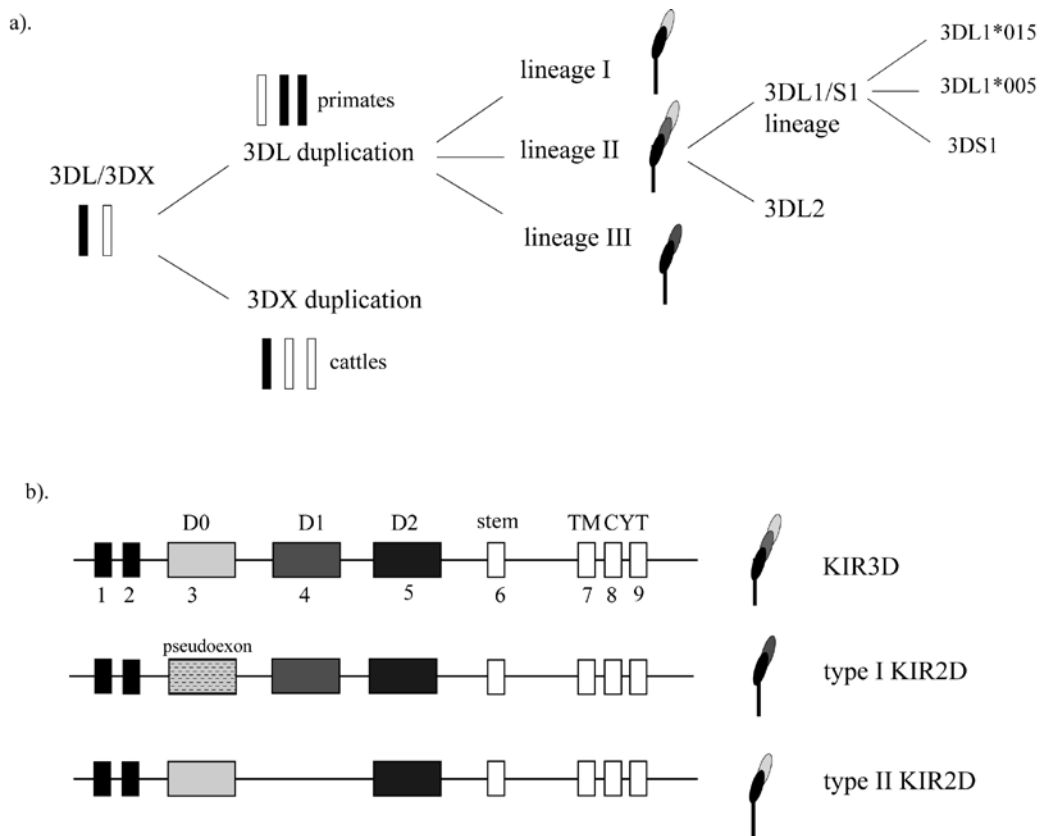
Fig 1-10. Evolution of 3DL/3DX

a) Illustration of KIR3DL/3DX expansion in non-primates and primates.

b) Genetic organization of KIR2D and KIR3D in human. Exons are shown in boxes as indicated.

1.5.1.2. KIR evolution

In humans, the diverse KIRs are grouped into three types (KIR3D, type I KIR2D and type II KIR2D) based on the number and type of extracellular Ig domains (Fig 1-9). Since KIR2Ds were identified first and their Ig domains were named as D1 and D2, the first Ig domain of KIR3D was then denoted as D0. Based on the contents of the Ig domains, KIR2D is divided into type I and II as illustrated in Fig 1-9. Type I KIR2D possess D1 and D2 domains, whereas type II have D0 and D2. In humans, type I includes KIR2DL1, KIR2DL2 and KIR2DL3, which recognize HLA-C molecules, and type II contains KIR2DL4 and KIR2DL5, which interact with non-classical MHC-I, such as HLA-G. Members of KIR3D contain three Ig domains (D0, D1 and D2 from membrane distal to proximal) as shown in Fig 1-9. Individual members of KIR3D have distinct ligands. For instance, KIR3DL1 recognizes HLA-A and B molecules carrying the Bw4 motif, while KIR3DL2 binds subsets of HLA-A molecules (114, 115).

The origin of human KIR is traced back to 135 million years ago when one of two ancient forms, 3DL and 3DX, diverged from a common ancestor before the diversification of modern placental mammals (116). Fig 1-10a illustrates the expansion of KIR families in non-primates and primates. 3DX diversified in non-primates, such as cattle, where 3DL remained as a single copy. Conversely, 3DL expanded in the primate/human lineage, while 3DX is maintained in the genome but is non-functional. The expansion of 3DL emerged approximately 31-44 million years ago when simian primates evolved (117, 118).

Comparative genetic studies in human KIRs reveal some information about the 3DL expansion. The genomic 3D gene is comprised of nine exons, as indicated in Figure 1-10b. Of note, exon 3, 4 and 5 encode extracellular Ig domains, D0, D1 and D2, respectively. Deletion of a region including exon 4 permitted the appearance of type II 2D that have homologous D0 and D2.

Replacement of exon 3 with a pseudoexon resulted in the emergence of type I 2D (D1 and D2) (101).

Three KIR lineages were defined during the course of studying the development of 3DL expansion. Human type I, II 2D and 3D belong to lineage III, I, and II, respectively (101) as shown in Fig 1-10a. Given the fact that 3D emerged prior to 2D and that high homology is shared by 3D and 2D, there is agreement that the 2D KIRs (lineage I and III) evolved from the 3D KIRs (lineage II). Individual lineages then further diversified as the result of gene duplications and deletions such as the KIR3DL/S1 lineage as shown in Fig 1-10a.

Comparison of genomic 3DL genes between other primates and humans show that 3D KIRs are present in all primates, while 2D KIRs appear only in some primates and correspond to the emergence of HLA-C (119). These studies reveal the co-evolutionary progression of KIR with MHC-I. Thus, KIR receptors are likely so diverse in order to keep up with their extremely polymorphic and rapidly evolving ligand, MHC-I.

1.5.1.3. KIR diversity

In humans, KIR genes are clustered in a 150 kilobase (kb) region with the LRC on the long arm of chromosome 19 (Fig 1-4a). Thus far, 17 unique KIR genes have been reported (45) (Table 1-4). These genes are arranged head to tail approximately 2 kb apart in continuous sequence in the direction of centromeric to telomeric (120) (Fig 1-4a). The intergenic regions are highly homologous to each other.

The distribution of KIR genes within populations is complicated for two reasons. First, the diversity of the number and type of genes present in the genome (haplotypic diversity), and second, the variation in DNA sequence in individual genes (allelic polymorphism) (121).

More than 50 different haplotypes have been reported thus far. This number is likely an underestimate as only a small number of groups were studied relative to the entire human population. The diverse haplotypes are likely generated by gene duplication, deletion, uneven recombination and reciprocal recombination (101). Based on gene content, most of the common haplotypes are conventionally divided into two groups, group A and group B. Despite the distinct gene content, these two groups have four fixed genes that are known as "framework" genes. They are KIR3DL3, KIR3DP1, KIR2DL4 and KIR3DL2. The KIR gene cluster is segregated from other gene families by two of these genes, KIR3DL3 and KIR3DL2. Within the 150 kb region, KIR3DL3 and KIR3DP1 form the frame for the centromeric region, whereas KIR2DL4 and KIR3DL2 mark the boundary of the telomeric region (Fig 1-11a). Most of the variations are within the centromeric and telomeric regions (122). For example, new sets of genes can be generated by means of reciprocal recombination occurring between KIR2DL4 and KIR3DP1 (Fig 1-11b). Non-reciprocal recombination outside the region of KIR3DP1-KIR2DL4 generated several unusual haplotypes including truncated haplotypes with frame shift deletions of some framework genes (123) as well as longer haplotypes containing duplicated genes (118, 124). Therefore, some of the resulting haplotypes are hard to place into the A or B group.

In addition to the framework genes, group A haplotypes have up to four additional genes, and two pseudogenes (Fig 1-11a). In group A haplotypes, the majority are inhibitory KIRs with one activating gene, KIR2DS4. Conversely, group B haplotypes have more genes encoding activating KIRs (125-127) (Fig 1-11a). Studies of populations from different geographic regions suggest that inhibitory KIRs are always present in A and B haplotypes, but the number of activating KIRs can vary a lot with higher frequency in B haplotypes. Although group A has a limited number of genes, the individual genes are polymorphic. Conversely, the genes specific to group B are less diverse but the organization of specific genes varies (128).

35

KIR gene polymorphism is second only to the MHC locus in terms of diversity in the human population. New alleles are generated due to point mutations and non-homologous recombination between intergenic regions (101). The recombination of one KIR gene with other KIR genes creates pairs of KIR containing highly similar extracellular domains but different signaling tails, such as KIR3DL1 and KIR3DS1. Another example of how recombination builds new KIR genes is KIR2DL2. KIR2DL2 is the hybrid product of the centromeric region of KIR2DL3 with the telomeric region of KIR2DL1. KIR2DL2 and KIR2DL3 are never found on the same haplotype and are now considered as alleles of the same locus, although they were first thought to be distinct genes (101). The allelic variation allows KIR haplotypes that are identical by gene content to be significantly different. Importantly, allelic polymorphism influences ligand recognition and alter the surface expression, which will be further described in section 1.5.1.7.

Collectively, the distribution of KIR genes in the entire human population is complicated by the results of haplotypic diversity, allelic variation and the inheritance of parental haplotypes (homozygous AA, heterozygous AB and homozygous BB). Therefore, there are barely any identical KIR genotypes between unrelated individuals across populations. The frequencies of the KIR genotypes are remarkably different though the distribution of group A/B haplotypes is relatively equal.
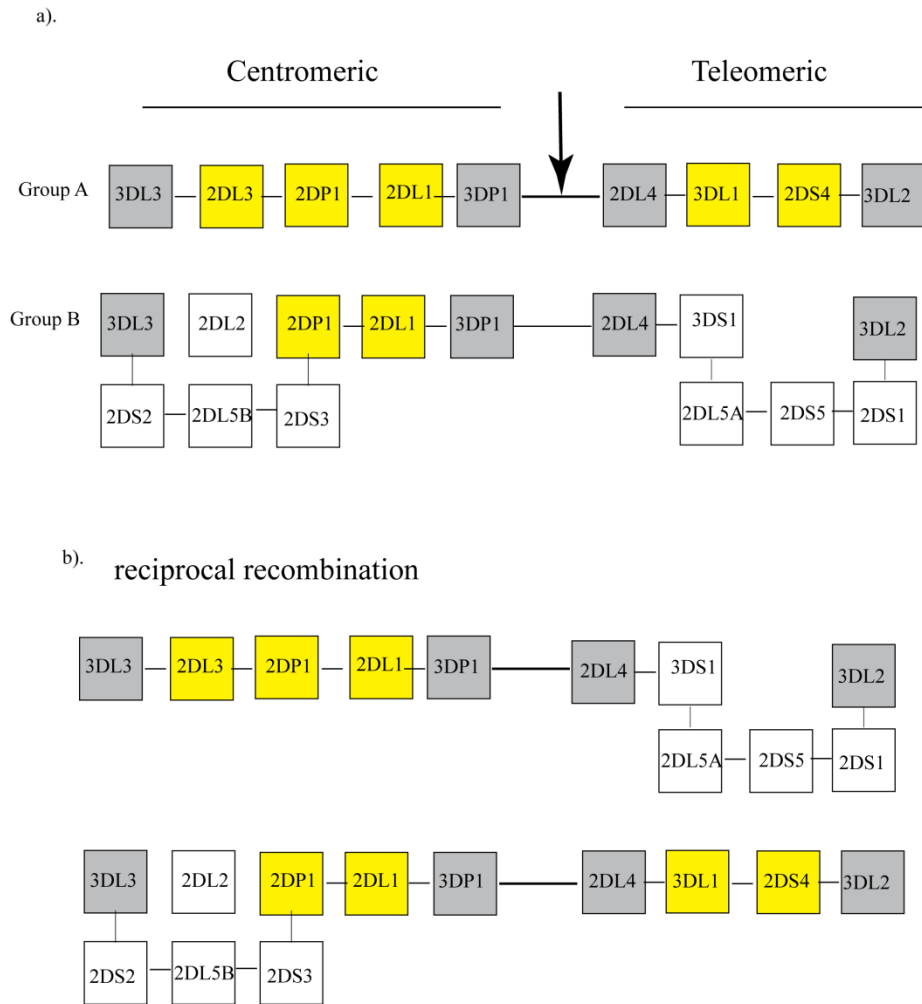
Fig 1-11. Organization of the human KIR locus.

a) Gene distributions in haplotype A and B are shown. Framework genes are shown in grey. Genes specific to A haplotypes are shown in yellow. *b)* An example of reciprocal recombination of KIR genes inherited from parents who have a genetic background as shown in *a)*. Recombination occurs between KIR3DP1 and KIR2DL4.

37

1.5.1.4. The regulation of variegated KIR expression on NK cells

Of all the studied KIR genes, the central framework gene, KIR2DL4, is the only gene expressed by every NK cell (129). The other KIRs are expressed "clonally" as described below. KIR genes are randomly expressed during NK cell development such that an individual NK cell expresses only a subset of KIR receptors encoded within their genome (101). Moreover, the presence of a given gene in the genome does not guarantee expression on the surface (130, 131). Between individuals, the frequency and level of expression of a given KIR gene varies and is controlled by elements in the promoter regions that are themselves polymorphic (113, 131). Collectively, NK cells express a pool of various KIR combinations, also known as the KIR repertoire. Individuals differ in the KIR repertoire unless they are identical twins. Once KIRs are developmentally turned on, the pattern of expression is stably maintained in individuals throughout life (123, 132, 133).

The mechanism of controlling variegated KIR expression has not been fully elucidated. However, research data have shown that KIR expression is regulated at the epigenetic and genetic level (134-136). Methylation is a typical epigenetic method of regulating KIR transcription as it causes inaccessibility of the promoter region (134, 136). It is proposed that KIR genes are epigenetically silenced by DNA methylation in early hematopoietic development (137). Demethylation occurs at the late stage and permits access to the open promoter, resulting in initiation of transcription (138). Subsequently, gene transcription is initiated by the proximal bidirectional promoter, which is present upstream of the coding region of the gene (135) as well as the more distal promoter. If the reverse transcription is strong, it leads to silencing of the distal promoter which normally takes over all transcription for the KIR gene in mature NK cells (139).

Additionally, expression of the KIR genes is also influenced by the presence of their specific MHC-I ligands. Providing evidence for this is the observation that

similar KIR surface phenotypes are observed only between KIR and HLA identical siblings (123). Studies of KIR distribution in populations from different geographic regions show that a high frequency of activating KIR alleles occurs when there is a lack of corresponding specific MHC-I (140). In contrast, an enhanced frequency of inhibitory KIRs appears when their specific MHC-I ligands are present (122).

1.5.1.5. KIRs and disease

Comparative studies across populations and species suggest that the rapid expansion of KIR genes is driven by survival from diseases and infections (119). Additionally, more and more evidence suggests the association of various KIR genotypes with diseases. In comparison to KIR alone, combinations of KIR alleles and MHC-I alleles are more strongly associated with susceptibility to disease and resistance to infection, though these two gene clusters are located on different chromosomes (chromosome 19 and 6, respectively) (43, 141).

Some paired KIR receptors recognize similar subsets of MHC-I ligands as shown in Table 1-4, but generally the inhibitory receptors have higher affinity than the activating receptors (142, 143). Therefore, KIRs could act as either inhibitory or activating during the development of diseases. Table 1-5 demonstrates some examples of the genetic linkages of KIR-MHC-I combinations with reported diseases including viral infection, autoimmune disease, cancer and pregnancy related disorders. In addition to associations with allelic variation, KIR haplotypes have also been linked to disease susceptibility. For example, women who are homozygous for the A haplotype are prone to preeclampsia (Table 1-5).

Despite the strong genetic correlations, the molecular basis and functional relationships of KIR-HLA with the related diseases are not yet clearly understood. Moreover, the stochastic expression pattern of KIR on NK cells adds more complexity to the task of investigating and understanding the mechanism of KIR

and HLA in disease. Nonetheless, all the published evidence suggests that higher affinity interactions triggering more inhibition is detrimental for pregnancy while weaker binding and thus less inhibition is beneficial for the clearance of viral infection (with the exception of HIV infection) and restriction of tumor growth. Those possessing haplotypes with more activating receptors are more likely prone to developing auto-immune diseases.

Given the clinical importance of inhibitory KIRs, I will describe several inhibitory KIR family members in the subsequent text. There will be a particular emphasis on the receptor that is studied in this thesis, KIR3DL1.

Table 1-5.   The association of KIR-HLA genotypes with disease

Disease	Combination of KIR-HLA	Role
HIV infection	KIR3DS1 - HLA-Bw4 (13) KIR3DL1-HLA-Bw4 (12)	Protection
HCV infection	KIR2DL3/HLA-C1 (11)	Protection
Psoriasis	KIR2DS1/HLA-Cw6	Promotion
Type I Diabetes	KIR2DS2/ HLA-C1 (144)	Promotion
Pre-eclampsia	KIR2DL1/HLA-C2 (145) Haplotype AA/HLA-C2 (146)	Promotion Promotion
Hepatocellular carcinoma	KIR3DS1/HLA-Bw4 (10, 11)	Protection
Cervical neoplasia	KIR2DL1/HLA-C2 (147)	Protection

1.5.1.6. Inhibitory KIR2D

As shown in Figure 1-9, inhibitory KIR2D members are grouped into two types, type I and type II. Here, I will only discuss the well studied type I members. The inhibitory type I 2D family consists of three members: KIR2DL1, KIR2DL2 and KIR2DL3. They all have extracellular domains D1 and D2 and contain long cytoplasmic tails. Of these receptors, KIR2DL1 is the most extensively studied dating back to the 1990's. The KIR2DL1 receptor recognizes HLA-C2 group members, with lysine (K) at position 80, such as HLA-Cw4 and Cw15. The other two members, KIR2DL2 and KIR2DL3, are allelic variants of the same locus. They bind to members of the HLA-C1 group, which have asparagine (N) at position 80, such as HLA-Cw3 and Cw7. In terms of binding affinity, KIR2DL1 has the highest and KIR2DL3 has the lowest for the same ligands (143, 148).

The crystal structure of KIR2DL1 demonstrates that D1 and D2 form a V shape at the interdomain region (149). The structure of the complex of KIR2DL1 with HLA-Cw4 demonstrates that the hinge region of the two Ig domains (D1 and D2) of KIR2DL1 orthogonally interacts with the region of HLA-C at the C-terminal end of the peptide-binding groove. The residues in HLA-C that are involved in the interaction are 77-80 (α1) and 145-151 (α2) (7, 150) (Fig 1-12a). At the binding site, the D1 domain interacts with the α1 domain while the D2 domain binds to the α2 domain. The interaction site overlaps with but is distinct from the site where the TCR binds (7). Mutagenesis studies have proven the critical role of methionine (M) at position 44 of KIR2DL1 (143) and lysine (K) at position 80 of HLA-Cw4 (151) in this interaction. In addition, the amino acids at position 7 and 8 of bound peptides contribute to the sensitivity of binding (149, 152).

KIR2DL2 has a similar overall binding mode as KIR2DL1 when interacting with HLA-Cw3, but with a weaker affinity (143). The amino acid difference at position 44 in the contact site along with other residue variations change the

interaction forces from electrostatic (KIR2DL1-Cw4) to hydrogen bonds (KIR2DL2-Cw3) and therefore alter the specificity (149). Interestingly, the KIR2DL1-Cw4 complex also formed a crystallographic dimer (149). In this dimer structure, two HLA-Cw4 molecules are connected by the interaction of α1 and $β_2$m, perhaps resulting in the facilitation of KIR clustering under normal conditions, though neighboring KIR2DL1 molecules do not contact each other (149) (Fig 1-12b). On the other hand, KIR2DL1 has a zinc binding motif with the consensus sequence HExxH. This sequence is able to drive dimerization of KIR2DL1 *in vitro* and enhances KIR avidity and signaling (153, 154).

There are a total of 43 alleles and 24 protein variants of KIR2DL1 according to the KIR Immuno Polymorphism Database (IPD-KIR database last dated 2013). Although all of the reported polymorphisms are found outside the contact regions, the polymorphisms have been shown to affect KIR2DL1 recognition (155).
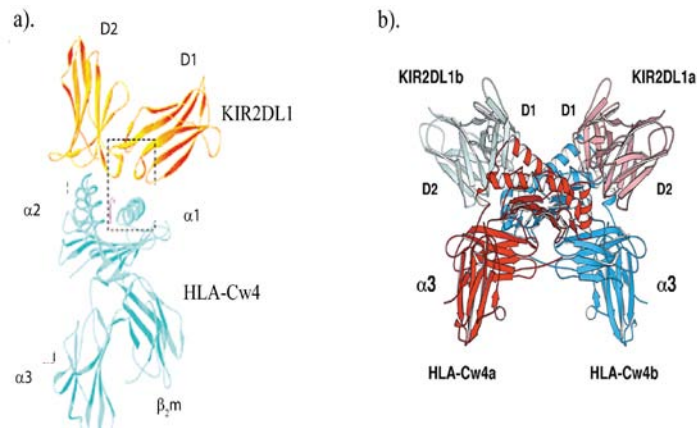
Fig 1-12. Crystal structure of HLA-C with KIR2DL1.

a). The ribbon diagram of the crystal structure of KIR2DL1 interacting with HLA-Cw4 (*149*). *b).* The ribbon diagram of a crystallographic dimer of KIR2DL1-HLA-Cw4 complex (*149*). Two KIR2DL1 molecules are shown in pink (KIR2DL1a) and gray (KIR2DL1b), and two HLA-Cw4 molecules are indicated in red (HLA-Cw4a) and blue (HLA-Cw4b). In this dimer structure, KIR2DL1a (pink) binds to HLA-Cw4a (red) to form one complex, while KIR2DL1b (gray) interacts with HLA-Cw4b (blue) to form the other complex.

1.5.1.7. KIR3DL1

KIR3DL1, the focus of this thesis, is of particular interest due to its genetic association with HIV infection and progression to Acquired Immunodeficiency Syndrome (AIDS) (12, 156). It is also of interest because it is highly polymorphic and there are numerous unknown aspects of how it functions.

Structurally, KIR3DL1 has three extracellular Ig domains (D0, D1 and D2) with a long cytoplasmic tail that contains two ITIMs to recruit phosphatases SHP-1 or SHP-2, which deliver an inhibitory signal. KIR3DL1 recognizes HLA molecules carrying the Bw4 epitope. Genetic combinations of KIR3DL1 and HLA-Bw4 appear to have a protective implication in decelerating progression to AIDS and reducing the risk of HIV exposure in an uninfected population (12, 156). Recently, a second critical role of inhibitory receptors such as KIR3DL1 has been described. During NK development, self-MHC-I recognition in mouse NK cells confers functional competence to be triggered by activating receptors, a process termed licensing (157), which is similar to positive selection in T cell development. Human NK cells are also subjected to this process such that NK cells expressing KIR3DL1 with HLA-Bw4 background are more responsive than those having HLA-Bw6 background (158), indicating the role of KIR3DL1 in maturation during NK development.

1.5.1.7.1. KIR3DL1 polymorphism

KIR3DL1 is the most diverse member in the KIR family likely due to the need to rapidly co-evolve with the extremely diverse HLA-B molecules. 73 alleles and 58 protein variants have been reported thus far for KIR3DL1 (45). Global genetic studies of distinct ethnic groups suggest that most of the naturally occurring KIR3DL1 subtypes diversified from two sources: *015 lineage and *005 lineage (159) (Fig 1-10). The extraordinary diversity of KIR and HLA influences KIR3DL1 expression, ligand recognition and function. The influence

of polymorphism on expression frequency, binding affinity and inhibition capacity is shown in Table 1-6.

Flow cytometric analysis of human NK cells using a KIR3DL1 specific antibody, DX9, revealed that KIR3DL1 subtypes are expressed at different levels (high, low or null) on the cell surface (160). This phenomenon is due, in part, to variations in the extracellular domains (161). The representative alleles for high, low and null are *015, *005 and *004, respectively (160). The poor expression of *004 is due to mutations in the D0 and D1 domains (162), which lead to retention of the protein in the ER (163). However, this allele is strongly linked to slow progression to AIDS by an unknown mechanism (12).

KIR3DL1 alleles also exhibit variation in their ability to inhibit NK activity upon encountering the same HLA-B allele (164). Allele *005 is a low density allele, and exerts weak inhibition in comparison to *015, which is a strong inhibitory allele. The functional difference is due to alterations in the D1 and D2 domains that influence affinity and/or expression. Besides the typical alleles derived from the described lineages, there are other variants that cannot fit with this classification, such as *001. Allele *001 is likely the recombinant product of *005 and *015, due to the fact that its D0 domain is homologous to that of *005 and its D1D2 domains are similar to that of *015. The *001 allele is well expressed at the cell surface and provides a strong inhibitory function. The frequencies of KIR3DL1 alleles across populations are varied. The frequencies of prototypical alleles such as *015 and *005 are largely altered in populations from different geographic regions. Conversely, *001 and *004 are present in high frequencies across various populations (159).

As shown in Table 1-7, polymorphisms are found across the entire coding region. Of note, D0 is the most diverse domain in comparison to the other two Ig domains. Polymorphism within the D0 domain not only contributes to ligand interaction, but also influences surface expression (161).

46

Table 1-6. The expression frequency, surface density and inhibition capacity

of different KIR3DL1 alleles

KIR3DL1 Allele	Frequency [a] (%)	Surface Density [b]	Inhibition Capacity [c]
*001	41	High	Strong
*002	24	High	Strong
*003	14	High	ND
*004	31	No	ND
*005	26	Low	Strong
*006	0	Low	ND
*007	11	Low	Low
*008	6	High	ND
*009	4	ND	ND
*015	ND	High	Medium
*020	ND	High	Medium

Note:

(a). The frequency data is adapted from Northern Irish populations (165) and European American data (12).

(b). The surface density is adapted from the literature (122) by DX9 staining.

(c). The inhibition capacity summary is adapted from the literature (122, 164).

The alleles described in Chapter 1 are indicated in red.

Table 1-7. Sequence comparison of KIR3DL1 alleles

		D0					D1		D2			S	TM	CYT	
Position	2	31	44	47	54	86	145	182	238	277	283	312	320	343	373
*001	M	R	R	I	I	S	R	P	G	R	W	S	I	C	E
*002	V	-	-	V	L	-	-	-	R	-	-	-	-	-	-
*003	V	-	-	V	L	-	-	-	-	-	-	C	-	-	-
*004	-	H	G	-	-	L	-	S	-	-	L	-	V	Y	Q
*005	-	-	-	-	-	-	-	S	-	-	L	-	-	-	-
*006	-	-	-	V	L	-	-	-	-	C	L	-	-	-	-
*007	V	-	-	V	L	-	-	-	-	-	-	-	V	-	Q
*008	V	H	-	V	L	-	-	-	-	-	-	-	-	-	-
*015	V	-	-	V	L	-	-	-	-	-	-	-	-	-	-
*020	V	-	-	V	L	-	S	-	-	-	-	-	-	-	-

Note: The alleles described in Chapter 1 are colored red.

1.5.1.7.2. KIR3DL1 ligand recognition

KIR3DL1 recognizes HLA-A and B molecules carrying the Bw4 epitope (160), which includes 20% of HLA-A allotypes and 33% of HLA-B allotypes (164, 166). In most human populations, 50% of HLA haplotypes encode an HLA-A and/or HLA-B allotype carrying the Bw4 epitope (159). Consequently, at least 50% of people have a cognate ligand for KIR3DL1. However, for a given individual, less than 40% of NK cells express the receptor.

KIR3DL1 variants differ in response to the same HLA-Bw4 molecule, and *vice versa*, such that the same KIR3DL1 molecule responds differently to diverse HLA-Bw4 allotypes (71). The Bw4 determinant is located in residues 77-80 of the α1 domain, but variations at position 80 are pivotal for determination of KIR3DL1 binding affinity. Isoleucine at position 80 confers strong affinity, such as in HLA-B*58:01, while threonine at this position provides weak affinity such as in HLA-B*27:05 (71). Aside from diversity within the Bw4 region, polymorphisms outside the Bw4 epitope also affect ligand interaction, particularly a polymorphism found in the α3 domain (167), which will be described in detail below.

1.5.1.7.3. The interaction of KIR3DL1 with ligand

When I started this project, the crystal structure of KIR3DL1 and the complex with its ligand had not been published. At that time, it was only known that the second and third Ig domain (D1 and D2) of KIR3DL1 had approximately 80% identity to the two Ig domains of KIR2DL1, and that these two Ig domains were responsible for binding specificity to HLA-Bw4 in a similar manner as KIR2DL1-HLA-C (168). However, the first Ig domain (D0) of KIR3DL1 was known to also be important for ligand recognition. The D0 domain was shown to be required for proper folding of the protein and ligand interaction using a cell based binding assay with variable combinations of extracellular Ig domains of

KIR3DL1 (169). Mutagenesis studies indicated that the D0 domain acted as an enhancer for ligand interaction, however, the mechanism was not clear (168). Interestingly, combined natural substitutions in the α1 and α3 domains of HLA-Bw4 reduced KIR3DL1 mediated inhibition (167).

1.5.2. Leukocyte Ig-like receptor 1 (LILRB1)

Another type of inhibitory receptor, LILRB1, has been reported to bind MHC-I molecules and influence KIR2D signaling (170, 171). In this thesis, I have examined whether LILRB1 also influences KIR3DL1 signaling. The LILRB1 receptor is discussed in the following sections.

1.5.2.1. General features of LILRB1

LILRB1 is also known as CD85j, Ig-like transcript 2 (ILT2) and LIR-1. It is expressed on various cells derived from myeloid and lymphoid lineages, such as monocytes, dendritic cells, B cells and a subset of NK and T cells (172). In comparison to KIR, LILRB1 is less polymorphic (173). Expression is variable between individuals and is affected by particular cytokines (174). Structurally, the receptor has four extracellular Ig domains named D1, D2, D3 and D4 from membrane distal to proximal, and contains four ITIM motifs in the cytoplasmic tail. Mutagenesis studies demonstrated that the predominant role of the two membrane distal ITIM motifs is recruitment of SHP-1 (175).

Changes in LILRB1 expression are correlated with Human Cytomegalovirus (HCMV) re-activation in transplant patients (176) and polymorphism in LILRB1 has been linked with autoimmune diseases, tumor growth and pregnancy related disorders (177).

1.5.2.2. LILRB1 ligands

LILRB1 recognizes classical (HLA-A, B and C) and non-classic MHC class I molecules (HLA-G) with different affinities. LILRB1 binds HLA-G with the

highest affinity (178). Although it only shares 25% homology with HLA molecules, the HCMV protein, UL18, binds with much higher affinity to LILRB1 than any of the HLA molecules (179). The interaction between LILRB1 with MHC-I can be blocked by LILRB1 specific antibodies (HPF1 and GHI/75) or by an antibody that reacts with all classes of HLA molecules, W6/32 (92, 171, 180).

1.5.2.3. The interaction of LILRB1 with MHC-I

The co-crystal structure of LILRB1-D1D2/HLA-A2 complex demonstrates that the interaction is largely dependent on the two membrane distal Ig domains (D1 and D2) (170). The tip of D1 binds to residues 193-200 of the α3 domain and the hinge region between D1 and D2 interdomain contacts β_2m (Fig 1-13a). LILRB1 has been reported to use a similar mode of interaction to bind UL18 (179, 181). Point mutants analyzed by surface plasmon resonance (SPR) revealed the critical role of a tyrosine (Y) at position 38 of LILRB1-D1 in recognition of UL18 (182). Although the role of the two membrane proximal Ig domains, D3 and D4, remains unclear, the comparison of binding to HLA molecules between the full length ectodomain and D1-D2 revealed that D3 and D4 mainly provide a support stem for the D1 and D2 domains and do not contact ligands (181, 182). LILRB1 is also found to interact with MHC-I on the same cell (*cis* interaction) (183) (Fig 1-13b).
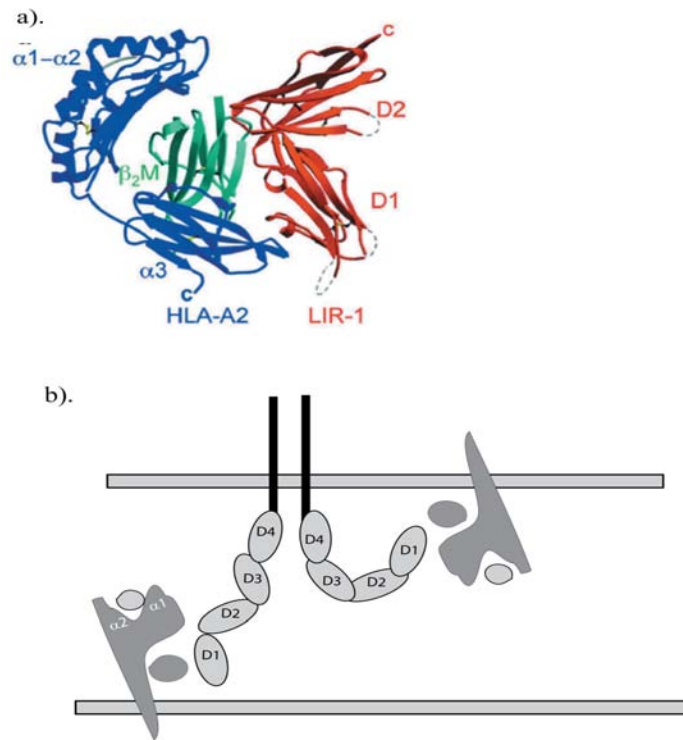
Fig 1-13. LILRB1 interacts with MHC-I in *trans* and *cis*

a). Ribbon diagram of crystal structure of D1D2 of LILRB1 bound to HLA-A2
(*adapted from Willcox B.E. et al, Nature Immunology, 2003, vol 4; 913).*

b) Illustration of LILRB1 interaction of MHC-I in *trans* and *cis* .

1.6. The immunological synapse (IS)

Previously, I have described fundamental mechanisms of how individual NK receptors control effector functions. Given the redundancy of receptors in regulating NK functions, I will now provide basic information of how receptors are involved in the events that occur on the cell surface and how these events occurring on the cell surface influence signaling inside the cells.

The immunological synapse (IS) defines a micrometer sized region formed at the cell surface between two immune cells in close contact. The IS is assembled by organization of surface receptors, adhesion molecules and intracellular signaling proteins in *trans*. The concept was first described in the 1990's at the organized cell-cell contact region between a T cell and an antigen presenting cell (APC), where the T cell receptor (TCR) interacts with MHC-I (184, 185). Subsequent studies have extended the observation and have shown the presence of IS for other types of immune cells, such as NK cells. Given that immune cells are highly motile, synapses that occur between immune cells and potential target cells are transient but dynamic, also called "make and break" synapses (186).

When an NK cell encounters a target cell, a number of events occur sequentially at the interface of the contact. To date, a total of three distinct stages are used to describe the time-dependent activating process in NK cells upon engagement of target cells, including the initial, effector and termination stages. The initial stage involves adhesion of the NK cell to the target cell, through clustering of adhesion molecules and activating receptors, and subsequent initiation of activating signals. Next, the effector stage is characterized by actin polymerization and re-orientation of lytic granules (187, 188). After lytic granules are released, the termination stage begins (188), this includes the detachment of the NK cell from the apoptotic target cell.

At the initial stage, events involved in assembling activating synapses (e.g., adhesion) and initiating activating signals (e.g. recruitment of signal molecules) are regulated by inhibitory receptors. Previously, our lab has shown that accumulation of inhibitory KIR2D (KIR clusters) occurring at the interface with a ligand bearing target cell correlated with inhibition of cytotoxicity and inhibition of adhesion (189, 190). A chimeric KIR2DL1 with an N-terminal EGFP moiety, which had less binding to the same ligands in comparison to KIR2DL1, formed smaller clusters (microclusters) of KIR2DL1 when engaged with HLA-C molecules (189). Consequently, there was less impact on cytotoxicity than adhesion (189, 190). Other studies have demonstrated clusters of KIR associated signaling molecules such as SHP-1 at the synapses (189-191). These clusters were shown to be independent of actin re-organization and ATP-driven cytoskeletal rearrangement (192, 193), but actin polymerization can enhance the process (194). In addition to KIRs, synapses with other inhibitory receptors, such as LILRB1 and NKG2A, have been studied. LILRB1 recognizes classical and non-classical MHC-I with highest affinity for HLA-G. However, visible accumulation of LILRB1 was not detected at the synapse when engaged with HLA-G (195).

In the following section, I will describe the influence of LILRB1 on KIR mediated signaling and how it led to the studies described in this thesis.

1.7. The influence of LILRB1 on KIR signaling

This is little evidence to support the concept that the binding strength of LILRB1 with classical HLA is sufficient to protect target cells from destruction in the absence of another inhibitory receptor. Interestingly, truncated KIR2DL1 that lacks a cytoplasmic tail loses most of its inhibitory function in some cells but not others. The observation of this residual inhibition indicated that other inhibitory receptors may be involved in the interaction (171). Using an NK cell line that co-expresses an ITIM-mutated KIR2DL1 and normal LILRB1, S. Kirwan in our lab showed that the presence of LILRB1 signaling is dependent on the presence of the

mutated KIR2DL1 (171). Given that the interaction of KIR2DL1 with HLA-C allows for the accumulation of HLA-C molecules at the synapse, the proposed model was that the accumulation causes the increased avidity of LILRB1 binding to HLA-C, facilitating LILRB1 signaling.

1.8. Research focus

When I began my studies, the KIR3DL1-D0 domain was known to somehow participate in the KIR3DL1 interaction. However, the mechanism remained unclear. The cognate ligands of KIR3DL1 are also known to bind with LILRB1. Given the known effect of LILRB1 on the KIR2DL1 signaling, my research began to test if LILRB1 either modifies KIR3DL1 signaling via engaging HLA-B molecules carrying the Bw4 motif or if the presence of the D0 domain might prevent such a phenomenon.

Surprisingly, during my initial investigations, I discovered that an anti-MHC-I antibody, W6/32, which was known to block LILRB1 interaction but had no impact on KIR2DL1 recognition, prevented inhibition mediated by KIR3DL1. Given the structural differences between KIR3DL1 and KIR2DL1, I speculated that the phenomenon was due to presence of the D0 domain. Therefore, the initial hypotheses to be tested in this thesis were:

1. LILRB1 can cooperate with KIR3DL1.

2. The D0 domain of KIR3DL1 is directly involved in KIR3DL1 mediated ligand binding

Chapter 2

MATERIALS AND METHODS

2. Materials and methods

2.1. Antibodies

Anti-KIR3DL1 mAb DX9 (IgG1), anti-KIR2DL1/S1 mAb HP-3E4 (IgM) and anti-HLA-ABC mAb DX17 (IgG1) were purchased from BD Biosciences (Mississauga, ON). Z27 specific for KIR3DL1/S1 was purchased from Beckman Coulter (Mississauga, ON). W6/32 (IgG2a) and control IgG2a (51.1) were purified by protein G-Agarose from the hybridomas obtained from ATCC. Control IgG1 MOPC-21 and control IgM MOPC-104E were purchased from Sigma-Aldrich (Oakville, ON). B27M1 (anti-B27 mAb) was kindly provided by Dr. Kane (University of Alberta). Anti-Bw4 was purchased from One Lambda. Full length LILRB1-Fc was purchased from R&D Systems (Minneapolis, MN, USA). B22-249 (anti-D^b α1) (196) , 28-14-8s (anti-D^b α3) (197), Y3 (anti-K^b α1) (198), 11-4.1(anti-2^k) (199), 34-5-8s (anti-H-$2D^d$) (200) were obtained from Dr. Kane (University of Alberta).

FITC-anti-HLA-G (IgG1) and FITC mouse-IgG1 isotype controls were obtained from eBioscience (San Diego, CA), PE-anti-HLA-E (IgG1) and PE-mouse-IgG1 isotype controls were purchased from Abcam (Cambridge, MA). Goat anti-human IgG Fc and alkaline phosphatase (AP) conjugated F(ab')$_2$ goat anti-mouse IgG and IgM were obtained from Jackson ImmunoResearch Laboratories (West Grove, PA). PE-conjugated anti-mouse IgG was purchased from Cedarlane (Burlington, ON).

2.2. Cell lines

Retroviral packaging cell line, Phoenix (obtained from Dr. S. Vidal's lab), were cultured in DMEM with 10% heat inactivated Hyclone characterized fetal bovine serum (FBS). NK92 (ATCC) was cultured in Iscoves medium with 12.5% heat inactivated Hyclone characterized FBS, 12.5% horse serum, 0.2 mM Inositol, 0.02 mM folic acid, 100 µM 2-mercaptoethanol (ME) and 2 mM L-glutamine.

NKL was maintained in Iscove's modified Dulbecco's medium with 10% Hyclone characterized FBS with 2mM L-glutamine. YTS cells, a subclone of YT cell line, obtained from G. Cohen was maintained in Iscove's modified Dulbecco's medium with 15% Hyclone characterized FBS / 50 µM 2- ME / 2mM L-glutamine. YTS transfectant, 2DL1.YTS produced in our lab were maintained in Iscove's modified Dulbecco's medium containing 15% FBS / 50 µM 2-mercaptoethanol / 2 mM L-glutamine and supplemented with 1 µg/ml puromycin where required (189). The mutant B lymphoblastoid cells 721.221, 221.G, HLA-B*58:01, B*27:05 and B*07:02 were provided by Eric Long and cultured in 10% FBS/Iscove's modified Dulbecco's medium supplemented with 0.5 mg/ml G418 (129, 201). Cos-7 cells from Dr. Kane (University of Alberta) were cultured in 10% FBS/DMEM. Primary NK cells were obtained from donors following written informed consent with approval from the Health Research Ethics Board at the University of Alberta. NK cells were purified from total PBMC using the StemSep Human NK Cell Enrichment Kit (StemCell Technologies). RMA and RMA/S (25, 202) (obtained from Dr. Kane, University of Alberta), R1E and R1E transfected with H-$2K^b m\beta_2 m$ or H-$2D^b m\beta_2 m$ (203) (provided from Dr. David Williams, University of Toronto) were maintained in RPMI 1640 medium supplement with glutamine and 10% FBS. NZB (murine lymphoma cell line from NZB animal) and RDM-4 (murine lymphoma cell line derived from AKR mice) (204) (provided from Dr. Kane's lab) were cultured in DMEM supplemented with 10% FBS. Rat cell line, RNK-16 and YB2/10 were maintained in RPMI 1640 medium supplement with 10% FBS. All the rat cell lines were provided from Dr. Kane (University of Alberta).

Table 2-1. List of surface receptors on NKL, NK92 and YTS cells

Cell lines	LIR-1	KIRs	NKG2A	NKG2D	CD8	CD16	CD28	CD56
NKL	Yes	No	Yes	Yes	No	No	No	Yes
NK92	Yes	No	Yes	Yes	No	No	Yes	Yes
YTS	No	No	No	No	No	No	Yes	Yes

2.3. Constructs

Cl42TGpMX. C-terminals of KIR2DL1* gene tagged with EGFP (cl42TG) in the context of pBabe vector was generated previously in our lab (189). The construct was digested with EcoRI and NotI at 37°C overnight, and the resulting fragment was subcloned into pMX-puro (gift from Dr. Lanier, UCSF).

KIR3DL1pMX, 3DL1Y^{2}FpMX. KIR3DL1*001 and its ITIM mutant 3DL1Y^{2}F were amplified and inserted into pSport vector by Johnason Huckle, a previous student in our lab. The constructs were digested with EcoRI and NotI, and the resulting fragments were subcloned into pMX-puro.

D02DL1pMX. The signal sequence and D0 domain of KIR3DL1*001 was linked to KIR2DL1 using PCR products with appropriate restriction sites as follows. KIR2DL1*0020101 was amplified by PCR from 2DL1 in the plasmid pMX with a forward primer complementary to the region just downstream of the signal sequence cleavage site and containing a BamH1 site (5'CAGGGGGCGGATCCGAACCACAGAAAACCTTCCCTCC3'), and the reverse primer complementary to the pMX backbone (5'CTAACTGACACACATTCCACAGC3') and reinserted into pMX with NotI and BamH1. The D0 of KIR3DL1 was amplified by PCR from KIR3DL1 in pMX with forward primer 5'CCTCTAGACTGCCGGATCTAGC3' complementary to the backbone of pMX upstream of KIR3DL1 signal peptide sequence and including a BamH1 site from the vector, and the reverse primer 5'CAGGGGGCGGATCCGCTCCTGTGACCATGATCACCACGG3' complementary to the region at the end of the KIR3DL1 D0 domain extended with a BamH1 restriction site. The resulting PCR product was digested with BamH1, and ligated into the BamH1-KIR2DL1 construct in pMX. The D0 boundary ends with IMVTG and is linked by ADPN to HRKPS at the beginning of the D1 domain of KIR2DL1 starting at the second histidine of the mature protein and corresponding to the beginning of KIR3DL1 D1's at the sequence NHRKP.

3DL1Y200ApMX. was generated using Quick Change Mutagenesis kit (Stratagene, LA Jolla, CA), confirmed by complete sequencing of the inserted DNA and subsequently subcloned in the pMX vector.

*HA.B*27:05.* DNA encoding HLA-B*27:05 was amplified by RT-PCR from RNA extraction of the cells stably expressing HLA-B27 (provided by Dr. Long's lab, NIH) with the forward primer B27fwdXmaI complementary to the region just downstream of the signal sequence cleavage site extended with a XmaI restriction site (5'-CCCCCGGGGGCTCCCACTCCATGAGG-3') and the reverse primer B27bwdSalI complementary to the end of HLA-B27 followed by SalI cloning site (5'-GC GTCGACTCAAGCTGTGAGAGACACATC-3'). The PCR product was cloned into the vector pCRII (Invitrogen, CA).

*HA.B*27:05I194A.* The mutation at position 194 from isoleucine (I) to alanine (A), I194A was generated by site directed mutagenesis of HLA-B*27:05 in pCRII using the QuickChange^{TM} (Stratagene) method. Primers used to generate HLA-B*27:05 I194A were 5'-GTGACCCACCACCCC<u>GCC</u>TCTGACCATGAGGC-3' and its reverse complement and 5'-GCCTCATGGTCAGA<u>GGC</u>GGGGTGGTGGGTCAC-3' and its reverse complement to change GCC to GGC.

HFE. HFE was amplified by RT-PCR using RNA extraction of 721.221 cells with the forward primer HFEfwdBgl that is complementary to the region just downstream of signal sequence cleavage site and extended with a BglII site (5'-AGATCTCGCTTGCTGCGTTCACAC-3') and the reverse primer HFEbwdSalI that is complementary to the stop codon region followed with a SalI site (5'-GTCGACTCACTCACGTTCAGCTAAGACG-3').

B27α1α2HFEα3. HLA-B*27:05α1α2 domain downstream of signal sequence was linked to HFE α3 using PCR fragments with PstI. B27α1α2 was amplified from HLA-B*27:05 in the plasmid pCRII with the B27fwdXmaI primer and the reverse primer that is complementary to the end of α2 region at residue 180, that naturally contains a PstI site (5'- CTGCAGCGTCTCCTTCCC-3') and inserted

into pDisplay with XmaI and PstI. The α3 of HFE was amplified by PCR from HFE in pCRII with forward primer 5'-CTGCAGCAACAAGTGCCTCCTTTGGTGAAGG-3' complementary to the region of the beginning of α3 domain of HFE extended with a PstI site and the reverse primer HFEbwdSalI. The resulting PCR product was digested with PstI and SalI, and ligated into the same site digested B27α1α2pDisplay. The α1α2 boundary of HLA-B27 ends with GKETLQ and is linked to the beginning of the α3 domain of HFE starting at residue 182 of mature protein by the amino acids as QQVPPLV.

HFEα1α2B27α3. The construct was generated with the similar strategy that link HFE α1α2 domain with B27α3 with KpnI. HFEα1α2 was amplified from HFE in pCRII with the forward primer that is complementary to the beginning of HFE downstream of the signal sequence with the additional of an XmaI site (5'-CCCGGGCGCTTGCTGCGTTCACACTC-3') and the backward primer complementary to the end of α2 domain of HFE followed by a KpnI site (5'-GGTACCGTCCAAAACACCTCTCCC -3'). The α3 domain of HLA-B*27:05 was amplified from B*27:05 in pCRII with a forward primer complementary to the region at the start of the α3 domain of HLA-B*27:05 at residue 181 and containing a KpnI site (5'- GGTACCCGCGCGGACCCCCCAAAG-3') and the backward primer B27bwdSalI. The α1α2 boundary of HFE ends with the amino acid sequence LGRGVLD and is linked by the amino acids GT to the beginning of B27α3 (RADPPK...).

All the PCR products were cloned into pCRII and the constructs were confirmed by sequencing. The pDisplay signal sequence and HA tag were fused in frame to the above constructs with XmaI and SalI except BglII and SalI for HFE insert. The constructs were subcloned into pMX-puro with EcoRI and NotI and transduced into 721.221 cells using the method described in chapter 2. The cells were selected in 1 µg/ml puromycin and stable clones established by single cell sorting based on W6/32 surface staining analyzed by flow cytometry.

3DL1Fc. The Cd5lneg1 vector containing human IgG Fc and the plasmids encoding 3DL1Fc and 2DL1Fc were provided by Dr. Long, NIH (169).

D0Fc, D0D1Fc, D1D2Fc. DNA encoding the first Ig domain D0 of KIR3DL1, the first and second Ig domains (D0D1) and the second, third Ig domains (D1D2) in cd51neg1 constructs (169) were kindly provided from Dr. Long's lab (NIH). The Fc fusion proteins were generated and purified as described in chapter 3.

D02DL1Fc. The chimeric construct D02D was generated by first linking D0 of KIR3DL1*001 to the D1 and D2 domain of KIR2DL1. The D0 domain of KIR3DL1 was amplified using the forward primer 5'-CAGGGGGCGCTAGCGCACATGGGTGGTCAGGACAAACC-3' corresponding to sequences immediately downstream of the signal sequence and containing an NheI site, and reverse primer 5'-CAGGGGGCGCTAGCGGTCCTGTGACCATGATC-ACCACGG-3' upstream of the D1 domain of KIR3DL1 and containing an NheI site. The segment with the KIR2DL1 Ig domains were amplified using the forward primer 5'CAGGGGGCGCGAGCGCATGAGGGAGTACACGAGAAACC-3' downstream of the signal sequence cleavage site and containing an NheI site, and reverse primer 5'-GAGGTCCCAGGATCCGCATGGTGCAGGTGTCTGGGGTTACC-3' upstream of the transmembrane region and containing a BamH1 site. In the resulting fusion, the D0 domain ends at IMVTG and is linked by amino acids PLA to the first histidine of the mature KIR2DL1 protein. D02D was inserted into Cd51neg1 vector with NheI and BamH1.

LILRB1-D1D2Fc. DNA encoding the first two extracellular domains (D1D2) of LILRB1 (residues 1-197) were amplified from LILRB1 in pSport using 5'-GCTAGCGGGGCACCTCCCCAAGCCCACC-3' as the forward primer and 5'-CGCTAGCCCTAGGACCAGGAGCTCCAGGAG-3' as the reverse primer. The resultant fragment was inserted into Cd51neg1 vector (provided by Dr. Long, NIH) with NheI.

63

LILRB1Fc. Fusion protein containing the extracellular domains of LILRB1 linked with human IgG1 Fc was purchased from R&D Systems Inc. (Cedarlane). The concentration was adjusted to 100 µg/ml as suggested by the manufacturer.

2.4. Optimized retroviral transduction protocol

The protocol was modified based on Dr. Nolan's protocol (http://www.stanford.edu/group/nolan/retroviral_systems/phx.html). Briefly, 2.5 x 10^6 cells of Phoenix cells were seeded in a 60 mm petridish at 37°C with 5% CO_2 for 12-16 hours. The following day, the medium was removed and the dish was replenished with 3 ml complete medium supplemented with 25 µM chloroquine. DNA/HBS mixture was prepared in a 15 ml tube as follows: up to 15 µg DNA were added into 450 µl sterile distilled water with 50 µl 2.5M $CaCl_2$, and then mixed with 500 µl 2X HEPES Buffered Saline (HBS) (50 mM HEPES, pH=7.05; 10 mM KCl; 12 mM Dextrose; 280 mM NaCl; 1.5 mM Na_2HPO_4). The DNA/HBS mixture was added drop wise to the cells, gently mixed. The cells were then incubated at 37°C for 8-10 hrs. The medium was changed to 3 ml NK culture medium, and the cells were incubated at 32°C with 5% CO_2 up to 48 hours. 48 hours post transfection, the supernatant containing retroviral particles were collected by centrifuge at 1200X rpm for 5 minutes. The harvested supernatant was then supplemented with 8 µg/ml polybrene to make infection cocktail. 0.5 million exponentially growing NK cells were suspended with the infection cocktail, and the suspension was plated into a 24 well plate with 0.5 ml per well. The plate was then spun at room temperature for 90 minutes at 1500 x rpm prior to another three hours subsequent incubation at 37°C with 5% CO_2. Next, the infected cells were pooled, pelleted and resuspended in 5 ml NK media. The cells were then placed into a 60mm petridish and incubated at 37°C with 5% CO_2 for 48 hours. 48 hours post infection, the expression of EGFP was measured by flow cytometry on a FACs Canto (BD Biosciences).

NK cell lines, NK92, NKL and YTS, were transduced with KIR3DL1*001pMX, KIR3DL1Y200A.pMX mutant or D02DL1pMX constructs using the described retroviral transduction. The positive cells were selected in 1 µg/ml (NKL and YTS) or 4 µg/ml puromycin (NK92).

2.5. Cell sorting

Subclones were isolated based on high KIR3DL1 expression by a single cell sorting (FACSAria) using FITC-conjugated anti-KIR3DL1 (DX9) antibody. In brief, all of the cells resistant to purimycin were pelleted and washed with 3 ml sterile FACs buffer (PBS with 1mM EDTA and 2% FBS). 5 µl FITC-coupled DX9 was diluted into 1 ml sterile FACs buffer and the diluted antibody solution was filter sterilized using 0.22 µm Millipore filter (Millpore). The sterilized antibody was then added to the washed cells using a ratio of 0.5 ml mAb to 1 million cells, and incubated at 4°C for 30 minutes. The isotype control was stained as described as DX9 but with less cells (0.5 million). The stained cells were then washed with 3 ml of sterile FACs buffer and resuspended in 1 ml of sterile FACs buffer. Prior to sorting, NK media supplemented with the appropriate amount of puromycin, 0.1% gentamycin (50 mg/ml, Cat#15750-060, Invitrogen) and 1% anti-fungi reagent, Antibiotic-Antimycotic (Cat # 15240-062, Invitrogen) were added to a 15 ml conical tube (10 ml) and a 96 well plate (100 µl per well). Next, the resulting cells were sorted into the plate as a single cell per well, and the remained cells were sorted into the tube. The sorted cells were maintained at 37°C with 5% CO_2 with the previous sorting media. The clones expressing high KIR3DL1 and containing a comparable lysis of 721.221 cells relative to parental NK cells were obtained for further functional examination.

221 cells were transduced with HA tagged B*27:05, I194A, HFE, HFEα1α2B27α3 or B27α1α2HFEα3 constructs using the optimized retroviral transduction method described in section 2.4. The positive cells were selected in 1 µg/ml puromycin. Subclones were isolated by a single cell sorting using anti-

65

MHC-I antibody, W6/32, and PE coupled anti mouse IgG. The clones expressing comparable levels of HA relative to wild type B*27:05 were obtained for further examination.

2.6. Virus titer determination

NIH 3T3 cells were seeded in a 6 well plate with 0.2 million cells per well and incubated at 37°C with 5% CO_2 for 12-18 hours. The following day, a serial dilution of the virus stock released from Phoenix cells was performed with standard fibroblast medium (SFM: containing 10% heat inactivated fetal bovine serum, 2mM L-glutamine in DMEM) supplemented with 15 µg/ml of polybrene. Next, NIH 3T3 cells were infected with 1 ml of each dilution for 24-48 hours at 37°C with 5% CO_2. 48 hours post infection, the cells were trypinsized and analyzed for EGFP expression as measured by flow cytometry. The virus titer (IU/ml) were calculated as (% positive cells expressing EGFP) X (the amount of target cells), and adjusted for the dilution factor (205).

2.7. Cytotoxicity assay

The cytotoxicity of transduced and parental NK cells was measured in a standard 4-h ^{51}Cr release assay (206) using 221 cells and 221 tranfectants expressing HLA class I as the target cells as follows. 0.5 million of target cells are labeled with 10 micro Currie (µCi) of ^{51}Cr at 37°C for one hour, and washed with 10 ml CTL medium (Iscove/5%FBS). The cell pellets were resuspended with 1 ml CTL medium, counted and adjusted at 2.5 X 10^4 cells/ml. Effector cells (NK cells) were collected and washed with CTL medium and dilution made for effector: target ratios from 9:1 and diluted to 3:1 and 1:1 with CTL medium. The effector and target cells were then placed into 96 well plate at 100 µl per well of each. The plates were spun at 400 rpm room temperature with no brake for 3 minutes and then incubated at 37°C with 5% CO2 for 4 hours. Post incubation, the plates were recentrifuged, and 25 µl of the supernatant was added to 100 µl scintillation liquid

(Perkin Elmer) per well in 96 well flex plates (Fisher). The ^{51}Cr in the supernatant was measured by 1450 Microbeta Trilux liquid Scintillation & Luminescence Counter (Wallac). The cytotoxicity was calculated as percentage lysis with the following formula: % lysis = (^{51}Cr release of sample – ^{51}Cr release of spontaneous) X 100 / (^{51}Cr release of maximum – ^{51}Cr release of spontaneous). For antibody reversal experiments, effector cells were preincubated with antibodies at room temperature for 10 minutes prior to adding the target cells. Unless otherwise indicated, the concentrations of the antibodies were: 2.5 µg/ml for anti-KIR3DL1 mAb (DX9), anti-KIR2DL1 (HP3E4) or anti-LILRB1 (M405), 5 µg/ml for anti-MHC-α3 mAb (W6/32). The same concentration of control IgG1 (MOPC-21), control IgG2a (51.1) and control IgM (MOPC-104E) were added for isotype controls. The results from at least three assays were aggregated and the significance of the differences determined using an unpaired Student *T* test.

2.8. Generation of Fc-fusion proteins

Fc-fusion proteins were generated by transfecting Cos-7 cells modified from the protocol provided from Dr. E. Long (148). In brief, 10 million cells were seeded per roller bottle (Cat#430849, Corning) in batchs of three bottles, and were incubated at 37°C with 5% CO_2 for two days. On the day of transfection, transfection medium (TM) was prepared as follows: 300 µg of DNA + 0.6 ml of 1M HEPES buffer (PH 7.4) + 0.6 ml of 40 mg/ml DEAE-Dextran (Cat#D9885, Sigma) + 240 µl of 25 µM chloroquine in plain DMEM medium in a total volume of 60 ml. The cells were washed with 25 ml plain DMEM three times prior to addition of 20 ml TM per roller bottle. Next, the cells replenished with TM were incubated at 37°C with CO_2 for 2 hours. Post incubation, the cells were washed once with plain DMEM and replenished with 50 ml fresh complete medium per roller bottle prior to incubation at 37°C with CO_2 overnight. The next day, the cells were washed with plain DMEM three times, and replenished with 50 ml DMEM supplemented with 5 ml Non-Essential Amino Acid (NEAA, Cat #11140-

67

050, Invitrogen). The cells were then incubated at 37°C with 5% CO_2. Every three to four days, supernatants were collected and clarified by centrifugation at 4000 X g for 20 minutes. To obtain enough of the proteins for purification, a total of three collections was done from 15 bottles.

2.9. Purification of Fc-fusion proteins

The various fusion proteins and control Fc protein were affinity purified on Protein G Plus-Agarose (Cat#IP08, Calbiochem) columns from serum free supernatants of transfected Cos-7 cells and dialyzed into PBS with Amicon® centrifugal filters (Cat#UFC910024, Millipore) essentially as described (148). Purity was verified by SDS-PAGE with Coomassie staining under non-reducing or reducing conditions. Protein concentrations were determined using the Micro Bicinchonic Acid assay (Pierce).

2.10. Capture-based ELISA

The folding of the purified and concentrated proteins was tested with conformationally sensitive anti-KIR antibodies using the following method. ELISA plates were coated with 25 µg/ml goat anti-human IgG Fc in 0.1M $NaHCO_3$ (pH=9.6) at 4°C overnight. The coated plate was then blocked with PBS with 2% BSA and 0.05% Tween-20 at room temperature for 1 hour. Next, the diluted Fc fusion proteins were added to the plate and incubated for 1 hr at room temperature prior to three washes with PBS/0.05% Tween-20. The bound proteins were incubated with 50 ng/ml DX9 or HP-3E4 at room temperature for 1 hour and then washed three times with PBS/0.05% Tween-20. Reactivity to antibodies was detected with alkaline phosphatase (AP) conjugated F(ab')$_2$ goat anti-mouse IgG or IgM (1:10,000 dilution) and the PNPP substrate (Pierce). The results were measured at 405 nM using Microplate Reader (Molecular Probe).

2.11. Western blot

Purified Fc fusion proteins were mixed with 2x SDS-PAGE reducing buffer (Fermenta) and denatured at 100°C for 10 minutes. The prepared samples were loaded on an 8 % polyacrylamide gel. The gels were run at 100 MV for 1.5 hours prior to transferring to 0.22 µm cellular membranes as instructed. The resulting membranes were incubated with 1:1 PBS/Li-Cor blocking buffer (Cat#927-40000, Odyssey) overnight at 4°C. Next, the membranes were blotted with 0.5 µg/ml anti-KIR3DL1 antibody, DX9 or purified goat anti-human-Fc mAb at room temperature for three hours. The antibodies were diluted in dilution buffer consisting of 1:1 PBS/Li-Cor blocking buffer supplemented with 0.1% Tween-20. Post incubation, the membranes were then washed with PBS/0.1% Tween-20 four times. Subsequently, the membranes were blotted with AlexFlour®680 goat anti-mouse-IgG (H+L) (Cat#A21057, Invitrogen) or AlexFlour®680 Donkey anti-goat-IgG (H+L) (Cat# A21084, Invitrogen) at room temperature for one hour covered with aluminum foil. The secondary antibodies were diluted 1: 10,000 in the dilution buffer. The membranes were then washed with PBS for three times. The binding of the antibodies was measured with Li-Cor Quantitative Fluorescent Imaging System (Odyssey).

2.12. Cell binding assay

In order to measure binding of Fc-fusion proteins to MHC-I, 2×10^5 of 721.221 cells or its derivatives expressing various MHC-I proteins were incubated in 20 µl with purified fusion proteins for 1 hour at 4°C with rotation. The incubation was maintained in 1.5 ml eppendorf tubes. The cells were washed and transferred into 5 ml Falcon tubes (Cat#352008, BD). The cells were then incubated with PE-conjugated goat anti-human Fc antibodies (eBioscience) for 30 min at 4°C, washed again, fixed in 5% formaldehyde/FACs buffer (PBS + 2% FBS + 1 µM EDTA) and analyzed by flow cytometry. To block the binding, the antibodies were incubated with the cells for 10 minutes at room temperature,

followed by addition of the purified proteins to a final concentration of 100 µg/ml in 30 µl. The significance of the binding was determined on aggregated data from at least three assays using an unpaired Student T test.

2.13. Generation of MHC-I conjugated streptavidin beads

100 µl of Dynobeads® M-280 streptavidin beads (cat#112.06D, Invitrogen) were washed with PBS and resuspended in 10 µl PBS buffer. 5 µg of biotinylated HLA-B*27:05 monomer (provided by Dr. Brook's Lab, Australia) or H-2K^b monomer (provided by Elsa Marquez and Dr. Kevin Kane, University of Alberta) were added. The samples were incubated at room temperature with rotation for 30 minutes prior to four washes with PBS/0.1% Tween-20. The monomer conjugated beads were used for further binding assay. The degree of conjugation was determined using MHC-I specific antibodies and flow cytometric analysis. The binding of Fc fusion proteins to beads was done similarly to the cell-binding assay (section 2.12) using 10 µl of Dynobeads. Fig 2-1 illustrates the process of conjugation and examination steps for analyzing antibody and Fc-fusion protein binding using flow cytometry.
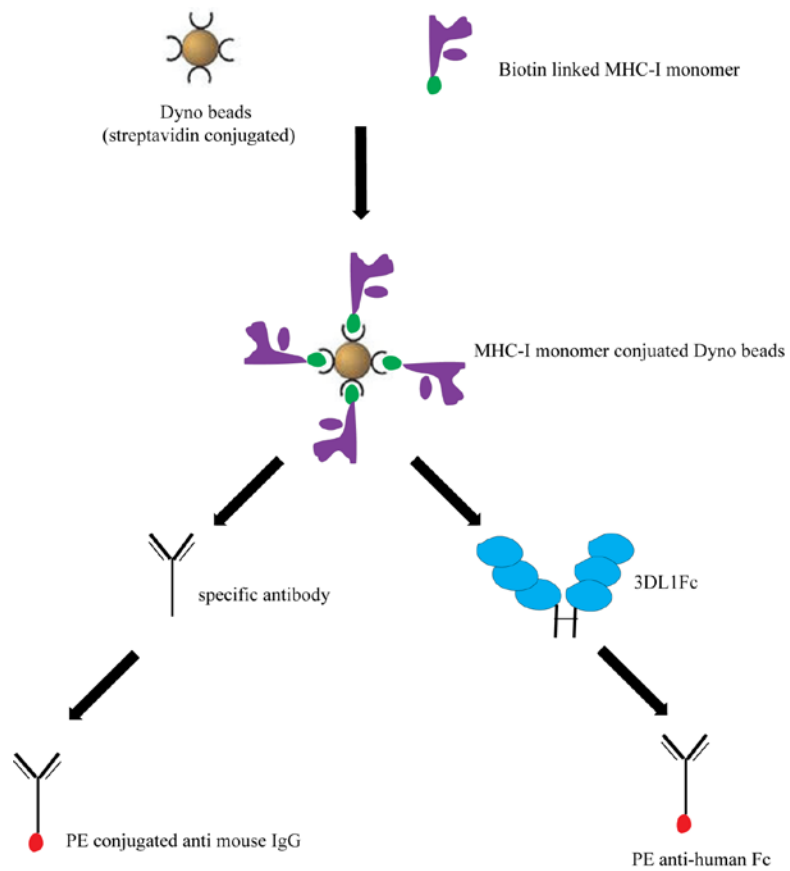
Figure 2-1. Illustration of MHC-I monomer conjugated Dyno®bead

Strepavidin coated Dynobeads® are coupled with biotinylated MHC-I monomer as illustrated. The resulting product then is detected for the binding of MHC-I using antibody.

2.14. Structural modelling of KIR3DL1

Structural models of KIR3DL1 and its interaction with HLA were created based on crystal structures of the HLA-Cw4/KIR2DL1 complex (PDB code 1IM9), or HLA-B*57:01/KIR3DL1*001 complex (PDB code 3VH8) and the LILRB1-HLA-A2 complex (PDB code 1P7Q). Superpositioning of models was performed with the SUPPOS program by Dr. Bart Hazes (University of Alberta) from the BIOMOL program package (unpublished results, University of Groningen) using the alpha carbon atoms of each residue. The model of KIR3DL1 alone was achieved by superimposing the D2 domain of a second copy of KIR2DL1 onto the D1 domain of the first copy (rmsd is 0.6Å for 57 superimposed residues) and using the resulting D1 position of the second copy as the model for the KIR3DL1 D0 domain. The KIR2DL1-HLA-Cw4 complex crystal structure was then used (PDB code 1IM9) to model binding of KIR3DL1 to MHC-I. For the complex we superimposed its D0 and D1 domains onto the D1 and D2 domains of the LILRB1-HLA-A2 complex (rmsd is 1.2Å for 99 superimposed residues). The images were prepared with the program PyMol (DeLano Scientific LLC, San Carlos, CA, USA. http://www.pymol.org).

Chapter 3

OPTIMIZATION OF A RETROVIRAL TRANSDUCTION SYSTEM FOR USE WITH NK CELL LINES AND FUNCTIONAL ANALYSIS OF KIR3DL1 IN THE PRESENCE OR ABSENCE OF ENDOGENOUS LILRB1

Preface

In this chapter, I optimized transferring genes of interest into NK cell lines by means of a retroviral transduction method. Using the optimized method, KIR3DL1 was stably introduced into three NK cell lines and the functions were carefully examined. I have performed all the experiments and the results have not yet been published.

3.1. Introduction

Natural killer (NK) cells are one of the front line defenses against virally infected and transformed cells by means of releasing cytolytic granules and secreting cytokines. The activities of NK cells are dependent on the balance of inhibitory and activating signals regulated by the interactions of surface receptors with their corresponding cognate ligands (8). Despite the enormous number of different receptors, all NK receptors are classified into two superfamilies: the immunoglobulin (Ig) like superfamily (IgSF) and the C-type lectin superfamily. The IgSF consists of the Killer Cell Ig-like Receptor (KIR) family and the Leukocyte Ig-like Receptor (LILR) family. Genetic variation of particular members of these families are known to be associated with susceptibility to auto-immunity and resistance to viral infections (4, 207). For instance, KIR3DL1, an inhibitory KIR receptor, is linked to the progression of Human Immunodeficiency Virus (HIV) infection (156). Variation of LILRB1, a well studied inhibitory LILR receptor, is associated with susceptibility to Rheumatoid Arthritis (RA) (208). Therefore, clarifying the mechanism of how these receptors regulate NK cells will allow us to better understand NK cell functions and explore therapies for these diseases.

In order to understand mechanisms, it is important to study individual receptors. Though multiple receptors are co-expressed on NK cells under physiological conditions, it is a good strategy to simplify the system in order to begin investigation. Cytolytic NK and T cells are notoriously difficult to transfect. However, a few methods have been reported to stably transfer genes into NK cells, such methods include electroporation (209), particle mediated gene transfer (210) and retroviral transduction (211, 212). Unfortunately, these methods are not highly efficient and are tailored to individual cell lines. NKL and NK92 cell lines express endogenous LILRB1 and YTS cells are LILRB1 negative, therefore, these cell lines can be used to study the influence of LILRB1 on KIR signaling. The

laboratory already had a working protocol to retrovirally transduce mouse NK cell lines, but not human NK cell lines. Given the high efficiency of transduction, I chose to pursue a retroviral transfection method to transduce a gene of interest into human NK cell lines.

A retrovirus is an RNA virus that is duplicated in a host cell using a reverse transcriptase to produce a DNA copy from its RNA genome. The resulting DNA is then incorporated into the host genome by an integrase enzyme. The virus proteins are transcribed and translated using host machinery, ultimately, to form a new virus. The natural retroviral mechnism of insertion into the genome makes them a good tool of stably introducing genes into target cells. For safety reasons, the genes that encode viral proteins are separated from the RNA genome, and they are inserted individually into packaging cell lines and retroviral vectors, respectively. Packaging cell lines are engineered to express the viral genes encoding for the retroviral envelope (*env*), the capsid proteins (*gag*) and the polymerase (*pol*). The retroviral vectors contain important viral elements, such as a viral packaging signal (Ψ), signals required for reverse transcription, and long terminal repeats (LTRs) for integration into host genome (213) (Fig 3-1). Packaging cells alone cannot produce virus due to lacking of these necessary replication elements. However, when transfected with the corresponding retroviral vectors, these cells can produce the virus and release it into the supernatant. The infectious supernatant can then be used for further infection of cells, in this case, NK cell lines (Fig 3-1). To transduce NK cell lines, we obtained Phoenix[TM]-Ampho, a packaging cell line generated in Dr. Nolan's lab, derived from the cell line, 293T. These cells are easily transfected with conventional methods such as calcium phosphate or lipid mediated methods. In addition, the produced virus is able to infect both murine and human cells because the envelope protein is amphotropic. Since they lack the genes encoding *gag-pol* and *env* that are needed for virus assembly, the transduced NK cells cannot produce retrovirus, and therefore are less hazardous and relatively safe to work with. Dr. Nolan's lab

provides a basic procedure for transduction (Fig 3-2) (http://www.stanford.edu/group/nolan/retroviral_systems/phx.html), however, in order to effectively introduce genes into NK cells, the basic protocol was modified. Several critical parameters influencing the transduction efficiency, such as the amount of DNA, temperature, infection methods and types of retroviral vectors were optimized. In this Chapter, I will review how I optimized the protocol for three KIR negative NK cell lines, NKL, NK92 and YTS, using a gene encoding enhanced green fluorescent protein (EGFP). KIR3DL1*001, was introduced into the three NK cell lines by this method to obtain the stable clones for the further investigation.

3.2. Results

3.2.1. Dose response of Phoenix transfection

The goal is to use as much DNA as possible to achieve maximal virus production without being toxic to the packaging cells. To optimize the protocol, I chose an easy to detect reporter gene encoding Enhanced Green Fluorescent Protein (EGFP) that was linked with an inhibitory KIR receptor, KIR2DL1, at the N-terminus (Cl42TG) (Fig 3-3a) previously generated in our lab (189). The EGFP tagged gene was subcloned into a retroviral vector, pBabe (189). The first variable tested was the amount of plasmid required for optimal expression in Phoenix cells. 8 µg of DNA was transfected into the Phoenix packaging cell line via the calcium phosphate method as described in *section 2.4*. 48 hours post transfection, the cells were trypsinized and analyzed for EGFP expression by flow cytometry. The majority of cells (around 80%) were observed to express a relatively high intensity of EGFP post transfection (Fig 3-3b). The results were not altered when the DNA amount was increased up to 15 µg (Table 3-1), suggesting that 8 µg DNA is sufficient for high transfection efficiency in Phoenix cells.
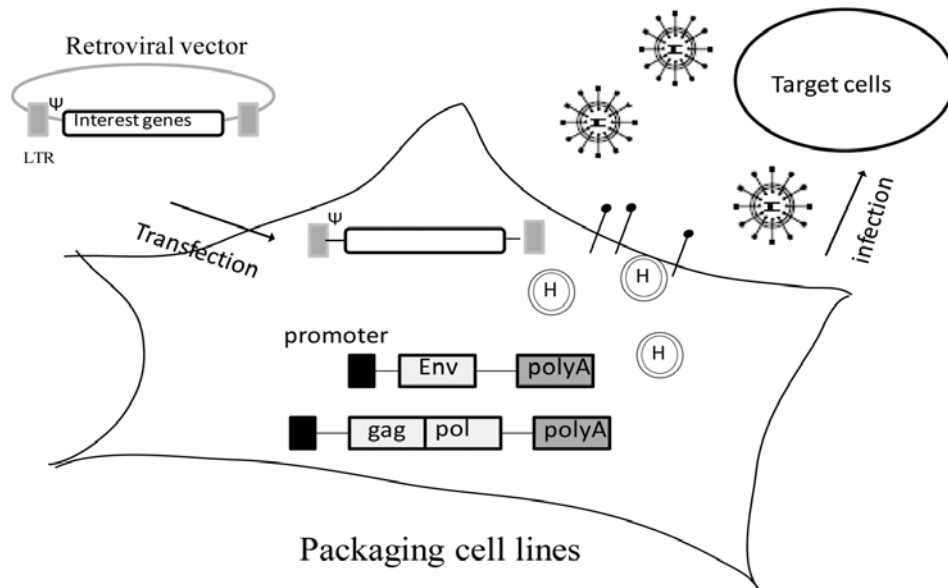
Figure 3-1. Illustration of retroviral transduction system.

Packaging cell lines make the *gag*, *pol* and *env* proteins. The retroviral vectors contain *cis*-acting viral elements including long terminal repeats (LTRs), polyadenylation signal (polyA), a viral packing signal (Ψ) and signals required for reverse transcription. The viral RNA genome is replaced with a gene of interest and a drug selection marker. When transfected with retroviral vectors, the packaging cell line produces viral particles that are released into the supernatant, and these are used to infect target cells.
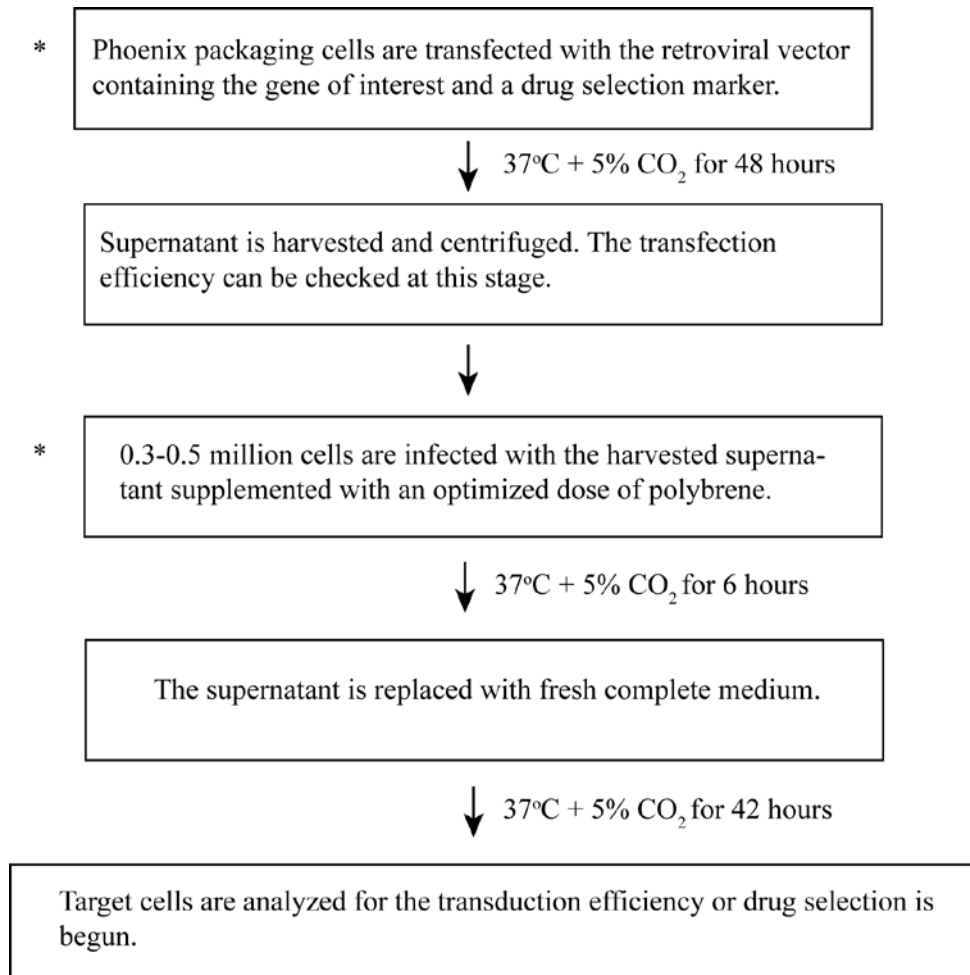
Figure 3-2. General procedure of retrovirus transduction provided by Dr. Nolan's lab.

* indicates the steps requiring optimization.

Table 3-1. Transfection efficiency in Phoenix cells using various amounts of plasmid DNA.

DNA Amount (μg)	% EGFP positive cell	Geometric Mean Fluorescence Intensity (Geo MFI)
8	77.5	630
10	80.5	650
12	76	630
15	79	665
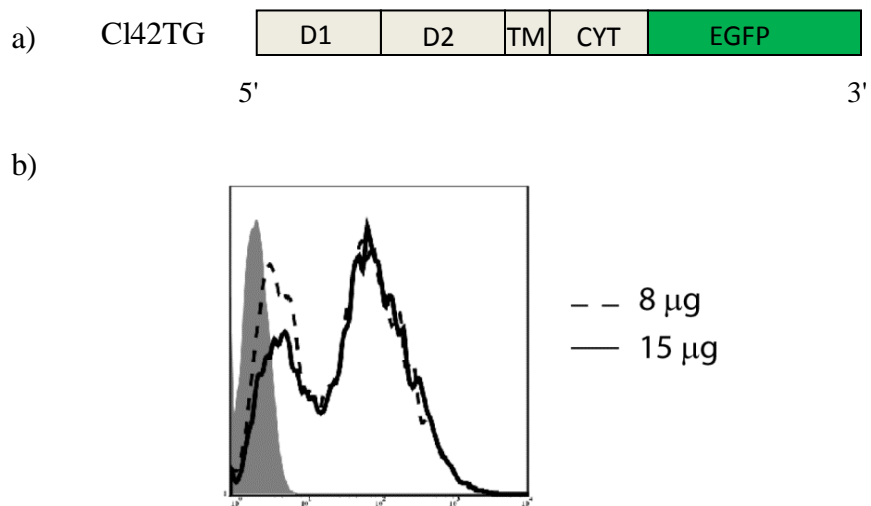
Figure 3-3. Comparison of EGFP expression with various amounts of DNA transfected into Phoenix packaging cells.

a) Schematic diagram of the KIR2DL1/GFP chimeric construct, Cl42TG. *b)* 8 μg or 15 μg cl42TGpBabe plasmid was transfected into Phoenix cells using the calcium phosphate mediated method. 48 hours post transfection, the cells were trypsinized and analyzed for EGFP expression by flow cytometry. The filled histogram represents the empty vector control. Representative of four experiments is shown.

3.2.2. Media change post transfection has no influence on Phoenix cell transfection efficiency

Phoenix cells are tolerant to various types of media, but NK cell lines are quite particular about the media they require. As the viral supernatant was to be directly used for infecting NK cell lines, using NK media (Iscove's media with various serum conditions) on Phoenix cells post transfection would be ideal to keep NK cells healthy during infection. Here, the transfection efficiency with several different types of NK media was compared to that of Phoenix complete medium (DMEM with 10% FBS). In addition, since high serum levels could diminish the infection efficiency, DMEM medium with decreased serum was tested as well. Fig 3-4 shows that reducing fetal bovine serum (FBS) to 1% has no effect on the percentage of EGFP positive cells or the EGFP intensity relative to 10% FBS. However, when changed to NK media, the proportion of cells expressing EGFP was slightly affected and the EGFP intensity was decreased (Fig 3-4), indicating that NK medium indeed does influence transfection efficiency in Phoenix cells. Given that a transfection of 30-60% is sufficient to produce high titer virus from Phoenix cells (214), incubating them with NK media is still acceptable.

3.2.3. 32°C increases production of retrovirus

Phoenix cells, a derivative of 293T cells, contain a temperature sensitive large T antigen for plasmid replication and are permissive to growth at 32°C (215). The retrovirus produced at 32°C has a longer half-life than at 37°C (http://www.stanford.edu/group/nolan/retroviral_systems/phx.html). Shifting cells to a lower incubation temperature post transfection has been reported to increase retroviral titers by 5 to 15 fold (216). Therefore, I compared viral titer between 32°C and 37°C 48 hours post transfection. In brief, 8 µg of DNA was transfected into Phoenix cells via the calcium phosphate method as described. 9 hours post transfection, the medium was replaced with NK medium and the cells were

incubated at either 32°C or 37°C. 48 hours post transfection, the supernatant was harvested as described and diluted 10 fold in NIH 3T3 medium. The diluted supernatant was then used to infect 0.2 million NIH 3T3 cells as described in *section 2.6*. 48 hours post infection, NIH 3T3 cells were trypsinized and analyzed for EGFP expression. The viral titer was then calculated as (% positive cells expressing EGFP) X (the number of target cells) / dilution factor. The results show that the infectious supernatant produced at 32°C causes an enhanced EGFP intensity on NIH 3T3 cells relative to that produced at 37°C (Fig 3-5). The viral titer was increased three fold, supporting the previous observation by the Nolan group that incubation at 32°C post transfection increases the viral titer.
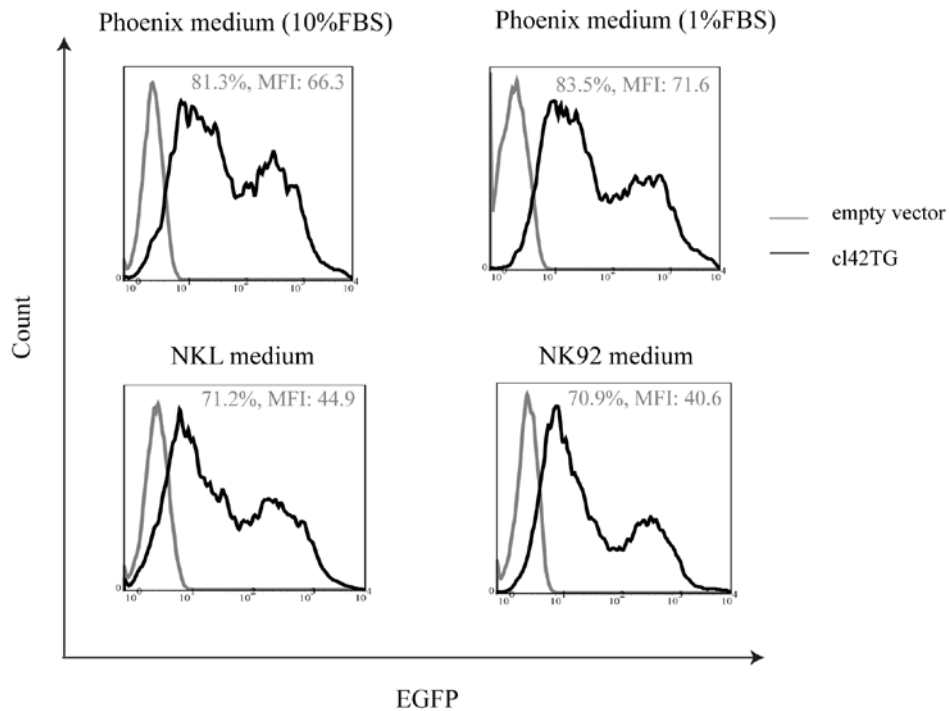
Figure 3-4. The influence of media composition on transfection efficiency.

 9 hours post transfection with cl42TGpBabe, Phoenix cells were incubated with 10% FBS in DMEM medium (the complete medium), 1% FBS-DMEM , NKL or NK92 medium for 40 hours. The cells were then trypsinized and analyzed for EGFP expression by flow cytometry. A representative of two experiments is shown.
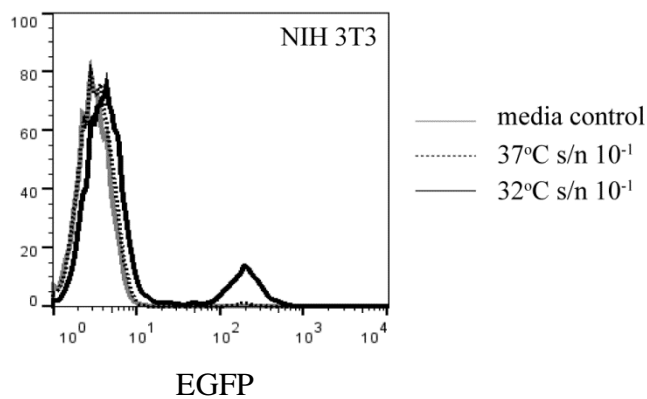
Figure 3-5. Infectivity is enhanced for virus produced at 32°C.

9 hours post transfection, Phoenix cells were resuspended in NK media and incubated at 37°C or 32°C. 48 hours post transfection, the supernatants were harvested and diluted 10 fold. The diluted supernatants or media control were then used to infect NIH 3T3 cells to determine the viral titer. 48 hours post infection, the NIH 3T3 cells were trypsinized and analyzed for EGFP expression by flow cytometry. The titer = (% EGFP positive cells X the number of NIH 3T3 cells used for infection) / Dilution Factor (IU/ml).

3.2.4. Spin infection enhances infection efficiency

Polybrene is a cationic agent utilized during the infection to neutralize the charge repulsion between viral particles and the sialic acid on the cell surface. The presence of polybrene therefore increases the infection efficiency (217). Other studies suggest that 2-8 µg/ml provides the best infection efficiency without becoming toxic and 4 µg/ml is often used for adherent cells (214, 218). A higher amount of polybrene might be detrimental to some cell types (218). First, to test if these amounts of polybrene are toxic to NK cells, I compared the viability of NKL and NK92 cells post treatment with 4 or 8 µg/ml polybrene. In brief, 0.5 million NKL or NK92 cells in log phase were treated with various amounts of polybrene for 6 hours at 37°C. The cell suspension was then centrifuged and resuspended in NK media. 48 hours post treatment, the cells were stained with trypan blue and analyzed to determine the percentage of live cells. As expected, 8 µg/ml of polybrene had no effect on the viability on NKL and NK92 cells compared to 4 µg/ml (80% and 82% vs 79% and 82%). Next, I examined if 8 µg/ml polybrene could increase infection. Phoenix cells were transduced and the supernatant incubated at 32°C was harvested as previously described. The infectious supernatant supplemented with 4 or 8 µg/ml of polybrene was used to infect 0.5 million NKL cells for 6 hours at 37°C. The cells were then cultured in fresh NK medium and continuously incubated at 37°C. 48 hours post infection, the cells were analyzed for EGFP expression by flow cytometry. However, 8 µg/ml only slightly increased EGFP expression on NKL cells compared to 4 µg/ml (Fig 3-6a). This was still too low to grow out the positive NK cells from the whole population. Nonetheless, the results do suggest that 8 µg/ml of polybrene is not toxic for NK92 and NKL cells.

The reason that NK cells are not infected well with even the highest acceptable amount of polybrene remains unclear. However, a method known as "spin infection" has been used to increase the infection efficiency in other cell

types (216). In this method, the cells suspended in the viral supernatant are centrifuged and this presumably concentrates the virus and cells together in the cell pellet. In brief, the cells suspended in the infection cocktail including 8 µg/ml polybrene were placed in a 12 well plate and centrifuged at 1500 rpm for 90 min at room temperature. The cells were subsequently incubated at 37°C for another 3 hours to adsorb the virus. After adsorption, the cells were washed and resuspended in complete medium and incubated for 48 hours prior to analysis of EGFP expression. 48 hours post infection, NKL cells treated with the spin infection dramatically increased EGFP expression in comparison to the traditional infection (Fig 3-6b), indicating the "spin infection" method increases the infection efficiency of NKL cells.

a)

b)
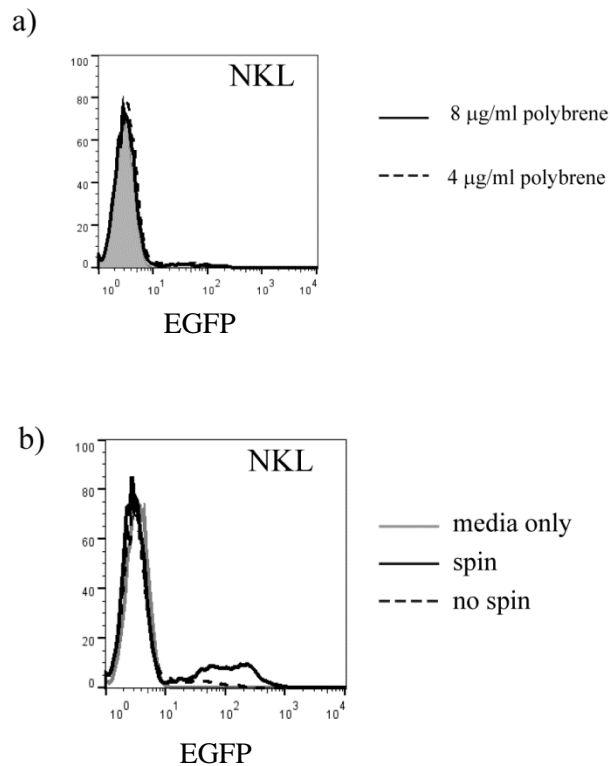
Figure 3-6. Transduction of NKL cells is improved by "spin -infection".

a) 4 µg/ml or 8 µg/ml polybrene was added to the supernatant containing viral particles. The resulting cocktail was then directly used to infect NKL cells for 6 hours at 37°C with 5% CO_2 prior to recovery in fresh complete NKL media. 48 hours post infection, the cells were analyzed for EGFP expression by flow cytometry. The filled histogram represents the media only control.   *b)* The infection cocktails containing 8 µg/ml polybrene or the media only control were used to infect NKL cells with the traditional direct infection or the spin infection. 48 hours post infection, the cells were analyzed for EGFP expression by flow cytometry.

3.2.5. Retrovirus vectors

The procedure of introducing EGFP in the context of the pBabe vector was optimized as described above. Different types of retroviral vector can also influence transduction efficiency for various cell types. For instance, another retroviral vector, pMX, which is a modified form of pBabe, contains an extended packaging signal derived from the MFG vector (219), perhaps resulting in the elevated production of viral particles. 8 µg of EGFP-pBabe or EGFP-pMX were compared for transfection and infection efficiencies. Interestingly, it appears that there was a greater portion of Phoenix cells expressing EGFP when transfected with the pBabe construct, in comparison to pMX (Fig 3-7a). However, the pBabe transfected cells produced less virus than the cells transfected with the pMX (1.034 X 10^6 IU/ml vs 4.72 X 10^6 IU/ml) as measured using NIH 3T3 cells. As a consequence, less NKL cells expressing EGFP were detected when infecting with the supernatant transfected with pBabe relative to that with pMX (27.97 % with MFI 113.60 compared to 53.49% with MFI 227.07) (Fig 3-7b). A similar observation was made in NK92 cells as well (9.26 % with MFI 68.95 vs 18.47 % with MFI 126.81). The results suggest that pMX enhances viral production and leads to greater transduction, even despite the decreased efficiency at the transfection stage relative to pBabe. The reason for lack of correlation between transfection efficiency and viral titer is perhaps due to more RNA copies being packaged instead of being translated when using the pMX vector. Although 30-60% transfection efficiency is enough to allow packaging cells to produce high titers of virus, my results indicate that the level of expressed EGFP on Phoenix cells is not always correlated with how many retroviral particles are produced by the cells. We have thus concluded that pMX is likely a better vector to use for our purposes.
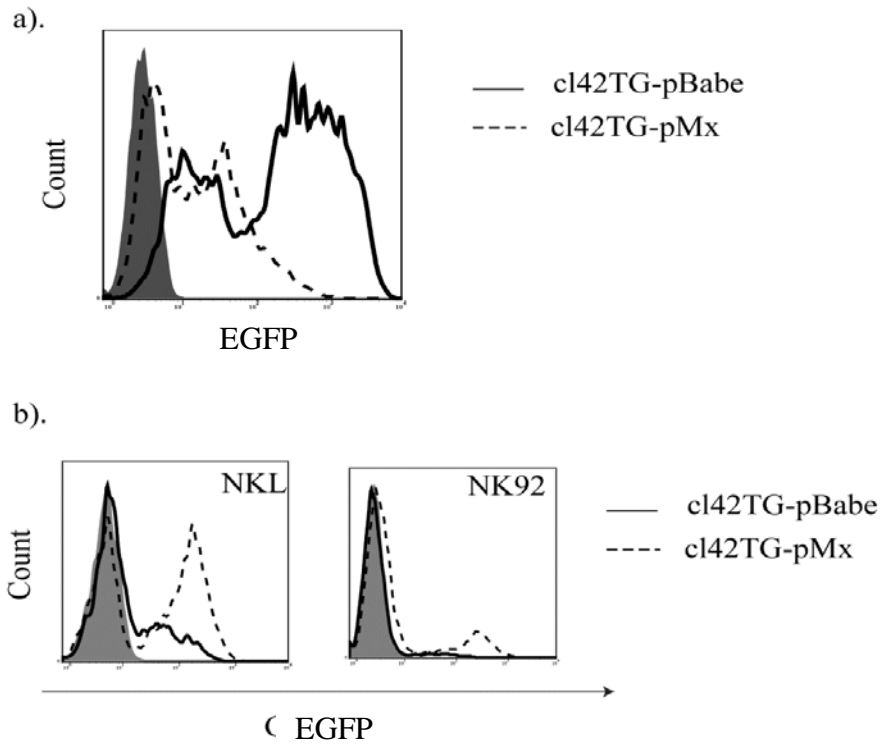
Figure 3-7. Comparison of transfection and infection efficiencies between pMX and pBabe vectors.

a) Comparison of EGFP expression on Phoenix cells transfected with cl42TGpBabe or cl42TGpMX. The filled histogram represents empty pMX vector only. *b)* Comparison of EGFP expression on NKL and NK92 cells with the two retroviral vectors. The supernatants obtained from *a)* were harvested and used to infect NKL or NK92 cells using the optimized protocol as described in this Chapter.

3.2.6. Drug selection and establishment of stable clones

As described above, the procedure of retroviral transfection into NK cell lines was optimized with modifications of the incubation temperature post transfection, cultured media post transfection, the infection method and the type of retroviral vectors. Next, I moved on to study a KIR receptor of interest, KIR3DL1. KIR3DL1*001 was chosen for the study because this allele is well expressed at the cell surface and induces strong inhibition upon engaging its ligand, HLA-Bw4 (see *section 1.5.1.7*). The cDNA of this receptor obtained from Dr. Long (NIH) was subcloned into the pMX-puro vector as described in Chapter 2.

I determined the optimal concentration of puromycin for NKL and NK92 using various titrations ranging from 0.5 to 6 µg/ml. Given puromycin is the drug selection marker in the pMX construct and it acts quickly to kill up to 99% of nonresistant cells in 2 days at low concentrations starting from 0.5 µg/ml (220), the cells were monitored 48 hours post treatment with trypan blue staining to determine viability. Treatment with 1 and 4 µg/ml puromycin led to the death of NKL and NK92, respectively. The results show that 1 and 4 µg/ml of puromycin are the optimal doses for NKL and NK92 cells, respectively.

To obtain KIR3DL1 expressing cell lines, the 3DL1pMX construct was retrovirally transduced into three KIR negative NK cell lines, NKL, NK92 and YTS as described in Chapter 2. 48 hours post infection, the optimal amounts of puromycin were added to transduced NKL and NK92 cells. Transduced YTS cells were treated with 1 µg/ml of puromycin as this is the reported effective dose (189). Approximately four to five days post treatment, puromycin resistant NKL, NK92 and YTS cells were observed, and in less than two weeks, the cells were confluent.

Next, KIR3DL1 expression was assessed by flow cytometry in the puromycin resistant cell population (Fig 3-8). The results show that only a small

percentage of the cells express KIR3DL1 and the expression is not stable as KIR3DL1 intensity diminished after one month in culture. Therefore, to ensure uniform and hopefully stable expression, I isolated the cells expressing KIR3DL1 using a FITC coupled anti-KIR3DL1 antibody and cell sorting (FACs Aria). The cells were sorted into a 96 well plate by single cell sorting and the remaining cells were collected into a 15 ml tube based on KIR3DL1 high expression. Comparison of KIR3DL1 expression between the mixed population (grown from the bulk sort) and subclones (obtained from the 96 well plate) showed that the level of KIR3DL1 on subclones was more stable during long term culture. Thus, the subclones were further screened for the expression of KIR3DL1 (Fig 3-8) and for maintenance of cytolytic capacity comparable to parental NKL cells using MHC-I negative target cells, 721.221. The resulting subclones were maintained in puromycin supplemented NK medium for use in functional assays.
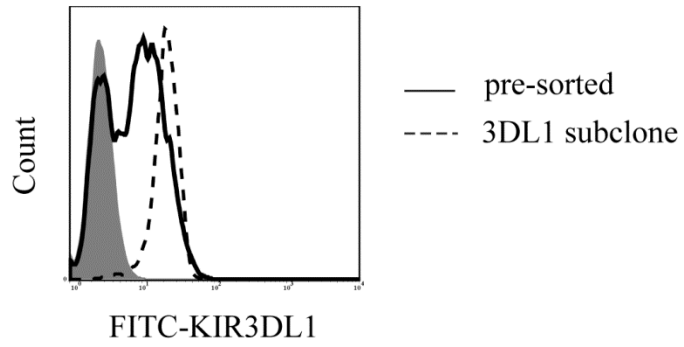
Figure 3-8. Comparison of the expression of KIR3DL1 on pre-sorted populations and a sorted subclone.

Expression of KIR3DL1*001 retrovirally transduced into NK92 cells is shown for the cells prior to sorting and stable clone. The cells were stained with FITC conjugated anti-KIR3DL1 (DX9) antibody and the results were analyzed by flow cytometry. Filled histogram represents the isotype control.

3.2.7. Application of retrovirally transduced cells to study KIR3DL1 function in NK cell lines with and without endogenous LILRB1

To examine KIR3DL1 function, I chose MHC-I negative 721.221 cells and 221 cells expressing a strong KIR3DL1 ligand, HLA-B*58:01 (abbreviated as B*58:01 in the subsequent text) as target cells. The lysis of selective target cells by NK cells expressing KIR3DL1 (Fig 3-9a) was examined using a ^{51}Cr release assay. Surprisingly, KIR3DL1 positive NK92 cells lysed targets expressing B*58:01 similar to parental 221 cells (Fig 3-9b). The results are representative of five independent subclones. However, a noticeable reduction of lysis was observed when KIR3DL1 positive YTS and NKL cells encountering 221 cells expressing B*58:01, relative to parental 221 cells (Fig 3-9c and d). These results suggest that KIR3DL1 expressed on YTS and NKL cells functions properly.

One explanation for the lack of KIR3DL1 signaling in NK92 cells is that the clones obtained may have mutations in signaling molecules required for KIR3DL1 to transmit a signal, for example, SHP-1 and SHP-2. To address the issue, I tested if these cells were able to transmit a negative signal. I used KIR2DL1 recombinant Vaccinia virus (KIR2DL1vv) generated by S. Kirwan in our lab (171) to express another KIR in the KIR3DL1 positive NK92 cells, and compared their lysis in response to the cells expressing KIR2DL1 ligand, HLA-Cw15, relative to B*58:01. Expression of KIR2DL1 in KIR3DL1^{+} NK92 subclones led to elimination of lysis in response to Cw15 relative to B*58:01 (Fig 3-10). The result suggests that the related downstream inhibitory signal molecules are not altered in the selected clones. Hence, the inability of inducing inhibition by KIR3DL1 expressed on NK92 cells is perhaps due to expression level being insufficient in these cells, even though it is similar to that on YTS and NKL cells (Fig 3-9a).
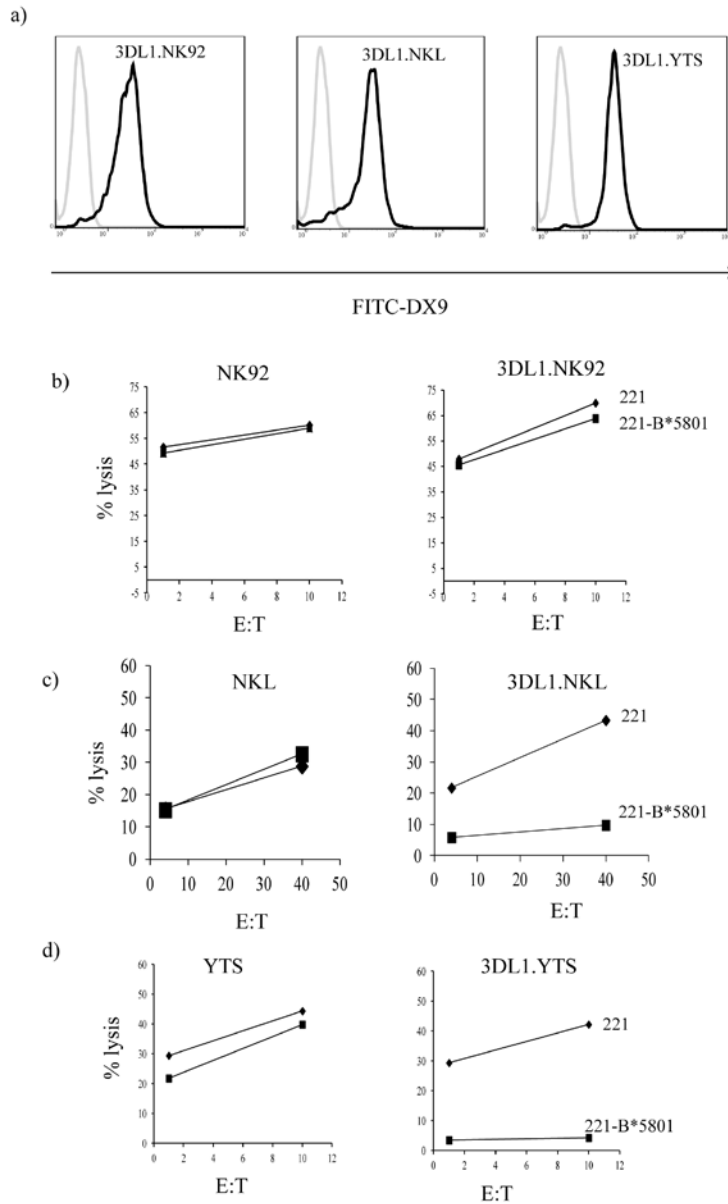
Figure 3-9. Analysis of 3DL1 function in NK92, NKL and YTS clones.

a). Flow cytometric analysis of subclones expressing KIR3DL1. *b-d).*The cytolysis of the indicated cells on parental 221 cells and 221 cells expressing KIR3DL1 ligand, HLA-B*58:01 was measured using a ^{51}Cr release assay as described in Chapter 2. E:T indicates the effector : target ratio. Representative of two experiments with triplicate measurements is shown.
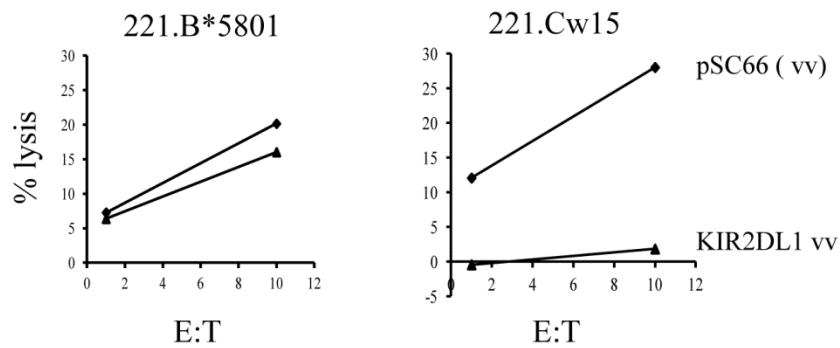
Figure 3-10. Inhibitory functional analysis of 3DL1$^+$NK92.

Vaccina virus encoding KIR2DL1(KIR2DL1 vv) or control virus (pSC66 vector only) were used to infect KIR3DL1.NK92 cells at 37°C for 2 hours with a multiplicity of infection of 10. The cytolysis mediated by the infected KIR3DL1 positive NK92 cells was measured using a ^{51}Cr release assay in response to cells expressing B*58:01 or KIR2DL1 ligand HLA-Cw15. Representative of two experiments with triplicate measurements is shown.

3.2.8. The influence of LILRB1 on KIR3DL1 signaling

LILRB1 has a broad specificity and interacts with both classical and non-classical HLA class I molecules but affinity depends on the subtype (181). It was previously reported that LILRB1 enhances signaling by KIR2DL1 when engaged by the KIR2DL1 ligand, HLA-Cw4 (171). However, whether LILRB1 influences KIR3DL1 signaling is not known. To study the role of LILRB1 in KIR3DL1 functional recognition in NKL cells, I first determined whether LILRB1 alone on the parental cells has an impact on NK lysis in response to KIR3DL1 ligand. The results show that the interaction between LILRB1 and B*58:01 does not alter lysis in comparison to the receptor alone (Fig 3-9c and 10). Importantly, LILRB1 specific antibody, M405, also did not influence the lysis (Fig 3-12a). These results suggest that the amount of endogenous LILRB1 on NKL cells (Fig 3-11b) is not sufficient to induce LILRB1 signaling or that LILRB1/B*58:01 interaction is too weak to induce a detectible inhibitory signal.

In order to reveal if LILRB1 can assist KIR3DL1 signaling, the two tyrosines (Y) in the ITIM motifs in the cytoplasmic tail of KIR3DL1 were mutated to phenylalanines (3DL1.Y^2F) (Fig 3-11a) to prevent KIR3DL1 signaling. The construct was introduced into YTS and NKL cells as described in *section 2.4*. The cells were then sorted and subclones were selected for comparable KIR3DL1 expression and cytotoxic capacity relative to wild type KIR3DL1 (Fig 3-11b and 11d). First, I examined if mutations of the ITIM motifs renders the loss of inhibition in the absence of LILRB1. As expected, the Y^2F mutant did not inhibit lysis of YTS cells in response to B*58:01 (Fig 3-11c), indicating that the two Ys within the ITIMs are important for transmitting the negative signal. A similar phenomenon was observed in the presence of endogenous LILRB1 in NKL cells (Fig 3-11e). These results suggest that mutations of Y398 and Y428 in the KIR3DL1 ITIMs disrupt the inhibitory signal and that LILRB1 cannot

compensate. However, in certain experiments, the lysis of B*58:01 did appear lower in comparison to that of parental 221 cells (Fig 3-12c).

Given we have observed some differences in the maximal lysis by various sublines of NKL, to better determine if there was any role for LILRB1 in KIR3DL1 signaling, I tested how various blocking antibodies affected the lysis. In agreement with previous reports (71), the anti-KIR3DL1 antibody, DX9, significantly reverted the inhibition seen with wildtype KIR3DL1 (Fig 3-12b). However, the strength of the inhibition in the presence of KIR3DL1 was perhaps slightly altered by M405, though not to a level reaching statistical significance relative to the matched isotype control (p=0.16, n=4) (7% lysis vs 5% lysis) (Fig 3-12b). Remarkably, the lysis was enhanced by the combination of DX9 and M405, relative to DX9 alone (p=0.0096, n=4) (Fig 3-12b), indicating a possible role for LILRB1 signaling in the presence of KIR3DL1.

To discriminate LILRB1 from KIR3DL1 in terms of inhibitory signaling, it is best done with the ITIM mutated KIR3DL1. As expected, the ITIM mutation resulted in reduction of the KIR3DL1 inhibitory signal in NKL cells (Fig 3-11c). Given that the clone expressing mutated KIR3DL1 has greater staining with DX9 than the cells expressing wild type KIR3DL1 (Fig 3-11d), the loss of inhibition was not due to less expression. In fact, a small reduction of lysis occurred when ITIM mutated KIR3DL1 interacted with B*58:01 relative to parental 221 cells based on the aggregated results from 4 experiments (Fig 3-12c). If LILRB1 enhances KIR3DL1 signaling as it does with KIR2DL1, the expectation is that there may be a decrease of lysis with the KIR3DL1Y^{2}F receptor, and that such a decrease should be reverted in the presence of DX9 or M405. Interestingly, relative to the isotype control, the lysis was increased by M405 (p= 0.07, n=4), but it was not further increased when both of DX9 and M405 were present (p=0.056, n=4) or significantly by DX9 alone (p=0.2, n=4) (Fig 3-12c). Together, the results indicate that if LILRB1 influences KIR3DL1 mediated signaling, the

influence is very weak. However, the one caveat to these experiments is the low level of KIR3DL1 expressed on the NKL cells relative to the levels on primary NK cells as shown by Fig 3-9a and 3-13. These levels may not drive MHC-I clustering sufficiently to invoke a LILRB1 signal.

3.2.9. *Anti-MHC-I-α3 antibody blocking of KIR3DL1 interaction with B*58:01*

Detectible LILRB1 signaling in response to B*58:01 was not observed in this system (Fig 3-12a). However, interestingly, a pan-reactive anti-MHC-I antibody, W6/32, that is known to block the interaction with LILRB1 (92, 171), slightly decreased NK lysis when LILRB1 was engaged with B*58:01. It must be noted that the same amount of the antibody as in other reports (92, 171) was used in this assay. Such a reduction was reproducible in three independent experiments but did not quite reach statistical significance (p = 0.06, n=4) (Fig 3-12a). Surprisingly, the same amount of W6/32 yielded a remarkable increase in the lysis similar to DX9 (p= 0.009, n=4) when KIR3DL1 was expressed at the cell surface (Fig 3-12b). Collectively, these results suggest that the enhancement in lysis by W6/32 is mainly caused by blocking KIR3DL1, and not the endogenous LILRB1.
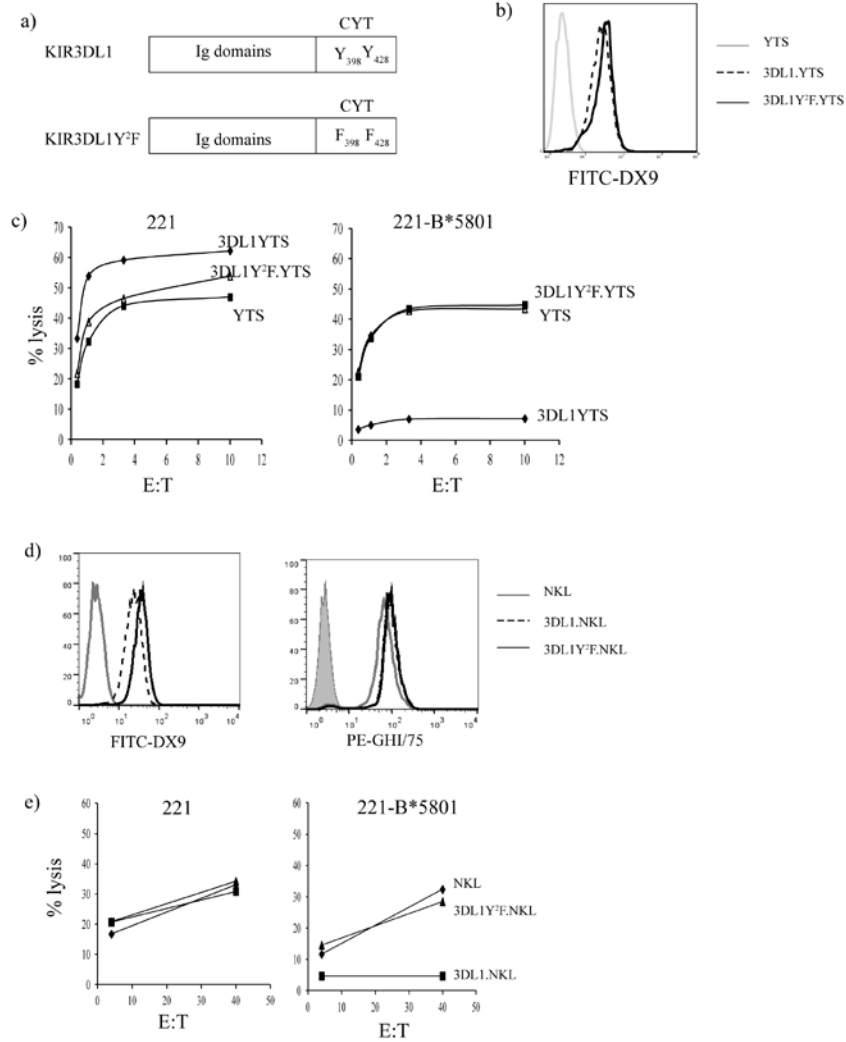
Figure 3-11. Mutating tyrosines to phenylalanines in the ITIMs of KIR3DL1 disrupts inhibitory signaling.

a) Schematic diagrams of wild type and ITIM mutated KIR3DL1. *b) and d)* Flow cytometric analysis of the indicated cells with FITC coupled anti-KIR3DL1 (DX9) or PE coupled anti-LILRB1 (GHI/75) antibodies. The filled histogram represents the matched isotype control. *c) and e)* The cytolytic analysis of the indicated cells at the various E:T ratios. A representative of three experiments is shown.
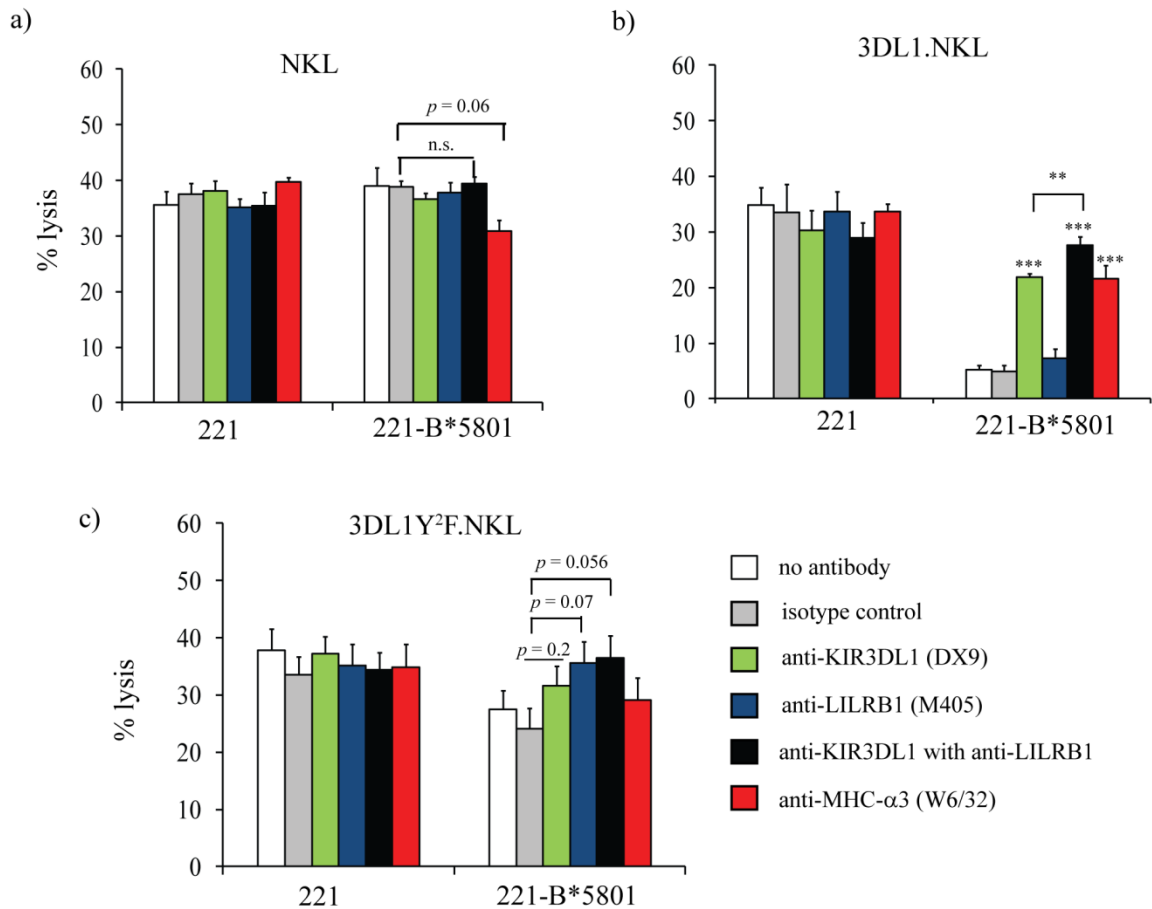
Fig 3-12. Antibody blocking of KIR3DL1 and LILRB1 on NKL cells.

The cytolysis of target cells by parental NKL *(a)*, NKL expressing wild type KIR3DL1 *(b)* and mutated 3DL1 *(c)* of 221 or 221 expressing HLA-B*58:01 was assessed at an E:T of 20:1 in the presence of 5 µg/ml of various antibodies (with the exception of W6/32 at 10 µg/ml) as shown in the legend beside *(c)*. The average of four experiments is shown with the standard error. ** indicates $p <$ 0.01-0.05, *** indicates $p <$ 0.01.
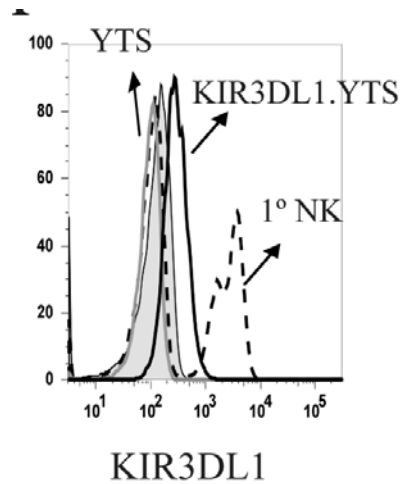
Fig 3-13. KIR3DL1 expression on primary NK cells and a stable KIR3DL1 expressing YTS clone.

Flow cytometric analysis of primary NK cells, parental YTS and YTS expressing KIR3DL1 using a FITC coupled DX9 antibody (anti-KIR3DL1). The filled histogram indicates the isotype control staining on primary NK cells.

3.3. Discussion

In this Chapter, I optimized the general retroviral transduction protocol supplied by Dr. Nolan's lab for transduction of three NK derived lymphoma lines, NKL, NK92 and YTS. This includes modification of incubation temperature to produce virus, incorporating a spin during the infection and the type of retroviral vector. Moreover, I successfully transferred the gene of interest, KIR3DL1*001 into three NK cell lines, NKL, NK92 (KIR$^-$LILRB1$^+$) and YTS (KIR$^-$LILRB1$^-$). However, I found that the lines did not express uniform amount of receptor and were not sufficiently stable when propagated as a mixed population. Therefore, I established subclones stably expressing KIR3DL1. I showed that the NKL and YTS clones expressing KIR3DL1 are able to induce KIR3DL1 inhibitory signaling when engaged by a cognate ligand, HLA-B*58:01. Furthermore, I studied the influence of LILRB1 on KIR3DL1 signaling by disrupting the intracellular signaling of KIR3DL1 in the presence of endogenous LILRB1. My results did not provide clear evidence that LILRB1 can cooperate with KIR3DL1 for inhibitory signaling, nor did they rule it out.

Of note, the KIR3DL1 positive YTS cells obtained here have less surface expression in comparison to primary NK cells (Fig 3-13) despite many attempts to obtain cells with higher expression. Although no direct comparison of KIR3DL1 surface level to primary NK cells was done for the NK92 and NKL subclones, these cells seem unable to express the receptor to a level similar to that being observed under physiological conditions, as suggested by Fig 3-9a. The reason for the limited expression may be a consequence of the expression system not producing enough transcript or may indicate that the cells lack other proteins required for optimal KIR3DL1 expression. Despite the relatively low surface level, KIR3DL1 presented on the surface of NKL and YTS was able to inhibit NK lysis, showing that the level of KIR3DL1 obtained is sufficient to induce inhibitory signaling in response to HLA-B*58:01, and suggesting that NKL and YTS cells are sensitive to inhibitory signaling. However, a similar level of KIR3DL1 on

NK92 cells failed to reduce NK lysis. Since possible defects in downstream inhibitory signaling molecules were ruled out, the lack of inhibition in NK92 cells is perhaps due to the high cytolytic capacity of NK92 as shown in Fig 3-9, which may be hard to be altered by the low level of KIR3DL1 obtained. As an alternative approach to obtain higher KIR3DL1 expression, I attempted to generate recombinant vaccina virus given that high expression with other KIRs have been obtained such as KIR2DL1, KIR2DL3 (171, 221) and KIR3DL1 (222). No KIR3DL1 positive recombinant viruses were obtained, in spite of the protocol being successful for other receptors in my hands.

LILRB1 enhances KIR2DL1 signaling though the signal derived from LILRB1 is hardly detectible when encountering with the KIR2DL1 ligand, HLA-C (171). Endogenous LILRB1 on NKL cells was also not able to trigger an inhibitory signaling in response to B*58:01 in this system (Fig 3-12a). However, in the presence of KIR3DL1 signaling, an additive effect by LILRB1 specific antibody, M405 (Fig 3-12b) suggests possible LILRB1 signaling. Here, I studied the potential effect of LILRB1 on KIR3DL1 signaling using the KIR3DL1Y^{2}F mutant. Mutation of the ITIM motifs caused the loss of KIR3DL1 signaling. If KIR3DL1 allows for LILRB1 signaling, the inhibitory signal induced by LILRB1 should have been observed and the inhibition should be reverted by anti-KIR3DL1, DX9, or anti-LILRB1 antibody, M405. However, my accumulated results with DX9 and M405 show only that there may be a weak inhibition in the presence of both of the receptors when KIR3DL1 lacks signaling ability. However, the blocking was not statistically significant. Hence, these results did not provide clear evidence for the role of LILRB1 in KIR3DL1 signaling.

KIR3DL1 is known to recognize HLA molecules carrying the Bw4 epitope, such as HLA-Bw4 or HLA-A2. Here, I have shown that W6/32 blocked KIR3DL1 interaction with HLA-B*58:01. The antibody is believed to react to the α2 and α3 domains of MHC-I (223) and block the LILRB1 mediated interaction

(92, 171). These results raise a possibility that KIR3DL1 interacts with or near the MHC-I-α3 domain. Moreover, it could perhaps explain why it is hard to detect any influence of LILRB1 on KIR3DL1 signaling if both of the receptors interact with MHC-I at the α3 domain. Given that W6/32 does not inhibit 2D KIRs and that the D1 and D2 domains provide the Bw4 specificity akin to KIR with 2D, the effect of W6/32 on KIR3DL1 is likely due to the D0 domain.

In summary, I established the optimized protocol of retroviral transduction and obtained NK clones stably expressing KIR3DL1. In addition, I tested the relationship of LILRB1 and KIR3DL1 on signaling in this system. In the course of these studies, new questions were raised for further examination regarding how KIR3DL1 interacts with HLA-B, such as why W6/32 blocks KIR3DL1 function.

Chapter 4

THE FIRST IG DOMAIN OF KIR3DL1 CONTACTS MHC CLASS I AT A SECONDARY SITE

Preface

Given the ill-defined role of the first Ig domain (D0) of KIR3DL1 and the observations in Chapter 3, the studies in this chapter were designed to explore the role of the KIR3DL1-D0 domain in ligand recognition. I have performed the majority of the experiments with the exception of Fig 4-21, which was done by Dr. Bart Hazes. I wrote the first draft of the manuscript. A major editorial contribution from my supervisor, Dr. Deborah Burshtyn, led to the final version of the paper. A version of this chapter has been published on *Journal of Immunology, 2011, 187:1816-1825.*

4.1. Introduction

The binding specificity of many of the inhibitory KIRs is understood. Particular KIRs bind subsets of class I HLA molecules that belong to defined groups with similar amino acids in region 77-80 of the α1-helix. For example, KIR2DL1 binds group 2 HLA-C molecules and KIR2DL2 and KIR2DL3 interact with group 1 HLA-C molecules. The interaction between these KIR2D receptors and their class I HLA ligands has been well defined by both mutagenesis and structural studies of the complex of the receptor and ligand (7, 70, 149). The inter-domain region between the Ig domains of KIR2D receptors makes contact with the top of the α1-α2 domain towards C-terminus end of the peptide binding groove (7, 149, 150, 224).

KIR3DL1 is highly polymorphic and can detect down-regulation of HLA-B molecules during HIV infection (225) and the combination of particular alleles of KIR3DL1 and HLA-B are associated with slower progression to AIDS (12). Despite the clear physiologic relevance of KIR3DL1, less is known about KIR3DL1 binding to its ligands compared to KIR2Ds. KIR3DL1 recognizes HLA-B and a few HLA-A molecules that possess the Bw4 epitope in the region on the α1-helix that corresponds to where KIR2D bind to HLA-C (168). Correspondingly, the Ig domains are named D0, D1 and D2 for the KIR3D receptors and D1 and D2 for the KIR2D receptors. Using Fc-fusion proteins, Long and colleagues first showed that the D1 and D2 domains were sufficient for the binding of HLA-B by KIR3DL1 (169). The specificity for Bw4 is determined by residues in KIR3DL1- D1 and D2 domains that are analogous to those in KIR2D that contact HLA-C (168). More importantly, the D0 domain has been reported to contribute to ligand recognition (168) but the mechanism of D0 contribution to binding has yet to be clearly defined. When these studies were initiated, the structure of KIR3DL1 had not been solved, and therefore, neither the orientation of D0 relative to D1 and D2 nor the points of contact of D0 with

MHC-I were known. Based on their studies of various human and chimpanzee receptors, Parham and colleagues proposed a model in which the D0 domain contacts both D1 and D2 to form a contiguous binding interface with the MHC-I (161). Curiously, they also identified a polymorphism in the α3 domain of HLA-Bw4 molecules that influences recognition by KIR3DL1 (167). The position of this residue (position 194) is on a loop at the base of the α3 domain near the membrane, and coincidentally, it is a contact residue with the broadly reactive receptor, LILRB1 (170).

Previously in Chapter 3, I showed an unexpected result that the anti-MHC-α3 antibody, W6/32, remarkably prevented KIR3DL1 mediated inhibition in comparison to the effect on LILRB1 using the NKL system. The result revealed a possibility that the first Ig domain (D0) of KIR3DL1 may play a role in the ligand recognition. In this Chapter, I present my study of the role of the D0 domain in binding and functional recognition of HLA-B molecules using soluble Fc fusion proteins and the YTS cell line. The results suggest that KIR3DL1-D0 domain interacts with HLA-B molecules carrying the Bw4 epitope, as well as other class I HLA molecules at a secondary site distance away from the conventional site.

4.2. Results

4.2.1. Characterization of KIR3DL1 specificity in YTS cells

To investigate KIR3DL1 function, I expressed KIR3DL1*001 in YTS cells which lack expression of endogenous KIR, LILRB-1, NKG2A and CD16 (Fig 4-1a). Subclones were isolated by cell sorting. However, it is important to note that the expression on the best clones was still significantly lower than on primary NK cells (Fig 4-1b). YTS cells expressing KIR3DL1 capable of lysing 221 cells at a similar level to parental YTS were inhibited when the target cells expressed HLA-B*58:01 (Fig 4-1c). As expected, expression of KIR2DL1, which does not interact with HLA-B, had no effect on YTS lysis of cells with B*58:01 relative to

parental 221 cells (Fig 4-1c). The recognition of B*58:01 by KIR3DL1 was blocked by the anti-KIR3DL1 antibody, DX9 (Fig 4-2).

4.2.2. Anti-MHC-a3 antibody blocking of KIR3DL1 mediated inhibition

The anti-MHC-α3 antibody, W6/32, has been reported to block LILRB1 interaction. In my hands, the antibody was shown to block KIR3DL1 mediated inhibition in the presence of LILRB1 (Fig 3-12b). To clarify the effect of W6/32 on KIR3DL1, here, I performed an antibody reversal experiment using KIR3DL1 transduced YTS cells as the cells lack LILRB1 expression. Interestingly, W6/32 blocked KIR3DL1 recognition of B*58:01, but as expected, it had no effect on KIR2DL1 recognition of HLA-Cw15 (Fig 4-2). These results confirm that an antibody that binds to the α3-region of MHC-I blocks KIR3DL1 in the absence of LILRBs.

To better understand if W6/32 blocks the same interaction as DX9, I tested if the combination of the antibodies was different than using each alone. I first established the dose that provides the maximal effect of DX9 or W6/32 alone (Fig 4-3a). Next, I determined the effects of combining the antibodies together using the optimal concentration of each antibody alone. Surprisingly, the combination of DX9 and W6/32 had a greater effect than either antibody alone (Fig 4-3b). Similar results were obtained with DX17 (Fig 4-3b), another antibody that binds to a broadly conserved epitope in class I HLA molecules and also likely in the α3-domain.

4.2.3. The functional recognition of non-Bw4 molecules by KIR3DL1

To further confirm the specificity of KIR3DL1 in YTS cells, I examined target cells with a weak Bw4$^+$ ligand, B*27:05 (226), as well as a Bw6$^+$ HLA-B molecule, B*07:02. As expected, the inhibition mediated by B*27:05 is less than that of B*58:01, and is blocked by DX9. Moreover, as we observed for 221-B*58:01 cells, W6/32 significantly increased the lysis of 221-B*27:05 cells (Fig

4-4) (226). Surprisingly, W6/32 increased the lysis of 221-B*07:02 cells whereas the anti-KIR3DL1 DX9 had no effect (Fig 4-4). The effect of W6/32 was small but reproducible and statistically significant ($p = 0.03$, n=4). The extra increase in lysis in the presence of W6/32 with DX9 for B*58:01, and particularly the increase of lysis of B*07:02 that lacks the Bw4 epitope only by W6/32, suggests that W6/32 blocks an interaction at a site distinct from the one blocked by anti-KIR3DL1, which is conserved and away from Bw4 epitope.
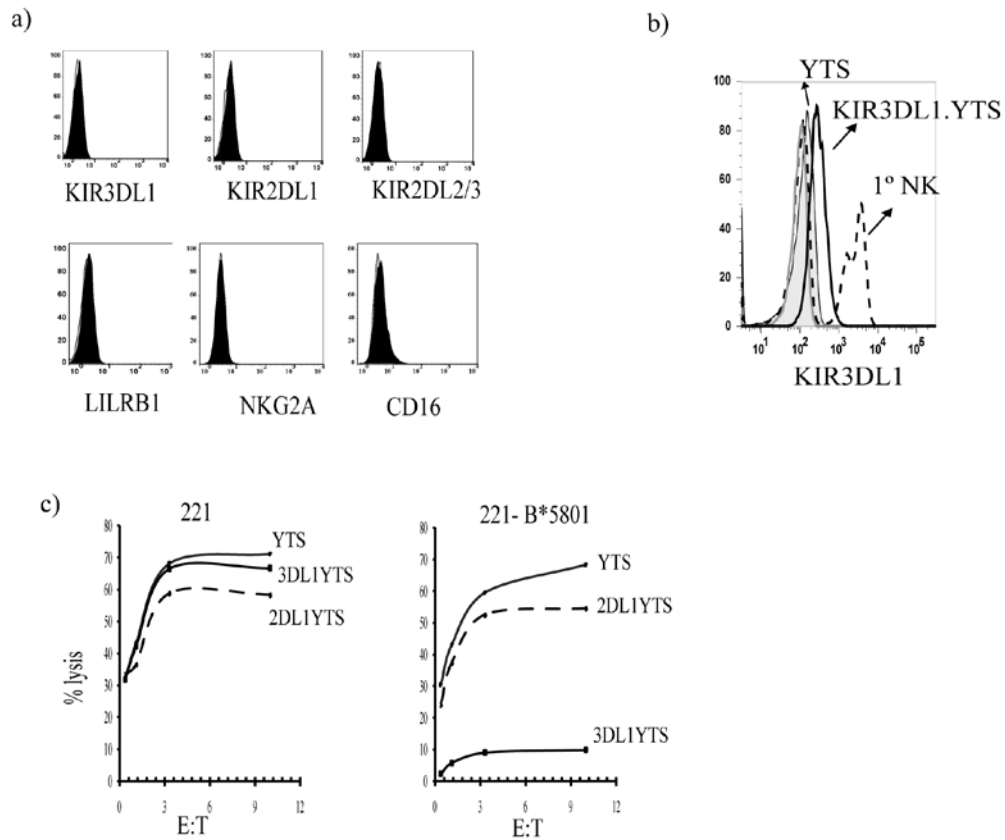
Figure 4-1. Characterization of YTS cells expressing KIR3DL1.

a) Surface staining of parental YTS cells with anti-KIR3DL1 (DX9), anti-KIR2DL1 (HP3E4), anti KIR2DL2/3 (DX27), anti-LILRB-1 (GHI/75), anti-NKG2A (Z199), followed by PE coupled anti mouse IgG (H+L). Fc receptor was stained with PE coupled anti-CD16 (eBioscience); *b)* Surface expression of KIR3DL1 on transduced YTS cells (3DL1.YTS) compared to primary NK cells. YTS cells (solid grey line), 3DL1.YTS cells (black line) or primary NK cells (dashed line) were stained with anti-KIR3DL1 (DX9). The isotype control is shown by the filled histogram for the YTS cells but is similar for all; *c)* KIR3DL1 recognition of B*58:01. Cytolysis of the indicated target cells was measured by ^{51}Cr release. The results are representative of three independent experiments with triplicate measurements.
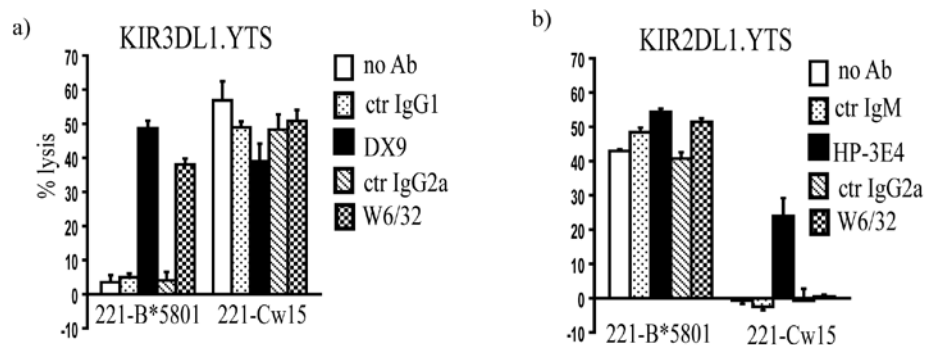
Figure 4-2. Anti-MHC-α3 blocks KIR3DL1 mediated inhibition.

Lysis of 221 cells expressing HLA-B*58:01 or HLA-Cw15 by YTS cells expressing KIR3DL1 *(a)* or KIR2DL1 *(b)*. The cytolysis was measured at an E:T of 1:1 in the presence of the indicated antibodies at 2.5 µg/ml. Representative of three experiments with triplicate measurements is shown and the error bars represent the standard error of the triplicates within the assay.
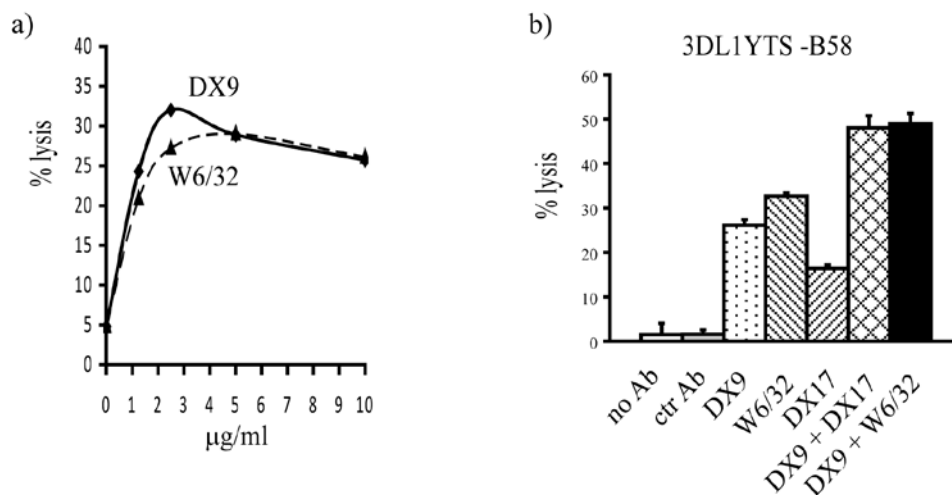
Figure 4-3. Antibodies blocking of functional recognition of HLA-B*58:01 by KIR3DL1.

a) Titration of antibodies blocking of KIR3DL1. 3DL1YTS lysis of 221-B*58:01 was performed with the indicated concentrations of antibodies. *b)* Combined effects of anti-KIR and anti-MHC-I antibodies. Lysis of 221 expressing HLA-B*58:01 cells by 3DL1.YTS cells was measured at an E:T =1:1 in the presence of 5 µg/ml DX17 or W6/32 and 2.5 µg/ml DX9. Representative of three experiments with triplicate measurements is shown and the error bars represent the standard error of the triplicates within the assay.
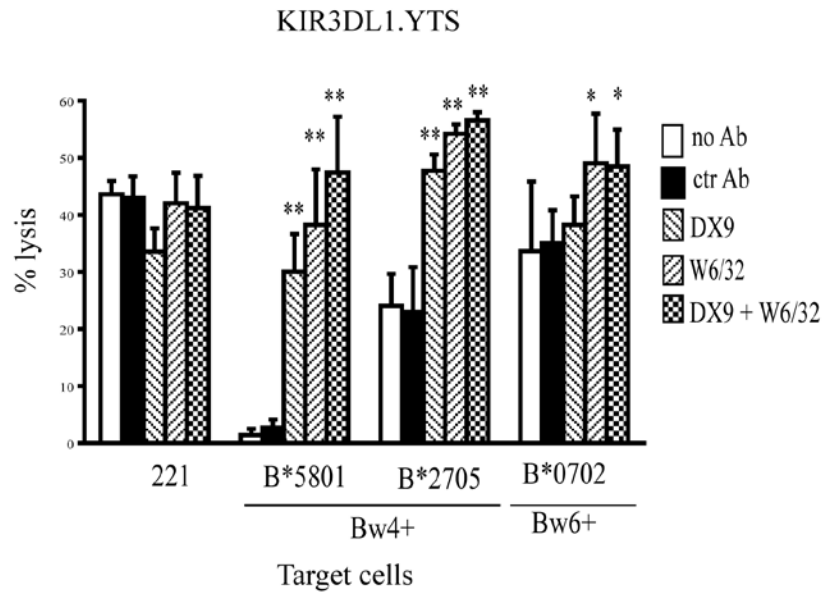
Figure 4-4. KIR3DL1 recognition of non-Bw4 ligands.

Lysis of 221 cells expressing the indicated ligands by YTS cells expressing KIR3DL1 was measured at an E:T=1:1. DX9 was added at 2.5 µg/ml and W6/32 at 5 µg/ml. The average of four experiments with triplicate measurement is shown. Error bars represent standard errors of the triplicates within the assay. ** indicates $p < 0.01$ and * indicates $p \leq 0.01\text{-}0.05$ compared to the corresponding control IgG.

4.2.4. *KIR3DL1 binding to Bw6$^+$ molecules*

To directly determine if KIR3DL1 bound non-Bw4 molecules and if W6/32 was blocking an independent binding site from DX9, I assessed the binding of KIR3DL1 to HLA-B molecules using a soluble Fc fusion protein, 3DL1Fc. The construct of 3DL1Fc was generated by means of linking extracellular Ig domains of KIR3DL1 with human IgG1 Fc fragment. The encoded protein was produced using Cos cells and confirmed with ELISA assay as described in Chapter 2. First, I performed a titration of 3DL1Fc protein and 221 cells expressing B*58:01 and B*07:02. As expected, 3DL1Fc bound to B*58:01 better than to B*07:02 (Fig 4-5a), in spite of there being a higher intensity of 221-B*07:02 than 221-B*58:01 based on W6/32 staining (Fig 4-5b). None-the-less, there was detectable binding to B*07:02 at high concentrations compared to the control Fc alone (Fig 4-5b).

Next, I examined how antibodies affected the binding. 3DL1Fc binding to B*58:01 was highly sensitive to W6/32 (Fig 4-6a). Virtually maximal blocking was achieved even at the lowest dose tested. Curiously, at the lowest concentration tested, DX9 potentiated the binding to B*58:01, but blocked at higher doses (Fig 4-6a). The requirement for the relatively high dose of DX9 compared with W6/32 is likely due to a requirement to saturate the amount of fusion protein in the assay (150 µg/ml). Finally, I tested the effect of combining DX9 and W6/32 at the maximal doses on binding to HLA-B58. I observed a consistent greater reduction of the binding than each antibody alone (p=0.007, n=4) according to Anova test (Fig 4-6b). I also observed weak but detectable binding of 3DL1Fc to B*07:02 that was blocked by W6/32 to a greater extent than DX9 (Fig 4-6b). These results are consistent with what we observed in the functional assays where both antibodies were required to fully block the receptor recognition of B*58:01 but only W6/32 blocked recognition of B*07:02. These results also suggest the binding being blocked by W6/32 is independent from that being blocked by DX9, although the two sites may synergize for higher binding.
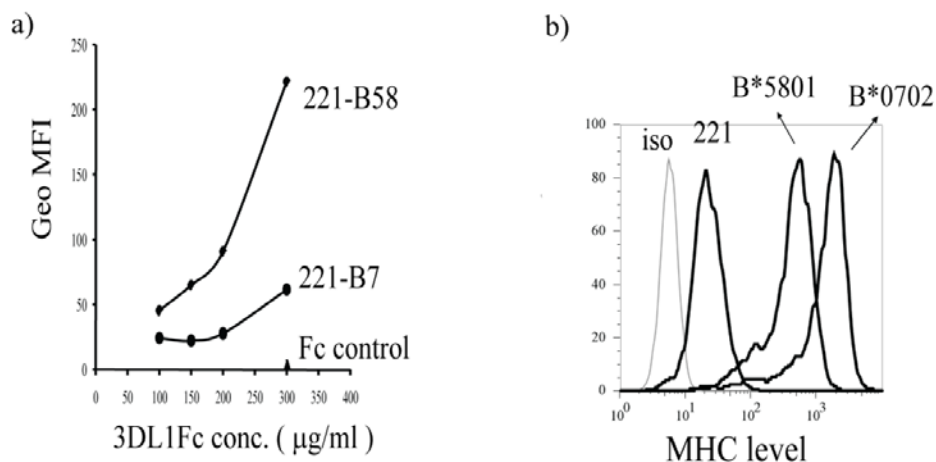
Fig 4-5. Titration of 3DL1Fc binding to HLA-B molecules.

a) Titration of purified 3DL1Fc to 221 cells expressing HLA-B*58:01 and HLA-B*07:02. The binding assay was performed at 4°C as described in Chapter 2, and the results were calculated as geometric mean fluorescent intensity (Geo MFI) of 3DL1Fc binding subtracted to Geo MFI of Fc control. The concentration of the 3DL1Fc is indicated on the x-axis. *b)* The indicated cells were stained with W6/32 and PE anti-mouse IgG. The isotype control is represented by the grey line histogram.
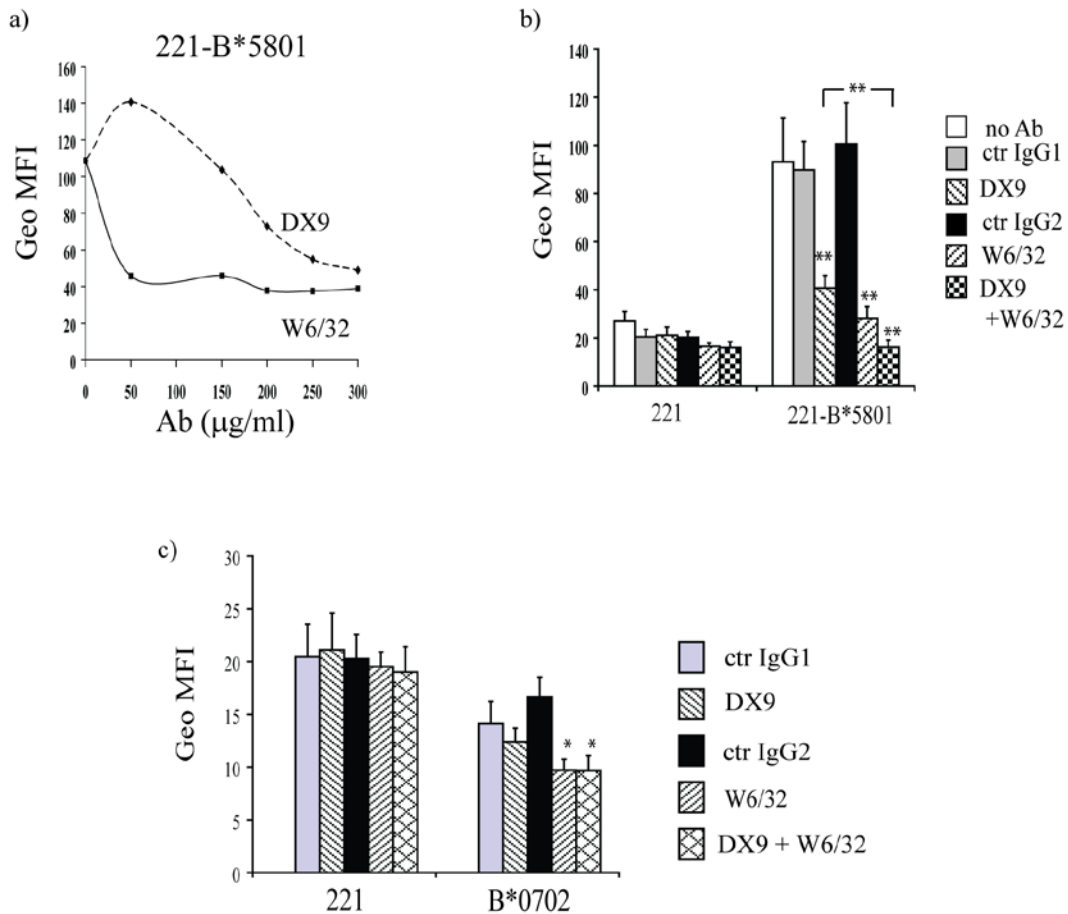
Fig 4-6. Antibodies blocking of 3DL1Fc binding to HLA-B molecules

*a)*Antibody blocking of 150 µg/ml 3DL1Fc binding to B*58:01. The concentration of the antibodies is indicated on the x-axis. *b)* Blocking by the combination of antibodies. The binding of 3DL1Fc was measured at 150 µg/ml with 50 µg/ml of W6/32 or 300 µg/ml of DX9 and control IgGs at the corresponding concentrations. *c)* W6/32 blocks 3DL1Fc binding to 221 cells expressing B*07:02. The binding of 3DL1Fc was measured at 150 µg/ml and the indicated antibodies were added as described in *b)*. For *b* and *c*, the average of three independent experiments with the error bars is shown. The statistical significance was calculated using Anova single factor test. ** indicates $p < 0.01$ and * indicates $p \leq 0.01\text{-}0.05$ compared to the corresponding control IgG.

4.2.5. D0 effects on 2DL1 mediated inhibition when engaging with HLA-Cw15

The simplest explanation for how W6/32 blocks KIR3DL1 but not KIR with only two Ig domains (e.g. KIR2DL1) is steric interference due to the presence of the D0 domain. To determine the effect of W6/32, I examined antibody blocking of KIR2DL1 mediated inhibition when EGFP was present at its N-terminus, HG (Fig 4-7a). The addition of EGFP at N-terminal of KIR2DL1 is known to interefere with the strength of the inihitory signal (189). Unlike the effect of W6/32 on KIR3DL1 (Fig 4-2), the antibody had only a minimal effect on function of KIR2DL1 in comparison to HP3E4 that binds to KIR2DL1 (Fig 4-7b). Interestingly, the combination of these two antibodies had a greater effect than each antibody alone, and the effect was statistically significant according to Anova single factor test (p=0.045, n=3) (Fig 4-7b). Since W6/32 does not interact with EGFP and KIR2DL1, the results suggest that W6/32 sterically interferes KIR2DL1 recognition of Cw15 in the presence of EGFP. However, steric interference does not explain the observation of the greater effect of W6/32 on KIR3DL1 interaction in comparison to HG (Fig 4-2 and 6c vs Fig 4-7b) and why DX9 does not prevent the recognition of B*07:02 by KIR3DL1 (Fig 4-4 and 4-6b).

Another possible explanation is that W6/32 blocks broad binding contributed by the D0 domain, while DX9 blocks the canonical and more Bw4-specific binding contributed by D1 and D2. Therefore, to determine if D0 is required for the effect of W6/32, I generated a chimeric receptor that links D0 of KIR3DL1 with KIR2DL1 (Fig 4-8a), and expressed it in YTS cells. It is worth noting that the N-terminal histidine of KIR2DL1 is missing, but I have previously shown a corresponding mutation in the wildtype receptor only minimally compromises the function of this receptor in YTS cells (189). The D02DL1 receptor was detectable at the cell surface with anti-KIR2DL1 (HP3E4) but not anti-KIR3DL1 (DX9) (Fig 4-8b). In the clones we obtained, the surface staining of the chimeric protein was less than wild type 2DL1 when detected by HP3E4

(Fig 4-8b). Functional recognition of Cw15 by D02DL1 was blocked by the presence of HP3E4 (Fig 4-8c). However, even at doses well beyond that required to interfere with KIR3DL1, W6/32 did not have an effect on D02DL1 (Fig 4-8c). This result indicates W6/32 blocking of KIR3DL1 is unlikely to be due to steric interference unless the orientation of the D0 domain in the chimera is quite different than in KIR3DL1. However, we also observed that the inhibition by D02DL1 was further reverted by anti-KIR2DL1 in combination with W6/32 (Fig 4-9a), which was not the case for 2DL1YTS cells (Fig 4-9b). The difference in lysis for the addition of W6/32 relative to HP3E4 alone was statistically significant for results pooled from several experiments using Anova test (p =0.02, n=4) (Fig 4-9). These results suggest that there may be some steric effect of W6/32 on the chimeric receptor interacting via the D1D2 domain but that this is only evident in the presence of HP3E4. This would imply HP3E4 cannot block the chimeric receptor as well as it blocks KIR2DL1. However, it is also possible that the D0 domain confers an independent binding interaction that is blocked W6/32.
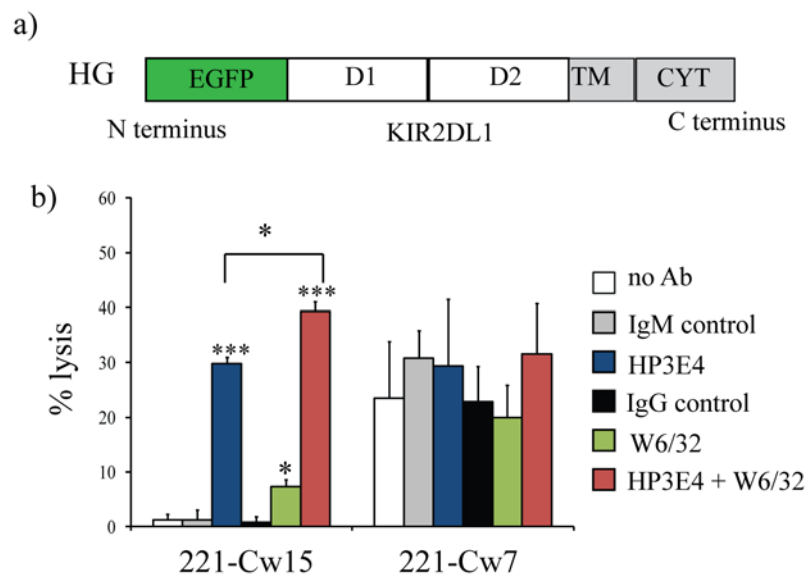
Fig 4-7. Steric interference of W6/32 on EGFP-KIR2DL1 inhibition.

a) Schematic diagram of HG. *b)* Cytolysis of 221 expressing Cw15 or Cw7 by YTS expressing HG at an E:T = 2:1. The statistical significance was calculated using Anova single factor test. The average of three independent experiments with the error bars is shown. *** indicates $p < 0.001$, ** indicates $p < 0.01$ and * indicates $p \leq 0.01$-0.05 compared to the corresponding control IgG.
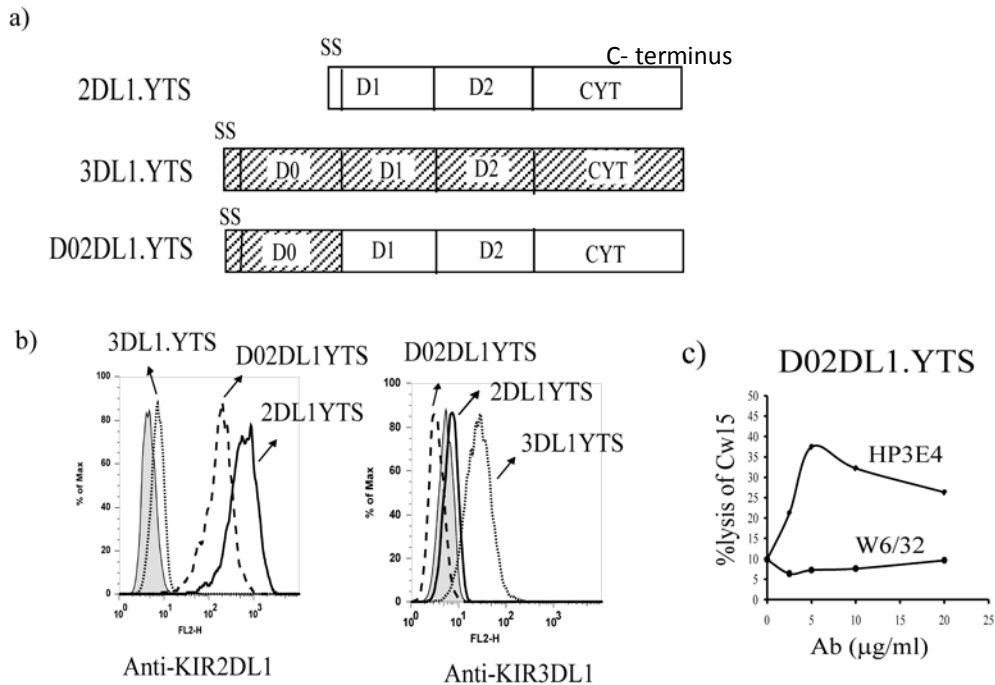
Fig 4-8. Characterization of D02DL1 chimeric receptor

*a)*Schematic diagram of 2DL1, 3DL1 and D02DL1 constructs. For the D02DL1 chimera, there is a linker between D0 of 3DL1 consisting of the residues ADPN. SS stands for signal sequence. *b)*Surface expression of D02DL1. YTS cells were stained by anti-KIR2DL1 (HP3E4) or anti-KIR3DL1 mAb (DX9) as indicated on the x-axis or the isotype control (MOPC21, filled histogram). *c)* Titration of antibody blocking of D02DL1YTS lysis of 221-Cw15. The concentrations of the antibodies are indicated on the x-axis. Representative of three experiments with triplicate measurements is shown.
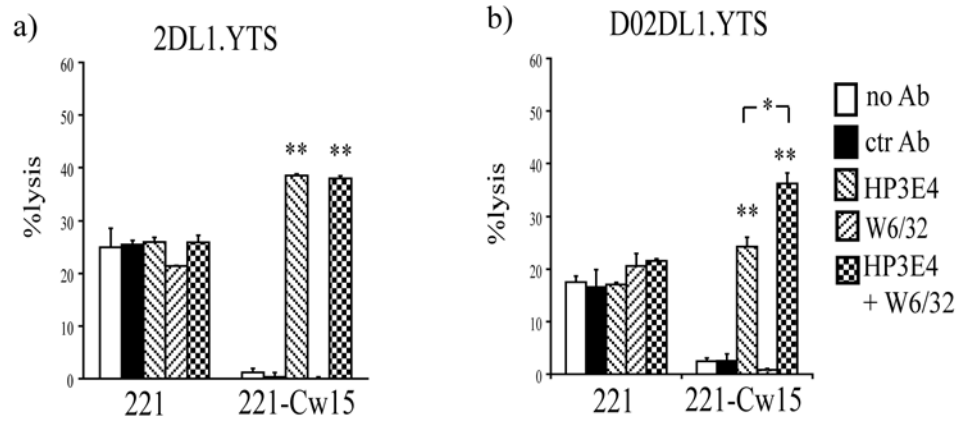
Fig 4-9. Effect of W6/32 on the functional interaction of 2DL1 chimeric receptors with Cw15.

KIR2DL1 *(a)* or D02DL1 *(b)* inhibits NK lysis of 221 cells expressing HLA-Cw15. Cytolysis was measured at an E:T of 2:1 in the presence of the indicated antibodies at 5 µg/ml. Statistical significance was calculated using Anova single factor test. The results are the average of four independent experiments with triplicate measurements and the error bars represent the standard errors of the triplicates within the assay.   ** indicates $p < 0.01$ and * indicates $p \leq 0.01\text{-}0.05$.

4.2.6. D0 effects on KIR2DL1 binding to HLA-Cw15

Based on the results with D02DL1 and the pattern of antibody blocking in the functional assays, I formulated the hypothesis that the D0 domain conferred weak but broad binding to MHC-I at a site blocked by W6/32. Therefore, as a strategy to isolate its binding characteristics, I generated a chimera of D0 from KIR3DL1 with KIR2DL1 as an Fc-fusion similar to what we expressed in YTS cells (Fig 4-10a). The resulting chimeric receptor D02DL1Fc has a three-residue linker (Pro.Leu.Ala) and maintains the N-terminal histidines of KIR2DL1. The intact chimeric D02DL1Fc appears slightly larger in size than wildtype 3DL1Fc under reducing conditions on SDS-PAGE. It is also quite smeared under non-reducing conditions, perhaps due to heterogeneous glycosylation or limited proteolysis (Fig 4-10b). Under non-reducing conditions, a product at about 70kDa was evident for KIR3DL1Fc and to some extent for D02DL1Fc, but not KIR2DL1. A smaller band for both also appeared under reducing conditions (~30kDa) suggesting the former was a breakdown product as opposed to monomeric receptor and again suggesting something in the D0 domain leads to protein instability. Western blotting confirmed the small fragments for 3DL1Fc contains the Fc portion of the protein (Fig 4-10c).

I next measured the reactivity of the fusion proteins with anti-KIR2DL1 and anti-KIR3DL1 antibodies that bind the folded cell surface receptors using a capture ELISA assay (Fig 4-11). As expected, D02DL1Fc reacted with the anti-KIR2DL1 antibody HP-3E4, but the sensitivity was less compared to wild type 2DL1Fc, suggesting that the addition of D0 somehow perturbs the accessibility of the epitope or folding of the KIR2DL1 domains. The D02DL1Fc chimera was not detected by the anti-KIR3DL1 antibody DX9, which fits our result that DX9 did not detect the chimeric receptor expressed on the YTS cells (Fig 4-8b) and published results that D0 alone had minimal reactivity with DX9 (169).

To determine the function of D02DL1Fc, I first tested its ability to bind to HLA-C proteins expressed on 221 cells. As expected, D02DL1Fc bound HLA-Cw15, a known ligand of KIR2DL1. However, the mean fluorescent intensity (MFI) corresponding to the binding to HLA-Cw15 was more than 10 fold less than 2DL1Fc used at the same concentration (Fig 4–12α). However, the high concentration of D02DL1Fc required to detect the interaction was similar to that required to detect binding of KIR3DL1 to its known HLA-Bw4 ligands. The anti-KIR2DL1 antibody, HP3E4, was able to block the interaction, but there was also an effect of W6/32 alone but it only partially blocked binding to HLA-Cw15 (Fig. 4-12b). In agreement with the functional results using YTS cells, anti-KIR2DL1, but not W6/32, fully blocked 2DL1Fc binding to Cw15 (Fig 4-12c). On the other hand, the binding of D02DL1Fc to Cw15 was blocked by anti-KIR2DL1 and partially by W6/32 but the two antibodies combined for a maximal effect (p=0.04, n=4) according to Anova single factor test (Fig 4-12c). The inability of anti-KIR2DL1 to fully block the binding of D02DL1, while it is blocked along with W6/32 suggests D0 can bind MHC-I independently of D1D2 and that the specificity of this interaction includes Cw15. If D0 confers binding to a second site on HLA-C, this might occur for KIR3DL1 and D02DL1 with various other MHC-I molecules. A very low level of binding to Cw7 was observed and there is a significant decrease in the presence of W6/32 (Fig 4-12d). However, the Cw7 cells coincidentally have considerably less staining with W6/32 relative to 221 expressing Cw15 (Fig 4-13a). Therefore, I reasoned that KIR3DL1 might also exhibit such binding to HLA-Cs if weak broad reactivity was due to the D0. Supporting this we observed very weak binding of 3DL1Fc to Cw7 and Cw15 (Fig 4-13b). The binding is reduced by W6/32 (Fig 4-13b). A functional interaction of KIR3DL1 and Cw7 blocked by W6/32 but not DX9 was also detected over repeated experiments (Fig 4-13c). It is not clear why a functional interaction with Cw7 was observed here and not with Cw15 (Fig 4-2).

123
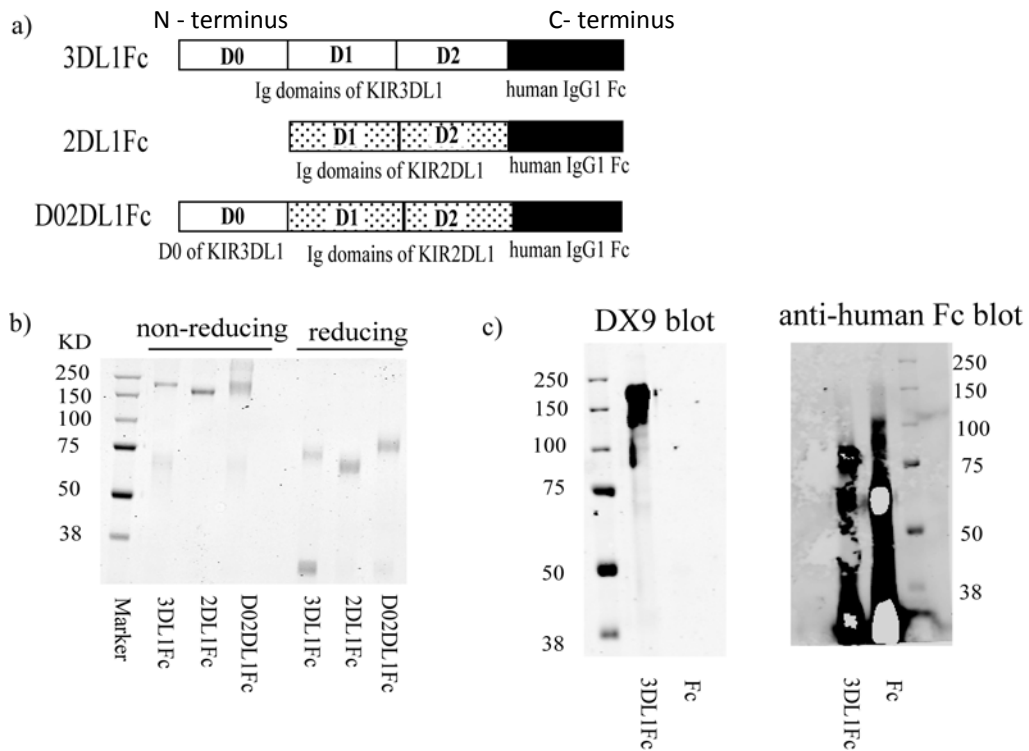
Fig 4-10. Characterization of fusion proteins.

*a)*Schematic diagram of 3DFc, 2DFc and D02DFc respectively indicating the corresponding regions of KIR2DL1 and KIR3DL1. *b)* SDS-PAGE analysis of purified fusion proteins. The samples were run under non-reducing (left lanes) and reducing (right lanes) conditions stained with Coomassie. 1 µg of samples were loaded on each lane. *c)* Western blot of 3DL1Fc and Fc with anti-KIR3DL1 (DX9) and anti-human Fc antibodies.
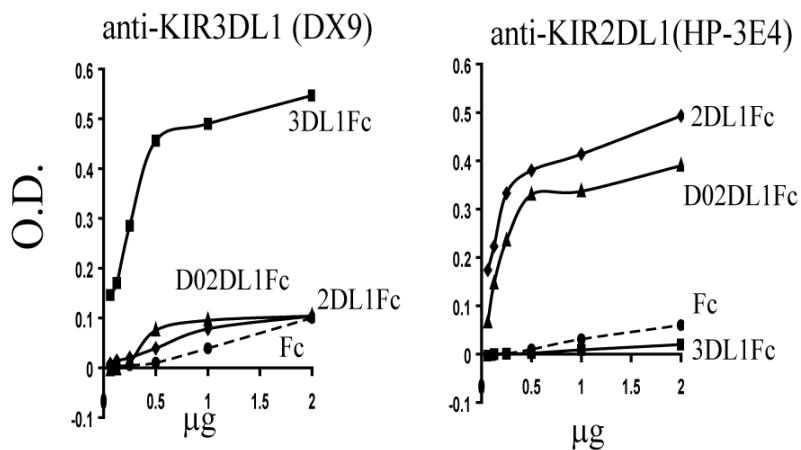
Fig 4-11. Detection of soluble Fc fusion by anti-KIR antibodies.

The indicated dilutions of Fc fusion proteins were captured on plates coated with anti-human IgG1 Fc mAb followed by the KIR-specific antibody and detection with AP-conjugated goat-anti-mouse IgG or IgM antibody for ELISA. See Chapter 2 for details. The results shown are representative of three experiments.
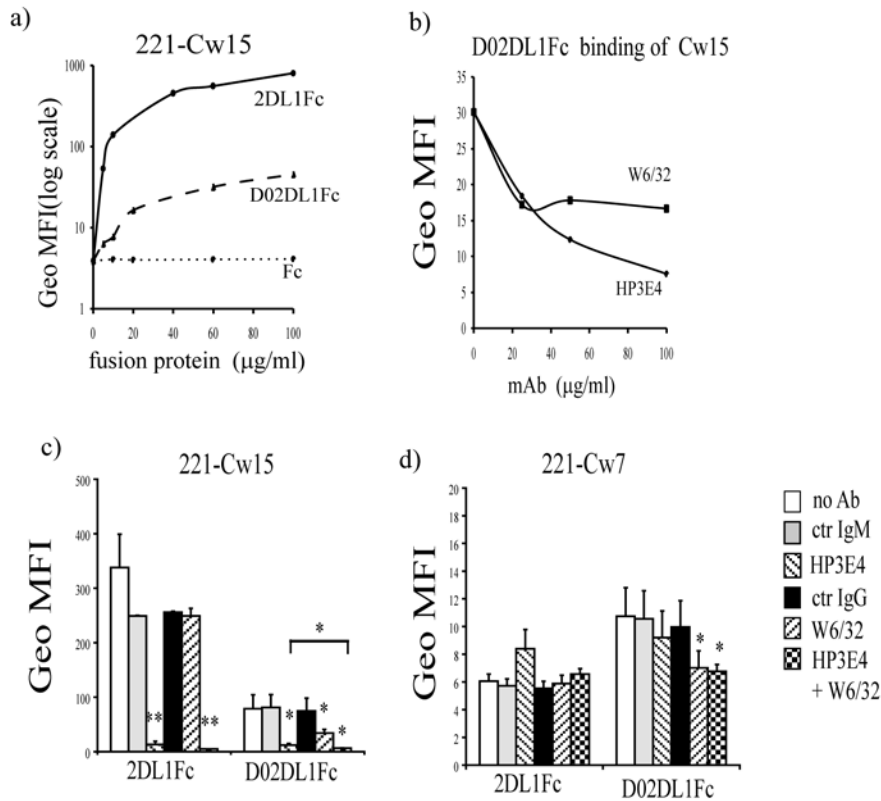
Fig 4-12. Binding of purified Fc fusion proteins to 221 cells expressing Cw15.

a) The purified D02DL1Fc, 2DL1Fc or Fc proteins were incubated at the concentration shown on the x-axis and the bound proteins were detected as described in Chapter 2. *b)* Antibody blocking of D02DL1Fc binding to cells expressing HLA-Cw15. The binding of D02DL1Fc at 100 µg/ml to Cw15-221 cells was measured with various amounts of HP-3E4 or W6/32 as indicated at x-axis. *c) and d)* Fc-fusion protein binding to the indicated cells in the presence of antibodies. 150 µg/ml HP-3E4 or 50 µg/ml W6/32 were incubated with target cells at room temperature for 10 min, then 10 µg/ml 2DL1Fc or 100 µg/ml D02DL1Fc were added and incubated at 4°C for 1 hr. The cells were washed and stained with PE anti-human Fcγ. The isotype matched IgM and IgG controls were added at 100 and 50 µg/ml respectively. The fusion proteins are indicated on the x-axis. Statistical significance was calculated using Anova single factor test. ** for $p < 0.01$ and * for $p \leq$ 0.01-0.05.

126
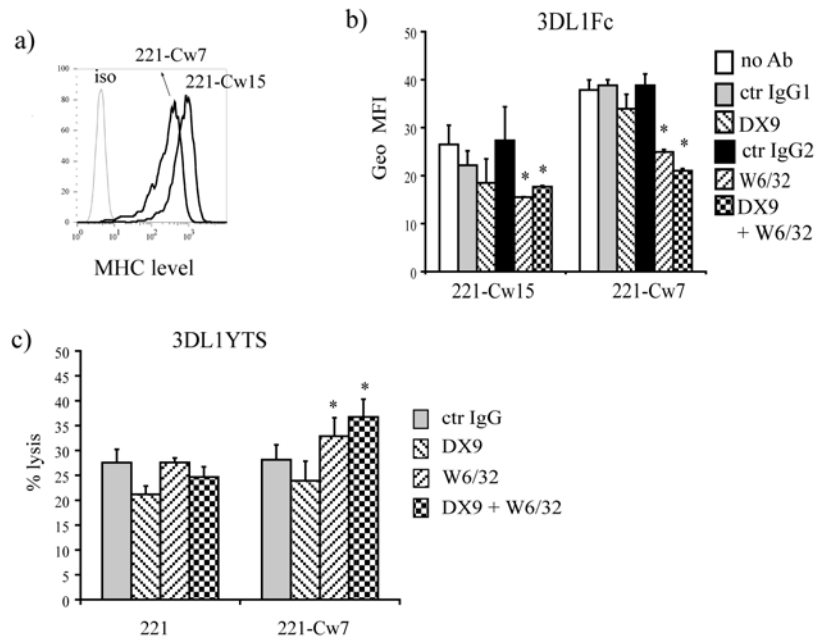
Fig 4-13. 3DL1Fc binds to HLA-Cw15.

a) Surface expression of MHC-I on 721.221 cells expressing Cw7 or Cw15. The indicated cells were stained with W6/32 and PE anti-mouse IgG. *b)* 3DL1Fc binding to HLA-Cw7 cells. 200 µg/ml DX9 or control IgG1(MOPC21) or 50 µg/ml W6/32 or control IgG2 (51.1) were preincubated with indicated cells at room temperature for 10 min. 200 µg/ml 3DFc was then added. *c)* 3DL1YTS cell lysis of targets at an E:T of 1:1. The indicated antibodies were added as *Fig 4-4*. Statistical significance was calculated using an unpaired student's *t* test. The means with standard error are shown as error bar with three to four independent experiments. The *p* values indicate the statistical significance relative to control antibodies with ** for $p < 0.01$ and * for $p \leq 0.01\text{-}0.05$.

4.2.7. D0 confers weak binding and recognition of HLA-B

To investigate if D0 conferred recognition of HLA-B molecules, we first examined the lysis of 221 expressing HLA-B*58:01 by YTS cells expressing the D0KIR2DL1 chimeric receptor (Fig 4-14). Although there was only a slight reduction in lysis of 221-B*58:01 cells relative to 221-Cw7, the reduction appeared to be specific to D02DL1 because it did not occur with 2DL1-YTS. Moreover, W6/32 specifically enhanced the lysis of HLA-B*58:01 targets compared to the matched isotype control and but HP3E4 did not. The effect is small but statistically significant (p=0.013, n=4). In parallel, we also tested if the soluble chimeric protein D02DL1 bound B*58:01. D02DL1Fc bound both B*58:01 and B*07:02 (Fig 4-15a), and the binding to B*58:01 was reduced by the anti-MHC-I α3 W6/32 relative to isotype matched control (Fig 4-15b). Curiously, the anti-KIR2DL1 antibody actually increased the binding compared to control IgM, but the increase was negated by W6/32 suggesting it was caused by specific binding to the MHC-I (Fig 4-15b). It is possible that multimerization of the chimera by the antibody actually enhances the binding via the D0 domain and similarly for DX9 with KIR3DL1 as seen in Figure 4-2a.

Together, these results suggest that D0 confers on 2DL1 the ability to interact with HLA-B molecules in a way that is independent of the conventional D1/D2 interaction, and blocked by the antibody binding to the MHC α3 domain.
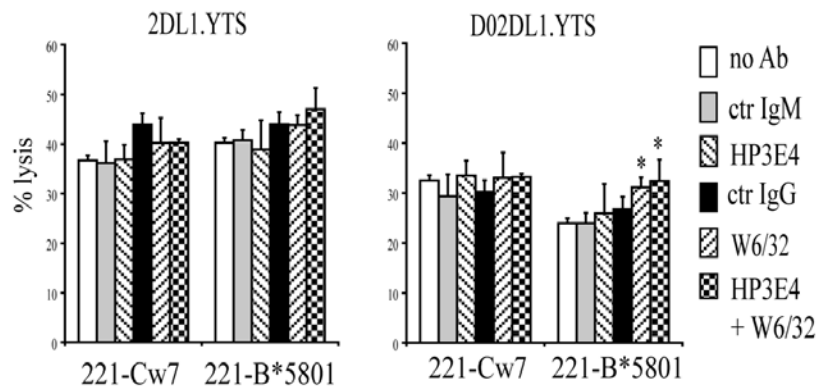
Fig 4-14. Cytolysis of 221-B*58:01 cells by YTS cells expressing D02DL1.

Lysis of 221 cells expressing the indicated ligands by YTS cells expressing KIR2DL1 or D02DL1 was performed at an E:T=1:1. The concentration of antibodies was added as Fig 4-4. The results are the average of three experiments with triplicate measurements, the error bars indicated standard error. The p values indicate the statistical significance relative to control antibody with * for $p \leq 0.01$-0.05.
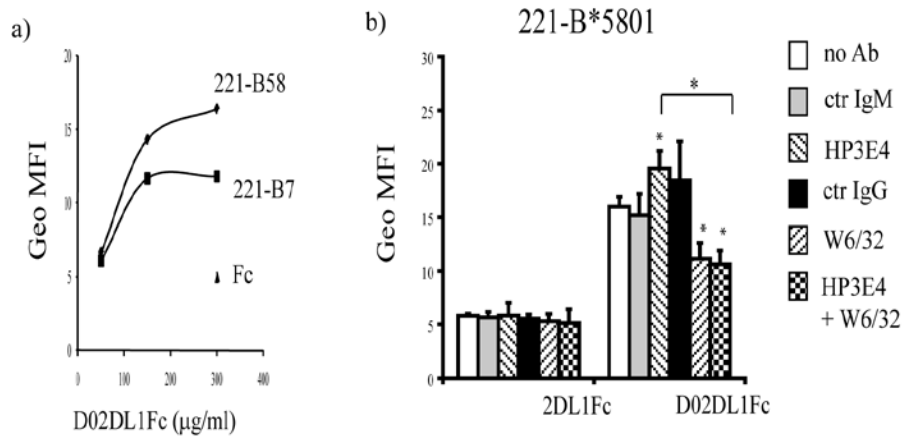
Fig 4-15. D02DL1Fc recognition of HLA-B*58:01.

a) The binding of D02DL1Fc to indicated cells. The concentration of the proteins (D02DL1Fc and Fc) was indicated at x-axis. A representative experiment was shown. *b)* D02DL1Fc binding to 221 and HLA-B*58:01 transduced 221 cells. The binding was done at 200 µg/ml D02DFc with 200 µg/ml HP3E4 and its IgM control or 50 µg/ml W6/32 and its IgG control. The results are the average of three experiments, the error bars indicated standard error. The *p* values indicate the statistical significance using Anova single factor test relative to control antibody with * for $p \leq 0.01\text{-}0.05$.

4.2.8. KIR3DL -D0 recognition of HLA-G

The results shown above with the soluble receptors suggests that the D0 domain of KIR3DL1 confers weak but significant amount of binding to a range of class I HLA and this binding is sensitive to inhibition by antibodies to a highly conserved region in the α3 domain of the MHC-I proteins. Therefore, we investigated the possibility that the D0 domain interaction would extend to a non-classical MHC-I molecule that is also reactive with the antibody W6/32, HLA-G. 3DL1YTS lysis of 221 cells expressing HLA-G was not reduced relative to 221 cells, but the presence of W6/32 increased the lysis compared to that of control antibody (Fig 4-16a). Although the effect is not strong, it was reproducible and significant for data aggregated from several experiments (Fig 4-16b). To further characterize the binding of 3DL1, and more specifically D0 to HLA-G, we tested if the soluble receptors could have some binding to 221 cells expressing HLA-G (Fig 4-17). Of note, these cells do not express HLA-E (Fig 4-17). We observed some binding of 3DL1Fc to HLA-G, and lower but detectable binding of D02DFc (Fig 4-17). Despite the relatively low degree of binding, W6/32 but not the relevant anti-KIR antibodies that bind the D1/D2 domains blocked the binding (Fig 6E and F). Similar to the binding of D02DL1 to B*58:01, the anti-KIR antibodies actually enhanced the binding of 3DL1Fc and D02DFc to HLA-G. These results support the idea that D0 confers weak but broad binding blocked by W6/32.
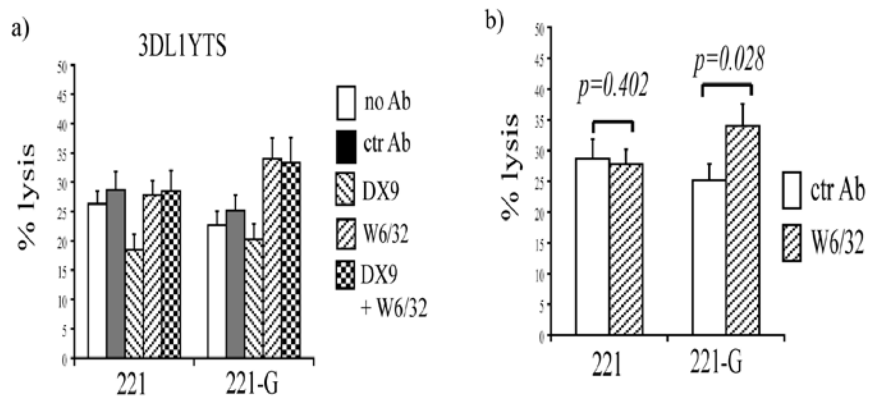
Fig 4-16. 3DL1YTS lysis of expressing HLA-G.

a) Cytolysis of 221 and 221 expressing HLA-G by 3DL1YTS at an E:T of 2:1, in the presence of antibodies as indicated in the legend. The concentrations of antibodies were added as Fig 4-4. *b)* The average lysis obtained under each condition as shown in *a)* for 10 experiments. The *p* values were calculated using student t test.
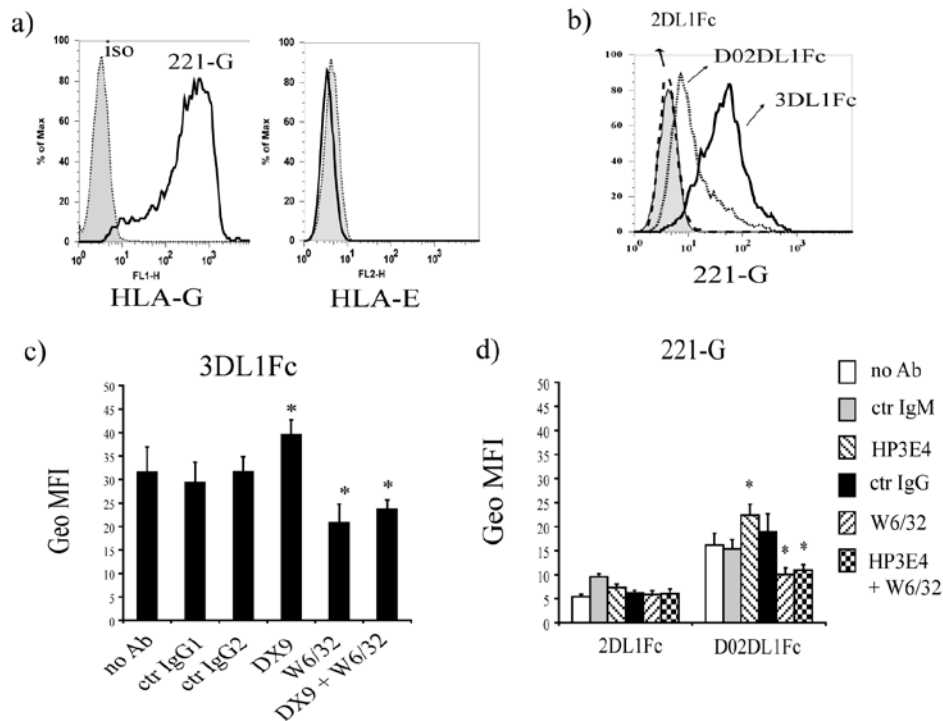
Fig 4-17. KIR3DL1-D0 binding to HLA-G.

a) The surface expression level of HLA-G. The cells were stained with control IgG (grey fill histograms) or anti-HLA-G or anti-HLA-E (black lines) as indicated on the x-axis and analyzed by flow cytometry. *b)* Binding of fusion proteins to 221-G cells. The indicated fusion proteins were added at 200 µg/ml. Fc alone is shown in grey filled histogram. *c)* W6/32 but not DX9 blocks 3DFc binding of 221-G. The blocking antibodies are indicated in x-axis. *d)* D02DFc blocked by W6/32 and not HP3E4. The binding of the fusion proteins indicated on the x-axis were measured as before. Antibodies and fusion proteins were added as Figure *4-15*. The results in *c)* and *d)* are the average of three experiments, the error bars indicated standard error. The *p* values indicate the statistical significance relative to control antibody with * for $p \leq 0.01\text{-}0.05$.

133

4.2.9. Z27 mAb recognizes D0 and blocks D0-MHC-I interactions

As an alternative method to test if W6/32 interfered with a distinct interaction of KIR3DL1, I expressed in YTS cells a mutated KIR3DL1 substituted Y200 to A in the D2 domain known to compromise recognition of B58 (168). This mutation disrupts the DX9 epitope, but not the epitope for another antibody, Z27 (Fig 4-18a). As expected the mutation reduced the inhibition and removed the ability of DX9 to increase the lysis for cells expressing B*58:01. However, for this mutant receptor, W6/32 also significantly increased the lysis specifically of the cells with B*58:01 (Fig 4-18b) again suggesting that the site W6/32 blocks was distinct from that of the Bw4 epitope. Given we had determined that Z27 still bound the mutant receptor, we tested if Z27 could in fact block KIR3DL1 recognition of the B*58:01. Z27 did block KIR3DL1 recognition of B*58:01, but when combined with W6/32, it did not augment the lysis significantly (Fig 4-19a). There was also no increased effect of combining DX9 with Z27 relative to each antibody alone, but the DX9 also blocks binding of Z27 to KIR3DL1 (Fig 4-19b). In view of the ability of Z27 to block KIR3DL1 recognition of B*58:01 and to bind to 3DL1Y200A, we tested if Z27 blocked the binding to molecules that lack the Bw4 epitope. Z27 blocked 3DL1Fc binding to B*07:02 with a dose response similar to W6/32 as opposed to DX9 (Fig 4-20a). Here we did not observe any augmentation of the binding with low doses of the antibody Z27. The results suggest that Z27 blocks KIR3DL1 function by preventing the binding of the D0 domain. To more directly test this, we determined that Z27 recognizes the D0 domain in the D02DL1 chimera (Fig 4-20b) and that it blocks the binding of D02DL1Fc to both B*58:01 and HLA-G (Fig 4-20c). Taken together these results suggest that Z27 binding to D0 blocks D0's interaction with a conserved region of the MHC-I that is distinct from the canonical specificity site corresponding to the Bw4 epitope.
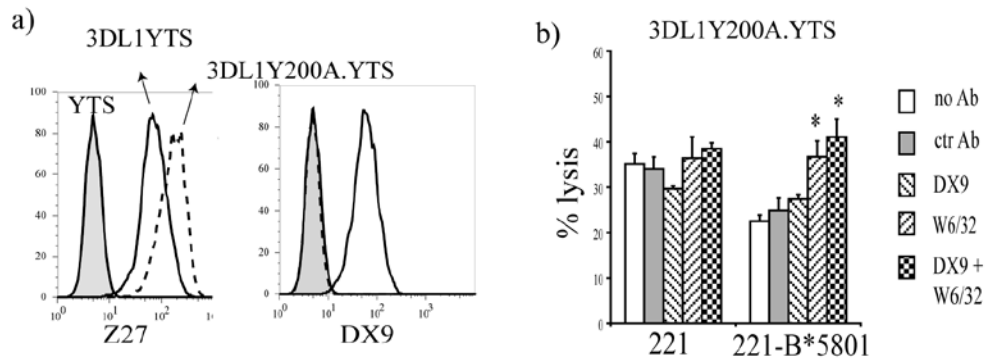
Fig 4-18. Y200A abolishes DX9 recognition.

a) The surface staining of YTS, 3DL1-YTS and 3DL1Y200A-YTS by PE coupled DX9 or PE coupled Z27 antibodies. *b)* Y200A interrupts 3DL1 inhibition. The assay was measured at an E:T= 2:1. Antibodies shown in the legend were added as methods. The results in are the average of three experiments with triplicate measurements, the error bars indicated standard error. The *p* values indicate the statistical significance relative to control antibody with * for $p \le 0.01$-0.05.
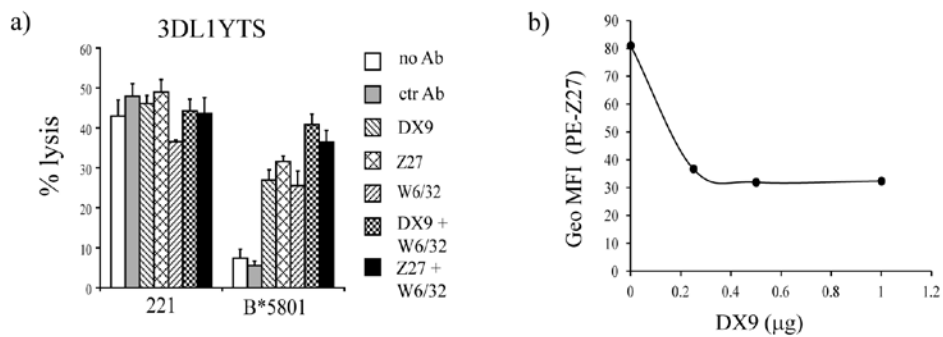
Fig 4-19. Z27 blocks 3DL1 mediated inhibition

a) 3DL1.YTS lysis of 221 expressing HLA-B*58:01. The lysis was measured at E:T=1:1 and the indicated antibodies were added at 5 µg/ml. One representative experiment was shown here. *b)* DX9 interferes with Z27 binding to HLA-B*58:01. 0.2 million of 221- B*58:01 cells were preincubated with the indicated concentrated DX9, the cells were then stained with PE conjugated Z27 antibody. The results were analyzed with flow cytometry. Representative of two experiments with triplicate measurements is shown.
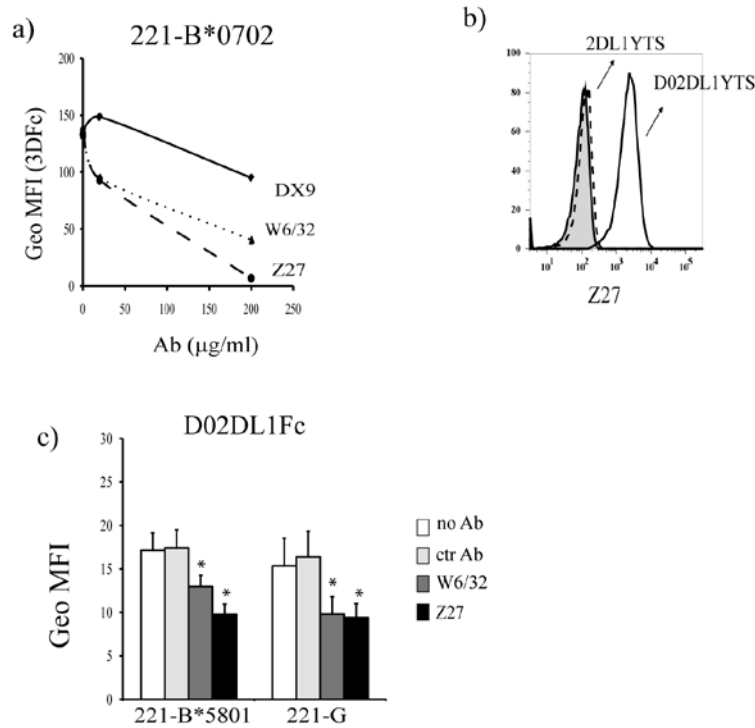
Fig 4-20. Z27 recognizes D0 and blocks the D02DL1Fc binding to B58 and G.

a) Z27 blocks 3DL1Fc binding of B*07:02. 3DL1Fc was added at 150 µg/ml to 221 cells expressing B*07:02. The indicated antibodies were added as shown on x-axis. The cells were incubated on ice for 2 hrs followed with PE-anti human Fcγ (eBioscience). *b)* Z27 binds D02DL1. Surface staining of YTS (filled grey), 2DL1YTS (dashed line) and D02DL1YTS (solid line) was done with PE-coupled Z27. *c)* Z27 blocks D02DL1Fc binding to B58 and HLA-G. 50 µg/ml W6/32 or 200 µg/ml Z27 was incubated with the indicated cells for 10 min prior to addition of 200 µg/ml D02DL1Fc. The results are the average of three experiments, the error bars indicate standard error. The *p* values indicate the statistical significance relative to control antibody with * for $p \leq 0.01$-0.05.

4.3. Discussion

Several previous studies have shown that the D0 domain contributes to MHC-I binding (161, 168, 169) but the mechanism of this contribution has not been understood. In this chapter, I have used the highly sensitive reporter system of YTS cells and chimeric soluble proteins with the D0 domain to show that D0 confers broad reactivity with classical MHC-I and even a non-classical MHC-I protein. In keeping with this idea, the D0 domain alone was previously shown to bind to cells with either B*51 or low levels of Cw4 (C1R), but the "binding" was considered as high levels of background due to poor folding of the isolated domain (169). I have shown that antibodies that bind to the MHC-I α3-domain and KIR3DL1-D0 domain but not antibodies that bind to the D1D2 domain prevent the binding and recognition via the D0 domain. These observations suggest that D0 contacts the MHC-I at a site that could be quite distinct from the canonical KIR site.

Our results suggest an explanation for how the D0 has an impact on the physiologic function of the receptor without contributing per se to the specificity. Although a binding of soluble KIR3DL1 to a variety of HLA-B, C and G molecules is detected, the interaction on its own is not strong and corresponds to a very weak level of functional recognition of molecules Cw7, B7 and G but not the Cw15. Nonetheless, the higher levels of lysis in the presence of antibodies for cells expressing B7 and HLA-G are indicative of a low degree of inhibition through KIR3DL1 at least in YTS cells. Recognition of these non-Bw4$^+$ molecule as ligands may be limited due to the low levels of receptor expressed on the YTS cells but fits with the observations that only Bw4 molecules serve as physiologic ligands of KIR3DL1 expressed in primary NK cells. Thus, while the D0 interaction appears to be functional in our system, it is secondary to the canonical interaction of KIR with the α1-region of MHC-I mediated by the D1 and D2 domains and, as will be discussed below, the role of the D0 domain is likely to

provide sufficient avidity for signalling. The ability of the D0 domain to bind to a distinct site might also explain how KIR3DL1 recognition of HLA-B27 heavy chain homodimers can be independent of the peptide (227). While the affinity of the D0 to a secondary site might be quite low, the dimer can provide an increase in avidity as has been reported LILRB1 binding to disulphide-linked dimers of HLA-G (228).

Parham and colleagues have proposed that the D0 domain may extensively contact the D1 and D2 domains (161) forming a single interface with the top surface of the MHC-I. Our observation that the presence of D0 influences the function of the D1 and D2 domain in KIR2DL1 fits with such a model where the D0 interfaces with D1 and D2 and has a conformational effect that influences their interaction with MHC-I. Specifically, I observe that D0 reduces reactivity with the KIR2DL1 antibody and binding to its normal ligand Cw15. The presence of the D0 domain also diminishes the yield of Fc fusion protein compared to KIR2DL1 and is similar to producing KIR3DL1 protein suggesting the D0 domain destabilizes the molecule overall which may also readout as the reduced binding. While our results do not directly refute the model in which the D0 forms a continuous surface with the D1 and D2 hinge region providing a larger face of interaction with the top of the MHC-I molecule, such a mode of interaction does not explain why W6/32 blocks KIR3DL1 recognition of its ligands but not the chimeric D02DL1 recognition the KIR2DL1 ligand Cw15. Therefore, I have considered other possibilities for the position of D0 based on two key points. First, the binding pattern of D0 is obviously reminiscent of how LILRB1 interacts with MHC-I that has very broad reactivity with diverse MHC-I molecules (HLA-A, B, C, E, G) but with relatively low affinity (178, 181). Second, perhaps it is not a mere coincidence that polymorphisms in residue 194 in the $\alpha 3$ domain of Bw4$^+$ molecules impact the interaction with KIR3DL1 (167) and structural studies have shown that the corresponding residue in HLA-A2 is bound by LILRB1 (170). Therefore, it is also possible that D0 retains LILRB1-like features and the D0

domain actually makes direct contact with residues in the conserved region, such as the α3 domain.

To explore this idea further, we tested the constraints on how D0 could interact with the α3-domain using molecular modelling(done by Dr. Bart Hazes). The KIR3DL1 domains D1 and D2 are closely related to the D1 and D2 domains of KIR2DL1 (77% and 88.4% sequence identity, respectively) and functional data indicate that they bind the α1-α2 domains of MHC-I in a similar manner (114, 168). Accordingly, we used the KIR2DL1-HLA-Cw4 crystal structure to model the two C-terminal domains of KIR3DL1 and their interaction with MHC-I. However, the KIR3DL1 D0 domain only shares 35% and 39% sequence identity with the KIR2DL1 D1 and D2 domains, respectively. LILRB1 D1 also shares only 36.8% and 36.7% sequence identity with the KIR2DL1 D1 and D2 domains, respectively, yet its D1 and D2 domains adopt the same relative orientation as the two KIR2DL1 domains (root mean square deviation, rmsd, is 1.2Å for 99 superimposed residues) and interact with MHC-I using the same surface of the hinge region between the domains (170). Therefore, because the linker between the KIR3DL1 D0 and D1 domains is the same length as that between the D1 and D2 domains of KIR2DL1 and LILRB1, and several key interacting residues in the domain interface are conserved, we explored possible binding mechanisms for KIR3DL1 assuming that its D0-D1 domain interface is equivalent to its D1-D2 interface (Fig 4-21). In this model, the D0 domain cannot reach the α3 domain while simultaneously engaging the peptide-binding groove via its D1 and D2 domains. Even if we allow considerable flexibility between the D0 and D1 domains, the short linker between them prevents interaction with α3. However, on its own the D0 could reach the same site contacted by LILRB1. Our modeling exercise suggests that D0 of KIR3DL1 could interact with MHC-I in a manner very similar to LILRB1 and that two KIRs could bind to a single MHC-I molecule without steric conflicts and with the receptors anchored in the membrane. In

140

addition, a single KIR3DL1 can bind to two MHC-I molecules simultaneously. Bridging together of KIR3DL1 molecules by MHC-I could drive receptor and ligand clustering. Perhaps in the confines of the membrane such bridging could potentiate the inhibitory signal as has been previously proposed for KIR2D based on a crystallographic contact (7). KIR2D receptors also possess features that might have replaced this function as KIR2D evolved from KIR3D (101) such as zinc-binding motifs that may dimerize the receptors (154) and a higher affinity for HLA-C as inferred by the KIR2DL1Fc-fusion protein's binding at much lower concentrations shown here.

In summary, I showed that KIR3DL1 weakly binds a broader range of HLA molecules than previously appreciated. In addition, I demonstrated that the antibody Z27 binds to the D0 domain of KIR3DL1 and blocks the interaction of KIR3DL1 with HLA-B*58:01 as well a chimeric receptor with the HLA-Bs and G. The results suggest that the D0 domain independently binds to MHC-I at a secondary site distinct from the conventional Bw4 epitope. However, the interaction site by the D0 domain remains unclear and whether the α3 domain of MHC-I is directly involved in the D0 interaction is not known. The remaining questions need to be further investigated.
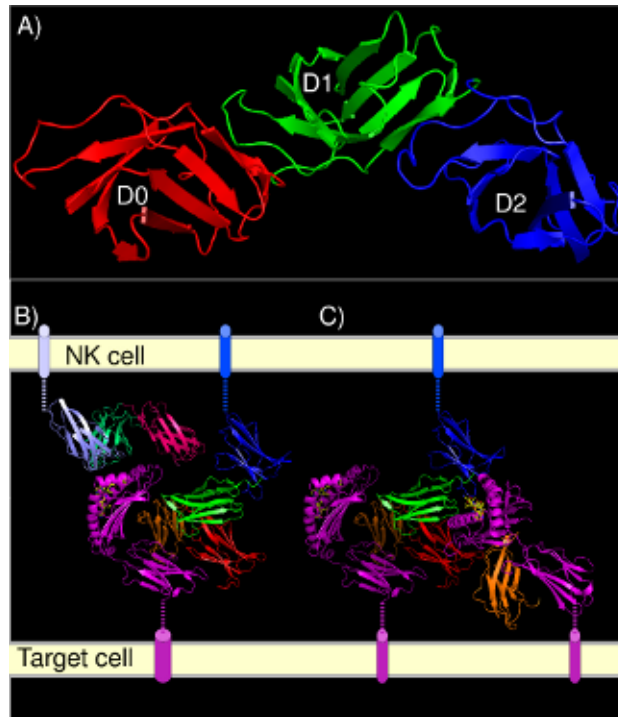
Fig 4-21. Ribbon diagram of proposed models.

A) A proposed structure of KIR3DL1 receptor. Each Ig domains are illustrated in different colors as indicated. *B*). A proposed model that KIR3DL1 interacts with ligands by 2 KIR3DL1 molecules binding to one MHC-I or one KIR3DL1 binding to 2 MHC-I molecules. MHC-I is colored purple.

Chapter 5

XENORECOGNITION OF MOUSE MHC-I

BY KIR3DL1

Preface

Based on my discovery that KIR3DL1 binds a conserved region of human MHC-I, the studies described in this chapter were designed to explore the possibility that KIR3DL1 recognizes xenogenic MHC-I. I have performed all of the experiments, but they have not yet been published.

5.1. Introduction

Previous studies described in Chapter 4 suggest that KIR3DL1-D0 directly contacts a conserved region of MHC-I at a secondary site. Following completion and publication of the study presented in Chapter 4, the crystal structure of the KIR3DL1-HLA-B*57:01 complex was published (229). In agreement with our studies, it clearly reveals that KIR3DL1 interacts with the HLA-Bw4 allele, HLA-B*57:01, at two separate contact sites (229). In brief, site 1 is contacted by two membrane proximal domains of KIR3DL1, D1D2, where it interacts with bound peptides and regions surrounding the peptide binding groove of MHC-I (Fig 5-1). Most importantly, site 2 involves the D0 domain as it contacts with conserved region of the α1 domain located in the two loops comprised of positions 14-18 and 88-92 (Fig 5-1). This site explains the broad recognition of classical and non-classical HLA molecules by the D0 domain as shown in Chapter 4. In addition, the KIR3DL1-D0 domain makes direct contact with a few residues in the β_2m domain (229).

As previously discussed in Chapter 4, antibody blocking of the interaction could be due to either steric interference or direct contact. In Chapter 4, W6/32 was shown to slightly block KIR2DL1 mediated inhibition when EGFP was present (Fig 4-7), suggesting that there is an effect of steric interference. However, this antibody has a greater effect on KIR3DL1 than it has on KIR2DL1, indicating a direct interaction aside from steric interference. Structurally, it is a bit difficult to model how W6/32 could sterically interfere with the binding when one KIR3DL1 interacts with one HLA-Bw4 molecule. Given that clustering of KIR receptors and their MHC-I ligands has been shown at the cell-cell interface when an NK cell encounters a target cell, interactions that might occur when the receptors accumulate at the synapse are not necessarily reflected by the crystallographic studies. Hence, the crystallographic study does not rule out the possibility that the α3 domain directly binds KIR3DL1 under physiological

conditions. To test if there is a role for the α3 domain in KIR3DL1 signaling in response to MHC-I on target cells, I considered making chimeras with the α1α2 domains of mouse MHC-I. However, I first needed to determine if KIR3DL1 could interact with mouse MHC-I.

Despite some amino acid variations in primary sequence, class I proteins from both species exhibit a very similar structure (230). However, the variations in particular residues do influence interaction between receptors and ligands. For instance, LILRB1 is known to broadly recognize classical and non-classical HLA molecules by means of making contact with the α3 domain and β_2m (170, 181, 182), but it interacts with only one member of mouse MHC-I, H-2D^b (231). The region of direct contact by LILRB1 is between residues 191-200 at the α3 domain, which is highly conserved among HLA alleles (Fig 5-2) (181, 182). However, there are significant differences in this region between mouse and human MHC-I molecules (Fig 5-2), suggesting why not all mouse α3 domains interact with LILRB1.

In Chapter 4, I demonstrated the recognition of Bw4$^-$ MHC-I molecules by the KIR3DL1-D0 domain (232). This interaction could be most likely due to direct contact with the α1 domain by the D0 domain. Alignment of several H-2 class I subtypes and HLA-class I revealed a high degree of identity at residues 14-18 and 88-92 on MHC-I molecules where KIR3DL1-D0 contacts (Fig 5-3). Therefore, KIR3DL1 may bind mouse MHC-I molecules. In this Chapter, I performed binding experiments with mouse cell lines using KIR3DL1 fusion proteins. Interestingly, I found xenorecognition of mouse MHC-I molecules by KIR3DL1. However, as will be shown and discussed, differences in which mouse MHC-I molecules cannot be readily explained by the recognition at site 2.
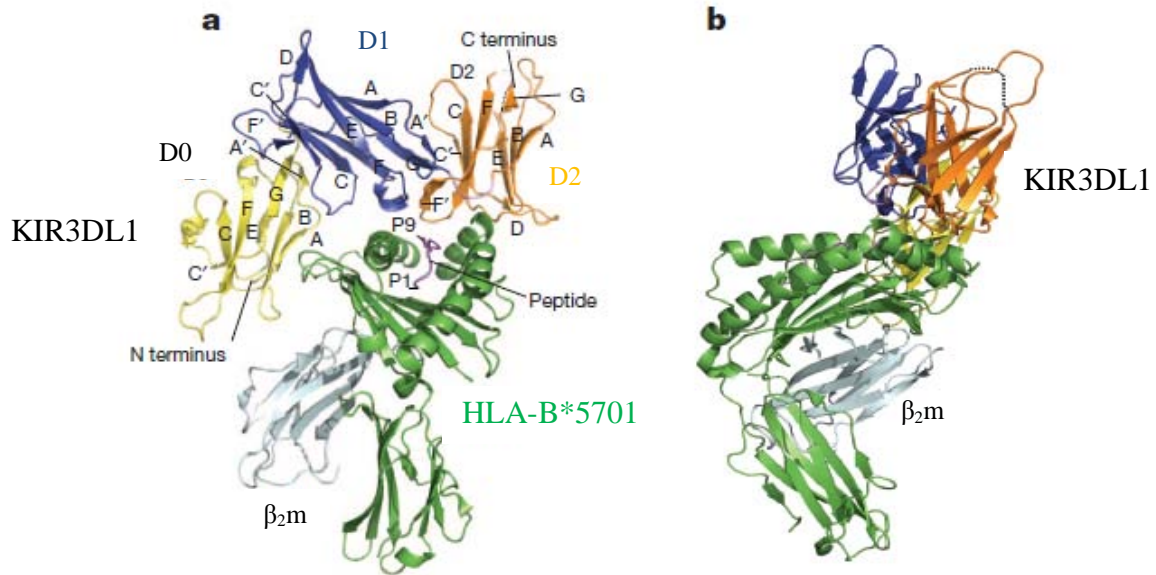
Fig 5-1: Structure of KIR3DL1-peptide bound HLA-B*57:01 complex (adapted from Nature, 2011, 479: 401)

The HLA and β_2-microglobulin are colored green and cyan, respectively. The three Ig domains of KIR3DL1, D0, D1 and D2 are colored as yellow, blue and orange, respectively. Front view (*a*) and side view (*b*) of the structure are shown.

```
AA Pos.              190       200       210       220       230

HLA-B*58:01  RADPPKTHVT HHPVSDHEAT LRCWALGFYP AEITLTWQRD GED-QTQDTEL
HLA-B*57:01  .......... ...I...... .......... .......... ...-.......
HLA-B*27:05  .......... ...I...... .......... .......... ...-.......
HLA-B*07:02  .......... ...I...... .......... .......... ...-.......
HLA-Cw1503   ..EH...... .......... .......... .......... ...-.......
HLA-Cw7      ..E....... ...L...... .......... .......... ...-.......
HLA-G        .......... ....F.Y... .......... ...I...... ...-....V..
H-2Dd        .T....A... ..RRPEGDV. .......... .D......LN ..E-L..EM..
H-2Kd        .T.S..A... Y..R.QVDV. .......... .D......LN ..D-L...M..
H-2Db        .T.S..A... ...R.KG.V. .......... .D......LN ..E-L...M..
H-2Kb        .T.S..A... ..SRPEDKV. .......... .D......LN ..E-L...M..
H-2Dk        HT.S..A... ...R.KV.V. .......... .D......LN ..E-L...M..
H-2Kk        .T.S..A... R.SRPEDKV. .......... .D......LN ..E-L...M..
HFE          QQV..LVK.. ..-.TSSVT. ...R..NY.. QN..MK.LK. KQPMDAKEF.P


AA Pos.              240       250       260       270

HLA.B*58:01  VETRPAGDRT FQKWAAVVVP SGEEQRYTCH VQHEGLPKPL TLRWE--PSSQSTIPIV
HLA-B*57:01  .......... .......... ....I....I. .......... .....--..........
HLA-B*27:05  .......... .......... .......... ...V...... ....-....V...
HLA-B*07:02  .......... .......... .......... .......... ...--....V...
HLA-Cw15     ........G. .......M.. .......... .......E.. ....--....P.....
HLA-Cw7      ........G. .......M.. ..Q....... M.....QE.. .....--...LP....M
HLA-G        ........G. .......... .......... .......E.. M...K--Q..LP....M
H-2Dd        ........G. .....S.... L.K..K.... .E.....E.. ....GKEEPPS..KTNT
H-2Kd        ........G. .....A.... L.K..N.... .H.K...E.. ....---KLPP..VSNT
H-2Db        ........G. .....S.... L.K..N...R .Y.....E.. ....---EPPP..DSYM
H-2Kb        ........G. .....S.... L.K..Y.... .Y.Q...E.. ....---EPPP..VSNM
H-2Dk        ........G. .....S.... L.K..N.... .Y.....E.. ....---EPPS..DSYM
H-2Kk        ........G. .....S.... L.K..Y.... .Y.Q...E.. ....---EPPP..VSNT
HFE          KDVL.N..G. Y.G.ITLA.. P........Q .E.P..DQ.. IVI..--..PSG.L-VI
```

Figure 5-2. Comparison of amino acid sequences of the α3 domain between HLAs, mouse MHC-Is and HFE.

Dots indicate amino acid identity to the HLA-B*58:01 sequence. Dashes indicate the absence of the amino acid relative to HLA-B*58:01. The boxed residues are the regions that interact with the LILRB1-D1 domain. Residue 194 is colored red. N-glycosylation sites are highlighted in red.

a). α1 domain

```
                                loop #1
AA Pos.            10         20         30         40         50
HLA-B*58:01   GSHSMRYFYT AMSRPGRGEP RFIAVGYVDD TQFVRFDSDA ASPRTEPRAP
HLA-B*57:01   .......... ..........  .......... .......... ....MA....
HLA-B*27:05   ........H. SV.......  ...T...... .L....... ....E.....
H-2Dd         .S..L...V. .V....F...  .YME.....N .E....... EN..Y....R
H-2Kd         .P..L...V. .V....L...  .......... .......... DN..F.....
H-2Db         .P......E. .V....LE..  .Y.S.....N KE....... EN..Y.....
H-2Kb         .P..L...V. .V....L...  .YME...... .E....... EN..Y....R
H-2Dk         .P..L...E. VV....L...  ...S.....N .E....... EN..D...VR
H-2Kk         .P..L...H. .V....L.K.  ...S...... .......... EN..Y...VR

AA Pos.            60         70         80         90
HLA-B*58:01   WIEQEGPEYW DGETRNMKAS AQTYRENLRI ALRYYNQSEA      loop #2
HLA-B*57:01   .......... .......... .......... ..........
HLA-B*27:05   .......... .R..QIC..K ...D..D..T L.........
H-2Dd         .......... ER...RA.GN E.SF.VD..T .........AG
H-2Kd         .M........ EEQ.QRA.SD E.IF.VS..T .Q......KG
H-2Db         .M........ ER..QKA.GQ E.WF.VS..N L.G....AG
H-2Kb         .M........ ER..QKA.GN E.SF.VD..T L.G....KG
H-2Dk         .M........ ER..QIA.GN E.WF.VD..T L........G
H-2Kk         .M..VE.... ERN.QIA.GN E.IF.VS..T ......AG
```

b). α2 domain

```
              loop #2
AA Pos.            100        110        120        130        140
HLA-B*58:01   GSHIIQRMYG CDLGPDGRLL RGHDQSAYDG KDYIALNEDL SSWTAADTAA
HLA-B*57:01   .....V... ..V....... .......... .......... ..........
HLA-B*27:05   ..TL.N... ..V....... ..YH.D.... .......... ..........
H-2Dd         ..TL.W.A. ..VES..... ..YW.F.... C......... KT.....M..
H-2Kd         ..TF...F. ..V.S.W... ..YQ.F.... R......... KT........
H-2Db         ..TL.Q.S. ....S.W... ..YL.F..E. R......... KT.....M..
H-2Kb         ..TI.VIS. .EV.S..... ..YQ.Y.... C......... KT.....M..
H-2Dk         ..T...LS. ..V.S.W... ..YE.F.... C......... KT.....M..
H-2Kk         ..TF..... .EV.S.W... ..YE.Y.... C......... KT.....M..

AA Pos.            150        160        170        180
HLA-B*58:01   QITQRKWEAA RVAEQLRAYL EGLCVEWLRR YLENGKETLQ RA
HLA-B85701    .......... .......... .......... .......... ..
HLA-B*27:05   .......... .......... ..E....... .......... ..
H-2Dd         ...R....Q. GA..RD.... ..E....... ..K..NA..L .T
H-2Kd         L..R....Q. GD..YY.... ..E....... ...L.N...L .T
H-2Db         ...R....QS GA..HYK... ..E.....H. ..K..NA..L .T
H-2Kb         L..KH...Q. GE..RL.... ..T....... .....NA..L .T
H-2Dk         L..KH...Q. GA..RD.... ..T....... ...L.NA..L HT
H-2Kk         L..KH...Q. GD..RD.... ..T....... ..QL.NA..P .T
```

Fig 5-3: Comparison of the amino acid sequences of the α1α2 domains between human and mouse MHC-I.

Dots represent identity with the reference sequence HLA-B*58:01. Residues corresponding to the Bw4 epitope are colored red. The boxed residues are the two loops that interact with KIR3DL1-D0. Contact residues with KIR3DL1-D0 are highlighted in yellow and glycosylation sites are highlighted in cyan. The underlined residues interact with KIR3DL1-D1D2, and cysteine residues are indicated in green.

5.2. Results:

5.2.1. 3DL1Fc binding to RMA cells

To test if the receptor, KIR3DL1, interacts with mouse class I MHC proteins, I chose a mouse cell line, RMA, that expresses endogenous H-2K^b and D^b, along with the MHC-I deficient variant RMA/S for comparison (233, 234). As expected, RMA cells express a high level of H-2D^b and K^b, while RMA/S had > 100 fold less expression of H-2D^b and K^b (Fig 5-4a). Not surprisingly, W6/32 also stained the RMA cells (Fig 5-4a) as it is well established that H-2D^b molecules gain the reactivity to W6/32 when they associate with bovine β_2m, as occurs in cell culture with FBS (235, 236). To explore if KIR3DL1 recognizes H-2^b, I examined the binding of the KIR3DL1 Fc fusion protein, 3DL1Fc, to the selected mouse cells. The results are shown proportional to Fc alone. Dose dependent and relatively high binding of 3DL1Fc to RMA cells was observed in comparison to RMA/S cells at concentrations ranging from 25 µg/ml to 150 µg/ml (Fig 5-4c). The results suggest that binding of KIR3DL1 with cells expressing H-2K^b and D^b. To explore the role of the D0 domain, the fusion protein composed of D0 and two Ig domains of 2DL1, D02DL1Fc, was used. In this case, the results are shown proportional to 2DL1Fc as the control, which had a similar minimal binding to RMA cells as Fc alone (Fig 5-4b). Noticeable binding of D02DL1Fc to mouse cells (Fig 5-4b and 4d) suggests the role of the D0 domain in the interaction.

To further investigate the interaction, I tested how various antibodies specific for the mouse class I proteins affect the interaction. The binding of RMA cells by 3DL1Fc and D02DL1Fc was blocked in the presence of antibodies against KIR3DL-D0 (Z27), H-2D^b (28.14.8S) (197), and K^b (Y3) (198) (Fig 5-5). Moreover, the blocking by Z27 and 28.14.8S were statistically significant. Interestingly, anti-3DL1-D1D2 antibody, DX9 (IgG) slightly reduced 3DL1Fc binding ($p = 0.06$, n=3). Given the tyrosine at position 200 in the KIR3DL1-D2

domain is critical for DX9 reactivity (168, 232) and for KIR3DL1 recognition of Bw4$^+$ molecules (168, 229, 232), the different level of blocking between DX9 and Z27 suggests that the D0 domain is important for binding to mouse MHC-I proteins. However, whether D1D2 domains of KIR3DL1 contribute to the binding still needs further examination as DX9 blocking could be the result of steric interference. In the case of D02DL1Fc, though the epitope of the antibody specific for KIR2DL1, HP3E4, is unknown, this antibody remarkably eliminated D02DL1 binding (p=0.03, n=3) with a similar degree to Z27 (Fig 5-5). Given the KIR2DL1 interaction pattern and the properties of the IgM structure of HP3E4, the elimination of binding by HP3E4 is likely due to steric interference. Overall, the preliminary results suggest that KIR3DL1 binds H-2D^b/K^b molecules but KIR2DL1 does not, and that the first Ig domain (D0) of KIR3DL1 is predominantly involved in this recognition.
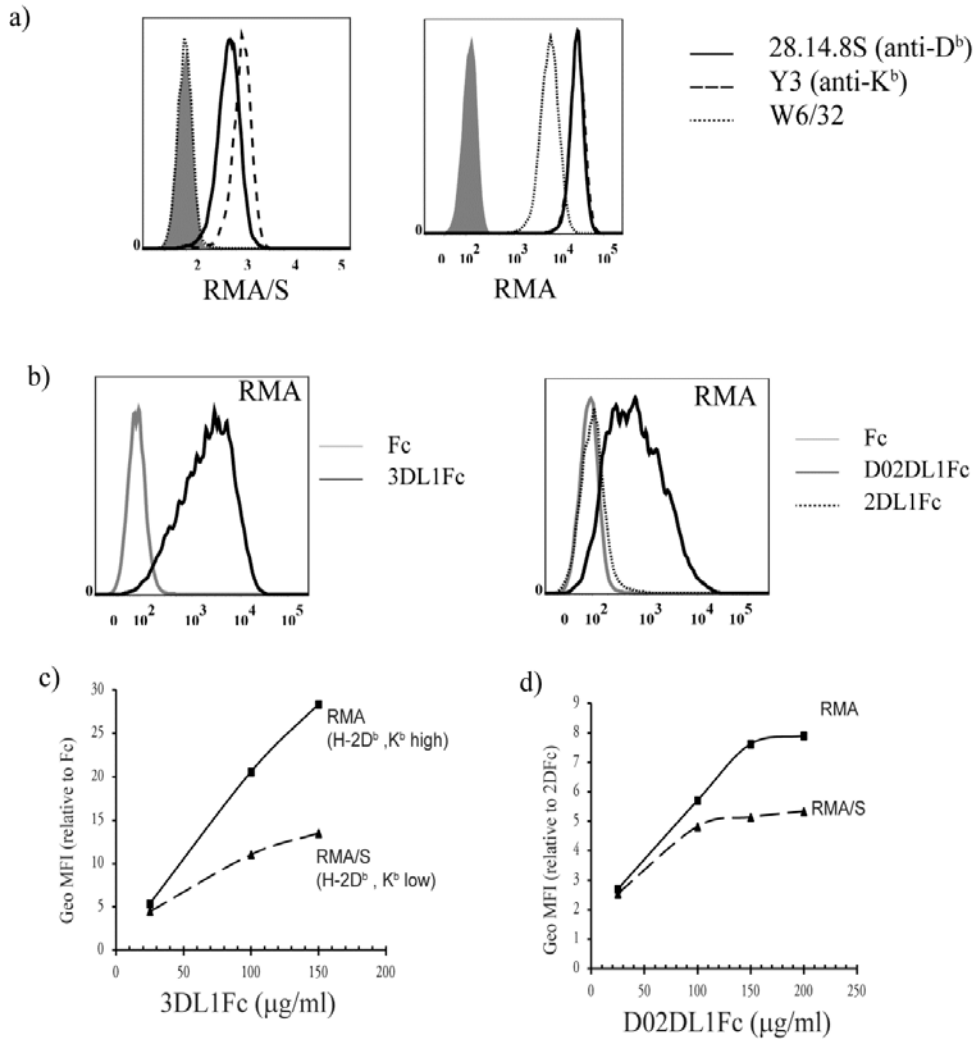
Fig 5-4. 3DL1Fc binding to RMA and RMA/S cells

a) Surface staining analysis of the murine cell lines RMA and RMA/S by flow cytometry with the indicated antibodies. The isotype control is shown as the filled histogram. *b)* Flow cytometric analysis of 150 µg/ml of 3DL1Fc (left panel) and D02DL1Fc (right panel) binding to RMA cells. *c-d)* Titration of 3DL1Fc *(c)* and D02DL1Fc *(d)* binding to the cells shown in *a. R*epresentative of three experiments is shown in *d* and *e.*

151
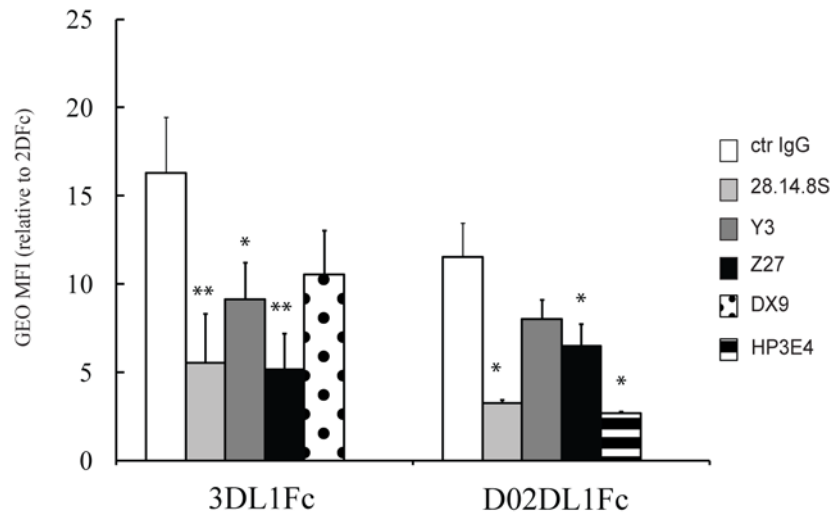
Fig 5-5. Anti-D^b-α3 and anti-D0 antibodies block 3DL1Fc and D02DL1Fc binding to RMA cells

RMA cells were incubated with 150 µg/ml of Z27 or the control IgG, and 50 µg/ml of 28.14.8S at room temperature for 10 minutes prior to 100 µg/ml fusion proteins. The binding was detected and analyzed as described in Chapter 2. Statistical significance was calculated using an unpaired student's *t* test. The average of four independent experiments with the standard error is shown. * indicates $p<0.05$, ** $p <0.01-0.05$

5.2.2. 3DL1Fc binding to various mouse MHC-I molecules

Having established that KIR3DL1 interacts with H-2^b, I questioned whether it binds other alleles of H-2. Therefore, I examined 3DL1Fc binding to the cell lines expressing H-2^d, such as NZB (H-2D^d), or cells expressing H-2^k, such as RDM4 (H-2D^k/K^k) (Fig 5-6a). The results are shown relative to Fc alone. Interestingly, though RDM4 cells highly express H-2D^k/K^k (Fig 5-6a), 3DL1Fc did not react with these cells at all (Fig 5-6b). In contrast, dose dependent binding to NZB cells was observed and the binding was saturated at 150 µg/ml (Fig 5-6b).

To clarify if 3DL1Fc binds D^b and/or K^b, I used R1E cells transfected with H-2D^b or K^b in combination with mouse β_2m (mβ_2m), H-2D^bβ_2m.R1E or H-2K^bβ_2m.R1E. Parental R1E cells are derived from C58 mouse thymoma with H-2^k background but lost expression of MHC-I on the surface due to lacking mβ_2m (203). When transfected with H-2D^b or K^b along with mβ_2m, R1E cells stably express the encoded proteins H-2D^b or K^b on the cell surface (Fig 5-8a), perhaps as well as endogenous K^k and D^k. It is worth noting that since 3DL1Fc did not bind H-2^k molecules on RDM4 cells (Fig 5-6b), the binding of 3DL1Fc to the R1E cells should only be due to D^b or K^b expressed on the R1E cells but not K^k or D^k molecules restored by the presence of mβ_2m. Interestingly, in contrast to NZB cells, R1E expressing H-2D^b or K^b exhibited a different binding trend (Fig 5-6b). The binding to D^b did not saturate in the range of 50 µg/ml to 200 µg/ml, though the absolute number of binding to R1E.D^b was similar to that to NZB at the concentration of 200 µg/ml. In the case of K^b, a more than 2-fold reduction of binding was observed relative to D^b (Fig 5-6b). The results suggest that KIR3DL1 interacts with H-2D^d, D^b, K^b, but not D^k/K^k, and that the strengths of binding to the various alleles of mouse MHC-I examined are different.
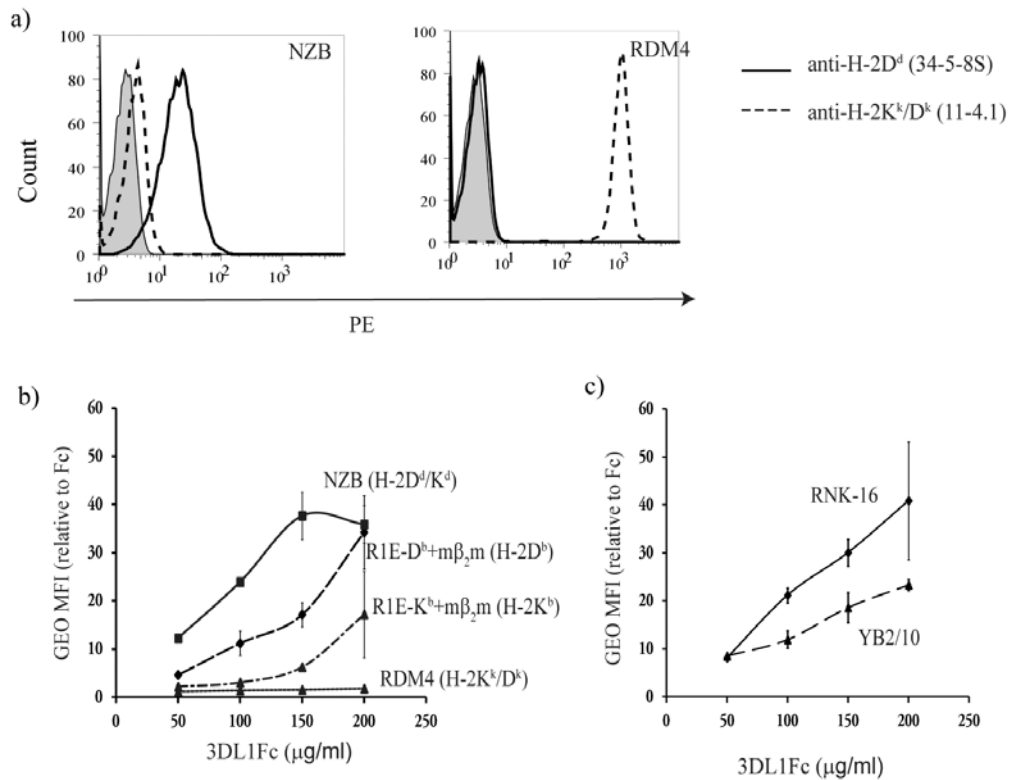
Fig 5-6. 3DL1Fc binding to various murine cell lines.

a) Flow cytometric analysis of the murine cell lines NZB and RDM4 using the indicated antibodies, the isotype control is shown by the filled histogram, the antibody staining was detected with PE coupled anti mouse IgG (H+L). *b)* Titration of 3DL1Fc on the indicated cells. The average of four experiments with the standard error is shown. *c)* Titration of 3DL1Fc binding to the rat cells RNK 16 and YB2/10. The results are relative to Fc control. The average of three experiments with the standard error is shown.

5.2.3. 3DL1Fc binding to rat cells

The genes in the rat MHC class I region encode structured class I proteins, known as RT1-A, similarly to human MHC-I (237). Therefore, it is possible that the receptor could also recognize rat MHC-I. To explore if KIR3DL1 binds rat MHC-I, I examined 3DL1Fc binding to the rat cells RNK-16 and YB2/10. Dose dependent binding to these cells as shown in Fig 5-6c suggests possible interaction of KIR3DL1 with rat MHC-I molecules. However, more experiments need to be performed to further investigate the interaction.

5.2.4. Anti H-2D^b-α3 blocking of D02DL1Fc binding to D^b and K^b

To test if the KIR3DL1-D0 domain is sufficient for binding to either D^b or K^b, I used D02DL1Fc. The results shown in Figures 5-7 demonstrate the binding to K^b and D^b by the D0 domain. Moreover, to dissect the regions involved in the binding, I examined D02DL1Fc binding in the presence of several antibodies including anti-D^b antibodies specific to the α1 domain (B22-249) (196) and to the α3 domain (28.14.8S) (197), and anti-Kb-α1 (Y3) (198). Using flow cytometry it is clear that these antibodies crossreact with other class I molecules as shown in Figure 5-7a. Both of the anti-D^b antibodies showed similar reaction with the cells expressing H-2D^b as measured by flow cytometry (Fig 5-7a). Surprisingly, the "D^b-specific" antibodies appear to cross-react to H-2K^b protein, and *vice versa* (Fig 5-7a). It must be noted that a greater intensity of H-2D^b than H-2K^b was detected on the transfected R1E cell surface when stained with the antibodies described as D^b-specific. This may be due to the variation of the antibody reactivity or actual higher expression of H-2D^b than K^b on R1E cells.

Similar to Fig 5-6b, the binding of D02DL1Fc was greater to D^b than to K^b at a fixed concentration of 100 µg/ml (Fig 5-7c). The binding to D^b was abrogated by either anti-D^b-α3 mAb (28.14.8S) or anti-D0 mAb (Z27), whereas it was partially blocked by anti-D^b-α1 antibody (B22-249) (Fig 5-7b and 7c). Given the pronounced effect of 28.14.8S compared to B22-249, it seems that the binding

region is near D^b-α3. Unfortunately, the antibody's epitope has not been precisely mapped, therefore, one cannot know if it is due to 28.14.8S sterically interfering with the interaction at site 2 on the α1 domain or blocking a contact with the α3 domain itself. There is also a significant reduction of binding of D02DL1Fc to D^b by the anti-K^b antibody, Y3, likely caused by cross-reaction of the antibody to D^b protein (Fig 5-7a). Remarkably, there is a noticeable reduction of binding to K^b by anti-Db-α3 mAb, 28.14.8S, which is greater than that observed with Y3 (Fig 5-7c). Given 28.14.8S has greater staining intensity on the R1E.K^b cells than Y3 does (Fig 5-7a, middle panel), the antibody cross-reaction and position of antibody likely explains the blocking of 3DL1-D0 binding shown in Fig 5-7c. As previously explained (235, 238), W6/32 reactivity is observed on the surface of R1E transfectants, whereas it is not present on parental R1E cells under the same culture conditions (Fig 5-7a). Interestingly, the presence of W6/32 attenuated the D02DL1Fc binding to H-2D^b and K^b based on four aggregated experiments with $p < 0.05$ (Fig 5-7b and 7c), further suggesting that the binding of the 3DL1-D0 domain to mouse MHC-I is in a region similar to where it binds human MHC-I and indicating the potential involvement of the α3 domain. Overall, the results reveal the participation of KIR3DL1-D0 in the xenorecognition of H-2D^b and K^b, perhaps through the α3 domain.
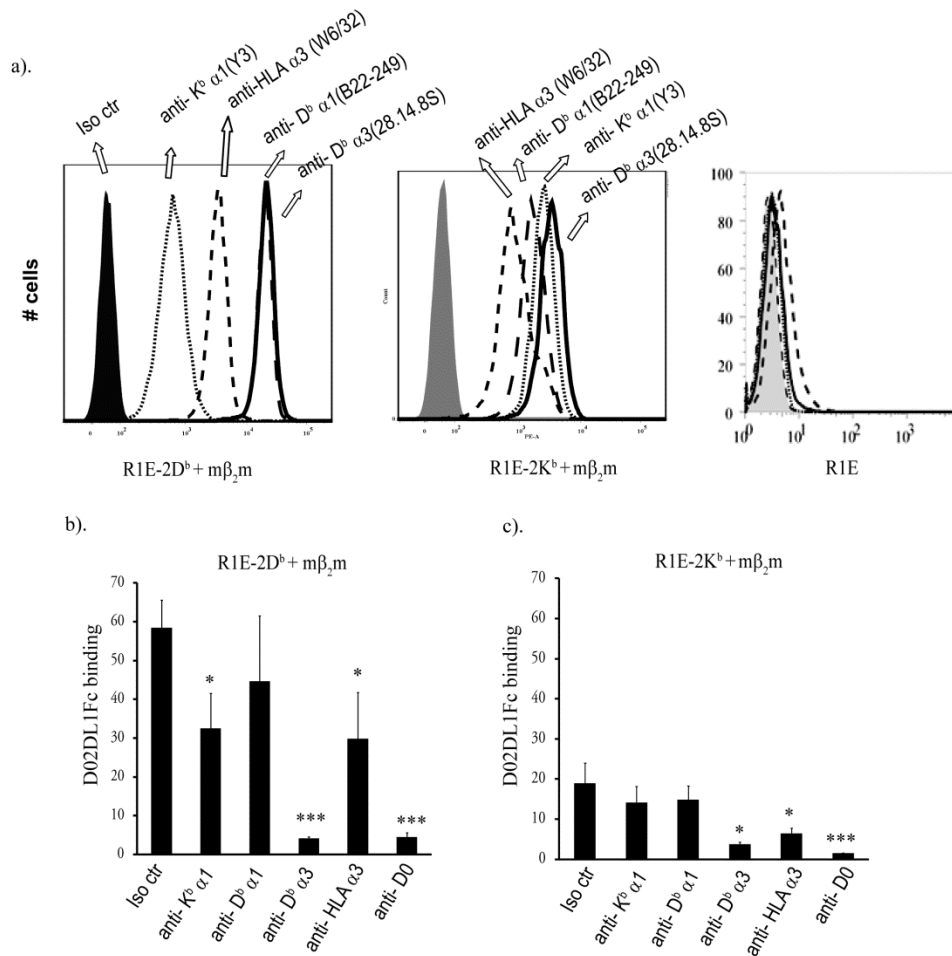
Fig 5-7. Antibody blocking of 3DL1-D0 binding to D^b and K^b.

a) Surface expression of MHC-I on R1E and R1E cells expressing H-$2D^b$ and K^b. The antibody staining was detected with PE coupled anti mouse IgG(H+L). *b-c)* Antibody blocking of D02DL1Fc binding to R1E cells expressing D^b *(b)* or K^b *(c)*. 150 µg/ml Z27 or 50 µg/ml anti MHC-I antibodies were pre-incubated with the indicated cells at room temperature for 10 minutes prior to the addition of 100 µg/ml D02DL1Fc . The results are shown proportional to Fc alone. The average of three experiments with the standard error is shown. The *p* value was calculated using an unpaired student's *t* test. *, $p<0.05$; *** , $p<0.001$.

157

5.2.5. D0 is responsible for the interaction with H-2D^b

To further explore the role of individual Ig domains of KIR3DL1 in xenorecognition, I generated the proteins encoded by constructs containing various combinations of Ig domains of KIR3DL1 generously provided by Dr. Long (169) (Fig 5-8a) using Cos-7 cells. The fusion proteins were then purified as described in Chapter 2. To assess the folding, I examined the purified proteins using a capture ELISA and various anti-KIR3DL1 antibodies. In brief, the same molar concentration of each protein was used with the human IgG Fc coated ELISA plates. The reactivity of anti-D1D2 antibody, DX9, or anti-D0 antibody, Z27 at various concentrations to the captured proteins was then detected with alkaline phosphatase (AP) conjugated anti mouse IgG. As previously reported (169, 232), the D1D2 domains, but not the D0 domain, are responsible for DX9 reactivity (Fig 5-8b, left panel) and D0 is detected by Z27 (Fig 5-8b, right panel). Moreover, at the same molar concentration, D0 alone had less reactivity with Z27 relative to full length KIR3DL1. However, in the context of D1 (D0D1Fc), the Z27 reactivity was restored and even exceeded the full length 3DL1 (Fig 5-8b, right panel). These results confirm that the presence of three Ig domains is required for proper protein assembly. These results also suggest that the D1 domain supports the D0 structure and that the D0 domain alone does not retain its conformation well. Alternatively, the D1 domain may contain part of the Z27 epitope.

Next, I examined the binding to R1E cells expressing H-2D^b using molar equivalents of the various fusion proteins. Dose dependent binding of D0D1Fc was observed with a saturation point at around 1.5 µM, while D1D2Fc did not show appreciable binding to D^b (Fig 5-9). Interestingly, D0Fc appears to have a greater binding than D0D1Fc at the highest concentration, 2 µM (Fig 5-9). The results again suggested that the D0 domain is essential for the binding to H-2D^b by KIR3DL1. Moreover, the results also explain the results shown in Fig 5-4 that 3DL1Fc has better binding to RMA cells than D02DL1Fc, which is perhaps due

to the fact that 3DL1-D1 interacts with D0 to produce the properly folded and intact protein.

5.2.6. D0Fc binds H-2K^b conjugated strepavidin beads

The D0 domain alone appears to be a poorly folded or unstable protein (169), which might cause low yields when Fc fusion protein is produced (169, 232) and background non-specific binding. The failure to saturate binding at 2 µM D0Fc to R1E.D^b cells, suggests that D0Fc binding might not be solely due to the D^b on the cells. Therefore, I checked the binding of D0Fc to the parental R1E cells. I observed quite high but surprisingly saturated binding of D0Fc to the parental R1E cells (Fig 5-10). Presumably, this binding is due to the instability of D0 itself or the recognition of unknown proteins on R1E cells.

Therefore, as an alternative approach to distinguish D0Fc binding to MHC-I proteins from spurious binding to the cells, I tested the binding to purified H-2K^b. I made streptavidin conjugated H-2K^b beads as described in the materials and methods (Chapter 2), and assessed D0Fc and 3DL1Fc binding to the beads. With the same strategy, HLA-B*27:05 monomer obtained from Dr. Brook (University of Melbourne) was conjugated to the beads as the positive control, and beads alone were used as the negative control. B*27:05 immobilized on beads was detectable by flow cytometry with B27 allele specific antibody, B27M1, the Bw4 specific antibody, anti-Bw4, and pan reactive anti MHC-I antibody, W6/32 (Fig 5-11a). The binding of 3DL1Fc relative to Fc control and control beads was remarkably high (Fig 5-11b), suggesting immobilization on the beads supports a B*27:05 structure conducive to receptor binding. In one experiment I performed, 3DL1Fc and D0Fc were shown to bind K^b-conjugated beads in comparison to control beads or Fc alone (Fig 5-11c). These results directly demonstrate that 3DL1Fc and the 3DL1-D0 domain bind H-2K^b. Interestingly, D0Fc exhibited higher background binding to the control beads than did 3DL1Fc. This result may indicate that there is also some non-specific binding to beads by D0 alone perhaps

159

due to the lability of the domain and further testing with fresh preparations of D0Fc and with blocking antibodies may clarify how much of the binding is specific. Together, the results clearly suggest 3DL1 and the 3DL1-D0 domain bind directly to H-2K^b without interference from other potential ligands.
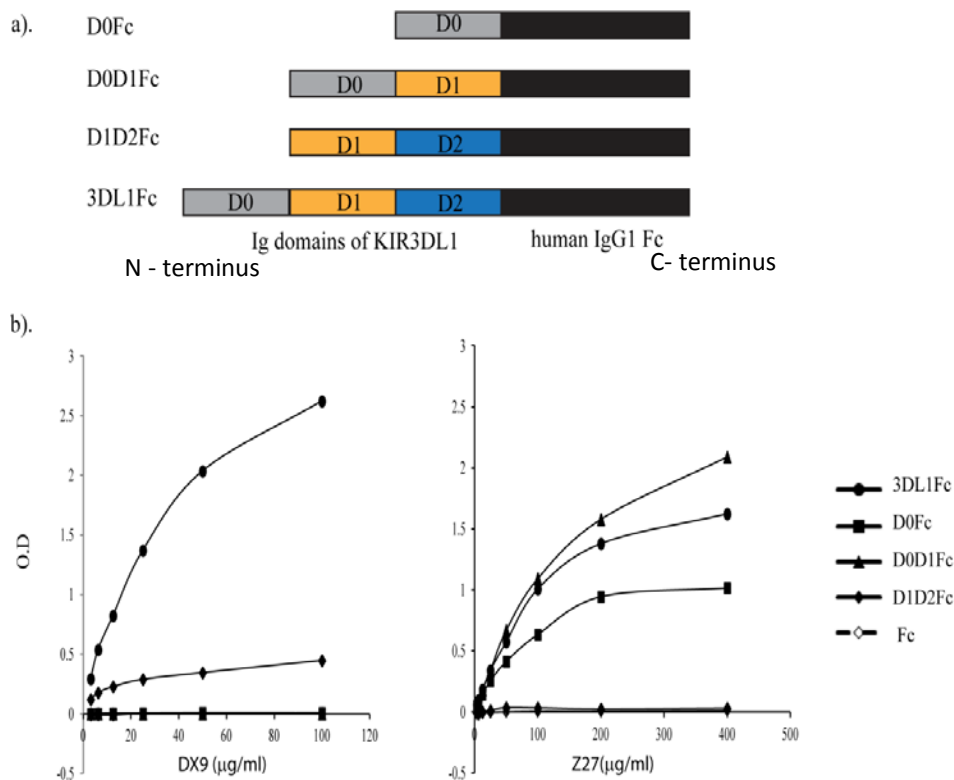
Fig 5-8. The reactivity of KIR3DL1 specific antibodies to various domains of KIR3DL1.

a) Schematic diagrams of the various constructs encoding the indicated fusion proteins. *b)* The reactivity of DX9 (left panel) or Z27 (right panel) to the indicated fusion proteins measured by a capture ELISA assay. In brief, 25 µg/ml anti-human Fc was coated to each well of an ELISA plate overnight prior to incubation with 10 nM of the Fc fusion proteins. The captured proteins were then detected by the titration of anti-KIR3DL1 antibodies and the subsequent addition of AP conjugated anti-mouse IgG. The results were analyzed with the Kinetic Microplate Reader (Molecular Device). Representative of three experiments with duplicate measurements is shown.
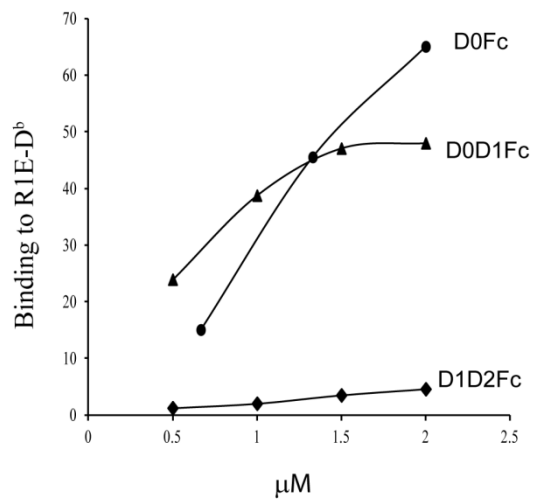
Fig 5-9. D0 is sufficient for 3DL1Fc binding to R1E cells expressing H-2D^b.

Binding of the indicated Fc fusion proteins to R1E-D^b+mβ_2m cells at various molar concentrations. The results are relative to Fc control. Representative of three experiments is shown.
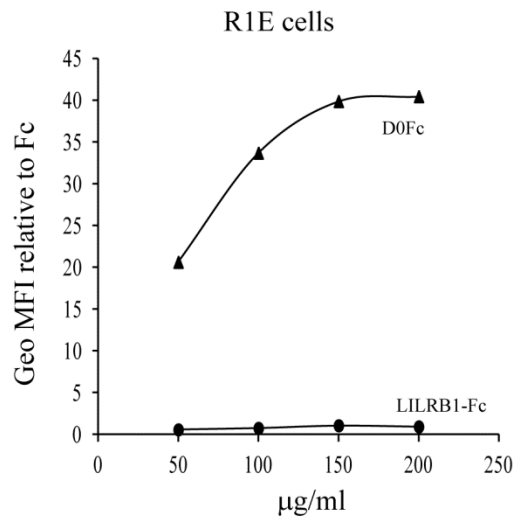
Fig. 5-10. D0Fc unexpectedly bind R1E cells

Binding of D0Fc or LILRB1-Fc (R&D) to the parental R1E cells at various concentrations. The results are proportional to Fc control. Representative of two experiments is shown.
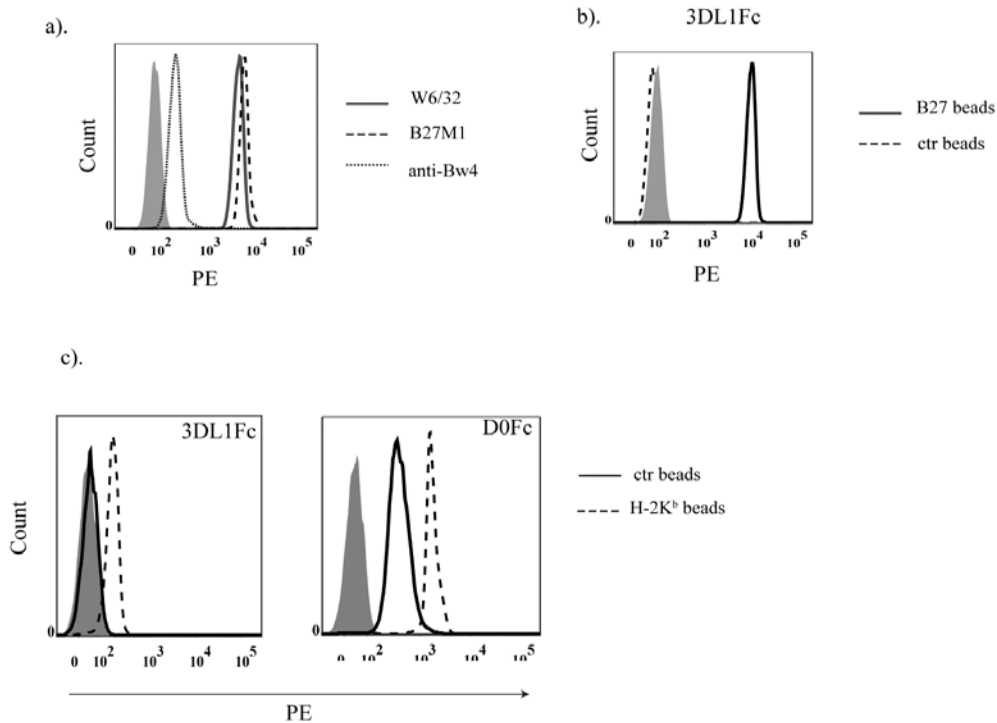
Fig 5-11. 3DL1Fc binding to H-2K^b conjugated streptavidin beads.

a) Detection of B*27:05 conjugating to streptavidin beads was performed using the indicated antibodies. The reactivity of immobilized B*27:05 on beads with the antibodies was detected by PE coupled anti mouse IgG (H+L). The results were analyzed by flow cytometry. Isotype control staining is indicated by the filled histogram. *b)* 3DL1Fc binding to the beads shown in *a). c)* The binding of 3DL1Fc or D0Fc to the H-2K^b conjugated streptavidin beads. For *b* and *c*, Fc alone is indicated as filled histogram. Representative of two experiments with duplicate measurements is shown in *a* and *b*, and only one experiment was performed in *c*.

5.2.7. KIR3DL1-D0 does not bind HFE

I have shown xenorecognition of H-2^b and H-2^d by KIR3DL1, therefore, they are not suitable for exploring if there is an interaction between KIR3DL1-D0 and the MHC-α3 domain. However, the ability of 28.14.8S to block this interaction again suggests that the α3 domain plays a role in KIR3DL1-D0 domain recognition of mouse MHC-I. Therefore, I considered more distantly related proteins that could be used instead, such as human hemochromatosis protein (HFE). HFE emerged as a good candidate to perform domain swaps with B*27:05 as well as to determine if 3DL1 might bind a highly divergent class I related protein. HFE is an MHC-I like molecule linked with iron metabolic disorder (98), that binds β$_2$m. HFE was successfully used to map the domains required for LILRB1 binding to MHC-I by making chimeric molecules due to lacking an interaction with LILRB1 (181). However, whether HFE is recognized by KIR3DL1 has not yet been reported, nor its expression on 221 cells known.

Here, HFE cDNA was produced from 221 cells and N-terminally tagged with the HA epitope to monitor expression of HFE and HFE-MHC-I chimeras with the same antibody. The resulting constructs were transduced into 221 cells as described in Chapter 2, and stable clones were isolated using single cell sorting with anti-HA mAb. There was no increase in W6/32 staining on these subclones indicating W6/32 does not react with HFE (Fig 5-12a). 721.221 cells are a mutated variant of Epstein-Barr virus-transformed lymphoblastoid cell line (LCL.721 cells) with loss of HLA-A, B and C expression (201) and they maintain a low level of reactivity with W6/32 relative to isotype control (Fig 5-12a). The results with the HA-HFE transfectants suggest HFE is not the protein that W6/32 recognizes on these cells.

In agreement with previous reports (169, 232), D0Fc alone showed some binding to 221 cells relative to Fc alone (Fig 5-12b). This is perhaps due to the unstable property of the D0 domain alone causing erratic background similar to with RIE cells or the potential recognition of unknown proteins expressed on the

cells. Interestingly, the presence of W6/32 did not alter D0Fc binding (Fig 5-12c), suggesting the binding observed on 221 cells is not because of any W6/32 reactive membrane proteins. However, no enhancement of D0Fc binding to HFE transfected 221 cells occurred relative to parental 221 cells (Fig 5-12b), despite HFE expression as detected with the anti-HA staining (Fig 5-12a), indicating that KIR3DL1-D0 domain does not bind HFE.

5.2.8. Swapping the B27-α3 domain with the HFE-α3 domain alters recognition by various antibodies

My previous studies in Chapter 4 revealed the potential role of the α3 domain in the KIR3DL1 mediated interaction (232). To investigate if the B27-α3 domain is required to obtain the binding by 3DL1-D0, I exchanged the α3 domain of HLA-B*27:05 with that of HFE and generated two chimeric constructs, HFEα1α2B27α3 and B27α1α2HFEα3 (Fig 5-13a). The constructs were linked to the HA epitope as described (Fig 5-13a) and transduced into 221 cells. Unfortunately, in the case of HFEα1α2B27α3, I could not obtain cells expressing a reasonable level of chimeric protein as indicated with anti-HA staining for further use (Fig 5-13b). A similar result occurred when the construct was transiently transfected into 293T cells (Fig 5-13c). The phenomenon may be due to a lack of compatibility between the HFE-α1α2 and B27-α3, or it may be that the artificial linker inserted between the segments somehow affects the tertiary structure resulting in a defect in protein expression. However, for B27α1α2HFEα3, I was able to select the cells with sufficient expression for further experiments (Fig 5-13d).

It is worth noting that generating the chimeric construct B27α1α2HFEα3 did not require an artificial linker between the fragments of HFEα1α2 and B27α3 due to the presence of a natural restriction site at the end of the B27-α2 sequence (Fig 5-13a). Subclones expressing comparable amounts of HA epitope relative to

HLA-B*27:05 were selected and maintained for further examination. It must be noted that B27^{low} was chosen based on comparable HA expression.

To characterize the conformation of the chimeric protein, I stained the transfected cells with antibodies specific for Bw4 (anti-Bw4), B27 (B27M1) and HLA (W6/32). As expected, the substitution of B*27:05-α3 with HFE-α3 caused the elimination of most of the W6/32 reactivity (Fig 5-13d), consistent with earlier studies showing that the W6/32 epitope requires the α3 domain (223, 235, 238-240). In addition, the substitution had no influence on the Bw4 epitope relative to the HA epitope although the anti-Bw4 antibody does not detect wild type B*27:05 very well in the first place (Fig 5-13d). Curiously, the chimera lost reactivity to anti-B27 antibody, B27M1 (Fig 5-13d), indicating that replacing the B27-α3 domain with the HFE-α3 domain somehow disrupts the B27M1 epitope. B27M1 reactivity is known to require solvent accessible residues 32, 41, 43, and at least one of the residues between 67-71 located in an α-helix in the α1 domain (241). Residue 32 contributes to the association with $β_2$m, while residues 41 and 43 are located in the loop at the N-terminus of the peptide groove (Fig 5-13e). Therefore, to my knowledge, B27M1 is a conformationally sensitive antibody detecting the B27/$β_2$m complex that requires the α3 domain participation, and the epitope is mapped mostly on the α1 domain. Overall, the results indicate that replacing the α3 domain of B*27:05 with that of HFE could possibly alter the α1 conformation.
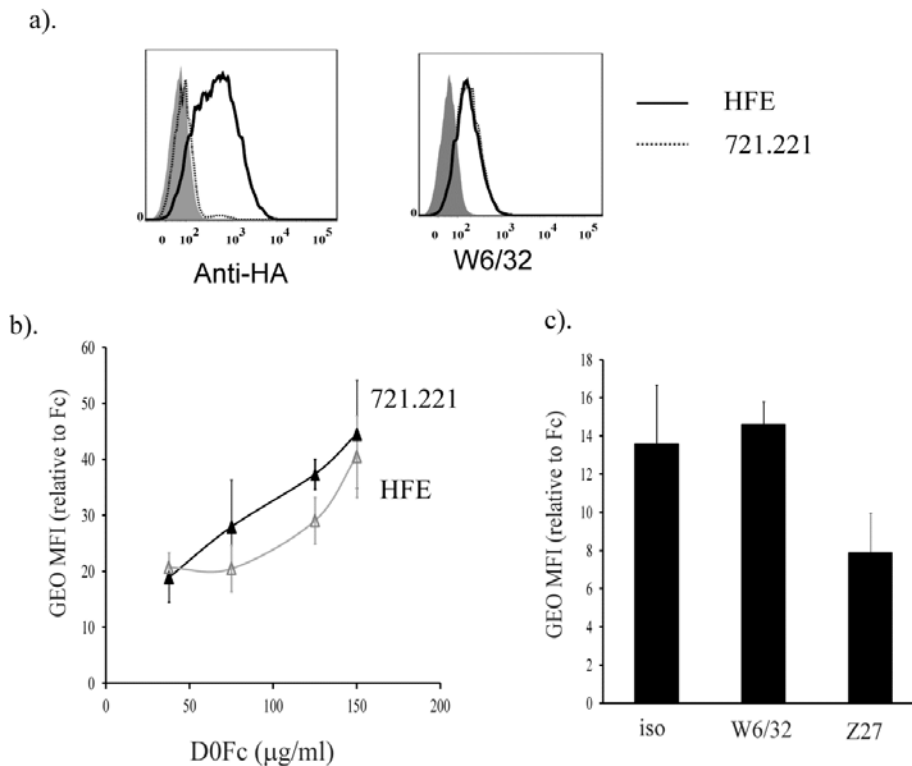
Figure 5-12. KIR3DL1-D0 domain does not bind HFE.

a) Surface expression of HA or MHC-I by flow cytometry with indicated antibodies staining. Isotype control is indicated with filled histogram. *b).* D0Fc titration on the 221 or 221 transfectant stably expressing HFE. c). Antibody blocking of D0Fc binding. 100µg/ml of the indicated antibodies were preincubated with 221 cells prior to 50 µg/ml of D0Fc being added. The same concentration of Fc only was added as the negative control. The readout was proportional to Fc only. The average of three experiments is shown with standard error.
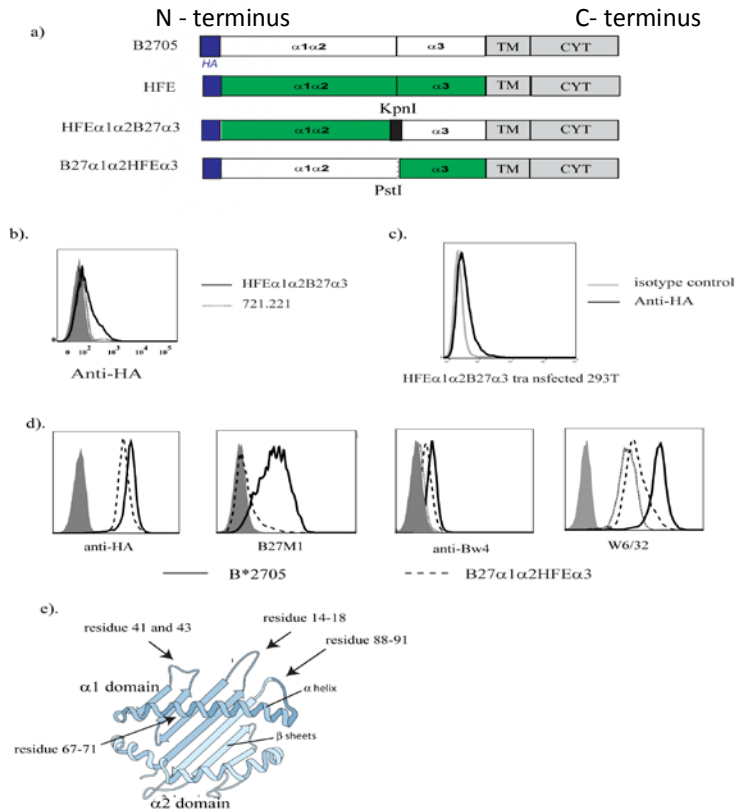
Figure 5-13. Swapping of the α3 domain of B27 with that of HFE alters recognition by various antibodies

a) Schematic diagram of the α3 domain swap. The domain composition of the two chimeric constructs HFEα1α2B27α3 and B27α1α2HFEα3 are shown. *b-c)* Surface staining of HFEα1α2B27α3 on 221 cells (*b*) or 293T cells (*c*) using anti-HA antibody or isotype control (indicated as filled histogram in Fig 5-13*b*) and followed with PE anti mouse IgG. The results were analyzed by flow cytometry. *d)* Surface staining of 221 cells or cells expressing chimeric protein B27α1α2HFEα3 with the indicated antibodies. Isotype control is shown with the filled histogram. Cells were stained with secondary PE conjugated anti mouse IgG to detect antibody binding. The results were analyzed by flow cytometry. The dotted line indicates parental 721.221 cells. *e)* Ribbon diagram showing the α1 and α2 domains of MHC-I molecule. Residues acquired for B27M1 reactivity indicated as orange, green and purple arrows. Red arrows indicate contact residues for 3DL1-D0 interaction based on the crystal structure. Image is modified from figure 8-4b, Kuby Immunology sixth edition.

169

5.2.9. Substituting the α3 domain affects LILRB1Fc, 3DL1Fc and D0Fc binding

As previously reported, soluble full-length LILRB1 protein does not bind HFE and the substitution of the α3 domain of HLA-B*07:02 with that of HFE was reported to cause the loss of LILRB1 interaction as measured by fluorescent microscopy (181). Similarly, in my hands, substitution of the B27-α3 domain with the HFE-α3 domain resulted in an absence of detectable LILRB1Fc binding relative to Fc alone analyzed by flow cytometry (Fig 5-14a). To address the role of MHC-I-α3 in KIR3DL1 binding, I examined the binding capacity by 3DL1Fc to the chimera. Surprisingly, I observed enhanced binding to cells expressing B27α1α2HFEα3 in comparison to wild type B*27:05 (Fig 5-14b). Moreover, D0 alone also bound the chimera better than wild type B*27:05 (Fig 5-14c). The enhancement of the binding in the presence of the HFE-α3 domain perhaps is caused by increased accessibility at site 2 for 3DL1-D0 and/or a conformational change in MHC-I structure augmenting the affinity of D0 to site 2 on the α1 domain. While binding to HFEα3 by KIR3DL1 is not completely ruled out in this chapter because I did not obtain sublines with HA-HFE with matched expression to the chimeras (compare Fig 5-12a and Fig 13d), the enhanced binding is not likely due to binding to the HFE-α3 domain because there was not detectable specific binding to HA-HFE.
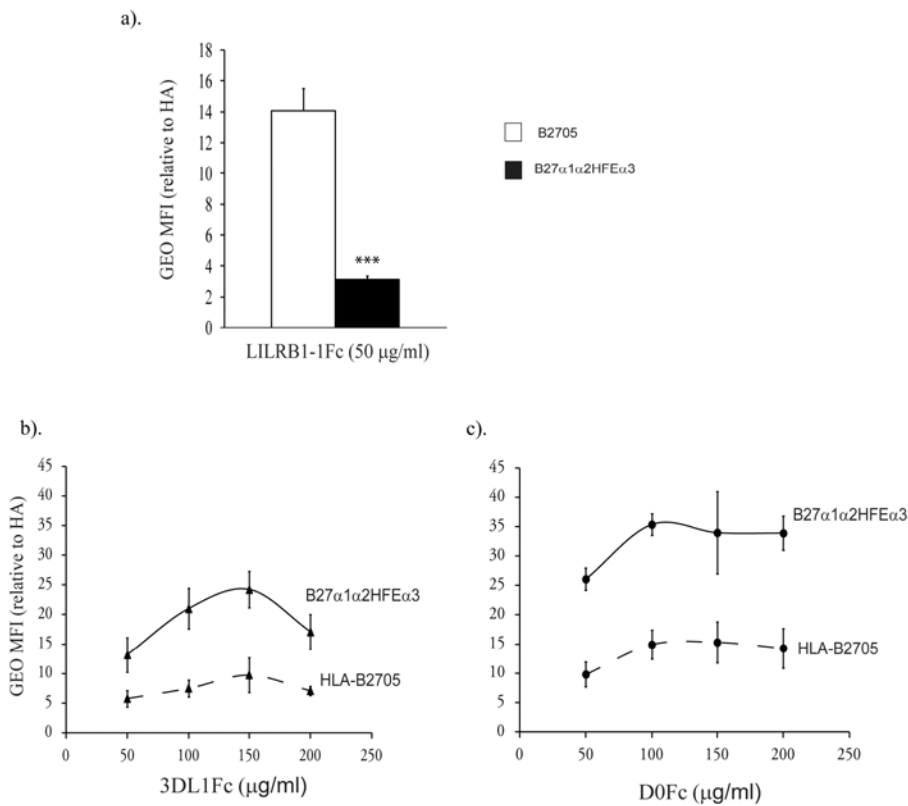
Fig 5-14. B27α1α2HFEα3 enhances 3DL1Fc and D0Fc binding.

a). Substitution of HFE-α3 results in the loss of LILRB1Fc binding. The binding was measured at 50 µg/ml of fusion proteins. The results are the average of four experiments with duplicate measurements and the error bars represent standard error. *** indicates $p < 0.001$. Titration of 3DL1Fc (*b*) or D0Fc (*c*) on the indicated cells. The mean with standard error is shown as error bars for four independent experiments.

5.3. Discussion

Using 3DL1Fc and D02DL1Fc fusion proteins and various murine cell lines, I showed xenorecognition of mouse MHC-I alleles, $H-2D^d$, D^b, K^b and perhaps rat MHC-I, but not $H-2D^k/K^k$ by KIR3DL1. With the addition of various specific antibodies, I showed that the interaction is dependent on the D0 domain, and that it is blocked by anti-D^b-$\alpha 3$ antibody, 28.14.8S. By means of various combinations of Ig domains, I further showed that the D0 domain is responsible for the recognition of $H-2D^b$ and for the reactivity to the antibody Z27, and that other Ig domains are also required for maintenance of optimal binding. By means of replacing the B27-$\alpha 3$ domain with the HFE-$\alpha 3$ domain, I showed that the MHC-I-$\alpha 3$ domain is important for maintaining reactivity with the B27 allele specific antibody, B27M1 and the pan reactive anti-MHC-I antibody, W6/32, but not for that of an anti-Bw4 antibody. Furthermore, I showed enhanced KIR3DL1-D0 binding to the chimeric protein with the $\alpha 3$ domain of HFE, presumably caused by the alteration of the tertiary structure of the $\alpha 1$ domain or greater binding to HFE-$\alpha 3$ domain.

I showed that D0Fc bound MHC-I negative cells and the streptavidin conjugated beads, and that the binding to cells did not saturate at the maximal concentration. The results suggest that the fusion protein, D0 alone with Fc, binds "non-specifically" to the cells perhaps due to the protein being denatured during purification and storage. In addition to its putative unstable property, D0Fc was already known for poor yield in comparison to other fusion proteins such as D02DL1Fc (169). Given that KIR2DL1 does not bind mouse MHC-I, at least $H-2D^b/K^b$, as suggested in Fig 5-4b, and that D0 supported by a D1 domain provides better binding (Fig 5-8 and 5-9), the fusion protein composing D0 in the context of 2DL1Fc (D02DL1Fc) seems to be a better tool for investigating the role of the D0 domain in binding to mouse MHC-I molecules. To discriminate KIR3DL1 binding specific to H-2 molecules from other unknown molecules, I immobilized biotinylated purified $H-2K^b$ monomer on streptavtidin coated beads and examined

172

3DL1Fc and D0Fc binding to the conjugated beads. Noticeable binding was observed in the one experiment performed, but further repeats and examination of binding to purified K^b in the presence of antibodies are required to solidify the results.

To distinguish the roles of individual Ig domains, I examined the antibody specificity of various combined fusion proteins as well as the binding to H-2D^b molecules. The results showed that D0Fc alone lost part of the reaction to Z27, but in the presence of D1, D0 displayed better binding to H-2D^b and gained a greater reaction with anti-D0 antibody, Z27. However, in the absence of D0, KIR3DL1-D1D2Fc did not bind H-2D^b. The results suggest that the D0 domain is essential for binding to mouse MHC-I by KIR3DL1, and that other Ig domains (especially the D1 domain) are also required to maintain optimal binding, perhaps by direct involvement in the binding or by helping proper folding or stability of the protein.

To understand the interaction of D^b and K^b with KIR3DL1, I used several available antibodies. B22-249, 28.14.8S and Y3 were thought to bind H-2D^b α1, α3 domain and H-2K^b α1 domain, respectively, and this was established in immunoprecipitation assays (231). However, by flow cytometry, I also showed the cross-reaction of D^b-specific antibodies to H-K^b. Similar to W6/32, 28.14.8S dramatically blocked 3DL1Fc and D02DL1Fc binding to H-2D^b, suggesting that the D^b-α3 domain perhaps interacts with KIR3DL1 or that 28.14.8S sterically interferes with the interaction. However, whether the α3 domain is involved in the binding to mouse MHC-I by KIR3DL1 still needs to be further clarified.

A crystallographic study has demonstrated that KIR3DL1 uses two separate sites to interact with HLA-B*57:01, including site 1 where the D1D2 domains contact the polymorphic region of α1α2, and site 2 where the D0 domain binds the conserved region of the α1 domain (229). Comparison of the α1α2 domains of human and mouse MHC-I molecules demonstrates a surprisingly high similarity

of the site 1 regions (underlined in Figure 5-3), implying the possibility that D1D2 also contacts mouse MHC-I. However, in the absence of D0, KIR3DL1-D1D2Fc does not bind (Fig 5-9), indicating that site 1 is not important in the interaction of KIR3DL1 with mouse MHC-I. Moreover, in this Chapter, I showed no detectable binding of 3DL1Fc to RDM4 cells expressing H-2D^k/K^k. A comparison of protein sequences at site 2 provides some hints regarding the residues required for the interaction. Particularly, residue 19 in H-2K^k is replaced from a negatively charged Glutamic acid (E) to a positively charged Lysine (K) (Fig 5-3). Therefore, it is possible that site 1 and 2 both contribute to the interaction of KIR3DL1 and H-2 alleles examined. In addition, anti-D^b-α3 and the anti-D0 antibody but not anti-α1α2 antibody fully block 3DL1Fc binding, indicating the potential involvement of the α3 domain or that anti-α3 blocks site 2. Collectively, like HLA, mouse MHC-I could supply multiple distinct regions for KIR3DL1 recognition.

Although surface expression of endogenous HFE on 221 cells was not determined, less binding to HFE stably transduced 221 cells by D0Fc relative to parental 221 cells (Fig 5-14b) indicates that the chance that the KIR3DL1-D0 domain binds full-length HFE is remote. However, the binding to HFE by D1D2 domains was not determined in this chapter. Therefore, thus far, whether KIR3DL1 binds HFE is still unknown. To clarify whether the α3 domain participates in KIR3DL1 interaction, I exchanged the HFE-α3 domain with the B27-α3 domain and compared their binding to wild type B*27:05 molecules. Surprisingly, the HFE-α3 substitution enhanced the binding of full-length 3DL1Fc and D0Fc. The enhancement may be due to a conformational change in the α1α2 domains. If the chimera with HFE is a less stable protein fold, it could lower the threshold to an induced fit with KIR3DL1. Alternatively, unlike LILRB1, KIR3DL1 could recognize HFE-α3 in the context of B27-α1α2. Given that there is direct contact with $β_2$m by the D0 domain as demonstrated in the crystal structure, HFE-α3 may make $β_2$m more accessible to facilitate the better binding relative to B27:05. The enhanced binding to the chimera, presumably at site 2,

may be masking the involvement of the α3-domain in a KIR3DL1 cognate interaction. Thus, other homologs (e.g. H-2K^k) could be used for further investigation. Moreover, the results that D0Fc is unlikely to bind HFE and its greater binding to the B27α1α2HFEα3 chimera imply that the α3 domain may not be required for KIR3DL1-D0 domain binding. However, further experiments need to be done for clarification.

In summary, the results presented in this Chapter firstly demonstrated xenorecognition of mouse MHC-I molecules by KIR3DL1 and indicate an important role for the D0 domain in the interaction. The results also raise many new questions that need further investigation.

Chapter 6

THE INFLUENCE OF POSITION 194 OF MHC-I

ON KIR3DL1-D0 BINDING

Preface

Based on evidence from the literature that the residue at position 194 influences
the interaction with KIR3DL1, the studies in this chapter were designed to explore
if the residue 194 is engaged in KIR3DL1-D0 binding. I have performed all of the
experiments, and they have not yet been published.

6.1. Introduction

In Chapter 4, I showed an effect of the anti-α3-antibody, W6/32, on KIR3DL1 binding. W6/32 is reported to react with a conformationally dependent epitope on the HLA heavy chain / β2 microglobulin (β2m) complex (242). Particular MHC-I alleles of other species, such as mice, rat, rabbit and guinea pig, which do not react with W6/32 when expressed in association with autologous β2m, can acquire W6/32 reactivity when cultured with bovine serum by association with free bovine β2m. This activity requires an arginine (R) at position 121 on the MHC-I-α2 domain (235). Moreover, residues near the first cysteine-comprised disulfide loop in the α2 domain play a role in W6/32 reactivity, likely by contributing to the stability of the heavy chain/β2m complex (240). Using mutations and a domain swap with H-2K^b, Tanabe et al. showed that W6/32 recognizes the HLA-α2 and α3 domains (223). Given the presumed location of W6/32 reactivity, its ability to block LILRB1 interaction with HLA-α3 and β2m (170, 171), and the observation that W6/32 does not block D02DL1 as well as it does 3DL1, I proposed that W6/32 is unlikely to alter the KIR3DL1 interaction that occurs on the top of α1α2 domains (site 1) as demonstrated by crystallographic studies (229), and perhaps directly contacts the α3-domain.

According to the structure of the KIR3DL1-HLA-B*57:01 complex, it is impossible for KIR3DL1-D0 to extend down and make contact with α3 of HLA while interacting with the top of the peptide groove of α1α2 on the same molecule (Fig 6-1). Although results presented in Chapter 5 indicate that a W6/32 reactive α3 domain is not required for KIR3DL1-D0 interaction, they do not rule out a potential presence of a third site of contact on the α3 domain by KIR3DL1. Curiously, the combination of natural substitutions at positions 77-83 (α1) and at position 194 (α3) in HLA-B*5101 remarkably influence the response of primary NK cells expressing only KIR3DL1 as measured by reductions in IFN-γ secretion (167). Coincidently, the amino acid at position 194 makes direct contact with residues of LILRB1-D1 (170). Therefore, the phenomenon was suggested to be

177

due to the interference of LILRs even though LILRB1 was not expressed on the selected NK cells and no other LILRs are thought to be expressed by NK cells. As illustrated in Fig 6-1, this residue sits near the first loop of the α3 domain at a substantial vertical distance away from the α1α2 domain and it faces towards the C-terminal end of the peptide binding groove that constitutes site 1. Therefore, there is a potential role for position 194 participating in the formation of a third contact site with KIR3DL1-D0. If this were so, LILRB1 then would be expected to compete with KIR3DL1 for this site. In this chapter, I examined whether position 194 influences KIR3DL1 binding using mutagenesis, and assessed if LILRB1 impacts KIR3DL1 signaling when residue 194 is mutated. For comparison, I also tested if mutation of position 194 alters LILRB1 binding.
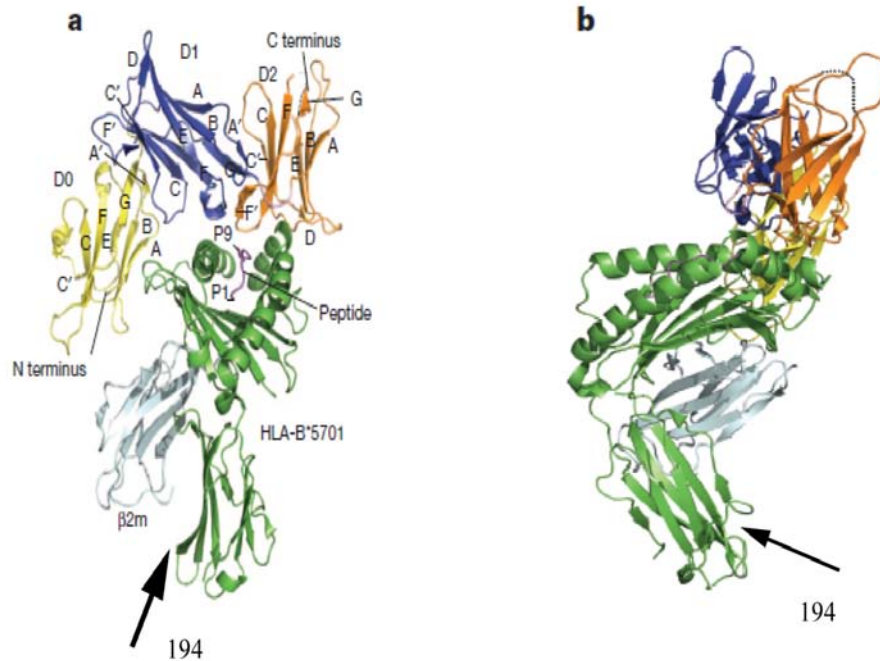
Fig 6-1: Illustration of the location of position 194 on the 3DL1-B*57:01 complex (Adapted from Nature, 2011, 479: 401)

The HLA and β₂-microglobulin are colored green and cyan, respectively. The three Ig domains of KIR3DL1, D0, D1 and D2 are colored as yellow, blue and orange, respectively. Front view (*a*) and side view (*b*) of the structure are shown. Arrows indicate the location of position 194 on MHC-I.

6.2. Results

*6.2.1. Establishment of B*27:05 and I194A stable clones*

The specificity of KIR3DL1 for HLA-Bw4 is dependent on the interaction of KIR3DL1-D1D2 with the peptide groove region of the HLA α1α2 domains. Therefore, to dissect if position 194 is involved in D0 binding to MHC-I, I chose a weak ligand of KIR3DL1, HLA-B*27:05, to maximize the chance of observing a difference in binding. To explore the role of position 194 in KIR3DL1 interaction, I generated the mutant I194A by replacing isoleucine (I) at position 194 on HLA-B*27:05 with alanine (A). The DNA sequence of wild type B*27:05 and mutant I194A were then tagged with human influenza hemagglutinin (HA) epitope at the N-terminus and transduced into 721.221 cells (an MHC-I negative cell line) as described (see Chapter 2). The transfected cells were puromycin selected and cells showing the highest surface level of MHC-I were isolated using single cell sorting. Stable clones expressing wild type or mutated HLA-B*27:05 were selected for further examination based on comparable surface levels using HA (Fig 6-2a).
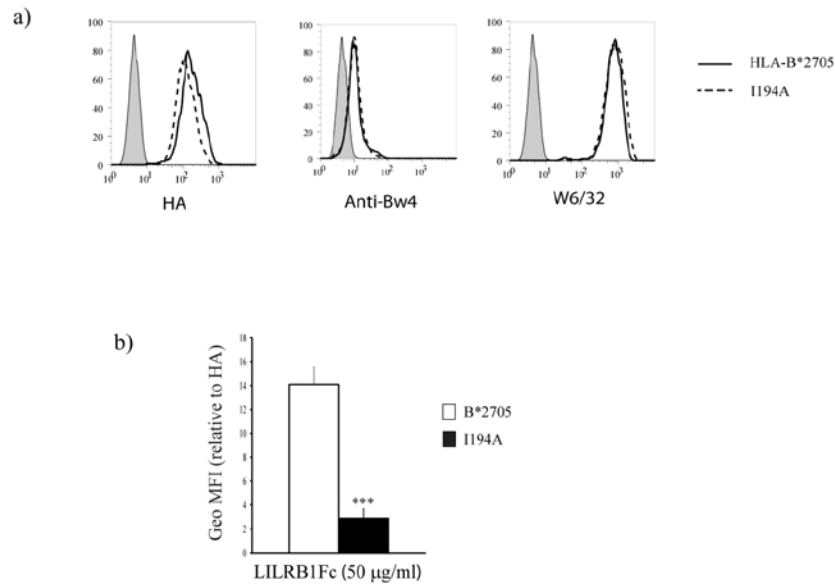
Fig 6-2. Mutation at position 194 of MHC-I eliminates LILRB1Fc binding.

a). Flow cytometric analysis of 221 cells stably expressing HA tagged HLA-B*27:05 and I194A mutant using surface staining with the indicated antibodies. The isotype control is shown with the filled histogram. *b).* LILRB1-Fc binding of the stable clones shown in *a)* at 50μg/ml. Statistical significance was calculated using an unpaired student's *t* test. The mean of three independent experiments is shown with standard error indicated by error bars (n=4). *** indicates $p < 0.001$.

6.2.2. Mutation at position 194 has no influence on Bw4 and W6/32 epitopes, but perturbs binding to LILRB1

To characterize the effect of the I194A mutation in B*27:05, I first evaluated the influence of position 194 on the reactivity to the antibody specific for Bw4 (anti-Bw4) and the antibody against an epitope shared by all HLA class I isoforms (W6/32). In comparison to the wild type, the mutation at position 194 did not significantly impact either antibodies' reactivity relative to the HA epitope using flow cytometric analysis (Fig 6-2a), suggesting that the substitution at position 194 with an alanine (A) has little effect on the Bw4 and W6/32 epitopes.

To examine the contribution of position 194 to the LILRB1-MHC-I interaction, I performed a binding assay with full-length soluble LILRB1-Fc (R&D). The relative binding was calculated as geometric mean fluorescent intensity (Geo MFI) of LILRB1Fc proportional to that of Fc / Geo MFI of HA in order to normalize between experiments. Mutation to A at position 194 diminished LILRB1-Fc binding, and the reduction was statistically significant ($p<0.001$, n=4) (Fig 6-2b), suggesting isoleucine (I) at position 194 on HLA-B*27:05 is pivotal for LILRB1 recognition. LILRB1 is known to contact the residue at position 194 of MHC-I using tyrosine (Y) at position 38 (170). However, the influence of the amino acid at residue 194 of MHC-I on the interaction has not been evaluated by mutagenesis. These results show that the interaction between Y at position 38 in LILRB1 with the residue at position 194 in HLA-B*27:05 contributes substantially to the binding.

6.2.3. The effect of mutagenesis at position 194 on KIR3DL1 binding

In Chapter 4, I showed a possible biphasic binding of soluble 3DL1Fc to HLA-B*58:01 with the second increase at around 300 µg/ml in comparison to the plateaued binding in the range of 100 to 200 µg/ml (Fig 4-5). Based on the previous results, here I examined the binding of soluble 3DL1Fc to B*27:05 in

the range of 25 µg/ml to 250 µg/ml. Moreover, to investigate the influence of I194 on 3DL1Fc binding, I compared the binding capacity of 3DL1Fc to wildtype and mutated B*27:05 relative to their anti-HA staining. In agreement with previous functional results (56, 71), I detected the binding by 3DL1Fc to the cells expressing HLA-B*27:05 relative to Fc alone (Fig 6-3b). Importantly, using this range of concentrations, the binding appears to have two distinct phases, with one saturation point between 100 and 150 µg/ml, and the second increase at the dose of 250 µg/ml (Fig 6-3b). However, although four experiments have been collated, the error bars are somewhat overlapping at several points. Therefore, to firm up the conclusion of biphasic binding, it will require more repetitions and testing at more concentrations between 150 and 250 µg/ml. A slightly different binding curve was observed for the I194A mutant. The increase was linear until 150 µg/ml but the binding at the highest concentration of 250 µg/ml was lower than with the wildtype sequence (Fig 6-3b). The results suggest that position 194 on HLA-B*27:05 may have a limited effect on the binding of full-length 3DL1, but they did hint at the presence of multiple binding sites and imply that the effect was only on the lowest affinity site.

In the co-crystal structure, KIR3DL1 predominantly contacts HLA-B*57:01 via site 1, and mutagenesis studies in the same publication revealed that the overall binding strength is enhanced with the addition of the D0 controlled site 2 (232). Thus, a potential third site of interaction mediated by D0 might be obscured by the ability to bind at site 1. To study the effect of mutating position 194 without an interaction at site 1, I tested binding of the D0 domain in the context of extracellular Ig domains of KIR2DL1, D02DL1Fc (described in Chapter 4). The readout is shown proportional to that of 2DL1Fc and then normalized to HA, although 2DL1Fc had a level of staining similar to that of Fc alone as before. Consistent with results shown in Fig 5-4, the overall binding of D02DL1Fc in these assays was less than the full-length 3DL1Fc (Fig 6-3c). Importantly, in comparison, there was a slight decrease in binding to the mutated

B*27:05 relative to wildtype B*27:05 (Fig 6-3c). The results suggest position 194 has an impact on KIR3DL1-D0 binding when the more dominant site 1 is excluded, but the limited binding overall makes it difficult to be conclusive.
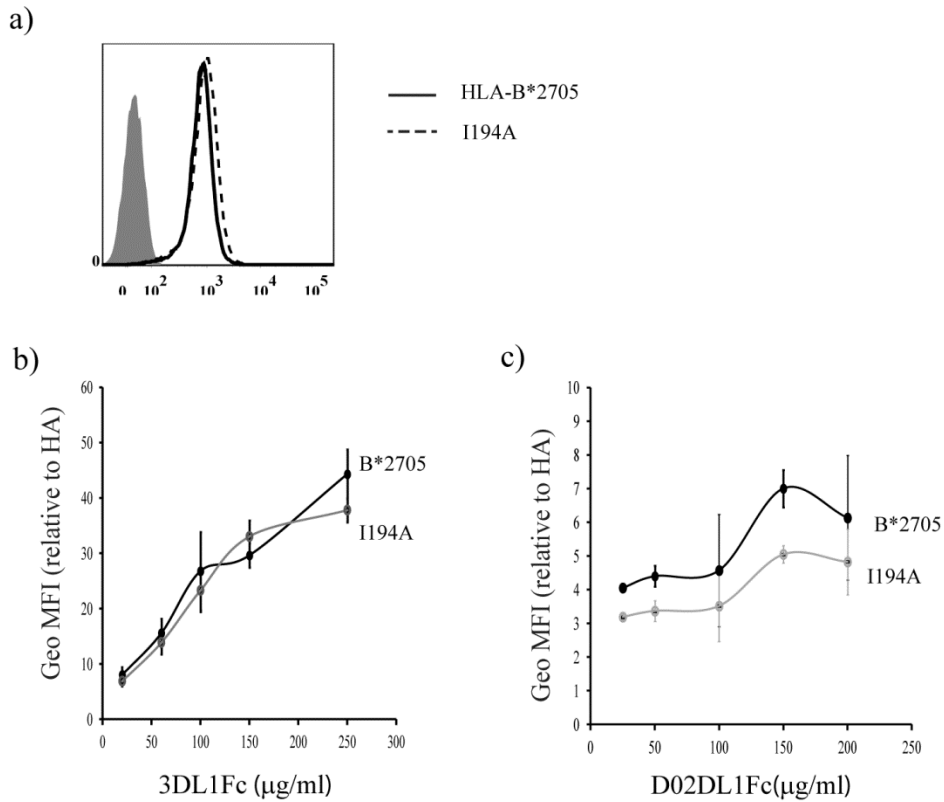
Fig 6-3. The influence of position 194 on 3DL1Fc and D02DL1Fc binding.

a). Surface expression of MHC on the indicated cells stained with anti-HA mAb. The filled histogram represents the isotype control staining. Titration of 3DL1Fc (*b*) or D02DL1Fc (*c*) on the indicated cells. The results were relative to Fc control (*b*) or 2DL1Fc (*c*) and then normalized to HA. The mean of four independent experiments is shown. Standard error is represented by error bars.

6.2.4. The effect of position 194 on KIR3DL1 functional recognition

In spite of the small effect of the mutation at position 194 on binding of full-length 3DL1 at 4°C, I went on to test the effect on functional recognition at 37°C where a third site of interaction might be required to stabilize the complexes and promote receptor clustering. I examined KIR3DL1$^+$YTS cells lysis of 221 transfectants at various effector:target ratios. In addition, YTS cells expressing a mutated KIR3DL1 in which Y200 was replaced with an A on the D2 domain, Y200A (described in Chapter 4), was also tested, as the replacement decreases KIR3DL1-mediated inhibition by disrupting binding at site 1 (229). Given the lysis of the three target cells by parental YTS cells was variable, and the cytolytic capacities among various YTS transfectents were inconsistent (Fig 6-4a), the lysis results of YTS transfectents normalized to that of YTS are also shown (Fig 6-4b). As expected, partial inhibition of lysis was observed with B*27:05, suggesting that the surface level of MHC-I expressed on the subclone that I used is sufficient to induce some KIR3DL1-mediated inhibitory signaling. A single experiment showed that the level of inhibition is unchanged when I was mutated to A at position 194 (Fig 6-4b, left panel). Interestingly, disruption of site 1 (KIR3DL1Y200A mutant) led to less inhibition of lysis in response to I194A mutation comparing to wild type B*27:05 at low E:T ratios starting from 3:1 (Fig 6-4b, right panel). The results suggest that at this level of MHC-I, residue 194 on HLA-B*27:05 does not influence KIR3DL1-D0 function except when the dominant site 1 interaction is compromised. Given the lack of a pronounced effect in this preliminary experiment, further studies with these target cells were not pursued.
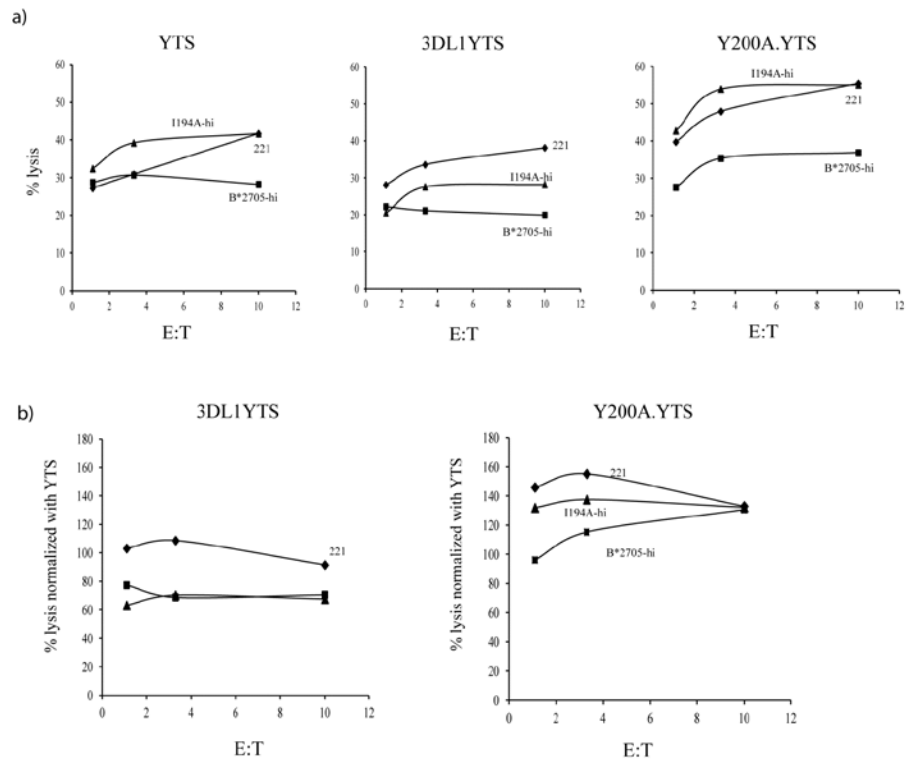
Fig 6-4. YTS lysis of 221 cells expressing wild type B27 or the I194A mutant.
a). One experiment of NK cytolysis. Cytolysis was measured in a standard chromium release assay. Parental YTS, YTS stably expressing KIR3DL1 or cells expressing Y200A mutant lyse target cells in Fig 4-5. *b).* The lysis results of 3DL1.YTS or Y200A.YTS were normalized to that of parental YTS shown in *a).* One experiment with triplicate measurements is shown.

6.2.5. The influence of substitution at position 194 on KIR3DL1-D0 binding when MHC-I level is low

Inhibitory KIRs, such as KIR3DL1, are geared to detect the loss of MHC-I during viral infection, thus, interaction with low levels of MHC-I is relevant and could reveal the phenotype of I194A more than when it is at high density. To test the effect of the I194A mutation at lower densities of MHC-I, I isolated clones using single cell sorting based on less W6/32 staining relative to previously selected clones (Fig 6-5a). The stable clones expressing wildtype or mutated B*27:05 with similarly low intensity of HA were selected and maintained for the binding experiments as described. Of note, approximately two-fold less surface MHC-I was observed for the low subclones, when analyzed using anti-HA or W6/32 staining (Fig 6-5b and c) (average Geo MFI of HA = 65.7 vs 35.4 or W6/32 as 523.57 vs 231.3, respectively). Obviously, the reduction did not alter the relative W6/32 reactivity (Fig 6-6a) nor the significance of I at position 194 on LILRB1-Fc binding (n=3, $p < 0.05$) (Fig 6-6b). More importantly, in comparison to the wild type, the binding to the mutated B*27:05 by full length KIR3DL1 was reduced in a dose dependent manner (Fig 6-6c, left panel). Notably, commercial 3DL1Fc was used in this assay, and the two sources of 3DL1Fc proteins showed somewhat different binding curves to B*27:05 (Fig 6-3b vs Fig 6-6c), which may be due to differences in glycosylation or the presence of denatured receptor in some of my preparations. As position 194 was influencing the contact with D0, I used D0 alone fused with human IgG1 Fc, D0Fc, and examined the binding to the cells expressing wildtype or mutated B*27:05. Similar to 3DL1Fc, D0Fc bound less to the I194A mutant relative to wild type B*27:05 (Fig 6-6c, right panel). The results suggest that with low levels of MHC-I, the residue at position 194 on MHC-I clearly alters LILRB1Fc and 3DL1Fc binding, and the influence on D0 domain binding is obvious.
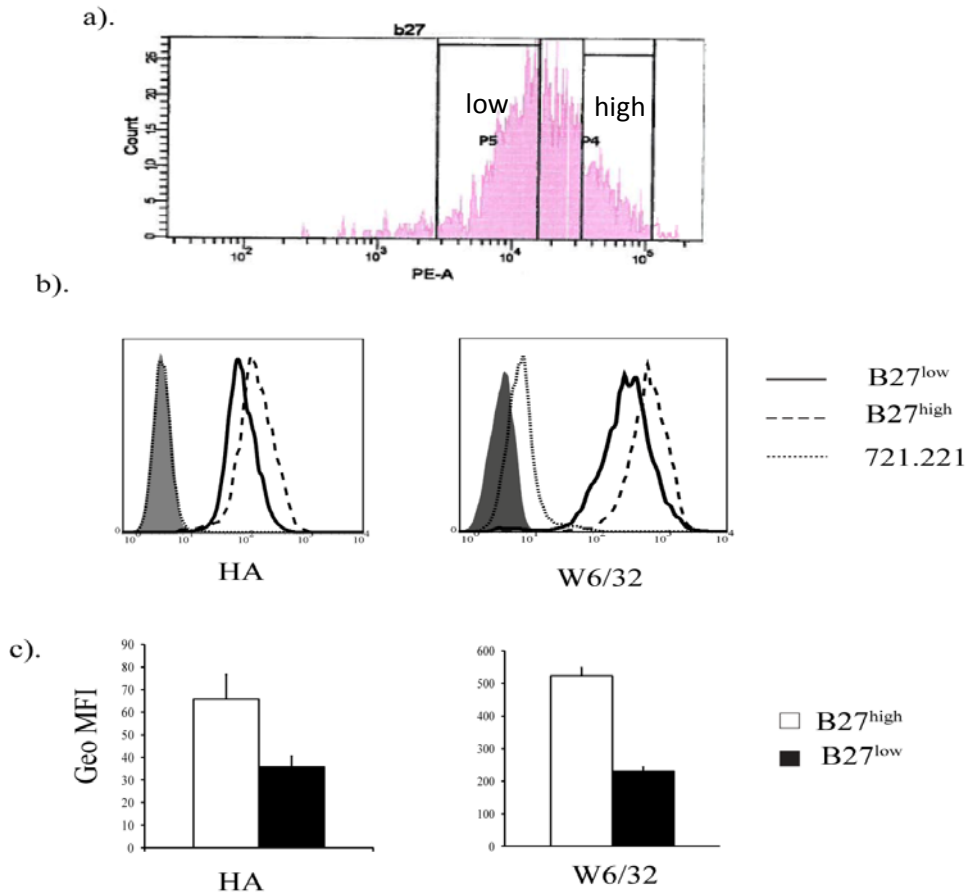
Fig 6-5: Isolation of low MHC-I population from 221 transfectants.

a). 221 cells transfected with HA tagged HLA-B*27:05 were sorted into MHC-I low and high populations. *b).* Surface staining of selected B*27:05^{high} or B*27:05^{low} subclones with the indicated antibodies followed by secondary antibodies. Samples were analyzed with flow cytometry. *c)* Approximately a 2 fold reduction of B27^{low} is shown in comparison to B27^{high} clones. The mean of five experiments with standard error are shown. Geo MFI of specific antibody staining is proportional to that of isotype control.
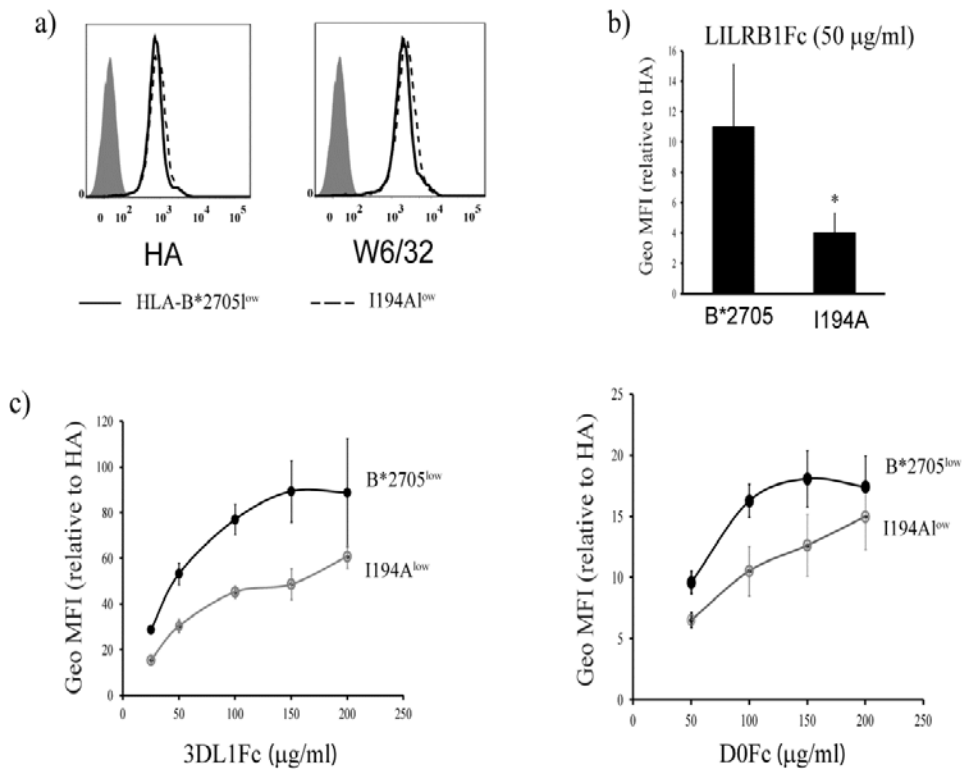
Fig 6-6. The influence of position 194 on LILRB1 and KIR3DL1 binding in low MHC-I population.

a). Surface anti-HA and anti-MHC-I staining on the low expressing clones of B*27:05 and I194A mutant. *b).* Mutation at position 194 eliminates LILRB1-Fc recognition. Binding by LILRB1Fc at 50 μg/ml to the indicated cells. The average of three experiments is shown. * indicates $p<0.05$. *c).* Titration of 3DL1Fc and D0Fc binding. The results were normalized to HA staining on each day. The mean of four independent experiments at each concentration is shown with standard error.

6.2.6. Antibody blocking of 3DL1Fc and D0Fc binding to B*27:05

Encouraged by the observation that mutating I at position 194 to A caused a discernible change of 3DL1-D0 binding on cells with low levels of MHC-I, I went further to characterize the interaction. I performed antibody reversal experiments using Z27, the antibody specific for 3DL1-D0, and the anti-MHC-I-α3 mAb, W6/32. As previously shown in Fig 6-6c, the mutation resulted in less binding to D0Fc at 100 µg/ml (Fig 6-7). In contrast to isotype control, Z27 totally disrupted D0Fc binding to the mutated B27, but only partially blocked binding to wild-type B27 (Fig 6-7), further supporting the idea that the mutation at position 194 influences D0 mediated interaction at an additional site. Surprisingly, a similar reduction occurred in the presence of W6/32 (Fig 6-7), though the reactivity to the antibody did not differ between the mutated and wild type B27 (Fig 6-6a). Currently, it is hard to explain why W6/32 has less effect on binding of KIR3DL1-D0 to wild type comparing to mutated B27 unless position 194 somehow influences the interaction at site 1. Nonetheless, the results suggest both the W6/32 and anti-D0 can prevent the residual binding by D0 to the mutated B27. However, how these antibodies block remains unclear.
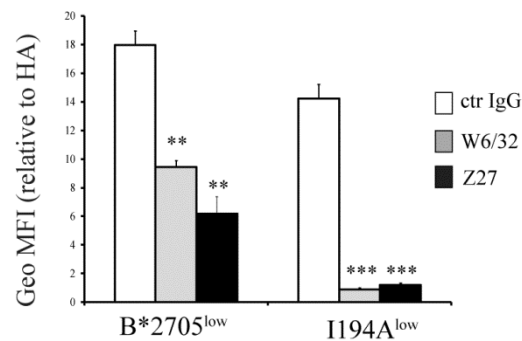
Fig 6-7. Antibody blocking of KIR3DL1-D0 binding to B*27:05

D0Fc binding to cells expressing a low level of wild type or mutated B27 in the presence of the indicated antibodies. 150 µg/ml Z27 or 50 µg/ml W6/32 were incubated with the indicated cells at room temperature for 10 min, then 100 µg/ml Fc or D0Fc were added and incubated at 4°C for 1 hr. The cells were washed and stained with PE anti-human Fcγ. The isotype matched IgG control was added at 150 µg/ml. Geometric MFI of binding was normalized with that of HA. The mean of three experiments were shown with error bar representing standard error. The p value is calculated with a student T test. **, $p<0.01$-0.05; *** , $p<0.001$.

6.2.7. Soluble LILRB1 does not prevent KIR3DL1 signaling

It is known that LILRB1 enhances KIR2DL1 mediated signaling upon engaging the same HLA-C molecule at a distinct site (171), but the limitations of my analysis presented in Chapter 3 did not clearly determine if LILRB1 influences KIR3DL1 signaling. However, the results with the I194A mutant suggest that LILRB1 should compete with KIR3DL1 if the effect of the mutation is because KIR3DL1 contacts position 194 directly. To address this issue, I generated a soluble form of the LILRB1 two membrane distal Ig domains with human IgG1 Fc, D1D2Fc, and tested if soluble LILRB1-D1D2Fc binding to MHC-I could prevent 3DL1 function on YTS cells. As expected, KIR3DL1 mediated inhibition of lysis was observed when cells expressed B*58:01 relative to parental 221 cells (Fig 6-8). As LILRB1-D1D2 is responsible for the interaction with the MHC-I-α3 domain, LILRB1-D1D2Fc is expected to block an α3 interaction that involves position 194. D1D2Fc of LILRB1 did not alter the inhibition (Fig 6-8), though the amount of LILRB1-D1D2Fc is sufficient for detecting LILRB1 binding to the cells expressing MHC-I at 4°C (Fig 6-2 and 6b). Unfortunately, in these assays, B*27:05 and the I194A mutant did not inhibit the 3DL1.YTS cells precluding detection of an effect of soluble LILRB1 on these interactions (Fig 6-8). The results suggest that the membrane distal two Ig domains of LILRB1 do not affect KIR3DL1 function in the YTS system. Although the concentration (50 μg/ml) used is enough for detecting the association of LILRB1 with MHC-I at 4°C, it is possible that during incubation at 37°C, the soluble protein dissociates too rapidly to prevent KIR3DL1 binding. Alternatively, the putative "site 3" interaction is not an interaction directly with position 194 or it is not required for KIR3DL1 function when its optimal interactions at site 1 and 2 are present.
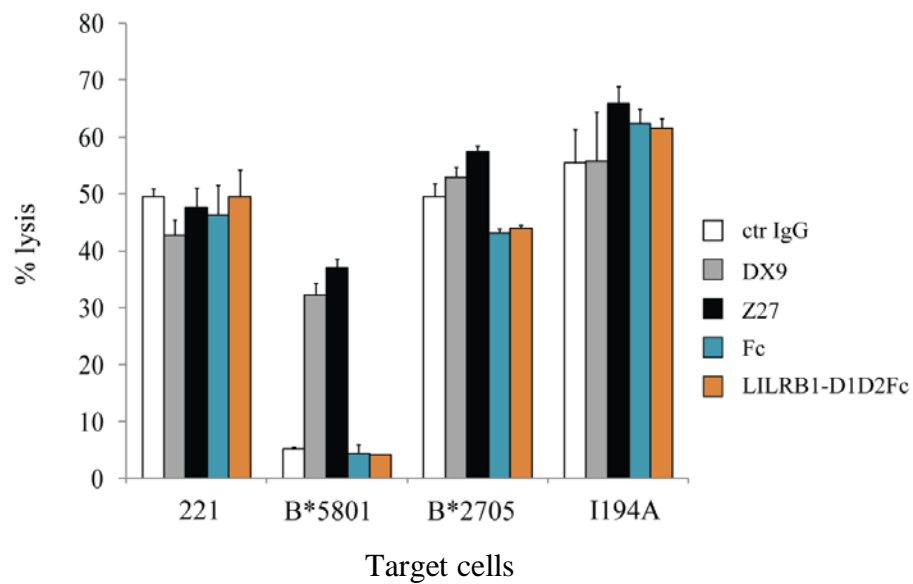
Figure 6-8. NK lysis of 221 transfectants in the presence of LILRB1-D1D2Fc.
Cytolysis by YTS-3DL1 was measured at an E:T of 3:1 in the presence of the indicated antibodies at 2.5 µg/ml. Fc or LILRB1-D1D2Fc was added at 50 µg/ml. Low MHC-I of stable clones were used here. Representative of two experiments with triplicate measurments is shown.

6.3. Discussion

KIR3DL1 is highly polymorphic and the variation is believed to allow optimal interaction with the diverse MHC-I molecules. The degree of association between KIR3DL1 and HLA-Bw4 is variable among different Bw4 subtypes, and the polymorphisms of KIR3DL1 and HLA-Bw4 influence the binding strength (161, 167). To study D0, I chose a weak 3DL1 ligand, HLA-B*27:05 and the 3DL1*001 allele as it has a strong interaction through D0 (159). In this study, I showed that mutating the I at position 194 to an A on HLA-B*27:05 dramatically eliminates the binding by LILRB1Fc, and that the mutation slightly altered KIR3DL1-mediated binding or functional recognition if the predominant site is excluded. Moreover, I showed that the influence appears to be more obvious when MHC-I density is limiting. Using antibodies that block the interaction of KIR3DL1-D0 with MHC-I, I further dissected how the mutation at position 194 influences binding with the D0-domain. The results suggest that this position is essential for LILRB1-mediated interaction and does appear to have a very limited effect on binding by KIR3DL1. In addition, the results also indicate that the threshold and the sensitivity of assays are important for detecting 3DL1Fc-mediated interaction due to the involvement of multiple binding sites. Using a truncated form of LILRB1 as a competitor, I attempted to test the relationship of LILRB1 and KIR3DL1 on signaling, and did not observe any interference with KIR3DL1 signaling by soluble LILRB1. However, these experiments are not entirely conclusive because the concentration of LILRB1Fc may have been too low.

The reproducible observation that W6/32 blocks the KIR3DL1 interaction with MHC-I molecules might be because the antibody epitope is near the D0 contact region of the α1 domain (site 2), thus resulting in steric hindrance. However, the failure of blocking KIR2DL1-Cw15 interaction in the presence of the D0 domain with W6/32 relative to a specific antibody against KIR2DL1 (Fig

4-2) suggests that this is not the case. It is possible that the extended artificial linker between KIR3DL1-D0 with KIR2DL1-D1D2 allows the D0 domain to move out of the way in the chimeric receptor to still maintain the tight association of KIR2DL1 with Cw15 in the presence of W6/32. However, in the case of KIR3DL1, the natural linker may restrict the flexibility of D0. Therefore, W6/32 would easily disturb the interaction by pushing the whole molecule away from the ligand. My studies in this chapter suggest different effects of residue 194 on KIR3DL1 and LILRB1 interaction in *trans*. My colleague, Nick Li, has shown that W6/32 blocks the *cis* interaction of LILRB1 with autologous MHC-I molecules (180). Therefore, there is a possibility that position 194 may contribute to LILRB1 interaction in *cis* on 221 cells and the mutation at this position perhaps alters the availability of MHC-I allowing for binding by KIR3DL1 fusion protein. The *cis* interaction of LILRB1 on 221 cells could perhaps also be part of the explanation as to how the anti-D0 antibody, Z27, has a bigger impact on binding to the mutated B*27:05 than wild type (Fig 6-7).

LILRB1 recognizes the majority of human MHC-I molecules and has a higher affinity for the viral MHC-I mimic molecule, UL18 (181). Point mutation of Y38 to an A on LILRB1 dramatically attenuates the affinity to UL18 by approximately 18-fold as measured with Biocore (182). As the crystal structure showed, Y38 of LILRB1 directly contacts the amino acid at position 194 on MHC-I (170). However, the role of this position on the LILRB1-mediated interaction has not been determined directly. Here, I demonstrated that position 194 on MHC-I is essential for LILRB1 recognition by mutagenesis and binding assays. LILRB1 is capable of assisting allele specific KIR2DL1 signaling when it engages with the KIR2DL1 ligand, HLA-C (171), hence, it is possible that LILRB1 can have some impact on KIR3DL1 signaling in response to HLA^{Bw4} molecules. In order to address this issue, in Chapter 3, I suppressed the intracellular signal of KIR3DL1 by means of mutating Y to phenylalanine (F) at the ITIM motif, and co-expressed it with LILRB1. The limited results in Chapter

3 are not conclusive, but they indicate that if endogenous LILRB1 does influence KIR3DL1 signaling, the effect is very weak (Fig 3-12). Conversely, in Chapter 4, W6/32 blocking of KIR3DL1 inhibition (Fig 3-12 and 4-2) suggests that LILRB1 may compete with KIR3DL1 for the interaction with MHC-I-α3 domain. In the studies shown in this Chapter, to further address this issue, I used the truncated LILRB1 Fc fusion protein, D1D2Fc. However, I failed to detect any change of lysis in the presence of LILRB1-D1D2Fc relative to Fc control (Fig 6-8), suggesting that LILRB1-D1D2 does not compete with KIR3DL1. The lack of a change could also be due to the low amount of fusion proteins used. To my knowledge, the apparently contradictory results presented in this thesis may be caused by the differences in the amount of LILRB1, the form of LILRB1 receptor used (full length vs D1D2) or most likely the level of KIR3DL1 expressed on the cells. Moreover, the *trans* and *cis* interactions of LILRB1 expressed on target and effector cells adds complexity for interpretation of the results. Further investigation is needed to clarify the effect of LILRB1 on KIR3DL1 signaling.

In summary, the results presented in this chapter have begun to clarify the role of position 194 on the MHC-I-α3 domain in the KIR3DL1-D0 mediated interaction and clearly demonstrated the essential role of this position in LILRB1 interaction. The results have also raised many new questions that need further investigation.

Chapter 7

FINAL DISCUSSION

7.1. Summary of results and questions arising

In this thesis, I examined the role of the D0 domain of KIR3DL1 in ligand recognition and found that this domain makes direct contact with HLA at a secondary site distinct from the conventional D1D2 domain contact site. The direct involvement of the D0 domain in ligand recognition could facilitate the clustering of KIR3DL1 and its ligand HLA-Bw4 at the NK-target interface, and therefore, enhance inhibitory signaling. The adjustment of the threshold for NK activation by the D0 domain becomes important when surface expression of HLA-B is downregulated during viral infection, such as HIV infection.

Moreover, I showed the binding of KIR3DL1 to mouse MHC-I molecules. This finding raises concerns for studies using KIR3DL1 transgenic mice. On the ligand side, residue 194 of the α3 domain of MHC-I was shown here to play a role in KIR3DL1 interaction. To further investigate the KIR3DL1-D0 domain and its biological relevance, more questions need to be resolved, including:

- Does the D0 domain from other KIRs confer broad binding similar to KIR3DL1-D0?
- Do D0 domains in receptors from other species interact with MHC-I in a similar fashion?
- Where does KIR3DL1 contact mouse MHC-I molecules?
- Does the KIR3DL1-D0 domain interact with other xenogenic MHC-I aside from rodent MHC-I?
- Is the α3 domain directly involved in KIR3DL1 interaction?
- How does position 194 of MHC-I influence KIR3DL1 binding?
- Does LILRB1 compete with KIR3DL1 during signaling if co-expressed on the same cell?

In the subsequent text, I will discuss these questions in detail and provide some possible methods to test outstanding questions.

7.2. The D0 domain in other KIR Receptors

KIR3DL1 uses three extracellular Ig domains to recognize HLA-A and B molecules carrying the Bw4 motif. Of these Ig domains, the membrane proximal Ig domains D1D2 have been extensively studied and are known to be responsible for the binding specificity to the Bw4 motif. In this thesis, I showed that the D0 domain confers broad but weak binding to both classical and non-classical human MHC-I molecules. Thus, I predicted that the D0 domain makes direct contact with MHC-I at a secondary site. Recent crystallographic studies provide evidence that the KIR3DL1-D0 domain directly interacts with a conserved region in the α1 domain (site 2). Additional mutagenesis studies revealed that the residue at position 9 of the D0 domain is critical for the D0 domain binding and residues at position 11 and 27 are required in maintaining optimal binding (229). However, in their studies, mutation of the residue at position 9 of the D0 domain (disruption of site 2) or position 200 of the D2 domain (disruption of site 1) led to a similar degree of abrogation of HLA-B*57:01 tetramer binding to the 3DL1 receptors expressed in 293T cells (229). These results are contradictory to the idea that site 1 predominates the binding. Therefore, my results (Fig 4-18) using YTS cells stably expressing KIR3DL1 and cytotoxicity assay fit well with the structural studies of the complex as they suggest that D0 and D1D2 bind independently of one another.

A large number of polymorphisms are distributed throughout KIR3DL1 including in the D0 domain (46). Interestingly, of the published polymorphisms in 3DL1-D0, residues involved in forming the site 2 interaction are quite conserved. This could explain why the D0 domain confers broad recognition. Parham and colleagues have already made a significant contribution to understanding how polymorphisms affect function of the receptor. Of particular relevance here, mutations at positions 50 and 51 in the D0 domain have been shown to influence the strength of the interaction of KIR3DL1 with HLA-B (168). These two

residues do not make contact at site 2 (colored in red in Fig 7-1), thus the effect is likely indirect. In fact, according to the KIR3DL1-HLA-B*57:01 crystal structure, these two residues are solvent exposed and located at the opposite face of the receptor from where it binds to site 2. Therefore, the influence could be due to conformational changes on the D0 domain or they may be involved in making contact with MHC-I via a third site or even dimerization of KIR3DL1.

Aside from KIR3DL1, the KIR family in human also has other members containing a homologous D0 domain, such as KIR3DS1, KIR3DL2, KIR3DL3, KIR2DL4 and KIR2DL5 (101). These KIRs have different specificity for HLA molecules. For example, KIR3DL2 binds to HLA-A and KIR2DL4 interacts with HLA-G, but the ligands for KIR3DS1, KIR2DL5 and KIR3DL3 remain unclear. KIR2Ds (type II) evolved through loss of the D0 domain and gaining strong binding to HLA-C molecules by the D1D2 domains (as suggested by Fig 4-14). However, KIR3DL1 kept the D0 domain that likely compensates for a weaker interaction with the Bw4 region of HLA molecules. Thus, another interesting question is whether homologous D0 domains in other KIRs play a similar role. Therefore, in the following section, the comparison of the amino acid sequences of the D0 domains from the previously described KIR receptors will be discussed.

KIR3DS1 is of the highest interest among the KIRs with D0 domains, as it is a variant of KIR3DL1 and its D0 domain shows approximately 98% identity to KIR3DL1-D0. There are only three amino acid differences in KIR3DS1-D0 compared to KIR3DL1-D0, and these are not residues shown to contact the MHC-I (229). However, there is little to no direct evidence demonstrating that KIR3DS1 can bind the ligands of KIR3DL1, the HLA molecules carrying the Bw4 epitope (HLA[Bw4]) (166, 243). The lack of interaction is likely due to alterations that occur in the D1 and D2 domains as suggested by mutagenesis studies (229, 244). Interestingly, like KIR3DL1, epistatic interaction of KIR3DS1 with HLA[Bw4] allows for AIDS patients to have a good survival rate (13). These observations

bring up an interesting question of how the combination of KIR3DS1 and HLA^{Bw4} is linked with protection against HIV infection. One possibility is that the physical interaction is below the level of detection in the assays used to date. I expect that the D0 domain of KIR3DS1 may have the ability to bind similarly to that of KIR3DL1 as there are only three conservative changes in the D0 domain and these changes are outside the region of site 2 (Fig 7-1). Similar to the KIR3DL1-D0 domain that I have shown interacts weakly with site 2 (232), KIR3DS1-D0 binding may be below the limit of detection by the assays previously used to test binding (244). Therefore, it is worth testing if KIR3DS1-D0Fc fusion protein binds HLA^{Bw4} and other HLAs as the binding may be detectable when the MHC-I can diffuse in the membrane to form higher order complexes.

Other D0 containing KIRs share less similarity with KIR3DL1 than KIR3DS1 (Fig 7-1). The alterations occurring within and outside the region of site 2 could dramatically affect the binding affinity. Given that most of the changes are non-conservative (some important changes are shown in Table 7-1), I predict that the D0 domains of KIR2DL4, KIR2DL5, KIR3DL2 and KIR3DL3 lost the features found in that of KIR3DL1 to bind at site 2. Future studies to test binding of HLA-B and HLA-G using fusion proteins comprised of the D0 domains of these receptors and an Fc fragment and/or in combination with 2DL1Fc could be performed. Moreover, mutagenesis of the specific residues that vary could be used to better understand the influence of these residues on D0 domain function.

```
                    10         20         30         40         50
3DL1*001-D0   HMGGQDKPFL SAWPSAVVPR GGHVTLRCHY RHRFNNFMLY KEDRIHIPIF
3DS1*013-D0   .......... .......... .......... .......... ......V...
3DL2*001-D0   .......... ..R..T.... ....A.Q... .RG....... ....S.V...
3DL3*001-D0   .V........ ....GT..SE ......Q.RS .LG..E.SES ...GS.MVPL
2DL4-D0       .V.......C .........Q .......... .RG..I.T.. .K.GVPV.EL
2DL5-D0       .E......L. .......... .....L.RS .LG.TI.S.. ...GVPV.EL


                    60         70         80         90
3DL1*001-D0   HGRIFQESFN MSPVTTAHAG NYTCRGSHPH SPTGWSAPSN PVVIMVT
3DS1*013-D0   .......G.. .......... .......... .......... .M.....
3DL2*001-D0   .........I .G...P.... T.R....R.. .L........ .......
3DL3*001-D0   YN...RN..L .G...P.... T.R.CS.... .L........ .......
2DL4-D0       YN...WN..L I....P.... T.....F... ...E...... .L.....
2DL5-D0       YNK..WK..L .G...P.... T.R......R ...IE..... .L..V..
```

Fig 7-1. Sequence alignment of D0 domains of KIRs in humans

Comparison of the D0 domains of KIR receptors in human. The dots indicate amino acid identity with the KIR3DL1 sequence. Cysteines are colored in green. The contact residues in the D0 domain are colored in red. The important residues suggested by mutagenesis studies are colored in red and underlined.

Table 7-1. Examples of non-conservative changes of D0 domains

Receptors	Within site 2	Outside site 2
KIR3DL2-D0	W to R (position 13) R to Q (position 27)	
KIR2DL4-D0		L to C (position 10)
KIR2DL5-D0	F to L (position 9) R to L (position 27)	

7.3. The features of D0 domain in KIRs from other species

KIR3DL diversified from the KIR3DL/3DX lineage and this occurred only in simian primates (Fig 1-10) (119). Simian primates include the Old World Monkeys, the New World Monkeys, apes and human. The Old World Monkeys such as Rhesus Macaque have diverse KIR3Ds and limited KIR2Ds in correspondence with expanded MHC-A and B and lack of MHC-C in these species. Conversely, apes (such as chimpanzee, banobo, gorilla and orangutan) and human have polymorphic KIR2Ds but limited KIR3Ds correlated with the emergence and rapid expansion of MHC-C (245). In terms of variations in KIR3DL, humans have both two KIR3DL1 and KIR3DL2 genes, while chimpanzees (*Pan troglodyte*) only have one gene, KIR3DL1/2. Conversely, Rhesus Macaques *(Macaca mulatta)* have more than 11 genes of KIR3DL (246). In the subsequent text, the counterparts of KIR3DL1 in chimpanzees and Rhesus Macaque are referred as *pt*KIR3DL1/2 and *Mamu*KIR3DL1, respectively (119).

In this thesis, I showed that the D0 domain in human KIR3DL1 (*hs*KIR3DL1) has broad binding for classical and non-classical human MHC-I molecules. The results raise an interesting question as to whether this feature occurs only in human KIRs or is maintained in KIRs from other species. A comparison of the amino acid sequences of the D0 domains of *pt*KIR3DL1/2 and *Mamu*KIR3DL1 with that of *hs*KIR3DL1 in Fig 7-2 shows that the D0 domains of *pt*KIR and *Mamu*KIR are ≥ 90% identical to that of *hs*KIR3DL1, particularly in the site 2 binding region. Interestingly, such similarity is even higher than what is observed in human KIR3DL2 and KIR3DL3. Therefore, I predict that these D0 domains will all share the property of binding to a broad range of MHC-I alleles at site 2.

*pt*KIR3DL1/2 interacts with MHC-A and MHC-B in chimpanzees (247). Interestingly, *pt*KIR3DL1/2 was also known to bind human HLA-B molecules regardless of whether they carry the Bw4 or Bw6 epitope using a highly sensitive reporter system (168). Swapping the D0 domain of *pt*KIR3DL1/2 with

*hs*KIR3DL1 resulted in enhanced binding to HLA-B molecules (168). This indicates that the D0 domain of *pt*KIR3DL1/2 is functional for the interaction with HLA-B molecules. Similarly, several KIR3DL1 allelic variants in Rhesus Macaques have been reported to bind human MHC-A, B and C using KIR-Fc fusion proteins. Interestingly, strong binding to HLA-C and to HLA^{Bw4} was observed (245). However, the role of the D0 domain was not dissected in these studies.

Based on the conservation of these D0 domains derived from *pt*KIR and *Mamu*KIR relative to *hs*KIR and the fact of broad binding to MHC-I by *hs*KIR3DL1-D0 domain, I now predict that *pt*KIR3DL1/2 and *Mamu*KIR3DL1 binding to HLA-B is mostly mediated by the D0 domain. Again, this could readily be tested using fusion proteins containing the D0 domain *Mamu*KIR3DL1, or *pt*KIR3DL1/2 and human IgG1 Fc fragment.

In contrast to the expansion of KIR3DLs in primates, limited KIR3DL genes occur in non-primates such as cattle (*Bos taurus*) and mice (*Mus musculus*) (119). However, these KIR genes and the encoded receptors are not well studied. It is known that the bovine genome consists of only four functional KIRs (*bt*KIRs), including *bt*KIR3DL1, *bt*KIR3DS1, *bt*KIR2DL1 and *bt*KIR2DS1 (116). The structure of *bt*KIR is similar to that of *hs*KIR but with some variations including a cysteine in the transmembrane region causing formation of a disulfide bonded dimer (248). Additionally, *bt*KIR contains only one ITIM in the tail, with the exception of *bt*KIR2DL1 (249). Two KIR genes are found in mice *(Mus musculus),* including KIR3DL1 (KIRL1) and KIRL2. Mouse KIR genes were translocated to the X chromosome (250, 251). Mouse KIR3DL1 is expressed on NK, NKT cells (252) and regulatory T cells (253), but the protein is difficult to express on non-NK and non-NKT cells (252) and remains poorly understood in terms of ligands.

A comparison of the amino acid sequence of the D0 domains of mouse and bovine KIR3DL1 to *hs*KIR3DL1 (Fig 7-2) reveals less homology with

*hs*KIR3DL1 than that for apes and monkeys. Therefore, it would be interesting to test *bt*KIR3DL1 and mouse KIR3DL1 binding to HLA.

```
                  10        20        30        40        50
hs3DL1-D0     HMGGQDKPFL SAWPSAVVPR GGHVTLRCHY RHR---FNNFMLY KEDRI-HIPIF
pt3DL1-D0     ....H..... ...S...... .......... .GG--....... .....-.V..-
Mamu3DL1-D0   YT.....T.. ..R...L..Q .......... .RGLYN.T..T.. .D..S-.V...
bt3DL1-D0     AV.EYE.LS. .....P...L .QT...Q..S HSP---LKR.R.F .T.GER.L.EL
mm3DL1-D0     .VGSH..... .....Y...L .QN...T.DS HRG---S.I.K.. ..EGS-PNHQL


                  60        70        80        90
hs3DL1-D0     HGRIFQESFN MSPVTTAHAG NYTCRGSHPH SPTGWSAPSN PVVIMVT
pt3DL1-D0     -......... .......... .......... .......... .......
Mamu3DL1-D0   P........L .G...P.... T.R....Y.. ...E...L.D .LA.R..
bt3DL1-D0     Q.HH.N-N.T LG...GE... S...S----- -EAY...P.D .LQ.V.S
mm3DL1-D0     .ETT..K.QV FG....E... T.R.F--..Q YANVL..H.E .LK.IIS
```

Fig 7-2. Sequence comparison of D0 domain of KIR3DL1 in humans and other species.

Comparison of the KIR3DL1-D0 domain in Chimpanzee (*Pan troglodytes,* *pt*3DL1), Rhesus Macaque (*Macaca mulatta, Mamu*3DL1), Cattle (*Bos taurus,* *bt*3DL1) *and* Mouse *(Mus musculus, mm3DL1)* to that of Human (*Homo sapiens*, *hs*3DL1)**.** Dashes indicate the absence of the amino acid relative to human KIR3DL1. Cysteines are colored in green. The contact residues in the D0 domain are colored in red. The important residues suggested by mutagenesis studies are colored in red and underlined.

207

7.4. How does KIR3DL1 interact with mouse MHC-I molecules?

KIR3DL1 uses two distinct sites to interact with HLA^{Bw4}. In this thesis, I demonstrated 3DL1Fc binding to mouse MHC-I molecules with the exception of H-2^k. To explore regions of 3DL1Fc binding, I used several mouse MHC-I specific antibodies. Strikingly, anti-D^b-α3 antibody (28.14.8S) and anti-D0 mAb (Z27) yielded a greater reduction of binding than anti-D^b-α1 mAb (B22-249) (Figs 5-4 and 5-5). Using various combinations of Ig domains of KIR3DL1, I found that D0Fc provided a remarkable amount of binding to D^b in comparison to D1D2Fc (Figs 5-8 and 5-9). The latter results suggest that the D0 domain of KIR3DL1 is necessary for xenorecognition, and the antibody blocking suggests the binding could involve a site near or in the α3 domain. However, given the site interaction of the antibodies chosen in this thesis have not been finely mapped, it is still too early to conclude the involvement of the α3 domain.

No detectable binding of 3DL1Fc to cells expressing H-2D^k/K^k was observed in my hands. The differences of amino acid sequences, in particular, at site 2, between H-2D^k/K^k and other H-2 alleles could hint at what is required for the binding. Moreover, several non-conservative differences in H-2D^k and H-2K^k to other H-2 molecules in the α1 and α3 domain (Table 7-2) could be the reason for a lack of binding. Particularly, the amino acid change from negatively charged glutamic acid (E) to positively charged lysine (K) at position 19 (contributing to formation of site 2) could lead to loss of D0 binding to H-2K^k (Table 7-2). In addition, a similar change in the α3 domain may cause loss of binding to H-2D^k (Table 7-2).

Based on the results with blocking antibody and the amino acid changes found between various mouse and human MHC-I proteins (Fig 5-2 and 5-3), there are a number of ways I can envision a KIR3DL1/H-2 interaction to occur as shown in Fig 7-3 and these models may not be mutually exclusive. First, it is possible that KIR3DL1 binds H-2 molecules in the same way it binds HLA

208

(model #1), and the anti-α3 antibody could sterically influence the binding. Another possibility is that the binding could only occur at the α3 domain (model #2). Alternatively, as shown in model #3, KIR3DL1 interacts with multiple H-2 molecules at multiple sites, and the interaction with the α3 domain facilitates clustering to increase KIR3DL1 avidity.

The finding of recognition of mouse MHC-I by human KIR3DL1 suggests that there is some conserved regions in MHC-I that allows for KIR3DL1 recognition. Understanding of the interaction between KIR3DL1 and mouse MHC-I may clarify how changes between human and mouse MHC-I affect KIR interaction. Various mutagenesis approaches may be explored to pinpoint interaction sites. The epitope of the anti-D^d-α3 antibody, 34-2-12s, has been mapped to position 227 of the α3 domain. A point mutation of D^d, Q227K was reported to totally abrogate the antibody reactivity (254, 255). Hence, 34-2-12s is a good tool for the assessment of the involvement of the α3 domain when engaging with KIR3DL1. Moreover, mutagenesis studies combined with domain swaps could be used to dissect the role of individual Ig domains of MHC-I in KIR3DL1 recognition.

Table 7-2. Examples of non-conservative amino acid changes in H-2^k

relative to other H-2 molecules

	α1 domain	**α3 domain**
H-2K^k	E to K (position 19)* E to V (position 55) G to E (position 56)	H to R (position 191)
H-2D^k		D to K (position 196)

Note: * refers to contact residues involved in site 2.
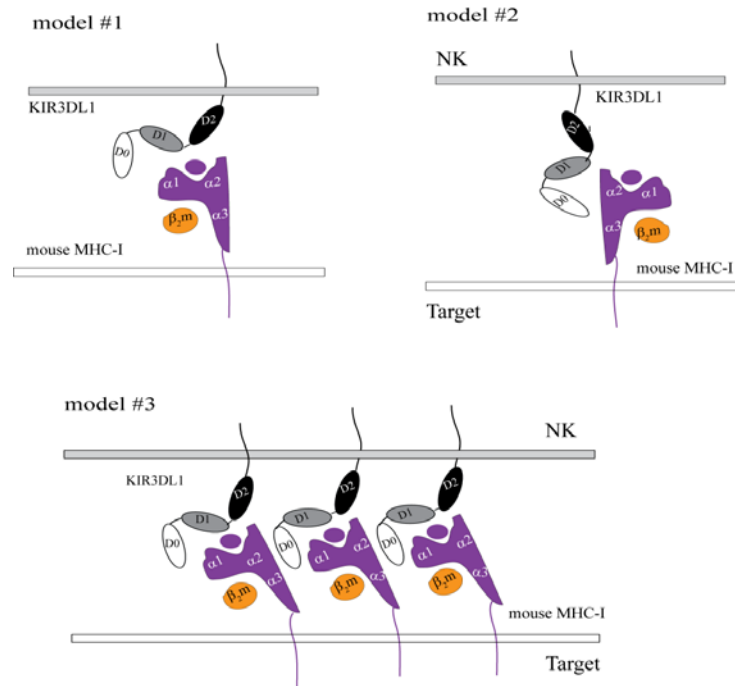
Fig 7-3. Proposed models of KIR3DL1 interaction with mouse MHC-I molecules.

Three models are shown to illustrate how KIR3DL1 interacts with mouse MHC-I proteins either in a 1:1 ratio (model #1 and #2) or a 1:2 ratio that allows for MHC-I clustering (model #3).

7.5. The recognition by KIR3DL1 of xenogenic MHC-I other than mouse MHC-I molecules

KIRs are diverse and rapidly co-evolve with MHC-I under natural selection. MHC is present in all jawed vertebrates, while KIR expansion only occurs in primates. Surprisingly, *pt*KIR3DL1/2 in chimpanzees not only binds *pt*MHC-I, but also interacts with human MHC-I, and *vice versa* that *hs*KIR3DL1 interacts with MHC-B molecules in chimpanzees and Rhesus Macaques (168). These observations suggest that *hs*KIR3DL1 interacts with MHC-I in species close to human, such as primates. In this thesis, I showed that *hs*KIR3DL1 binds to MHC-I molecules derived from mice, a mammalian species.

Cartilaginous fish are the earliest jawed vertebrate possessing organized MHC genes, including MHC-I, II and III regions, while the chicken has the "simplest but essential" MHC genes. Therefore, it could be interesting to test if cells expressing MHC-I molecules from cartilaginous fish and from chicken are bound by 3DL1Fc. Moreover, the assessment of binding by the D0 domains of KIRs from non-primates, high primates and human described in *section 7.3* would clarify how the D0 domain has evolved in pace with the alterations of MHC-I in various species.

7.6. The role for the α3 Domain of MHC-I in the KIR3DL1 interaction

In my hands, the anti-MHC-I-α3 domain antibody, W6/32, dramatically reduced 3DL1Fc binding. Using an N-terminal EGFP linked KIR2DL1 receptor, I concluded that steric interference by W6/32 was not the likely explanation because the additional EGFP did not make the 2DL1 receptor blockable by W6/32 (Fig 4-7 vs 4-3). A bridging model with D0 binding to the base of the α3 domain was proposed in Chapter 4 to explain how the KIR3DL1-D0 domain might facilitate the assembly of KIR3DL1 clustering (Fig 4-21). However, the co-crystal structure that emerged demonstrated that the conserved region bound by the

KIR3DL1-D0 domain is actually located in the α1 domain (site 2). Similar to what has been observed with Ly49 (256), it remains possible that a third site for binding exists, though it is not evident in the structure.

To further test the involvement of the α3 domain, the α3 domain of HLA-B*27:05 was swapped with that of HFE because the α3 domain of HFE could support α1α2 folding but was not expected to bind KIR3DL1. However, elevated binding was observed compared to HLA-B*27:05 (Fig 5-14). The enhanced binding could be explained by the HFE-α3 domain improving the binding at site 1 or site 2 by allosteric effects. The results suggest that the α3 domain is not required for the binding. However, additional experiments need to be done for clarification. Alternatively, another explanation would be that the conformational changes in the α1 domain override the actual loss of a putative site 3.

Although the results presented in Chapter 5 did not provide clear evidence for binding to the α3 domain, a single point mutation at position 194 did show some effect on 3DL1Fc binding and will be discussed in *section 7.7*. The complex of KIR3DL1 and HLA-B*57:01 illustrated how the specificity of KIR3DL1 is dependent on the D1D2 domains as they occupy 70% of overall binding area and the interaction is stabilized by salt bridges and hydrogen bonds, while the D0 domain only contributes 30% of the overall binding area and the binding forces are formed by van der Waals interactions (229). The D0 contacting region is perpendicular to the axis of the peptide binding groove. Therefore, it remains feasible that the α3 domain could be bound by the other face of the KIR3DL1-D0 domain and the interaction does not overlap with the other two published sites.

In our updated model incorporating recent structural and mutagenesis results (Fig 7-4), the 3DL1-D0 domain makes weak contact with the α3 region of MHC-I to form a third site when multiple MHC-I molecules are engaged between two opposing cell membranes. Of note, since multiple sites are involved and site 1 is essential for the specificity, the interaction at site 3 on the α3 domain may be

quite subtle. The putative site 3 would be important for ligands with a weak site 1 (e.g. HLA-B*27:05) or when KIR3DL1 or MHC-I levels are relatively low. The interaction at site 3 would allow 3DL1-D0 to bridge MHC-I molecules together and facilitate receptor clustering.
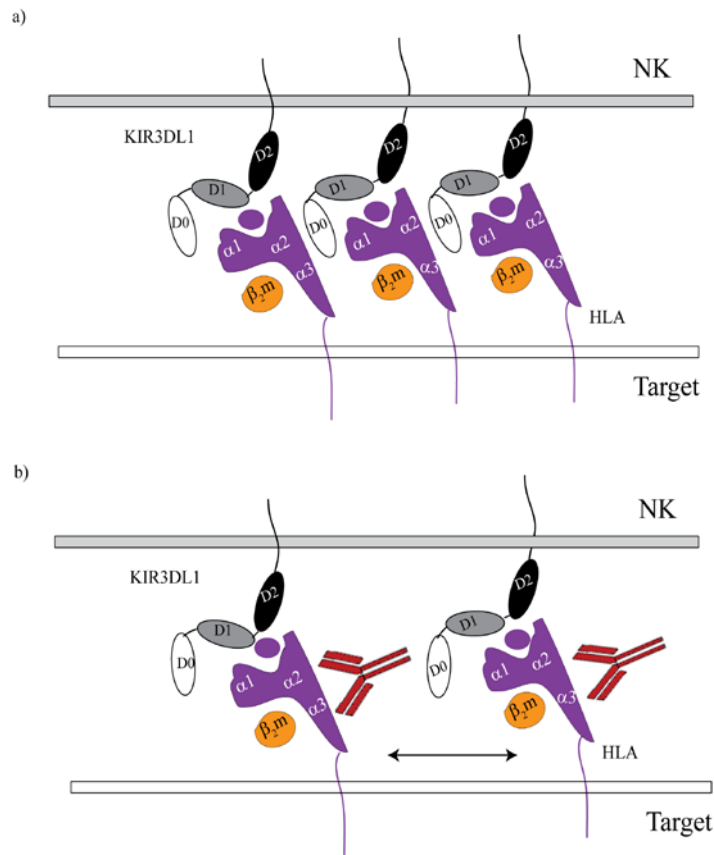
Figure 7-4. Proposed model of KIR3DL1 bridging HLA clustering.

a) The interaction of KIR3DL1-D0 domain with the α3 domain of HLA facilitates HLA clustering, thus, enhancing KIR3DL1 signaling. *b)* Illustration of W6/32 effect on KIR3DL1 binding to HLA-Bw4 moleucles. The interaction of W6/32 with the α2 and α3 domains of HLA-B results in disruption of clustering and sterically causes loss of site 2 interaction.

7.7. How does position 194 influence KIR3DL1 binding in *trans?*

Natural variants at position 194 of various HLA molecules are found in the population, including isoleucine (I), valine (V) and leucine (L). V at position 194 in HLA-B molecules was recently reported to be linked with HIV progression (257). Changing V to I was predicted by these investigators to dramatically interfere with the network of interactions between contact residues of the α3 domain and LILRB1 (257). In comparison to V, I at position 194 can reach closer to residue 38 of LILRB1 (257). Therefore, theoretically, I194 should produce a stronger interaction to LILRB1 relative to V194. This I to V polymorphism on HLA-B molecules has been shown to impact IFN-γ secretion on primary KIR3DL1$^+$ NK cells in combination with position 82 (167), one of residues involved in formation of the Bw6 epitope. Whether this influence is KIR3DL1 dependent was not determined in these studies. As suggested by my previous results and the crystallographic studies, position 194 may be in contact with the D0 domain. Thus, in a single experiment, I attempted to test if I to V at position 194 affect KIR3DL1-D0 binding using D02DL1Fc. It seemed that the I194V mutant caused a slight decrease in binding at 200 µg/ml (Appendix A). Additional experiments are required to determine whether the effect is consistent.

In order to maximally assess the role of position 194, I mutated I to A to abrogate all the potential interactions mediated by isoleucine (I). A reduction of 3DL1Fc binding was observed when HLA is expressed at relatively low level (Fig 6-6). However, at such a level, wild type B*27:05 did not invoke inhibition, making it difficult to interpret the impact of the mutation. Interestingly, when the expression level was elevated approximately 2-fold to where some KIR3DL1 mediated inhibition occurred, the I to A mutation at position 194 showed a small influence on NK lysis when combined with the mutation of Y200 to prevent a site 1 interaction (Fig 6-4). Oddly, little difference for 3DL1Fc fusion protein binding was detected when the molecules were at this level (Fig 6-3). The lack of

agreement of the binding results with the functional data could be due to variable amounts of KIR3DL1 in these assays. The results suggest that there is a possible involvement of position 194 in KIR3DL1 binding, but cannot determine if it participates directly in the binding. The impact of position 194 on binding might be very limited due to the presence of the other two sites as seen in the crystal structure, particularly, high affinity site 1. But interestingly, this position has biological relevance as reported for HIV susceptibility (257).

In terms of the mechanism, I predict three possibilities. First, position 194 could be one of the contact residues bound by the KIR3DL1-D0 domain as illustrated in Fig 7-3. Another possibility is that the residue at position 194 could associate with other molecules on target cells to assist KIR3DL1 binding, such as LILRB1. In that case, LILRB1 would bind MHC-I on 221 cells in *cis* and perhaps allosterically alter how KIR3DL1 binds at site 1 and site 2. Alternatively, since the influence of position 194 on KIR3DL1 binding without the interference of LILRs was only tested using HLA-B*27:05, it is possible that the influence is B*27:05 specific, which will be discussed below.

7.8. Is the influence of position 194 of HLA-B*27:05 on KIR3DL1 interaction representative?

Since residues in the Bw4 epitope of B*27:05 have a weaker site 1 interaction (71), this allele was used to explore the potential involvement of the α3 domain and the role of position 194. In this thesis, I showed some effect of position 194 of HLA-B*27:05 on KIR3DL1 binding when the expression level was low. Given the fact that HLA-B*27:05 has an unique extra cysteine (C) at position 67 (C67), which renders an unusual homodimer containing only the B27 free heavy chain (hereafter called $B27_2$), my results in Chapter 6 raise an interesting question: is the influence of position 194 in HLA-B*27:05 on KIR3DL1 interaction representative of all Bw4 or unique to B*27?

B27$_2$ has been extensively studied as it is associated with susceptibility to several seronegative arthritic diseases, such as ankylosing spondylitis and Reiter's syndrome (258, 259). B27$_2$ has been observed on primary NK cells and B27 transfectants (52). Binding to B27$_2$ but not B27/β_2m by KIR3DL2 (ligand known is subsets of HLA-A) has been reported (227), suggesting that C67 does impact KIR3DL2 binding. In relation to my findings, KIR3DL1 binds B27$_2$ and the B27/β_2m complex (64, 227). Therefore, it is possible that C67 can affect KIR3DL1 binding. In the co-crystal structure, KIR3DL1-D0 contacts HLA-B*57:01 at the loop comprising residues 13-20 in the α1 domain (Fig 5-1) along with a few residues in β_2m. As residue 67 is situated in the α-helix in close proximity to the D0 contacting loop, thus, it is possible that C67 alters KIR3DL1 interaction resulting in different KIR3DL1 binding to B27$_2$ in comparison to B27/β_2m and B*57:01.

Mutating C67 to serine (S) prevents formation of B27$_2$, suggesting that this residue is pivotal for the formation of B27$_2$. I have now shown that position 194 of HLA-B*27:05 influences 3DL1Fc and D02DL1Fc binding. However, whether this influence is attributed to B27$_2$ and/or B27/β_2m complex or whether the influence observed on HLA-B*27:05 also occurs with other HLA-Bw4 alleles was not determined in these studies. In my opinion, B27$_2$ homodimers could lead to a possible interaction of the amino acid at position 194 with residues in the α2 or α3 domain of another B27 molecule involved in such dimerization (Fig 7-5). Such an interaction could enhance KIR3DL1 binding avidity and/or facilitate MHC-I clustering. Thus, to better understand the interaction mode, additional experiments could be done, such as comparing C67S mutation of B27 and studying the role of position 194 on other weak ligands of KIR3DL1 such as HLA-B*15:13 (56).
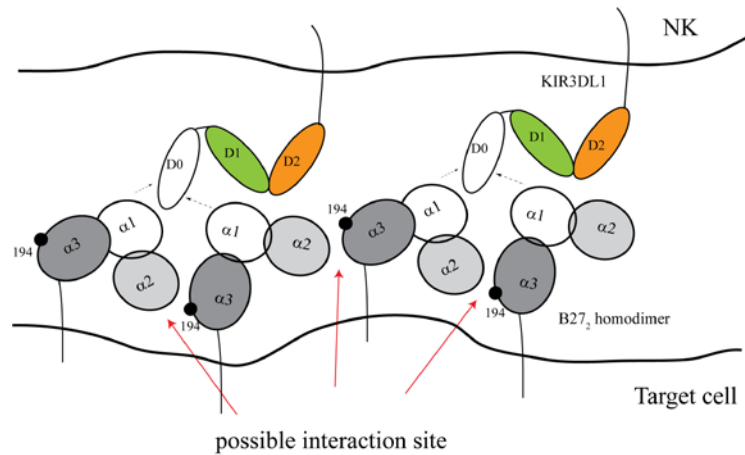
Figure 7-5. Proposed model of the role of position 194 in KIR3DL1 interaction.

Interaction of the residue at position 194 (dark dot) with residues in the α2 domain could help form $B27_2$ homodimer. Such dimers could increase the binding avidity by the D0 domain indicated as dotted arrows and facilitate MHC-I clustering. Sites are indicated by red arrows.

7.9. KIR3DL1 modulation of adhesion to target cells and the effect of position 194 on KIR3DL1 interaction

Multiple events occur sequentially at the NK activating synapse. However, the process of activation is regulated by inhibitory receptors at the initial stage (e.g. adhesion). The enrichment of KIR2DL receptors and associations with other related molecules (e.g. SHP-1) have been demonstrated at the synapse between an NK cell and a target cell (190, 191). Such enrichment is known to disrupt the adhesion, prevent lytic granule polarization and inhibit actin reorganization (189, 260, 261). To date, studies of inhibitory synapses have been with KIR2D receptors, which have high affinity for their ligands, HLA-C. However, the inhibitory synapse mediated by KIR3DL1 at the interface has not yet been determined.

Our lab showed that KIR2DL1 with an N-terminal EGFP led to formation of smaller clusters (microclusters) relative to the wild type, and such microclusters were still able to prevent adhesion but to a lesser extent relative to wild type (189). Despite the reduced size, KIR microclusters were associated with strong inhibition of cytolysis (189). These previous results in our lab suggest that disruption of adhesion is not necessary for disruption of cytolysis, although these two events occur sequentially. Since KIR3DL1 has a weaker interaction with HLA relative to KIR2DL1, it is possible that in comparison to KIR2DL1, KIR3DL1 has a lesser effect on preventing cell-cell adhesion and this might be useful to tease out the effects of my mutants, such as I194A. YTS cells expressing KIR3DL1 were analyzed for adhesion to HLA-B*58:01 using a conjugation assay. The preliminary data showed that KIR3DL1 causes disruption of adhesion but to a lesser extent when ligated with HLA-B*58:01 in comparison to KIR2DL1 to HLA-Cw15 (Appendix B), suggesting that KIR3DL1 can prevent adhesion, but not as well as KIR2DL1 in the same system.

If the formation of large receptor clusters is required to antagonize the adhesion, it is possible that the putative "site 3" enhances enrichment of the receptor at the synapse. I have already tested the effect on adhesion using HLA-B*27:05 and the I194A mutant tagged with yellow fluorescent protein (YFP) at the C-terminus (B*27:05YFP and I194AYFP). In comparison to B*58:01, ligation of KIR3DL1 with B*27:05 on these cells did not disrupt adhesion (Appendix C), though the weak interaction was sufficient to induce some degree of inhibition of cytolysis (Fig 4-4). Therefore, these transfectants cannot be used to discern the role of position 194 in KIR3DL1 signaling. Nonetheless, the results indicate that higher binding affinity/avidity is required to prevent adhesion than to inhibit cytolysis and are consistent with the previous studies of Borszcz et al in 2003 (189). Further studies using high resolution imaging of the synapses could be used to see if KIR3DL1 behaves similarly to KIR2DL1 with the N-terminal EGFP moiety in forming microclusters. Moreover, mutation of I194A on B*58:01 might clarify if there is a role for this residue in KIR3DL1 signaling that can be discerned in the effects on cell-cell adhesion.

7.10. Does LILRB1 play a role in KIR3DL1 signaling?

When this work was started, whether LILRB1 could affect KIR3DL1 signaling was not known. In this thesis (Chapter 3 and 6), I examined the influence of LILRB1 on ITIM-mutated KIR3DL1 signaling using NKL cells. However, I did not observe much LILRB1 signaling when the mutated KIR3DL1 interacted with HLA-B molecules (Fig 3-12). Moreover, I tested if LILRB1 fusion protein containing only the first two Ig domains (D1D2) could disrupt KIR3DL1 signaling when engaging HLA-B*58:01 or B*27:05, but found no effect (Fig 6-8). These results suggest that masking the region of MHC-I bound by LILRB1-D1D2 does not interfere with KIR3DL1 signaling. However, more experiments with positive controls could be done for the correct conclusion, such as LILRB1-D1D2Fc blocking of LILRB1 signaling.

The co-crystal structure that was published during the course of my thesis suggests that LILRB1 could interact with the MHC-I while engaged by KIR3DL1. However, based on the functional results, it seems unlikely that LILRB1 cooperates with KIR3DL1 for inhibitory signaling. The bridging model proposed in *section 7.6* shows that KIR3DL1-D0 domain facilitates MHC-I clustering via contacting the α3 domain (Fig 7-2). If the model is correct, LILRB1 then should compete with KIR3DL1 for binding to the α3 domain of MHC-I molecules. Since LILRB1 can interact with MHC-I in *trans* and in *cis,* endogenous LILRB1 expression on effector and target cells adds complexity to interpretation of the results obtained in these studies. I found that the I194A mutant abrogated LILRB1 binding in *trans* (Fig 6-6). Therefore, examination of binding to cells expressing MHC-I molecules and an I194A mutant using soluble LILRB1 and/or KIR3DL1 proteins may be a better approach to explore the relationship of LILRB1 and KIR3DL1 on ligand interaction. Given around 30% of primary NK cells co-express KIR3DL1 and LILRB1, further studies of the relationship of LILRB1 and KIR3DL1 on signaling could provide a possible explanation of how LILRB1 contributes to currently known or yet undiscovered associations between KIR3DL1 and disease susceptibility (257).

7.13. Concluding remarks:

Pathogens, from viruses to parasitic worms, have rapidly evolved in an attempt to invade the host's body and avoid the immune response, while the immune system has developed multiple defense mechanisms to respond to the invasion, including the innate and adaptive immune responses. Of these, NK cells are one of the critical components to evoke innate immune responses as they recognize and rapidly terminate virus-infected cells at early stages using diverse receptors, including KIR and LILR families. The more recent and rapidly evolving KIR family members have a high degree of specificity for MHC-I. The rapid evolution of KIR is thought to be driven by pathogens. During KIR

evolution, the "2D" KIR arose by loss of the D0 domain but compensated at site 1 to maintain recognition specificity and affinity. Until recently, the role of the D0 domain in KIR3D receptors remained enigmatic. In this thesis, I have presented that the D0 domain of KIR3DL1 confers broad but weak binding to classical and non-classical human and mouse MHC-I molecules. My attempts to dissect where D0 binds MHC-I yielded results that are difficult to reconcile in terms of the "site 2" shown by crystallographic and mutagenesis studies without invoking a putative third site on the α3 domain. Based on the results in this thesis, site 3 may be distinct from the LILRB1 site, and the binding at this site is subtle. Future studies should be conducted to determine how the various D0 domains modulate ligand binding and to resolve the issue of how position 194 influences D0 binding. The results may shed light on how KIRs evolved from LILRs and be used to interpret genetic association of KIR with diseases such as HIV/AIDS.

BIBLIOGRAPHY

1. Herberman, R. B., M. E. Nunn, H. T. Holden, and D. H. Lavrin. 1975. Natural cytotoxic reactivity of mouse lymphoid cells against syngeneic and allogeneic tumors. II. Characterization of effector cells. *Int. J. Cancer* 16: 230-239.

2. Herberman, R. B., M. E. Nunn, and D. H. Lavrin. 1975. Natural cytotoxic reactivity of mouse lymphoid cells against syngeneic acid allogeneic tumors. I. Distribution of reactivity and specificity. *Int. J. Cancer* 16: 216-229.

3. Trinchieri, G. 1989. Biology of natural killer cells. *Adv. Immunol.* 47: 187-376.

4. Biron, C. A., K. B. Nguyen, G. C. Pien, L. P. Cousens, and T. P. Salazar-Mather. 1999. Natural killer cells in antiviral defense: function and regulation by innate cytokines. *Annu. Rev. Immunol.* 17: 189-220.

5. Cooper, M. A., T. A. Fehniger, and M. A. Caligiuri. 2001. The biology of human natural killer-cell subsets. *Trends Immunol.* 22: 633-640.

6. Miletic, A., A. Krmpotic, and S. Jonjic. 2013. The evolutionary arms race between NK cells and viruses: who gets the short end of the stick? *Eur. J. Immunol.* 43: 867-877.

7. Boyington, J. C., S. A. Motyka, P. Schuck, A. G. Brooks, and P. D. Sun. 2000. Crystal structure of an NK cell immunoglobulin-like receptor in complex with its class I MHC ligand. *Nature* 405: 537-543.

8. Lanier, L. L. 2005. NK cell recognition. *Annu. Rev. Immunol.* 23: 225-274.

9. Colucci, F., J. P. Di Santo, and P. J. Leibson. 2002. Natural killer cell activation in mice and men: different triggers for similar weapons? *Nat. Immunol.* 3: 807-813.

10. Lopez-Vazquez, A., L. Rodrigo, J. Martinez-Borra, R. Perez, M. Rodriguez, J. L. Fdez-Morera, D. Fuentes, S. Rodriguez-Rodero, S. Gonzaez, and C. Lopez-Larrea. 2005. Protective effect of the HLA-Bw4I80 epitope and the killer cell immunoglobulin-like receptor 3DS1 gene against the development of hepatocellular carcinoma in patients with hepatitis C virus infection. *J. Infect. Dis.* 192: 162-165.

11. Khakoo, S. I., C. L. Thio, M. P. Martin, C. R. Brooks, X. Gao, J. Astemborski, J. Cheng, J. J. Goedert, D. Vlahov, M. Hilgartner, S. Cox, A. M. Little, G. J. Alexander, M. E. Cramp, S. J. O'Brien, W. M. Rosenberg, D. L. Thomas, and M. Carrington. 2004. HLA and NK cell inhibitory receptor genes in resolving hepatitis C virus infection. *Science* 305: 872-874.

12. Martin, M. P., Y. Qi, X. Gao, E. Yamada, J. N. Martin, F. Pereyra, S. Colombo, E. E. Brown, W. L. Shupert, J. Phair, J. J. Goedert, S. Buchbinder, G. D. Kirk, A. Telenti, M. Connors, S. J. O'Brien, B. D. Walker, P. Parham, S. G. Deeks, D. W. McVicar, and M. Carrington. 2007. Innate partnership of HLA-B and KIR3DL1 subtypes against HIV-1. *Nat. Genet.* 39: 733-740.

13. Martin, M. P., X. Gao, J. H. Lee, G. W. Nelson, R. Detels, J. J. Goedert, S. Buchbinder, K. Hoots, D. Vlahov, J. Trowsdale, M. Wilson, S. J. O'Brien, and M. Carrington. 2002. Epistatic interaction between KIR3DS1 and HLA-B delays the progression to AIDS. *Nat. Genet.* 31: 429-434.

14. Tang, A. W., Z. Alfirevic, and S. Quenby. 2011. Natural killer cells and pregnancy outcomes in women with recurrent miscarriage and infertility: a systematic review. *Hum. Reprod.* 26: 1971-1980.

15. Shegarfi, H., F. Naddafi, and A. Mirshafiey. 2012. Natural killer cells and their role in rheumatoid arthritis: friend or foe? *Scientificworldjournal* 2012: 491974.

16. Langers, I., V. M. Renoux, M. Thiry, P. Delvenne, and N. Jacobs. 2012. Natural killer cells: role in local tumor growth and metastasis. *Biologics* 6: 73-82.

17. De Santis, D., A. Bishara, C. S. Witt, A. Nagler, C. Brautbar, S. Slavin, and F. T. Christiansen. 2005. Natural killer cell HLA-C epitopes and killer cell immunoglobulin-like receptors both influence outcome of mismatched unrelated donor bone marrow transplants. *Tissue Antigens* 65: 519-528.

18. Snell, G. D. and G. F. higgins. 1951. Alleles at the histocompatibility-2 locus in the mouse as determined by tumor transplantation. *Genetics* 36: 306-310.

19. Bach, F. H., M. L. Bach, and P. M. Sondel. 1976. Differential function of major histocompatibility complex antigens in T-lymphocyte activation. *Nature* 259: 273-281.

20. Cudkowicz, G. and M. Bennett. 1971. Peculiar immunobiology of bone marrow allografts. I. Graft rejection by irradiated responder mice. *J. Exp. Med.* 134: 83-102.

21. Cudkowicz, G. and M. Bennett. 1971. Peculiar immunobiology of bone marrow allografts. II. Rejection of parental grafts by resistant F 1 hybrid mice. *J. Exp. Med.* 134: 1513-1528.

22. Cudkowicz, G. and J. H. STIMPFLING. 1964. Deficient Growth of C57bl Marrow Cells Transplanted in F1 Hybrid Mice. Association with the Histocompatibility-2 Locus. *Immunology* 7: 291-306.

23. Daley, J. P. and I. Nakamura. 1984. Natural resistance of lethally irradiated F1 hybrid mice to parental marrow grafts is a function of H-2/Hh-restricted effectors. *J. Exp. Med.* 159: 1132-1148.

24. Karre, K., H. G. Ljunggren, G. Piontek, and R. Kiessling. 1986. Selective rejection of H-2-deficient lymphoma variants suggests alternative immune defence strategy. *Nature* 319: 675-678.

25. Ljunggren, H. G. and K. Karre. 1985. Host resistance directed selectively against H-2-deficient lymphoma variants. Analysis of the mechanism. *J. Exp. Med.* 162: 1745-1759.

26. Kavathas, P., F. H. Bach, and R. DeMars. 1980. Gamma ray-induced loss of expression of HLA and glyoxalase I alleles in lymphoblastoid cells. *Proc. Natl. Acad. Sci. U. S. A.* 77: 4251-4255.

27. Ljunggren, H. G. and K. Karre. 1990. In search of the 'missing self': MHC molecules and NK cell recognition. *Immunol. Today* 11: 237-244.

28. Vivier, E., E. Tomasello, and P. Paul. 2002. Lymphocyte activation via NKG2D: towards a new paradigm in immune recognition? *Curr. Opin. Immunol.* 14: 306-311.

29. Gazit, R., R. Gruda, M. Elboim, T. I. Arnon, G. Katz, H. Achdout, J. Hanna, U. Qimron, G. Landau, E. Greenbaum, Z. Zakay-Rones, A. Porgador, and O. Mandelboim. 2006. Lethal influenza infection in the absence of the natural killer cell receptor gene Ncr1. *Nat. Immunol.* 7: 517-523.

30. Arnon, T. I., H. Achdout, N. Lieberman, R. Gazit, T. Gonen-Gross, G. Katz, A. Bar-Ilan, N. Bloushtain, M. Lev, A. Joseph, E. Kedar, A. Porgador, and O. Mandelboim. 2004. The mechanisms controlling the recognition of tumor- and virus-infected cells by NKp46. *Blood* 103: 664-672.

31. Arase, H., E. S. Mocarski, A. E. Campbell, A. B. Hill, and L. L. Lanier. 2002. Direct recognition of cytomegalovirus by activating and inhibitory NK cell receptors. *Science* 296: 1323-1326.

32. Dokun, A. O., S. Kim, H. R. Smith, H. S. Kang, D. T. Chu, and W. M. Yokoyama. 2001. Specific and nonspecific NK cell activation during virus infection. *Nat. Immunol.* 2: 951-956.

33. Mandelboim, O., N. Lieberman, M. Lev, L. Paul, T. I. Arnon, Y. Bushkin, D. M. Davis, J. L. Strominger, J. W. Yewdell, and A. Porgador. 2001. Recognition of haemagglutinins on virus-infected cells by NKp46 activates lysis by human NK cells. *Nature* 409: 1055-1060.

34. GORER, P. A. 1948. The significance of studies with transplanted tumours. *Br. J. Cancer* 2: 103-107.

35. DAUSSET, J. 1958. Iso-leuko-antibodies. *Acta Haematol.* 20: 156-166.

36. Kelley, J., L. Walter, and J. Trowsdale. 2005. Comparative genomics of major histocompatibility complexes. *Immunogenetics* 56: 683-695.

37. Raychaudhuri, S., C. Sandor, E. A. Stahl, J. Freudenberg, H. S. Lee, X. Jia, L. Alfredsson, L. Padyukov, L. Klareskog, J. Worthington, K. A. Siminovitch, S. C. Bae, R. M. Plenge, P. K. Gregersen, and P. I. de Bakker. 2012. Five amino acids in three HLA proteins explain most of the association between MHC and seropositive rheumatoid arthritis. *Nat. Genet.* 44: 291-296.

38. Relle, M. and A. Schwarting. 2012. Role of MHC-linked susceptibility genes in the pathogenesis of human and murine lupus. *Clin. Dev. Immunol.* 2012: 584374.

39. Sadovnick, A. D. 2012. Genetic background of multiple sclerosis. *Autoimmun. Rev.* 11: 163-166.

40. Kubinak, J. L., J. S. Ruff, C. W. Hyzer, P. R. Slev, and W. K. Potts. 2012. Experimental viral evolution to specific host MHC genotypes reveals fitness and virulence trade-offs in alternative MHC types. *Proc. Natl. Acad. Sci. U. S. A.* 109: 3422-3427.

41. McLaren, P. J., S. Ripke, K. Pelak, A. C. Weintrob, N. A. Patsopoulos, X. Jia, R. L. Erlich, N. J. Lennon, C. M. Kadie, D. Heckerman, N. Gupta, D. W. Haas, S. G. Deeks, F. Pereyra, B. D. Walker, P. I. de Bakker, and International HIV Controllers Study. 2012. Fine-mapping classical HLA variation associated with durable host control of HIV-1 infection in African Americans. *Hum. Mol. Genet.* 21: 4334-4347.

42. Gonzalez, A., V. Rebmann, J. LeMaoult, P. A. Horn, E. D. Carosella, and E. Alegre. 2012. The immunosuppressive molecule HLA-G and its clinical implications. *Crit. Rev. Clin. Lab. Sci.* 49: 63-84.

43. Trowsdale, J. and A. Moffett. 2008. NK receptor interactions with MHC class I molecules in pregnancy. *Semin. Immunol.* 20: 317-320.

44. Shiina, T., K. Hosomichi, H. Inoko, and J. K. Kulski. 2009. The HLA genomic loci map: expression, interaction, diversity and disease. *J. Hum. Genet.* 54: 15-39.

45. Robinson, J., J. A. Halliwell, H. McWilliam, R. Lopez, and S. G. Marsh. 2012. IPD--the Immuno Polymorphism Database. *Nucleic Acids Res.*

46. Robinson, J., J. A. Halliwell, H. McWilliam, R. Lopez, and S. G. Marsh. 2013. IPD--the Immuno Polymorphism Database. *Nucleic Acids Res.* 41: D1234-40.

47. Madden, D. R. 1995. The three-dimensional structure of peptide-MHC complexes. *Annu. Rev. Immunol.* 13: 587-622.

48. Groothuis, T. A., A. C. Griekspoor, J. J. Neijssen, C. A. Herberts, and J. J. Neefjes. 2005. MHC class I alleles and their exploration of the antigen-processing machinery. *Immunol. Rev.* 207: 60-76.

49. Gattoni-Celli, S., K. Kirsch, R. Timpane, and K. J. Isselbacher. 1992. Beta 2-microglobulin gene is mutated in a human colon cancer cell line (HCT) deficient in the expression of HLA class I antigens on the cell surface. *Cancer Res.* 52: 1201-1204.

50. Hochman, J. H., Y. Shimizu, R. DeMars, and M. Edidin. 1988. Specific associations of fluorescent beta-2-microglobulin with cell surfaces. The affinity of different H-2 and HLA antigens for beta-2-microglobulin. *J. Immunol.* 140: 2322-2329.

51. Macdonald, W. A., A. W. Purcell, N. A. Mifsud, L. K. Ely, D. S. Williams, L. Chang, J. J. Gorman, C. S. Clements, L. Kjer-Nielsen, D. M. Koelle, S. R. Burrows, B. D. Tait, R. Holdsworth, A. G. Brooks, G. O. Lovrecz, L. Lu, J. Rossjohn, and J. McCluskey. 2003. A naturally selected dimorphism within the HLA-B44 supertype

alters class I structure, peptide repertoire, and T cell recognition. *J. Exp. Med.* 198: 679-691.

52. Allen, R. L., C. A. O'Callaghan, A. J. McMichael, and P. Bowness. 1999. Cutting edge: HLA-B27 can form a novel beta 2-microglobulin-free heavy chain homodimer structure. *J. Immunol.* 162: 5045-5048.

53. van ROOD, J. 1962. Leukocyte groups. *Ned. Tijdschr. Geneeskd.* 106: 692-694.

54. Ayres, J. and P. Cresswell. 1976. HLA-B specificities and w4, w6 specificities are on the same polypeptide. *Eur. J. Immunol.* 6: 794-799.

55. Rodey, G. E. and T. C. Fuller. 1987. Public epitopes and the antigenic structure of the HLA molecules. *Crit. Rev. Immunol.* 7: 229-267.

56. Gumperz, J. E., V. Litwin, J. H. Phillips, L. L. Lanier, and P. Parham. 1995. The Bw4 public epitope of HLA-B molecules confers reactivity with natural killer cell clones that express NKB1, a putative HLA receptor. *J. Exp. Med.* 181: 1133-1144.

57. Muller, C. A., G. Engler-Blum, V. Gekeler, I. Steiert, E. Weiss, and H. Schmidt. 1989. Genetic and serological heterogeneity of the supertypic HLA-B locus specificities Bw4 and Bw6. *Immunogenetics* 30: 200-207.

58. Wan, A. M., P. Ennis, P. Parham, and N. Holmes. 1986. The primary structure of HLA-A32 suggests a region involved in formation of the Bw4/Bw6 epitopes. *J. Immunol.* 137: 3671-3674.

59. Barber, L. D. and P. Parham. 1993. Peptide binding to major histocompatibility complex molecules. *Annu. Rev. Cell Biol.* 9: 163-206.

60. Clayberger, C., M. Rosen, P. Parham, and A. M. Krensky. 1990. Recognition of an HLA public determinant (Bw4) by human allogeneic cytotoxic T lymphocytes. *J. Immunol.* 144: 4172-4176.

61. Voorter, C. E., S. van der Vlies, M. Kik, and E. M. van den Berg-Loonen. 2000. Unexpected Bw4 and Bw6 reactivity patterns in new alleles. *Tissue Antigens* 56: 363-370.

62. Kostyu, D. D., P. Cresswell, and D. B. Amos. 1980. A public HLA antigen associated with HLA-A9, Aw32, and Bw4. *Immunogenetics* 10: 433-442.

63. Layet, C., T. Delovitch, P. Ferrier, D. H. Caillol, B. R. Jordan, and F. A. Lemonnier. 1985. Expression of an HLA-Bw6-related specificity by the HLA-Cw3 molecule. *Immunogenetics* 21: 469-478.

64. Kollnberger, S., L. Bird, M. Y. Sun, C. Retiere, V. M. Braud, A. McMichael, and P. Bowness. 2002. Cell-surface expression and immune receptor recognition of HLA-B27 homodimers. *Arthritis Rheum.* 46: 2972-2982.

65. Colonna, M., E. G. Brooks, M. Falco, G. B. Ferrara, and J. L. Strominger. 1993. Generation of allospecific natural killer cells by stimulation across a polymorphism of HLA-C. *Science* 260: 1121-1124.

66. Colonna, M., T. Spies, J. L. Strominger, E. Ciccone, A. Moretta, L. Moretta, D. Pende, and O. Viale. 1992. Alloantigen recognition by two human natural killer cell clones is associated with HLA-C or a closely linked gene. *Proc. Natl. Acad. Sci. U. S. A.* 89: 7983-7985.

67. Snary, D., C. J. Barnstable, W. F. Bodmer, and M. J. Crumpton. 1977. Molecular structure of human histocompatibility antigens: the HLA-C series. *Eur. J. Immunol.* 7: 580-585.

68. Neefjes, J. J. and H. L. Ploegh. 1988. Allele and locus-specific differences in cell surface expression and the association of HLA class I heavy chain with beta 2-microglobulin: differential effects of inhibition of glycosylation on class I subunit association. *Eur. J. Immunol.* 18: 801-810.

69. Falk, C. S. and D. J. Schendel. 1997. HLA-C revisited. Ten years of change. *Immunol. Res.* 16: 203-214.

70. Biassoni, R., M. Falco, A. Cambiaggi, P. Costa, S. Verdiani, D. Pende, R. Conte, C. Di Donato, P. Parham, and L. Moretta. 1995. Amino acid substitutions can influence the natural killer (NK)-mediated recognition of HLA-C molecules. Role of serine-77 and lysine-80 in the target cell protection from lysis mediated by "group 2" or "group 1" NK clones. *J. Exp. Med.* 182: 605-609.

71. Gumperz, J. E., L. D. Barber, N. M. Valiante, L. Percival, J. H. Phillips, L. L. Lanier, and P. Parham. 1997. Conserved and variable residues within the Bw4 motif of HLA-B make separable contributions to recognition by the NKB1 killer cell-inhibitory receptor. *J. Immunol.* 158: 5237-5241.

72. Braud, V., E. Y. Jones, and A. McMichael. 1997. The human major histocompatibility complex class Ib molecule HLA-E binds signal sequence-derived peptides with primary anchor residues at positions 2 and 9. *Eur. J. Immunol.* 27: 1164-1169.

73. Lee, N., M. Llano, M. Carretero, A. Ishitani, F. Navarro, M. Lopez-Botet, and D. E. Geraghty. 1998. HLA-E is a major ligand for the natural killer inhibitory receptor CD94/NKG2A. *Proc. Natl. Acad. Sci. U. S. A.* 95: 5199-5204.

74. Llano, M., N. Lee, F. Navarro, P. Garcia, J. P. Albar, D. E. Geraghty, and M. Lopez-Botet. 1998. HLA-E-bound peptides influence recognition by inhibitory and triggering CD94/NKG2 receptors: preferential response to an HLA-G-derived nonamer. *Eur. J. Immunol.* 28: 2854-2863.

75. Brooks, A. G., F. Borrego, P. E. Posch, A. Patamawenu, C. J. Scorzelli, M. Ulbrecht, E. H. Weiss, and J. E. Coligan. 1999. Specific recognition of HLA-E, but not classical, HLA class I molecules by soluble CD94/NKG2A and NK cells. *J. Immunol.* 162: 305-313.

76. Tomasec, P., V. M. Braud, C. Rickards, M. B. Powell, B. P. McSharry, S. Gadola, V. Cerundolo, L. K. Borysiewicz, A. J. McMichael, and G. W. Wilkinson. 2000. Surface expression of HLA-E, an inhibitor of natural killer cells, enhanced by human cytomegalovirus gpUL40. *Science* 287: 1031.

77. Nattermann, J., H. D. Nischalke, V. Hofmeister, G. Ahlenstiel, H. Zimmermann, L. Leifeld, E. H. Weiss, T. Sauerbruch, and U. Spengler. 2005. The HLA-A2 restricted T cell epitope HCV core 35-44 stabilizes HLA-E expression and inhibits cytolysis mediated by natural killer cells. *Am. J. Pathol.* 166: 443-453.

78. Heatley, S. L., G. Pietra, J. Lin, J. M. Widjaja, C. M. Harpur, S. Lester, J. Rossjohn, J. Szer, A. Schwarer, K. Bradstock, P. G. Bardy, M. C. Mingari, L. Moretta, L. C. Sullivan, and A. G. Brooks. 2013. Polymorphism in human cytomegalovirus UL40 impacts on recognition of HLA-E by natural killer cells. *J. Biol. Chem.*

79. Michaelsson, J., C. Teixeira de Matos, A. Achour, L. L. Lanier, K. Karre, and K. Soderstrom. 2002. A signal peptide derived from hsp60 binds HLA-E and interferes with CD94/NKG2A recognition. *J. Exp. Med.* 196: 1403-1414.

80. Nattermann, J., H. D. Nischalke, V. Hofmeister, B. Kupfer, G. Ahlenstiel, G. Feldmann, J. Rockstroh, E. H. Weiss, T. Sauerbruch, and U. Spengler. 2005. HIV-1 infection leads to increased HLA-E expression resulting in impaired function of natural killer cells. *Antivir Ther.* 10: 95-107.

81. Pietra, G., C. Romagnani, P. Mazzarino, M. Falco, E. Millo, A. Moretta, L. Moretta, and M. C. Mingari. 2003. HLA-E-restricted recognition of cytomegalovirus-derived peptides by human CD8+ cytolytic T lymphocytes. *Proc. Natl. Acad. Sci. U. S. A.* 100: 10896-10901.

82. Pietra, G., C. Romagnani, C. Manzini, L. Moretta, and M. C. Mingari. 2010. The emerging role of HLA-E-restricted CD8+ T lymphocytes in the adaptive immune response to pathogens and tumors. *J. Biomed. Biotechnol.* 2010: 907092.

83. Lee, N. and D. E. Geraghty. 2003. HLA-F surface expression on B cell and monocyte cell lines is partially independent from tapasin and completely independent from TAP. *J. Immunol.* 171: 5264-5271.

84. Lee, N., A. Ishitani, and D. E. Geraghty. 2010. HLA-F is a surface marker on activated lymphocytes. *Eur. J. Immunol.* 40: 2308-2318.

85. Ishitani, A., N. Sageshima, N. Lee, N. Dorofeeva, K. Hatake, H. Marquardt, and D. E. Geraghty. 2003. Protein expression and peptide binding suggest unique and interacting functional roles for HLA-E, F, and G in maternal-placental immune recognition. *J. Immunol.* 171: 1376-1384.

86. Geraghty, D. E., X. H. Wei, H. T. Orr, and B. H. Koller. 1990. Human leukocyte antigen F (HLA-F). An expressed HLA gene composed of a class I coding sequence linked to a novel transcribed repetitive element. *J. Exp. Med.* 171: 1-18.

87. Boyle, L. H., A. K. Gillingham, S. Munro, and J. Trowsdale. 2006. Selective export of HLA-F by its cytoplasmic tail. *J. Immunol.* 176: 6464-6472.

88. Goodridge, J. P., A. Burian, N. Lee, and D. E. Geraghty. 2010. HLA-F complex without peptide binds to MHC class I protein in the open conformer form. *J. Immunol.* 184: 6199-6208.

89. Lepin, E. J., J. M. Bastin, D. S. Allan, G. Roncador, V. M. Braud, D. Y. Mason, P. A. van der Merwe, A. J. McMichael, J. I. Bell, S. H. Powis, and C. A. O'Callaghan. 2000. Functional characterization of HLA-F and binding of HLA-F tetramers to ILT2 and ILT4 receptors. *Eur. J. Immunol.* 30: 3552-3561.

90. Davis, D. M., H. T. Reyburn, L. Pazmany, I. Chiu, O. Mandelboim, and J. L. Strominger. 1997. Impaired spontaneous endocytosis of HLA-G. *Eur. J. Immunol.* 27: 2714-2719.

91. Boyson, J. E., R. Erskine, M. C. Whitman, M. Chiu, J. M. Lau, L. A. Koopman, M. M. Valter, P. Angelisova, V. Horejsi, and J. L. Strominger. 2002. Disulfide bond-mediated dimerization of HLA-G on the cell surface. *Proc. Natl. Acad. Sci. U. S. A.* 99: 16180-16185.

92. Gonen-Gross, T., H. Achdout, T. I. Arnon, R. Gazit, N. Stern, V. Horejsi, D. Goldman-Wohl, S. Yagel, and O. Mandelboim. 2005. The CD85J/leukocyte inhibitory receptor-1 distinguishes between conformed and beta 2-microglobulin-free HLA-G molecules. *J. Immunol.* 175: 4866-4874.

93. Le Discorde, M., P. Moreau, P. Sabatier, J. M. Legeais, and E. D. Carosella. 2003. Expression of HLA-G in human cornea, an immune-privileged tissue. *Hum. Immunol.* 64: 1039-1044.

94. Crisa, L., M. T. McMaster, J. K. Ishii, S. J. Fisher, and D. R. Salomon. 1997. Identification of a thymic epithelial cell subset sharing expression of the class Ib HLA-G molecule with fetal trophoblasts. *J. Exp. Med.* 186: 289-298.

95. Kovats, S., E. K. Main, C. Librach, M. Stubblebine, S. J. Fisher, and R. DeMars. 1990. A class I antigen, HLA-G, expressed in human trophoblasts. *Science* 248: 220-223.

96. Feder, J. N., A. Gnirke, W. Thomas, Z. Tsuchihashi, D. A. Ruddy, A. Basava, F. Dormishian, R. Domingo Jr, M. C. Ellis, A. Fullan, L. M. Hinton, N. L. Jones, B. E. Kimmel, G. S. Kronmal, P. Lauer, V. K. Lee, D. B. Loeb, F. A. Mapa, E. McClelland, N. C. Meyer, G. A. Mintier, N. Moeller, T. Moore, E. Morikang, C. E. Prass, L. Quintana, S. M. Starnes, R. C. Schatzman, K. J. Brunke, D. T. Drayna, N. J. Risch, B. R. Bacon, and R. K. Wolff. 1996. A novel MHC class I-like gene is mutated in patients with hereditary haemochromatosis. *Nat. Genet.* 13: 399-408.

97. Lebron, J. A., M. J. Bennett, D. E. Vaughn, A. J. Chirino, P. M. Snow, G. A. Mintier, J. N. Feder, and P. J. Bjorkman. 1998. Crystal structure of the hemochromatosis protein HFE and characterization of its interaction with transferrin receptor. *Cell* 93: 111-123.

98. Feder, J. N. 1999. The hereditary hemochromatosis gene (HFE): a MHC class I-like gene that functions in the regulation of iron homeostasis. *Immunol. Res.* 20: 175-185.

99. Borges, L. and D. Cosman. 2000. LIRs/ILTs/MIRs, inhibitory and stimulatory Ig-superfamily receptors expressed in myeloid and lymphoid cells. *Cytokine Growth Factor Rev.* 11: 209-217.

100. Cella, M., H. Nakajima, F. Facchetti, T. Hoffmann, and M. Colonna. 2000. ILT receptors at the interface between lymphoid and myeloid cells. *Curr. Top. Microbiol. Immunol.* 251: 161-166.

101. Vilches, C. and P. Parham. 2002. KIR: diverse, rapidly evolving receptors of innate and adaptive immunity. *Annu. Rev. Immunol.* 20: 217-251.

102. Barber, D. F., M. Faure, and E. O. Long. 2004. LFA-1 contributes an early signal for NK cell cytotoxicity. *J. Immunol.* 173: 3653-3659.

103. Burshtyn, D. N., A. M. Scharenberg, N. Wagtmann, S. Rajagopalan, K. Berrada, T. Yi, J. P. Kinet, and E. O. Long. 1996. Recruitment of tyrosine phosphatase HCP by the killer cell inhibitor receptor. *Immunity* 4: 77-85.

104. Long, E. O. 1999. Regulation of immune responses through inhibitory receptors. *Annu. Rev. Immunol.* 17: 875-904.

105. Binstadt, B. A., K. M. Brumbaugh, C. J. Dick, A. M. Scharenberg, B. L. Williams, M. Colonna, L. L. Lanier, J. P. Kinet, R. T. Abraham, and P. J. Leibson. 1996. Sequential involvement of Lck and SHP-1 with MHC-recognizing receptors on NK cells inhibits FcR-initiated tyrosine kinase activation. *Immunity* 5: 629-638.

106. Purdy, A. K. and K. S. Campbell. 2009. SHP-2 expression negatively regulates NK cell function. *J. Immunol.* 183: 7234-7243.

107. Stebbins, C. C., C. Watzl, D. D. Billadeau, P. J. Leibson, D. N. Burshtyn, and E. O. Long. 2003. Vav1 dephosphorylation by the tyrosine phosphatase SHP-1 as a mechanism for inhibition of cellular cytotoxicity. *Mol. Cell. Biol.* 23: 6291-6299.

108. Yusa, S. and K. S. Campbell. 2003. Src homology region 2-containing protein tyrosine phosphatase-2 (SHP-2) can play a direct role in the inhibitory function of killer cell Ig-like receptors in human NK cells. *J. Immunol.* 170: 4539-4547.

109. Long, E. O. 2008. Negative signaling by inhibitory receptors: the NK cell paradigm. *Immunol. Rev.* 224: 70-84.

110. Marsh, S. G., P. Parham, B. Dupont, D. E. Geraghty, J. Trowsdale, D. Middleton, C. Vilches, M. Carrington, C. Witt, L. A. Guethlein, H. Shilling, C. A. Garcia, K. C. Hsu, and H. Wain. 2003. Killer-cell immunoglobulin-like receptor (KIR) nomenclature report, 2002. *Tissue Antigens* 62: 79-86.

111. Kikuchi-Maki, A., T. L. Catina, and K. S. Campbell. 2005. Cutting edge: KIR2DL4 transduces signals into human NK cells through association with the Fc receptor gamma protein. *J. Immunol.* 174: 3859-3863.

112. Rajagopalan, S., Y. T. Bryceson, S. P. Kuppusamy, D. E. Geraghty, A. van der Meer, I. Joosten, and E. O. Long. 2006. Activation of NK cells by an endocytosed receptor for soluble HLA-G. *PLoS Biol.* 4: e9.

113. Faure, M. and E. O. Long. 2002. KIR2DL4 (CD158d), an NK cell-activating receptor with inhibitory potential. *J. Immunol.* 168: 6208-6214.

114. Gumperz, J. E., J. C. Paterson, V. Litwin, N. Valiante, L. L. Lanier, P. Parham, and A. M. Little. 1996. Specificity of two anti-class I HLA monoclonal antibodies that block class I recognition by the NKB1 killer cell inhibitory receptor. *Tissue Antigens* 48: 278-284.

115. Pende, D., R. Biassoni, C. Cantoni, S. Verdiani, M. Falco, C. di Donato, L. Accame, C. Bottino, A. Moretta, and L. Moretta. 1996. The natural killer cell receptor specific for HLA-A allotypes: a novel member of the p58/p70 family of inhibitory receptors that is characterized by three immunoglobulin-like domains and is expressed as a 140-kD disulphide-linked dimer. *J. Exp. Med.* 184: 505-518.

116. Guethlein, L. A., L. Abi-Rached, J. A. Hammond, and P. Parham. 2007. The expanded cattle KIR genes are orthologous to the conserved single-copy KIR3DX1 gene of primates. *Immunogenetics* 59: 517-522.

117. Trowsdale, J., R. Barten, A. Haude, C. A. Stewart, S. Beck, and M. J. Wilson. 2001. The genomic context of natural killer receptor extended gene families. *Immunol. Rev.* 181: 20-38.

118. Martin, A. M., E. M. Freitas, C. S. Witt, and F. T. Christiansen. 2000. The genomic organization and evolution of the natural killer immunoglobulin-like receptor (KIR) gene cluster. *Immunogenetics* 51: 268-280.

119. Parham, P., L. Abi-Rached, L. Matevosyan, A. K. Moesta, P. J. Norman, A. M. Older Aguilar, and L. A. Guethlein. 2010. Primate-specific regulation of natural killer cells. *J. Med. Primatol.* 39: 194-212.

120. Wilson, M. J., M. Torkar, A. Haude, S. Milne, T. Jones, D. Sheer, S. Beck, and J. Trowsdale. 2000. Plasticity in the organization and sequences of human KIR/ILT gene families. *Proc. Natl. Acad. Sci. U. S. A.* 97: 4778-4783.

121. Trowsdale, J. 2001. Genetic and functional relationships between MHC and NK receptor genes. *Immunity* 15: 363-374.

122. Yawata, M., N. Yawata, M. Draghi, A. M. Little, F. Partheniou, and P. Parham. 2006. Roles for HLA and KIR polymorphisms in natural killer cell repertoire selection and modulation of effector function. *J. Exp. Med.* 203: 633-645.

123. Shilling, H. G., N. Young, L. A. Guethlein, N. W. Cheng, C. M. Gardiner, D. Tyan, and P. Parham. 2002. Genetic control of human NK cell repertoire. *J. Immunol.* 169: 239-247.

124. Williams, F., L. D. Maxwell, I. A. Halfpenny, A. Meenagh, C. Sleator, M. D. Curran, and D. Middleton. 2003. Multiple copies of KIR 3DL/S1 and KIR 2DL4 genes identified in a number of individuals. *Hum. Immunol.* 64: 729-732.

125. Wilson, M. J., M. Torkar, and J. Trowsdale. 1997. Genomic organization of a human killer cell inhibitory receptor gene. *Tissue Antigens* 49: 574-579.

126. Pyo, C. W., L. A. Guethlein, Q. Vu, R. Wang, L. Abi-Rached, P. J. Norman, S. G. Marsh, J. S. Miller, P. Parham, and D. E. Geraghty. 2010. Different patterns of evolution in the centromeric and telomeric regions of group A and B haplotypes of the human killer cell Ig-like receptor locus. *PLoS One* 5: e15115.

127. Middleton, D., A. Meenagh, and P. A. Gourraud. 2007. KIR haplotype content at the allele level in 77 Northern Irish families. *Immunogenetics* 59: 145-158.

128. Middleton, D. and F. Gonzelez. 2010. The extensive polymorphism of KIR genes. *Immunology* 129: 8-19.

129. Rajagopalan, S. and E. O. Long. 1999. A human histocompatibility leukocyte antigen (HLA)-G-specific receptor expressed on all natural killer cells. *J. Exp. Med.* 189: 1093-1100.

130. Goodridge, J. P., C. S. Witt, F. T. Christiansen, and H. S. Warren. 2003. KIR2DL4 (CD158d) genotype influences expression and function in NK cells. *J. Immunol.* 171: 1768-1774.

131. Trundley, A. E., S. E. Hiby, C. Chang, A. M. Sharkey, S. Santourlidis, M. Uhrberg, J. Trowsdale, and A. Moffett. 2006. Molecular characterization of KIR3DL3. *Immunogenetics* 57: 904-916.

132. Valiante, N. M., M. Uhrberg, H. G. Shilling, K. Lienert-Weidenbach, K. L. Arnett, A. D'Andrea, J. H. Phillips, L. L. Lanier, and P. Parham. 1997. Functionally and structurally distinct NK cell receptor repertoires in the peripheral blood of two human donors. *Immunity* 7: 739-751.

133. Pascal, V., N. Schleinitz, C. Brunet, S. Ravet, E. Bonnet, X. Lafarge, M. Touinssi, D. Reviron, J. F. Viallard, J. F. Moreau, J. Dechanet-Merville, P. Blanco, J. R. Harle, J. Sampol, E. Vivier, F. Dignat-George, and P. Paul. 2004. Comparative analysis of NK cell subset distribution in normal and lymphoproliferative disease of granular lymphocyte conditions. *Eur. J. Immunol.* 34: 2930-2940.

134. Chan, H. W., J. S. Miller, M. B. Moore, and C. T. Lutz. 2005. Epigenetic control of highly homologous killer Ig-like receptor gene alleles. *J. Immunol.* 175: 5966-5974.

135. Davies, G. E., S. M. Locke, P. W. Wright, H. Li, R. J. Hanson, J. S. Miller, and S. K. Anderson. 2007. Identification of bidirectional promoters in the human KIR genes. *Genes Immun.* 8: 245-253.

136. Santourlidis, S., H. I. Trompeter, S. Weinhold, B. Eisermann, K. L. Meyer, P. Wernet, and M. Uhrberg. 2002. Crucial role of DNA methylation in determination of clonally distributed killer cell Ig-like receptor expression patterns in NK cells. *J. Immunol.* 169: 4253-4261.

137. Uhrberg, M. 2005. Shaping the human NK cell repertoire: an epigenetic glance at KIR gene regulation. *Mol. Immunol.* 42: 471-475.

138. Gardiner, C. M. 2008. Killer cell immunoglobulin-like receptors on NK cells: the how, where and why. *Int. J. Immunogenet.* 35: 1-8.

139. Stulberg, M. J., P. W. Wright, H. Dang, R. J. Hanson, J. S. Miller, and S. K. Anderson. 2007. Identification of distal KIR promoters and transcripts. *Genes Immun.* 8: 124-130.

140. Single, R. M., M. P. Martin, X. Gao, D. Meyer, M. Yeager, J. R. Kidd, K. K. Kidd, and M. Carrington. 2007. Global diversity and evidence for coevolution of KIR and HLA. *Nat. Genet.* 39: 1114-1119.

141. Parham, P. 2005. MHC class I molecules and KIRs in human history, health and survival. *Nat. Rev. Immunol.* 5: 201-214.

142. Biassoni, R., A. Pessino, A. Malaspina, C. Cantoni, C. Bottino, S. Sivori, L. Moretta, and A. Moretta. 1997. Role of amino acid position 70 in the binding affinity of p50.1 and p58.1 receptors for HLA-Cw4 molecules. *Eur. J. Immunol.* 27: 3095-3099.

143. Winter, C. C., J. E. Gumperz, P. Parham, E. O. Long, and N. Wagtmann. 1998. Direct binding and functional transfer of NK cell inhibitory receptors reveal novel patterns of HLA-C allotype recognition. *J. Immunol.* 161: 571-577.

144. van der Slik, A. R., B. P. Koeleman, W. Verduijn, G. J. Bruining, B. O. Roep, and M. J. Giphart. 2003. KIR in type 1 diabetes: disparate distribution of activating and inhibitory natural killer cell receptors in patients versus HLA-matched control subjects. *Diabetes* 52: 2639-2642.

145. Hiby, S. E., J. J. Walker, K. M. O'shaughnessy, C. W. Redman, M. Carrington, J. Trowsdale, and A. Moffett. 2004. Combinations of maternal KIR and fetal HLA-C genes influence the risk of preeclampsia and reproductive success. *J. Exp. Med.* 200: 957-965.

146. Hiby, S. E., R. Apps, A. M. Sharkey, L. E. Farrell, L. Gardner, A. Mulder, F. H. Claas, J. J. Walker, C. W. Redman, L. Morgan, C. Tower, L. Regan, G. E. Moore, M. Carrington, and A. Moffett. 2010. Maternal activating KIRs protect against human reproductive failure mediated by fetal HLA-C2. *J. Clin. Invest.* 120: 4102-4110.

147. Carrington, M., S. Wang, M. P. Martin, X. Gao, M. Schiffman, J. Cheng, R. Herrero, A. C. Rodriguez, R. Kurman, R. Mortel, P. Schwartz, A. Glass, and A. Hildesheim. 2005. Hierarchy of resistance to cervical neoplasia mediated by combinations of killer immunoglobulin-like receptor and human leukocyte antigen loci. *J. Exp. Med.* 201: 1069-1075.

148. Winter, C. C. and E. O. Long. 2000. Binding of soluble KIR-Fc fusion proteins to HLA class I. *Methods Mol. Biol.* 121: 239-250.

149. Fan, Q. R., E. O. Long, and D. C. Wiley. 2001. Crystal structure of the human natural killer cell inhibitory receptor KIR2DL1-HLA-Cw4 complex. *Nat. Immunol.* 2: 452-460.

150. Fan, Q. R., L. Mosyak, C. C. Winter, N. Wagtmann, E. O. Long, and D. C. Wiley. 1997. Structure of the inhibitory receptor for human natural killer cells resembles haematopoietic receptors. *Nature* 389: 96-100.

151. Mandelboim, O., H. T. Reyburn, M. Vales-Gomez, L. Pazmany, M. Colonna, G. Borsellino, and J. L. Strominger. 1996. Protection from lysis by natural killer cells of group 1 and 2 specificity is mediated by residue 80 in human histocompatibility leukocyte antigen C alleles and also occurs with empty major histocompatibility complex molecules. *J. Exp. Med.* 184: 913-922.

152. Malnati, M. S., M. Peruzzi, K. C. Parker, W. E. Biddison, E. Ciccone, A. Moretta, and E. O. Long. 1995. Peptide specificity in the recognition of MHC class I by natural killer cell clones. *Science* 267: 1016-1018.

153. Fan, Q. R., E. O. Long, and D. C. Wiley. 2000. Cobalt-mediated dimerization of the human natural killer cell inhibitory receptor. *J. Biol. Chem.* 275: 23700-23706.

154. Rajagopalan, S. and E. O. Long. 1998. Zinc bound to the killer cell-inhibitory receptor modulates the negative signal in human NK cells. *J. Immunol.* 161: 1299-1305.

155. Bari, R., T. Bell, W. H. Leung, Q. P. Vong, W. K. Chan, N. Das Gupta, M. Holladay, B. Rooney, and W. Leung. 2009. Significant functional heterogeneity among KIR2DL1 alleles and a pivotal role of arginine 245. *Blood* 114: 5182-5190.

156. Boulet, S., M. Kleyman, J. Y. Kim, P. Kamya, S. Sharafi, N. Simic, J. Bruneau, J. P. Routy, C. M. Tsoukas, and N. F. Bernard. 2008. A combined genotype of KIR3DL1 high expressing alleles and HLA-B*57 is associated with a reduced risk of HIV infection. *Aids* 22: 1487-1491.

157. Kim, S., J. Poursine-Laurent, S. M. Truscott, L. Lybarger, Y. J. Song, L. Yang, A. R. French, J. B. Sunwoo, S. Lemieux, T. H. Hansen, and W. M. Yokoyama. 2005. Licensing of natural killer cells by host major histocompatibility complex class I molecules. *Nature* 436: 709-713.

158. Kim, S., J. B. Sunwoo, L. Yang, T. Choi, Y. J. Song, A. R. French, A. Vlahiotis, J. F. Piccirillo, M. Cella, M. Colonna, T. Mohanakumar, K. C. Hsu, B. Dupont, and W. M.

Yokoyama. 2008. HLA alleles determine differences in human natural killer cell responsiveness and potency. *Proc. Natl. Acad. Sci. U. S. A.* 105: 3053-3058.

159. Norman, P. J., L. Abi-Rached, K. Gendzekhadze, D. Korbel, M. Gleimer, D. Rowley, D. Bruno, C. V. Carrington, D. Chandanayingyong, Y. H. Chang, C. Crespi, G. Saruhan-Direskeneli, P. A. Fraser, K. Hameed, G. Kamkamidze, K. A. Koram, Z. Layrisse, N. Matamoros, J. Mila, M. H. Park, R. M. Pitchappan, D. D. Ramdath, M. Y. Shiau, H. A. Stephens, S. Struik, D. H. Verity, R. W. Vaughan, D. Tyan, R. W. Davis, E. M. Riley, M. Ronaghi, and P. Parham. 2007. Unusual selection on the KIR3DL1/S1 natural killer cell receptor in Africans. *Nat. Genet.* 39: 1092-1099.

160. Gardiner, C. M., L. A. Guethlein, H. G. Shilling, M. Pando, W. H. Carr, R. Rajalingam, C. Vilches, and P. Parham. 2001. Different NK cell surface phenotypes defined by the DX9 antibody are due to KIR3DL1 gene polymorphism. *J. Immunol.* 166: 2992-3001.

161. Sharma, D., K. Bastard, L. A. Guethlein, P. J. Norman, N. Yawata, M. Yawata, M. Pando, H. Thananchai, T. Dong, S. Rowland-Jones, F. M. Brodsky, and P. Parham. 2009. Dimorphic motifs in D0 and D1+D2 domains of killer cell Ig-like receptor 3DL1 combine to form receptors with high, moderate, and no avidity for the complex of a peptide derived from HIV and HLA-A*2402. *J. Immunol.* 183: 4569-4582.

162. Pando, M. J., C. M. Gardiner, M. Gleimer, K. L. McQueen, and P. Parham. 2003. The protein made from a common allele of KIR3DL1 (3DL1*004) is poorly expressed at cell surfaces due to substitution at positions 86 in Ig domain 0 and 182 in Ig domain 1. *J. Immunol.* 171: 6640-6649.

163. Taner, S. B., M. J. Pando, A. Roberts, J. Schellekens, S. G. Marsh, K. J. Malmberg, P. Parham, and F. M. Brodsky. 2011. Interactions of NK cell receptor KIR3DL1*004 with chaperones and conformation-specific antibody reveal a functional folded state as well as predominant intracellular retention. *J. Immunol.* 186: 62-72.

164. Carr, W. H., M. J. Pando, and P. Parham. 2005. KIR3DL1 polymorphisms that affect NK cell inhibition by HLA-Bw4 ligand. *J. Immunol.* 175: 5222-5229.

165. Halfpenny, I. A., D. Middleton, Y. A. Barnett, and F. Williams. 2004. Investigation of killer cell immunoglobulin-like receptor gene diversity: IV. KIR3DL1/S1. *Hum. Immunol.* 65: 602-612.

166. O'Connor, G. M., K. J. Guinan, R. T. Cunningham, D. Middleton, P. Parham, and C. M. Gardiner. 2007. Functional polymorphism of the KIR3DL1/S1 receptor on human NK cells. *J. Immunol.* 178: 235-241.

167. Sanjanwala, B., M. Draghi, P. J. Norman, L. A. Guethlein, and P. Parham. 2008. Polymorphic sites away from the Bw4 epitope that affect interaction of Bw4+ HLA-B with KIR3DL1. *J. Immunol.* 181: 6293-6300.

168. Khakoo, S. I., R. Geller, S. Shin, J. A. Jenkins, and P. Parham. 2002. The D0 domain of KIR3D acts as a major histocompatibility complex class I binding enhancer. *J. Exp. Med.* 196: 911-921.

169. Rojo, S., N. Wagtmann, and E. O. Long. 1997. Binding of a soluble p70 killer cell inhibitory receptor to HLA-B*5101: requirement for all three p70 immunoglobulin domains. *Eur. J. Immunol.* 27: 568-571.

170. Willcox, B. E., L. M. Thomas, and P. J. Bjorkman. 2003. Crystal structure of HLA-A2 bound to LIR-1, a host and viral major histocompatibility complex receptor. *Nat. Immunol.* 4: 913-919.

171. Kirwan, S. E. and D. N. Burshtyn. 2005. Killer cell Ig-like receptor-dependent signaling by Ig-like transcript 2 (ILT2/CD85j/LILRB1/LIR-1). *J. Immunol.* 175: 5006-5015.

172. Colonna, M., F. Navarro, T. Bellon, M. Llano, P. Garcia, J. Samaridis, L. Angman, M. Cella, and M. Lopez-Botet. 1997. A common inhibitory receptor for major histocompatibility complex class I molecules on human lymphoid and myelomonocytic cells. *J. Exp. Med.* 186: 1809-1818.

173. Davidson, C. L., N. L. Li, and D. N. Burshtyn. 2010. LILRB1 polymorphism and surface phenotypes of natural killer cells. *Hum. Immunol.* 71: 942-949.

174. Li, N. L., C. L. Davidson, A. Humar, and D. N. Burshtyn. 2011. Modulation of the inhibitory receptor leukocyte Ig-like receptor 1 on human natural killer cells. *Front. Immunol.* 2: 46.

175. Bellon, T., F. Kitzig, J. Sayos, and M. Lopez-Botet. 2002. Mutational analysis of immunoreceptor tyrosine-based inhibition motifs of the Ig-like transcript 2 (CD85j) leukocyte receptor. *J. Immunol.* 168: 3351-3359.

176. Berg, L., G. C. Riise, D. Cosman, T. Bergstrom, S. Olofsson, K. Karre, and E. Carbone. 2003. LIR-1 expression on lymphocytes, and cytomegalovirus disease in lung-transplant recipients. *Lancet* 361: 1099-1101.

177. Brown, D., J. Trowsdale, and R. Allen. 2004. The LILR family: modulators of innate and adaptive immune pathways in health and disease. *Tissue Antigens* 64: 215-225.

178. Shiroishi, M., K. Kuroki, L. Rasubala, K. Tsumoto, I. Kumagai, E. Kurimoto, K. Kato, D. Kohda, and K. Maenaka. 2006. Structural basis for recognition of the nonclassical MHC molecule HLA-G by the leukocyte Ig-like receptor B2 (LILRB2/LIR2/ILT4/CD85d). *Proc. Natl. Acad. Sci. U. S. A.* 103: 16412-16417.

179. Willcox, B. E., L. M. Thomas, T. L. Chapman, A. P. Heikema, A. P. West Jr, and P. J. Bjorkman. 2002. Crystal structure of LIR-2 (ILT4) at 1.8 A: differences from LIR-1 (ILT2) in regions implicated in the binding of the Human Cytomegalovirus class I MHC homolog UL18. *BMC Struct. Biol.* 2: 6.

180. Li, N. L., L. Fu, H. Uchtenhagen, A. Achour, and D. N. Burshtyn. 2013. Cis association of leukocyte Ig-like receptor 1 with MHC class I modulates accessibility to antibodies and HCMV UL18. *Eur. J. Immunol.*

181. Chapman, T. L., A. P. Heikeman, and P. J. Bjorkman. 1999. The inhibitory receptor LIR-1 uses a common binding interaction to recognize class I MHC molecules and the viral homolog UL18. *Immunity* 11: 603-613.

182. Chapman, T. L., A. P. Heikema, A. P. West Jr, and P. J. Bjorkman. 2000. Crystal structure and ligand binding properties of the D1D2 region of the inhibitory receptor LIR-1 (ILT2). *Immunity* 13: 727-736.

183. Mori, Y., S. Tsuji, M. Inui, Y. Sakamoto, S. Endo, Y. Ito, S. Fujimura, T. Koga, A. Nakamura, H. Takayanagi, E. Itoi, and T. Takai. 2008. Inhibitory immunoglobulin-like receptors LILRB and PIR-B negatively regulate osteoclast development. *J. Immunol.* 181: 4742-4751.

184. Monks, C. R., B. A. Freiberg, H. Kupfer, N. Sciaky, and A. Kupfer. 1998. Three-dimensional segregation of supramolecular activation clusters in T cells. *Nature* 395: 82-86.

185. Grakoui, A., S. K. Bromley, C. Sumen, M. M. Davis, A. S. Shaw, P. M. Allen, and M. L. Dustin. 1999. The immunological synapse: a molecular machine controlling T cell activation. *Science* 285: 221-227.

186. Davis, D. M. and M. L. Dustin. 2004. What is the importance of the immunological synapse? *Trends Immunol.* 25: 323-327.

187. Carpen, O., I. Virtanen, and E. Saksela. 1982. Ultrastructure of human natural killer cells: nature of the cytolytic contacts in relation to cellular secretion. *J. Immunol.* 128: 2691-2697.

188. Orange, J. S., K. E. Harris, M. M. Andzelm, M. M. Valter, R. S. Geha, and J. L. Strominger. 2003. The mature activating natural killer cell immunologic synapse is formed in distinct stages. *Proc. Natl. Acad. Sci. U. S. A.* 100: 14151-14156.

189. Borszcz, P. D., M. Peterson, L. Standeven, S. Kirwan, M. Sandusky, A. Shaw, E. O. Long, and D. N. Burshtyn. 2003. KIR enrichment at the effector-target cell interface is more sensitive than signaling to the strength of ligand binding. *Eur. J. Immunol.* 33: 1084-1093.

190. Treanor, B., P. M. Lanigan, S. Kumar, C. Dunsby, I. Munro, E. Auksorius, F. J. Culley, M. A. Purbhoo, D. Phillips, M. A. Neil, D. N. Burshtyn, P. M. French, and D. M. Davis. 2006. Microclusters of inhibitory killer immunoglobulin-like receptor signaling at natural killer cell immunological synapses. *J. Cell Biol.* 174: 153-161.

191. Schleinitz, N., M. E. March, and E. O. Long. 2008. Recruitment of activation receptors at inhibitory NK cell immune synapses. *PLoS One* 3: e3278.

192. Standeven, L. J., L. M. Carlin, P. Borszcz, D. M. Davis, and D. N. Burshtyn. 2004. The actin cytoskeleton controls the efficiency of killer Ig-like receptor accumulation at inhibitory NK cell immune synapses. *J. Immunol.* 173: 5617-5625.

193. Davis, D. M., I. Chiu, M. Fassett, G. B. Cohen, O. Mandelboim, and J. L. Strominger. 1999. The human natural killer cell immune synapse. *Proc. Natl. Acad. Sci. U. S. A.* 96: 15062-15067.

194. Barreira da Silva, R., C. Graf, and C. Munz. 2011. Cytoskeletal stabilization of inhibitory interactions in immunologic synapses of mature human dendritic cells with natural killer cells. *Blood* 118: 6487-6498.

195. Favier, B., J. Lemaoult, E. Lesport, and E. D. Carosella. 2010. ILT2/HLA-G interaction impairs NK-cell functions through the inhibition of the late but not the early events of the NK-cell activating synapse. *Faseb j.* 24: 689-699.

196. Lemke, H., G. J. Hammerling, and U. Hammerling. 1979. Fine specificity analysis with monoclonal antibodies of antigens controlled by the major histocompatibility complex and by the Qa/TL region in mice. *Immunol. Rev.* 47: 175-206.

197. Ozato, K., T. H. Hansen, and D. H. Sachs. 1980. Monoclonal antibodies to mouse MHC antigens. II. Antibodies to the H-2Ld antigen, the products of a third polymorphic locus of the mouse major histocompatibility complex. *J. Immunol.* 125: 2473-2477.

198. Hammerling, G. J., E. Rusch, N. Tada, S. Kimura, and U. Hammerling. 1982. Localization of allodeterminants on H-2Kb antigens determined with monoclonal antibodies and H-2 mutant mice. *Proc. Natl. Acad. Sci. U. S. A.* 79: 4737-4741.

199. Oi, V. T., P. P. Jones, J. W. Goding, L. A. Herzenberg, and L. A. Herzenberg. 1978. Properties of monoclonal antibodies to mouse Ig allotypes, H-2, and Ia antigens. *Curr. Top. Microbiol. Immunol.* 81: 115-120.

200. Evans, G. A., D. H. Margulies, B. Shykind, J. G. Seidman, and K. Ozato. 1982. Exon shuffling: mapping polymorphic determinants on hybrid mouse transplantation antigens. *Nature* 300: 755-757.

201. Shimizu, Y., D. E. Geraghty, B. H. Koller, H. T. Orr, and R. DeMars. 1988. Transfer and expression of three cloned human non-HLA-A,B,C class I major histocompatibility complex genes in mutant lymphoblastoid cells. *Proc. Natl. Acad. Sci. U. S. A.* 85: 227-231.

202. Karre, K., H. G. Ljunggren, G. Piontek, and R. Kiessling. 2005. Selective rejection of H-2-deficient lymphoma variants suggests alternative immune defence strategy. 1986. *J. Immunol.* 174: 6566-6569.

203. Allen, H., J. Fraser, D. Flyer, S. Calvin, and R. Flavell. 1986. Beta 2-microglobulin is not required for cell surface expression of the murine class I histocompatibility antigen H-2Db or of a truncated H-2Db. *Proc. Natl. Acad. Sci. U. S. A.* 83: 7447-7451.

204. Mehdi, S. Q., D. J. Recktenwald, L. M. Smith, G. C. Li, E. P. Armour, and G. M. Hahn. 1984. Effect of hyperthermia on murine cell surface histocompatibility antigens. *Cancer Res.* 44: 3394-3397.

205. Yang, J., M. S. Friedman, H. Bian, L. J. Crofford, B. Roessler, and K. T. McDonagh. 2002. Highly efficient genetic transduction of primary human synoviocytes with concentrated retroviral supernatant. *Arthritis Res.* 4: 215-219.

206. Miller, R. G. and M. Dunkley. 1974. Quantitative analysis of the 51Cr release cytotoxicity assay for cytotoxic lymphocytes. *Cell. Immunol.* 14: 284-302.

207. Orange, J. S. and Z. K. Ballas. 2006. Natural killer cells in human health and disease. *Clin. Immunol.* 118: 1-10.

208. Kuroki, K., N. Tsuchiya, M. Shiroishi, L. Rasubala, Y. Yamashita, K. Matsuta, T. Fukazawa, M. Kusaoi, Y. Murakami, M. Takiguchi, T. Juji, H. Hashimoto, D. Kohda, K. Maenaka, and K. Tokunaga. 2005. Extensive polymorphisms of LILRB1 (ILT2, LIR1) and their association with HLA-DRB1 shared epitope negative rheumatoid arthritis. *Hum. Mol. Genet.* 14: 2469-2480.

209. Liu, J. H., S. Wei, D. K. Blanchard, and J. Y. Djeu. 1994. Restoration of lytic function in a human natural killer cell line by gene transfection. *Cell. Immunol.* 156: 24-35.

210. Tam, Y. K., G. Maki, B. Miyagawa, B. Hennemann, T. Tonn, and H. G. Klingemann. 1999. Characterization of genetically altered, interleukin 2-independent natural killer cell lines suitable for adoptive cellular immunotherapy. *Hum. Gene Ther.* 10: 1359-1373.

211. Miller, J. S., J. Tessmer-Tuck, N. Blake, J. Lund, A. Scott, B. R. Blazar, and P. J. Orchard. 1997. Endogenous IL-2 production by natural killer cells maintains cytotoxic and proliferative capacity following retroviral-mediated gene transfer. *Exp. Hematol.* 25: 1140-1148.

212. Nagashima, S., R. Mailliard, Y. Kashii, T. E. Reichert, R. B. Herberman, P. Robbins, and T. L. Whiteside. 1998. Stable transduction of the interleukin-2 gene into human natural killer cell lines and their phenotypic and functional characterization in vitro and in vivo. *Blood* 91: 3850-3861.

213. Cepko, C. and W. Pear. 2001. Overview of the retrovirus transduction system. *Curr. Protoc. Mol. Biol.* Chapter 9: Unit9.9.

214. Cepko, C. 2001. Preparation of a specific retrovirus producer cell line. *Curr. Protoc. Mol. Biol.* Chapter 9: Unit9.10.

215. Heinzel, S. S., P. J. Krysan, M. P. Calos, and R. B. DuBridge. 1988. Use of simian virus 40 replication to amplify Epstein-Barr virus shuttle vectors in human cells. *J. Virol.* 62: 3738-3746.
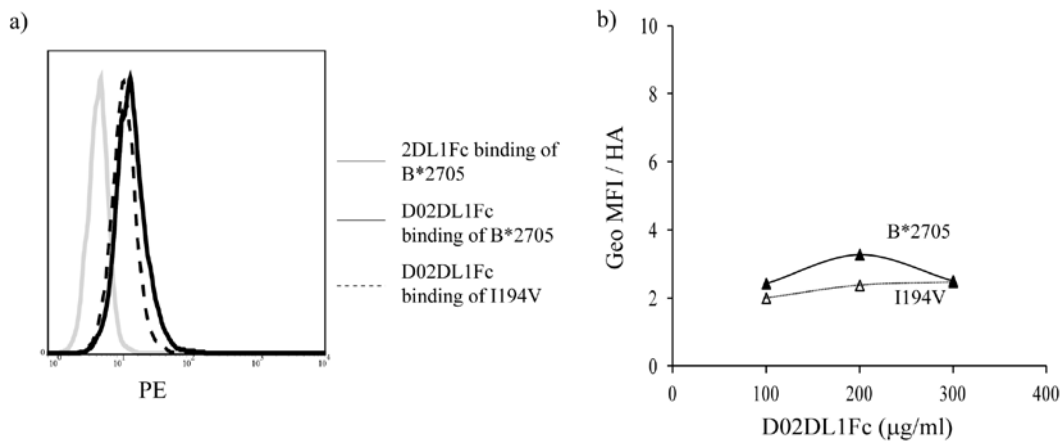
216. Kotani, H., P. B. Newton 3rd, S. Zhang, Y. L. Chiang, E. Otto, L. Weaver, R. M. Blaese, W. F. Anderson, and G. J. McGarrity. 1994. Improved methods of retroviral vector transduction and production for gene therapy. *Hum. Gene Ther.* 5: 19-28.

217. Burns, J. C., T. Friedmann, W. Driever, M. Burrascano, and J. K. Yee. 1993. Vesicular stomatitis virus G glycoprotein pseudotyped retroviral vectors: concentration to very high titer and efficient gene transfer into mammalian and nonmammalian cells. *Proc. Natl. Acad. Sci. U. S. A.* 90: 8033-8037.

218. Pear, W. 2001. Transient transfection methods for preparation of high-titer retroviral supernatants. *Curr. Protoc. Mol. Biol.* Chapter 9: Unit9.11.

219. Onishi, M., S. Kinoshita, Y. Morikawa, A. Shibuya, J. Phillips, L. L. Lanier, D. M. Gorman, G. P. Nolan, A. Miyajima, and T. Kitamura. 1996. Applications of retrovirus-mediated expression cloning. *Exp. Hematol.* 24: 324-329.

220. de la Luna, S., I. Soria, D. Pulido, J. Ortin, and A. Jimenez. 1988. Efficient transformation of mammalian cells with constructs containing a puromycin-resistance marker. *Gene* 62: 121-126.

221. Wagtmann, N., S. Rajagopalan, C. C. Winter, M. Peruzzi, and E. O. Long. 1995. Killer cell inhibitory receptors specific for HLA-C and HLA-B identified by direct binding and by functional transfer. *Immunity* 3: 801-809.

222. Bakker, A. B., J. H. Phillips, C. G. Figdor, and L. L. Lanier. 1998. Killer cell inhibitory receptors for MHC class I molecules regulate lysis of melanoma cells mediated by NK cells, gamma delta T cells, and antigen-specific CTL. *J. Immunol.* 160: 5239-5245.

223. Tanabe, M., M. Sekimata, S. Ferrone, and M. Takiguchi. 1992. Structural and functional analysis of monomorphic determinants recognized by monoclonal antibodies reacting with the HLA class I alpha 3 domain. *J. Immunol.* 148: 3202-3209.

224. Maenaka, K., T. Juji, D. I. Stuart, and E. Y. Jones. 1999. Crystal structure of the human p58 killer cell inhibitory receptor (KIR2DL3) specific for HLA-Cw3-related MHC class I. *Structure* 7: 391-398.

225. Cohen, G. B., R. T. Gandhi, D. M. Davis, O. Mandelboim, B. K. Chen, J. L. Strominger, and D. Baltimore. 1999. The selective downregulation of class I major histocompatibility complex proteins by HIV-1 protects HIV-infected cells from NK cells. *Immunity* 10: 661-671.

226. Cella, M., A. Longo, G. B. Ferrara, J. L. Strominger, and M. Colonna. 1994. NK3-specific natural killer cells are selectively inhibited by Bw4-positive HLA alleles with isoleucine 80. *J. Exp. Med.* 180: 1235-1242.

227. Kollnberger, S., A. Chan, M. Y. Sun, L. Y. Chen, C. Wright, K. di Gleria, A. McMichael, and P. Bowness. 2007. Interaction of HLA-B27 homodimers with

KIR3DL1 and KIR3DL2, unlike HLA-B27 heterotrimers, is independent of the sequence of bound peptide. *Eur. J. Immunol.* 37: 1313-1322.

228. Shiroishi, M., K. Kuroki, T. Ose, L. Rasubala, I. Shiratori, H. Arase, K. Tsumoto, I. Kumagai, D. Kohda, and K. Maenaka. 2006. Efficient leukocyte Ig-like receptor signaling and crystal structure of disulfide-linked HLA-G dimer. *J. Biol. Chem.* 281: 10439-10447.

229. Vivian, J. P., R. C. Duncan, R. Berry, G. M. O'Connor, H. H. Reid, T. Beddoe, S. Gras, P. M. Saunders, M. A. Olshina, J. M. Widjaja, C. M. Harpur, J. Lin, S. M. Maloveste, D. A. Price, B. A. Lafont, D. W. McVicar, C. S. Clements, A. G. Brooks, and J. Rossjohn. 2011. Killer cell immunoglobulin-like receptor 3DL1-mediated recognition of human leukocyte antigen B. *Nature* 479: 401-405.

230. Shields, M. J., W. Hodgson, and R. K. Ribaudo. 1999. Differential association of beta2-microglobulin mutants with MHC class I heavy chains and structural analysis demonstrate allele-specific interactions. *Mol. Immunol.* 36: 561-573.

231. Liang, S., W. Zhang, and A. Horuzsko. 2006. Human ILT2 receptor associates with murine MHC class I molecules in vivo and impairs T cell function. *Eur. J. Immunol.* 36: 2457-2471.

232. Fu, L., B. Hazes, and D. N. Burshtyn. 2011. The first Ig domain of KIR3DL1 contacts MHC class I at a secondary site. *J. Immunol.* 187: 1816-1825.

233. Powis, S. J., A. R. Townsend, E. V. Deverson, J. Bastin, G. W. Butcher, and J. C. Howard. 1991. Restoration of antigen presentation to the mutant cell line RMA-S by an MHC-linked transporter. *Nature* 354: 528-531.

234. Attaya, M., S. Jameson, C. K. Martinez, E. Hermel, C. Aldrich, J. Forman, K. F. Lindahl, M. J. Bevan, and J. J. Monaco. 1992. Ham-2 corrects the class I antigen-processing defect in RMA-S cells. *Nature* 355: 647-649.

235. Kahn-Perles, B., C. Boyer, B. Arnold, A. R. Sanderson, P. Ferrier, and F. A. Lemonnier. 1987. Acquisition of HLA class I W6/32 defined antigenic determinant by heavy chains from different species following association with bovine beta 2-microglobulin. *J. Immunol.* 138: 2190-2196.

236. Jefferies, W. A. and G. G. MacPherson. 1987. Expression of the W6/32 HLA epitope by cells of rat, mouse, human and other species: critical dependence on the interaction of specific MHC heavy chains with human or bovine beta 2-microglobulin. *Eur. J. Immunol.* 17: 1257-1263.

237. Rudolph, M. G., J. Stevens, J. A. Speir, J. Trowsdale, G. W. Butcher, E. Joly, and I. A. Wilson. 2002. Crystal structures of two rat MHC class Ia (RT1-A) molecules that are associated differentially with peptide transporter alleles TAP-A and TAP-B. *J. Mol. Biol.* 324: 975-990.

238. Kievits, F. and P. Ivanyi. 1987. Monomorphic anti-HLA monoclonal antibody (W6/32) recognizes polymorphic H-2 heavy-chain determinants exposed by

association with bovine or human but not murine beta 2-microglobulin. *Hum. Immunol.* 20: 115-126.

239. Ladasky, J. J., B. P. Shum, F. Canavez, H. N. Seuanez, and P. Parham. 1999. Residue 3 of beta2-microglobulin affects binding of class I MHC molecules by the W6/32 antibody. *Immunogenetics* 49: 312-320.

240. Maziarz, R. T., J. Fraser, J. L. Strominger, and S. J. Burakoff. 1986. The human HLA-specific monoclonal antibody W6/32 recognizes a discontinuous epitope within the alpha 2 domain of murine H-2Db. *Immunogenetics* 24: 206-208.

241. McCutcheon, J. A., K. D. Smith, A. Valenzuela, K. Aalbers, and C. T. Lutz. 1993. HLA-B*0702 antibody epitopes are affected indirectly by distant antigen residues. *Hum. Immunol.* 36: 69-75.

242. Brodsky, F. M. and P. Parham. 1982. Monomorphic anti-HLA-A,B,C monoclonal antibodies detecting molecular subunits and combinatorial determinants. *J. Immunol.* 128: 129-135.

243. Carr, W. H., D. B. Rosen, H. Arase, D. F. Nixon, J. Michaelsson, and L. L. Lanier. 2007. Cutting Edge: KIR3DS1, a gene implicated in resistance to progression to AIDS, encodes a DAP12-associated receptor expressed on NK cells that triggers NK cell activation. *J. Immunol.* 178: 647-651.

244. O'Connor, G. M., E. Yamada, A. Rampersaud, R. Thomas, M. Carrington, and D. W. McVicar. 2011. Analysis of binding of KIR3DS1*014 to HLA suggests distinct evolutionary history of KIR3DS1. *J. Immunol.* 187: 2162-2171.

245. Older Aguilar, A. M., L. A. Guethlein, M. Hermes, L. Walter, and P. Parham. 2011. Rhesus macaque KIR bind human MHC class I with broad specificity and recognize HLA-C more effectively than HLA-A and HLA-B. *Immunogenetics* 63: 577-585.

246. Moreland, A. J., L. A. Guethlein, R. K. Reeves, K. W. Broman, R. P. Johnson, P. Parham, D. H. O'Connor, and B. N. Bimber. 2011. Characterization of killer immunoglobulin-like receptor genetics and comprehensive genotyping by pyrosequencing in rhesus macaques. *BMC Genomics* 12: 295-2164-12-295.

247. Khakoo, S. I., R. Rajalingam, B. P. Shum, K. Weidenbach, L. Flodin, D. G. Muir, F. Canavez, S. L. Cooper, N. M. Valiante, L. L. Lanier, and P. Parham. 2000. Rapid evolution of NK cell receptor systems demonstrated by comparison of chimpanzees and humans. *Immunity* 12: 687-698.

248. Dissen, E., S. Fossum, S. E. Hoelsbrekken, and P. C. Saether. 2008. NK cell receptors in rodents and cattle. *Semin. Immunol.* 20: 369-375.

249. McQueen, K. L., B. T. Wilhelm, K. D. Harden, and D. L. Mager. 2002. Evolution of NK receptors: a single Ly49 and multiple KIR genes in the cow. *Eur. J. Immunol.* 32: 810-817.

250. Hoelsbrekken, S. E., O. Nylenna, P. C. Saether, I. O. Slettedal, J. C. Ryan, S. Fossum, and E. Dissen. 2003. Cutting edge: molecular cloning of a killer cell Ig-like receptor in the mouse and rat. *J. Immunol.* 170: 2259-2263.

251. Welch, A. Y., M. Kasahara, and L. M. Spain. 2003. Identification of the mouse killer immunoglobulin-like receptor-like (Kirl) gene family mapping to chromosome X. *Immunogenetics* 54: 782-790.

252. Wilson, E. B., C. A. Parachoniak, C. Carpenito, D. L. Mager, and F. Takei. 2007. Expression of murine killer immunoglobulin-like receptor KIRL1 on CD1d-independent NK1.1(+) T cells. *Immunogenetics* 59: 641-651.

253. Qin, H., Z. Wang, W. Du, W. H. Lee, X. Wu, A. D. Riggs, and C. P. Liu. 2011. Killer cell Ig-like receptor (KIR) 3DL1 down-regulation enhances inhibition of type 1 diabetes by autoantigen-specific regulatory T cells. *Proc. Natl. Acad. Sci. U. S. A.* 108: 2016-2021.

254. Potter, T. A., J. A. Bluestone, and T. V. Rajan. 1987. A single amino acid substitution in the alpha 3 domain of an H-2 class I molecule abrogates reactivity with CTL. *J. Exp. Med.* 166: 956-966.

255. Shen, L., T. A. Potter, and K. P. Kane. 1996. Glu227-->Lys substitution in the acidic loop of major histocompatibility complex class I alpha 3 domain distinguishes low avidity CD8 coreceptor and avidity-enhanced CD8 accessory functions. *J. Exp. Med.* 184: 1671-1683.

256. Back, J., E. L. Malchiodi, S. Cho, L. Scarpellino, P. Schneider, M. C. Kerzic, R. A. Mariuzza, and W. Held. 2009. Distinct conformations of Ly49 natural killer cell receptors mediate MHC class I recognition in trans and cis. *Immunity* 31: 598-608.

257. Grifoni, A., C. Montesano, P. Palma, A. Salerno, V. Colizzi, and M. Amicosante. 2013. Role of HLA-B alpha-3 domain amino acid position 194 in HIV disease progression. *Mol. Immunol.* 53: 410-413.

258. Schlosstein, L., P. I. Terasaki, R. Bluestone, and C. M. Pearson. 1973. High association of an HL-A antigen, W27, with ankylosing spondylitis. *N. Engl. J. Med.* 288: 704-706.

259. Breur-Vriesendorp, B. S., A. J. Dekker-Saeys, and P. Ivanyi. 1987. Distribution of HLA-B27 subtypes in patients with ankylosing spondylitis: the disease is associated with a common determinant of the various B27 molecules. *Ann. Rheum. Dis.* 46: 353-356.

260. Huse, M., S. Catherine Milanoski, and T. P. Abeyweera. 2013. Building tolerance by dismantling synapses: inhibitory receptor signaling in natural killer cells. *Immunol. Rev.* 251: 143-153.

261. Das, A. and E. O. Long. 2010. Lytic granule polarization, rather than degranulation, is the preferred target of inhibitory receptors in NK cells. *J. Immunol.* 185: 4698-4704.
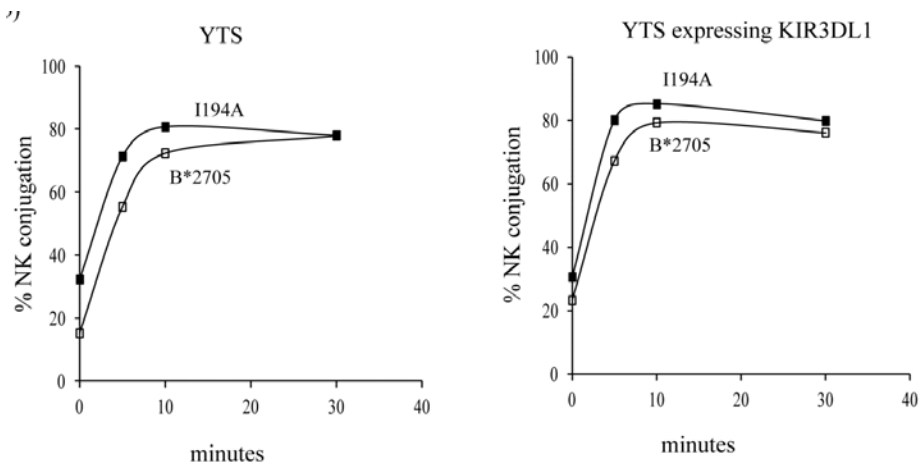
APPENDICES

a)

2DL1Fc binding of B*2705

D02DL1Fc binding of B*2705

D02DL1Fc binding of I194V

PE

b)

Geo MFI / HA

B*2705

I194V

D02DL1Fc (µg/ml)

Appendix A. The influence of isoleucine/valine at position 194 on D02DL1Fc binding

a) Flow cytometric analysis of D02DL1Fc (200 µg/ml) binding to 221 cells expressing B*27:05 or the I194V mutant. *b)* Titration of D02DL1Fc binding to 221 cells expressing B*27:05 or I194V. Expression of HLA on target cells were comparable between wild type and the mutant measured by W6/32 and HA staining. The binding results were normalized to HA staining on target cells. Only one experiment was performed.
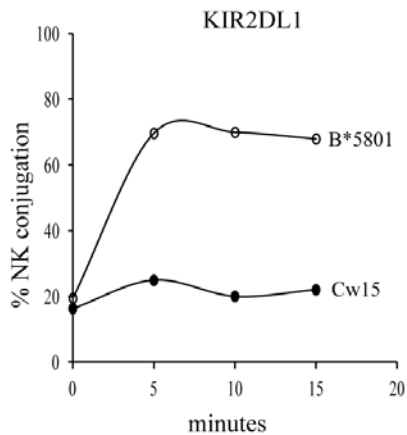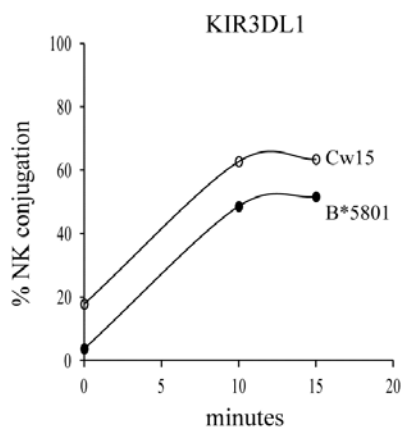
Appendix B. The influence of the D0 domain on adhesion.

Adhesion to the indicated target cells by KIR3DL1 or KIR2DL1 was measured

using a conjugation assay. The results were calculated as percentage of NK

conjugation = (conjugates of NK-target cells / total number of NK cells) X 100.

Only one experiment was performed.

Appendix C. The influence of position 194 on KIR3DL1 mediated adhesion.

Adhesion to the indicated target cells by parental YTS cells or YTS cells expressing KIR3DL1 was measured using a conjugation assay. The results were calculated as percentage NK conjugation as Appendix B. Only one experiment was performed.